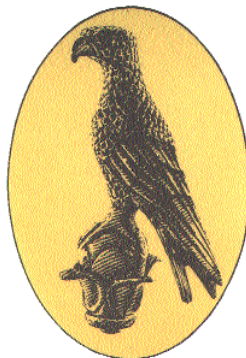**Πανεπιστήμιο Ιωαννίνων**
Σχολή Θετικών Επιστημών
Τμήμα Φυσικής

Μελέτη ιδιοτήτων λύσεων μελανών οπών στα πλαίσια τετραδιάστατων και πολυδιάστατων θεωριών βαρύτητας

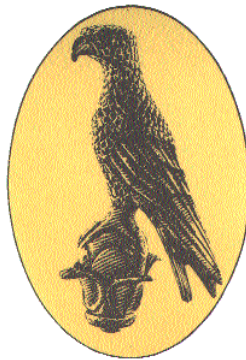**Παππάς Νικόλαος**

ΔΙΔΑΚΤΟΡΙΚΗ ΔΙΑΤΡΙΒΗ

ΙΩΑΝΝΙΝΑ 2013

University of Ioannina
Physics Department

Study of black hole solution properties in the context of 4- and higher- dimensional gravity theories

Nikolaos Pappas

PhD Thesis

IOANNINA 2013

ΠΡΑΚΤΙΚΟ
ΔΗΜΟΣΙΑΣ ΠΑΡΟΥΣΙΑΣΗΣ, ΕΞΕΤΑΣΗΣ ΚΑΙ ΑΞΙΟΛΟΓΗΣΗΣ
ΔΙΔΑΚΤΟΡΙΚΗΣ ΔΙΑΤΡΙΒΗΣ

Σήμερα Τρίτη **25-6-2013**, ώρα **16.00μ.μ.** στην αίθουσα **Σεμιναρίων του Τμήματος Φυσικής, κτίριο Φ2,** του Πανεπιστημίου Ιωαννίνων, πραγματοποιήθηκε, σύμφωνα με το άρθρο 12, παρ. 5 του Ν.2083/92, η διαδικασία της δημόσιας παρουσίασης, εξέτασης και αξιολόγησης της εργασίας του υποψήφιου για την απόκτηση Διδακτορικής Διατριβής **κ. Νικολάου Παππά.**

Την Επταμελή Εξεταστική Επιτροπή, που συγκροτήθηκε με απόφαση της Γενικής Συνέλευσης Ειδικής Σύνθεσης του Τμήματος Φυσικής (συν. 422/27-5-2013), αποτελούν τα ακόλουθα μέλη:

1) Παναγιώτα Καντή, Αναπληρώτρια Καθηγήτρια του Τμήματος Φυσικής του Παν/μίου Ιωαννίνων (Επιβλέπουσα)

2) Κυριάκος Ταμβάκης, Καθηγητής του Τμήματος Φυσικής του Παν/μίου Ιωαννίνων

3) Λέανδρος Περιβολαρόπουλος, Καθηγητής του Τμήματος Φυσικής του Παν/μίου Ιωαννίνων

4) Κωνσταντίνος Βαγιονάκης, Καθηγητής του Τμήματος Φυσικής του Παν/μίου Ιωαννίνων

5) Γεώργιος Λεοντάρης, Καθηγητής του Τμήματος Φυσικής του Παν/μίου Ιωαννίνων

6) Ιωάννης Ρίζος, Αναπληρωτής Καθηγητής του Τμήματος Φυσικής του Παν/μίου Ιωαννίνων

7) Χαράλαμπος Κολάσης, Επίκουρος Καθηγητής του Τμήματος Φυσικής του Παν/μίου Ιωαννίνων

Παρόντα ήταν και τα 7 μέλη της εξεταστικής επιτροπής. Το θέμα της διδακτορικής διατριβής που εκπόνησε ο κ. Παππάς και που παρουσίασε σήμερα είναι **«Μελέτη Ιδιοτήτων Λύσεων Μελανών Οπών στα πλαίσια Τετραδιάστατων και Πολυδιάστατων Θεωριών Βαρύτητας».**
Ο υποψήφιος παρουσίασε και ανάπτυξε το θέμα και απάντησε σε σχετικές ερωτήσεις τόσο των μελών της εξεταστικής επιτροπής όσο και του ακροατηρίου. Στη συνέχεια αποσύρθηκε η εξεταστική επιτροπή και μετά από συζήτηση κατέληξε στα ακόλουθα:

α) Η συγγραφή της διατριβής έγινε με τρόπο που δείχνει ιδιαίτερη μεθοδικότητα και πλήρη ενημέρωση του υποψήφιου πάνω στη σχετική βιβλιογραφία.
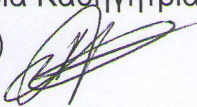
β)   Η ερευνητική εργασία καταλήγει σε σημαντικά αποτελέσματα τα οποία προάγουν την επιστήμη. Από την εργασία αυτή έχουν προκύψει πέντε εργασίες δημοσιευμένες σε έγκριτα επιστημονικά περιοδικά, μία έκτη εργασία υποβληθείσα για δημοσίευση σε διεθνές επιστημονικό περιοδικό, και μία ανακοίνωση σε διεθνές συνέδριο που έγινε από τον υποψήφιο καθώς και δημοσίευση στα πρακτικά.

γ)   Η παρουσίαση και ανάπτυξη του θέματος της εργασίας από τον υποψήφιο και οι εύστοχες απαντήσεις στις ερωτήσεις που του τέθηκαν έδειξαν πλήρη γνώση του θέματος και γενικότερων σχετικών θεμάτων Φυσικής Στοιχειωδών Σωματιδίων και Βαρύτητας.
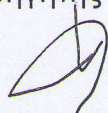
Με βάση τα ανωτέρω, τα μέλη της Επταμελούς Εξεταστικής Επιτροπής εγκρίνουν ομόφωνα την εργασία και εισηγούνται ανεπιφύλακτα την απονομή Διδακτορικού Διπλώματος στον κ. Νικόλαο Παππά με βαθμό Άριστα.

Τα μέλη της Εξεταστικής Επιτροπής

1. Αναπληρώτρια Καθηγήτρια Π. Καντή
(Επιβλέπουσα)

2. Καθηγητής Κ. Ταμβάκης

3. Καθηγητής Λ. Περιβολαρόπουλος
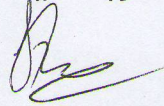
4. Καθηγητής Κ. Βαγιονάκης
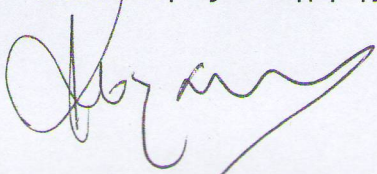
5. Καθηγητής Γ. Λεοντάρης

6. Αναπληρωτής Καθηγητής Ι. Ρίζος

7. Επίκουρος Καθηγητής Χ. Κολάσης

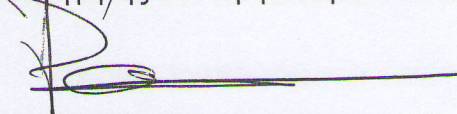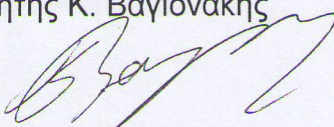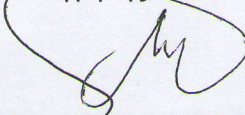<u>Three-member advisory committee.</u>

- P. Kanti, Associate Professor, Department of Physics, University of Ioannina (supervisor)

- K. Tamvakis, Professor, Department of Physics, University of Ioannina

- L. Perivolaropoulos, Professor, Department of Physics, University of Ioannina

<u>Dissertation evaluation committee</u>

- P. Kanti, Associate Professor, Department of Physics, University of Ioannina (supervisor)

- K. Tamvakis, Professor, Department of Physics, University of Ioannina

- L. Perivolaropoulos, Professor, Department of Physics, University of Ioannina

- C.E. Vayonakis, Professor, Department of Physics, University of Ioannina

- G.K. Leontaris, Professor, Department of Physics, University of Ioannina

- J. Rizos, Associate Professor, Department of Physics, University of Ioannina

- Ch. Kolassis, Assistant Professor, Department of Physics, University of Ioannina

Acknowledgements

In our complicated and highly interactive world no activity can be regarded as independently realized by a single person. The same holds true for the present dissertation as well. It would be just impossible to conduct my research without the contribution of many different people at many different levels. I owe an enormous debt to all of them who assisted, encouraged, inspired, guided and, more often than not, led me during my study. Hereby, I wish grab the chance to thank:

- My supervisor, Ass. Professor P. Kanti for all the time and energy that she devoted during the past years being the best supervisor one could have. She has always been there for me – to guide me through the difficulties of the scientific research, to give me valuable advices and to support me both morally and financially. It has been a great honor and a privilege for me to meet her and to have her as a teacher, as a collaborator and as a friend. Her striking generosity, her infinite patience along with her deep scientific knowledge have been of catalytic importance for the completion of my PhD studies, which have been realized under rather unconventional circumstances, but nevertheless were proven to be fruitful.

- Prof. K. Tamvakis for our stimulating discussions on physics and philosophy as well as for helping me on multiple occasions. I'd also like to thank him for his advices and guidance. And for giving me some important lessons regarding both physics and life.

- Prof. L. Perivolaropoulos for our successful collaboration on various issues at several occasions.

- Prof. C.E. Vayonakis, Ass. Prof. A. Dedes and Assist. Prof. Ch. Kolassis for some very interesting discussions and their encouragement.

- All seven members of the dissertation evaluation committee for the time they devoted to read it and their valuable remarks.

- Hideo Kodama, Alexander Zhidenko, Roman Konoplya and Katarzyna Zuleta Estrugo for our collaboration at various stages of my research that resulted to the publication of two papers. Also Marc Casals for his valuable help with the normalization factors of the spin-weighted spheroidal harmonics and Athanasios Dedes for useful discussions regarding our numerical codes in *MATHEMATICA*.

- All the teachers I had during my under- and post-graduate studies for their self-evident contribution to my education.

- Ass. Professor G. Throumoulopoulos for a brave and open-minded decision of his, which allowed my journey in Physics to start a decade ago.

- My colleagues, fellow PhD students and friends Michalis Paraskevas and Christos Soutzios for the amusing moments, the very interesting discussions and the ideas that we shared over the past years and for helping me at several occasions with practical issues.

- Mr. Spyros Kosmas for his valuable help at so many levels during my research. And for being such a good friend.

Finally, there are not enough words to express my gratitude to my wife Valia and my son Petros for being an endless source of happiness and inspiration for me.

Outline

The dissertation is dedicated to the study of black hole physics. In particular, we have studied various aspects of the Hawking radiation spectrum of higher-dimensional rotating black holes. Furthermore, we also sought for an answer to the question of whether some conventional field living in the bulk could support the existence of a rational black hole solution in the context of the Randall-Sundrum one brane model. Finally, we turned our attention to issues concerning information and unitarity preservation in a system that involves an evaporating black hole. The results of our study have been published in the following articles:

- *"Graviton Emission in the Bulk by a Simply Rotating Black Hole"*, P. Kanti, H. Kodama, R.A. Konoplya, N. Pappas and A. Zhidenko, *Phys. Rev.* D **80**, 084016 (2009).

- *"Emission of Massive Scalar Fields by a Higher-Dimensional Rotating Black-Hole"*, P. Kanti and N. Pappas, *Phys. Rev.* D **82**, 024039 (2010).

- *"Bulk decay of (4 + n)-dimensional simply rotating black holes: Tensor-type gravitons"*, N. Pappas, *J. Phys. Conf. Ser.* **283** 012028 (2011).

- *"A New approach to information loss (no) problem for Black Holes"*, N. Pappas, *Int. J. Theor. Math. Phys.* **2N2**, 5-9 (2012).

- *"On the preservation of unitarity during black hole evolution and information extraction from its interior"*, N. Pappas, *Mod. Phys. Lett.* A**27**, 12501 (2012).

- *"Angular profile of Particle Emission from a Higher-dimensional Black Hole: Analytic Results"*, P. Kanti and N. Pappas, *JHEP* **1212**, 019 (2012).

- *"On the Localization of 4-Dimensional Brane-World Black-Holes"*, P. Kanti, N. Pappas and K. Zuleta Estrugo (submitted for publication to Class. Quant. Grav.).

The first chapter tries to encapsulate all the theoretical knowledge necessary for someone to understand the questions we tried to answer, the techniques we used and the implications of our findings. Therefore, it includes an introduction to General Relativity, brane world models, 4- and higher-dimensional black hole solutions, the Hawking radiation mechanism, the thermodynamical properties of black holes and the information loss paradox. In chapter 2 we study the emission of tensor-type gravitons

in the bulk as well as massive scalars both in the bulk and on the brane by a higher-dimensional rotating black hole. Even more, we deal with the angular profile of the Hawking radiation of such a black hole in the case of the emission of fermions, bosons and scalars on the brane. In chapter 3 we show that no well-defined field configuration in the bulk can support the existence of a 5-dimensional, yet localized on the brane, black hole in the context of the Randall-Sundrum II model. In chapter 4 we turn our attention to the famous (or, even, notorious) information paradox for black holes and we present a couple of ideas to resolve it. Finally, in chapter 5 we make a review of our work and proceed to a discussion about the significance of our results. In the three appendices following, we give some details about the properties of the spin-weighted spheroidal harmonics (app. A and B), while in app. C some indicative codes we wrote for the *MATHEMATICA* computer programme and used throughout the studies presented in chapter 2 are given.

Preface

There is one, and only one, fundamental distinction between the questions one can ask about Nature. On the one hand are the "Why?"s and on the other the "How?"s. Even though there is a connection between them through a dialectic interaction, where the ones trigger off the others, at the same time they stand on a completely different ground. Posing the question is of sublime significance in the process of expanding our understanding. More often than not, even formulating a question is a big step forward. And it is exactly this function, in reference to which the two question types differ so much. The "How?"s live in a specific knowledge frame, which they cannot surpass, since their role is to check the compatibility of this frame with reality and give us feedback on the limitations and failures of the former. The "Why?"s, on the other hand, can play a more radical role. Whereas they are formed based on notions and input coming from an already existing frame, the very fact that they were actually put forward can lead to the birth of a new paradigm. To put it in another way, asking "how does an apple move when falling off a tree?" leads to the answer "with a constant acceleration of $9.81 m/s^2$" (details concerning friction, latitude etc. are irrelevant, since they do not change the essence of the argument). By asking "why do apples always fall towards the earth?" one ends up with "Gravity" for an answer (if this one is someone like Newton, of course, but in any case the formulation of the question is prerequisite for the discovery of Gravity).

Following the distinction of the questions, scientists can also be categorized as "Why-ers" and "How-ers" accordingly. However, contrary to the dialectic relation between "Why?"s and "How?"s, there is a huge gap dividing the two tribes, that is only occasionally bridged. Interestingly enough, belonging to the one or the other group is, actually, not at all a conscious choice. It is, rather, an internal tendency and sometimes need to try to answer questions starting primarily with a "why" or a "how". There is a flame inside the mind and soul, that sparkles when coming across these questions, but, mistake not, if it is the "Why?"s, that cause this, then the "How?"s can't and vise versa. It is that simple and that definite. After all, how on earth could it be a conscious choice to feel uneasy with the potential existence of naked singularities

somewhere in the Universe, when driving? Or to worry about the non-existence of black hole solutions in the context of brane modles, during lunch? Or to get puzzled about the origin of time, while being at a bank queue? It comes as no surprise then that, when coming to Physics, "Why-ers" naturally become theoretical physicists.

The naturalness of this fact becomes evident when bearing in mind the very special property of Theoretical Physics to be the only scientific activity characterized by such an enormous freedom and width. No time or energy scale is big or small enough not to be considered. No technical limitation can forbid the examination of systems like the Universe as a whole or the interior of black holes. Nor is our thought obliged to remain "trapped" inside a four-dimensional space-time or times later than the Big Bang (if we wish to adopt the Big Bang hypothesis at all!). What more charming, can a scientist think of, than the freedom to consider any process (no matter how complicated it may be), any phenomenon (even if it has never been observed), any particle or dimension (real or alleged), any notion (no matter where it comes from) in order to formulate a model or give an explanation? No human activity, other than Poetry, incorporates this magnitude of freedom of thought. And that is why these two preserve the hope that the world could evolve in a direction that would make our lives more meaningful. Besides, what makes humans different from all other creatures is not the efficiency with which they dominate over their environment, but the fact that they can wonder about causes, that they raise questions that surpass their sad material existence, that their mind can fly from the tiniest to the largest scale, from the deepest sentiments to the most admirable truths.

Paying tribute to the crown jewel of Science, then, hereby I present my first (and wishfully not last) contributions to Theoretical Physics.

Contents

Chapter 1

Introduction

General Relativity is, if anything, a theory of gravity. The most important notion in the theory is the notion of space-time, that is the idea that space and time co-form a continuum which can be encountered as a 4-dimensional manifold, in terms of Differential Geometry. This idea was conceived by Hermann Minkowski, whose famous quotation

"... Henceforth space by itself, and time by itself, are doomed to fade away into mere shadows, and only a kind of union of the two will preserve an independent reality..."

emphatically underlines the necessity to deal with space and time as indispensable parts of the same entity [1]. Apart from the notion of space-time, there are two key ideas that form the kernel of the theory.

The first idea goes by the name *Mach's principle*, which in reality is a set of ideas concerning the relation between the space-time properties and the matter-energy distribution in it. The general concept is that this distribution should play a crucial role in the definition of properties like "acceleration" and "rotation", which also means that in an empty Universe these concepts are devoid of meaning. In other words, space-time has a dynamical behavior since its properties should change following changes of the matter distribution in it.

The second idea is the *equivalence principle*, which is usually expressed as the fact that the gravitational and inertial mass of all bodies are identical. Furthermore, it suggests that all bodies are affected by gravity and they fall in the same way in a gravitational field. Because the trajectories (geodesics since we talk about free falling objects) are independent of the nature of the bodies, one can consider them as indicating the existence of a curved space-time region, to the structure of which we can ascribe properties of the gravitational field that we study.

Combining all these ideas together, Einstein was able to formulate General Relativity as the theory of space, time and gravitation. There the intrinsic observer-independent properties of space-time are described by a space-time metric, which does not in general or necessarily has the flat form known from Special Relativity and Newtonian physics. Instead, space-time could be curved (that is deviate from flatness) with its curvature to account for the physical effects we usually ascribe to gravitational
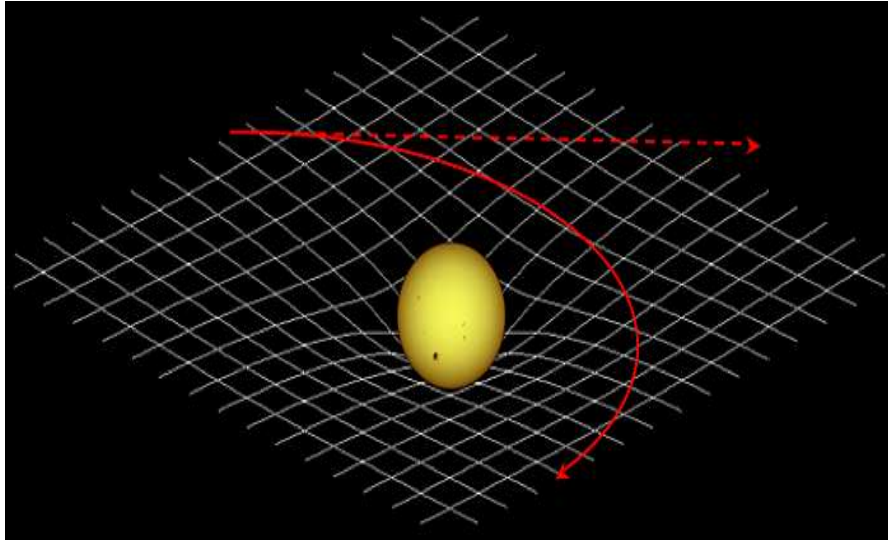
Figure 1.1: The existence of a massive object (yellow ball) causes the deformation of the space-time continuum (represented by the white lattice). A freely moving object instead of traveling in a straight light (dashed line) naturally follows a curved route (solid line) even though no force is exerted on it [2].

fields. Moreover, the aforementioned curvature is related to the energy-momentum tensor ($T_{\mu\nu}$), that encapsulates all information about the energy and matter content of space-time, and can vary with time depending on the time evolution of this tensor.

General Relativity [3, 4, 5, 6, 7, 8, 9, 10, 11, 12, 13] is an extremely successful theory. A number of its predictions differ significantly from those of classical physics, especially concerning the passage of time, the geometry of space, the motion of bodies in free fall, and the propagation of light. Examples of such differences include gravitational time dilation, gravitational lensing, the gravitational redshift of light and the gravitational time delay. All predictions have been confirmed in all observations and experiments to date. Nonetheless, unanswered questions remain, the most fundamental being how General Relativity can be reconciled with the laws of quantum physics to produce a complete and self-consistent theory of quantum gravity. In order to explore the limits of the validity region of General Relativity and get some insights concerning quantum gravity we turn to the study of the most extreme and fascinating objects predicted to exist in the context of the former, namely the black holes [24, 25].

There is good reason for that choice. Back in the $70's$ black holes were shown by Bekenstein to possess, classically unexpected, thermodynamic properties [26], that we will extensively present in section 1.3.3. Shortly after Hawking, following a semiclassical approach, proved that black holes radiate thermally (see section 1.3.2 for a detailed presentation) and, thus, have a measurable radiation spectrum, that, once recorded, could reveal all kinds of information about their properties. However, the huge value of their -predicted- entropy and the thermal nature of the emitted radiation raised a series of puzzling questions. These mainly concern the fate of information that ends

in the black holes and the consistency of their evolution with the rules of Quantum Mechanics, as it seemed that they evolve in a non-unitary way (see section 1.3.4 for details). The fact that these questions remain more or less unanswered until now, motivated the work presented in chapter 4 [17] [18]. Furthermore, during the last couple of decades string theory-inspired models postulating the existence of large extra spacelike dimensions were proposed (namely the ADD and Randall-Sundrum models - presented in section 1.2). Since black holes are purely gravitational objects, their behavior (ergo also their spectrum) should in principle be determined by the properties of space-time, making them impeccable probes of the actual space-time geometry. The fact that General Relativity allows for the existence of black holes of any mass combined with the prediction of the aforementioned models of a significantly lower (of TeV order) fundamental energy scale, than the traditional 4-dimensional Planck scale (of order 10^{19}GeV), made it legitimate to expect that miniature black holes could be produced in ground-based experiments (like the LHC). In this case we would be able to witness their evaporation through the emission of Hawking-type radiation and find direct evidence about the existence of extra dimensions. Therefore, it is very important to have a clear knowledge of the expected spectrum for different parameter combinations. Our contribution to this effort [19] [20] [21] is presented in chapter 2. Finally, inspired by previous works on the subject, we explored the possibility of finding a classical black hole solution on a brane and reached a no-go result concerning the potential field theories required to support such a solution, that we present in chapter 3 [22].

1.1 Elements of General Relativity

As stated earlier the space-time continuum can be treated as a manifold. A manifold is a space that may be curved and/or have a complicated topology, but locally looks like the Euclidean n-dimensional space (R^n). This basically means that functions and coordinates work (locally) much in the same way as in R^n. We construct a manifold of dimension n by smoothly sewing together a set of well-behaved, Euclidean patches, all of which are of the same dimensionality n. In this way one can study functions on the manifold by converting them locally to functions in Euclidean space.

The most important mathematical tool, when it comes to the study of curved manifolds, is the metric tensor (usually referred simply as "the metric") symbolized as $g_{\mu\nu}$ (when it comes to Minkowski space we write $\eta_{\mu\nu}$ instead). It has to be symmetric and nondegenerate, which means that its determinant $g \equiv |g_{\mu\nu}|$ doesn't vanish. In this case we also define the inverse metric $g^{\mu\nu}$ through the relation

$$g^{\mu\nu} \, g_{\nu\sigma} = g_{\lambda\sigma} \, g^{\lambda\mu} = \delta^\mu_\sigma. \qquad (1.1)$$

Both versions can be used to raise and lower indices on tensors. Nevertheless, the importance of the metric tensor goes far beyond that use. Following Sachs and Wu [23] we cite that the metric also:
(**1**) - supplies a notion of "past" and "future";
(**2**) - allows the computation of path length and proper time;

(3) - determines the "shortest distance" between two points and, therefore, the trajectory of test particles;

(4) - replaces the Newtonian gravitational field;

(5) - provides a notion of locally inertial frames and, consequently, a sense of "no rotation";

(6) - determines causality, by defining the speed of light faster than which no signal can travel;

(7) - replaces the traditional three-dimensional Newtonian picture of Nature.

A useful characterization of the metric is obtained by converting $g_{\mu\nu}$ into its canonical form, where it is written as a diagonal matrix, with the elements being its eigenvalues (it can be shown that at any point there exists a suitable coordinate system in which $g_{\mu\nu}$ takes its canonical form[1]). The signature of the metric is the number of positive and negative eigenvalues. If all of them are positive, the metric is called Euclidean or Riemannian or positive definite. If there is a single negative one, then we characterize the metric as Lorentzian or pseudo-Riemannian. Space-times that admit Lorentzian metrics are the most interesting ones and, therefore, we shall focus our study solely on such.

Since neither the time nor the space interval between events has an absolute significance, in accordance to the statement of Minkowski, we shall turn our attention to the quantity

$$ds^2 = g_{\mu\nu}\, dx^\mu\, dx^\nu. \tag{1.2}$$

The above defines the space-time interval between two events with an infinitesimal coordinate separation (also known as the line-element), which is observer-independent (i.e. its value is the same for all sets of global inertial coordinates) and, thus, capable to describe the space-time properties in a well defined way. The term $g_{\mu\nu}$ is of course the metric tensor of the manifold, the exact form of which is determined by the mass distribution considered. Because of the close relation between ds^2 and $g_{\mu\nu}$, the terms "metric" and "line-element" are often used interchangeably.

The metric tensor and the quantities derived from it play a crucial role in the formulation of General Relativity. More specifically, we define the following key quantities for the study of curved manifolds:

- The "affine connection" $\Gamma^\lambda_{\mu\nu}$ as

$$\Gamma^\lambda_{\mu\nu} = \frac{1}{2}\, g^{\lambda\rho}\, (\partial_\mu g_{\nu\rho} + \partial_\nu g_{\rho\mu} - \partial_\rho g_{\mu\nu}), \tag{1.3}$$

which is very useful while treating free falling objects and, therefore determining the geodesics (the straightest possible lines) of a curved region.

- The Riemann tensor $R^\rho{}_{\sigma\mu\nu}$ as

$$R^\rho{}_{\sigma\mu\nu} = \partial_\mu \Gamma^\rho_{\nu\sigma} - \partial_\nu \Gamma^\rho_{\mu\sigma} + \Gamma^\rho_{\mu\lambda}\Gamma^\lambda_{\nu\sigma} - \Gamma^\rho_{\nu\lambda}\Gamma^\lambda_{\mu\sigma}, \tag{1.4}$$

where all information about the curvature of the space-time manifold is included.

- The Ricci tensor $R_{\mu\nu}$ as

$$R_{\mu\nu} = R^\lambda{}_{\mu\lambda\nu} \tag{1.5}$$

---

[1]We usually refer to these coordinates as locally inertial coordinates.

and the scalar curvature R, defined as the trace of the Ricci tensor

$$R = R^{\mu}{}_{\mu} = g^{\mu\nu} R_{\mu\nu}. \tag{1.6}$$

- The Einstein tensor

$$G_{\mu\nu} = R_{\mu\nu} - \frac{1}{2} R\, g_{\mu\nu}, \tag{1.7}$$

whose property to be divergence-free

$$\nabla^{\mu} G_{\mu\nu} = 0 \tag{1.8}$$

is equivalent to the twice-contracted Bianchi identity.
Finally, the most important equation that every system has to satisfy in the context of General Relativity is the famous Einstein equation

$$G_{\mu\nu} = R_{\mu\nu} - \frac{1}{2} R\, g_{\mu\nu} = 8\pi\, G\, T_{\mu\nu}, \tag{1.9}$$

where G is Newton's constant of gravitation and $T_{\mu\nu}$ the energy-momentum tensor. It is evident from eq. (1.9) that the geometrical features of space-time as expressed by $R_{\mu\nu}$ and R are directly connected to the exact form of the energy-momentum tensor, which serves as the source of the gravitational field, that we encounter as equivalent to the curved space-time manifold. It seems natural then to try to solve the above equation to find $g_{\mu\nu}$ after having specified $T_{\mu\nu}$. However, this is a very tricky approach since, until $g_{\mu\nu}$ is determined, we don't know how to physically interpret $T_{\mu\nu}$. Therefore, with the exception of some special cases, both $g_{\mu\nu}$ and $T_{\mu\nu}$ are to be determined and understood simultaneously, while solving eq. (1.9).

A particularly interesting route to Einstein's equation is through the principle of least action. The idea is to use notions of the classical field theory to give $g_{\mu\nu}$ field equations of its own since our dynamical variable is now the metric itself. Hilbert figured out that the simplest Lagrangian one can write for the gravitational field is the Ricci scalar itself and, consequently, proposed the action

$$S_H = \int d^4x \sqrt{-g}\, R, \tag{1.10}$$

known ever since as the Hilbert (or Einstein-Hilbert) action, as the starting point of the analysis. Then we consider the behavior of S_H under small variations of the metric (in fact we make variations with respect to the inverse metric $g^{\mu\nu}$, which are equivalent to the ones with respect to $g_{\mu\nu}$, while more convenient to calculate). Using the *Palatini identity*

$$\delta R_{\mu\nu} = \left(\delta\Gamma^{\lambda}_{\mu\lambda}\right)_{;\nu} - \left(\delta\Gamma^{\lambda}_{\mu\nu}\right)_{;\lambda}, \tag{1.11}$$

the covariant form of Gauss's theorem, stating that if V^{μ} vanishes at infinity then

$$\int d^4x \sqrt{-g}\, V^{\mu}{}_{;\mu} = 0, \tag{1.12}$$

and the fact that

$$\delta g^{\mu\nu} = -g_{\mu\rho}\,g_{\nu\sigma}\,\delta g^{\rho\sigma} \quad \text{and} \quad \delta\sqrt{-g} = -\frac{1}{2}\sqrt{-g}\,g_{\mu\nu}\,\delta g^{\mu\nu}, \tag{1.13}$$

we arrive at the expression

$$S_H = \int d^4x \sqrt{-g} \left[R_{\mu\nu} - \frac{1}{2}\,R\,g_{\mu\nu} \right] \delta g^{\mu\nu}. \tag{1.14}$$

Bearing in mind that for the functional derivative of the action applies that

$$S = \int \sum_i \left(\frac{\delta S}{\delta \Phi^i}\,\delta \Phi^i \right) d^4x, \tag{1.15}$$

where Φ^i is the set of all fields being varied (which in our case is the $g^{\mu\nu}$ alone), and that for stationary points $\frac{\delta S}{\delta \Phi^i} = 0$, we find

$$\frac{1}{\sqrt{-g}}\frac{\delta S_H}{\delta g^{\mu\nu}} = R_{\mu\nu} - \frac{1}{2}\,R\,g_{\mu\nu} = 0, \tag{1.16}$$

which is the Einstein's equations in vacuum. The fact that eq. (1.16) is the vacuum solution should come as no surprise since in the action eq. (1.10) we considered only the purely gravitational quantity R and no additional terms for matter fields were included. In the case of non-vacuum conditions we use the generalized action

$$S = \frac{1}{16\pi G}\,S_H + S_M, \tag{1.17}$$

where S_M is the action for matter, S_H is the gravitational (Einstein-Hilbert) action and the factor $\frac{1}{16\pi G}$ is used for normalization reasons. Following the same steps as before we get

$$\frac{1}{\sqrt{-g}}\frac{\delta S}{\delta g^{\mu\nu}} = \frac{1}{16\pi G}\left(R_{\mu\nu} - \frac{1}{2}\,R\,g_{\mu\nu} \right) + \frac{1}{\sqrt{-g}}\frac{\delta S_M}{\delta g^{\mu\nu}} = 0. \tag{1.18}$$

We define the energy-momentum tensor $T_{\mu\nu}$ as

$$T_{\mu\nu} = -2\frac{1}{\sqrt{-g}}\frac{\delta S_M}{\delta g^{\mu\nu}} \tag{1.19}$$

and then we straightforwardly end up with the complete form of the Einstein equation

$$G_{\mu\nu} = R_{\mu\nu} - \frac{1}{2}\,R\,g_{\mu\nu} = 8\pi\,G\,T_{\mu\nu}. \tag{1.20}$$

The derivation of the Einstein equation with the use of Lagrangian formulation is a very interesting fact since it manifests a not-at-all-self-evident connection between General Relativity and field theory. In addition, it provides us with a relatively easy way of constructing new models by adding terms in the Lagrangian, either gravitational

invariant quantities or terms concerning matter fields, and then studying their impact on the field equations derived from them.

It is worth noting here that, even though we usually speak about a 4-dimensional space-time continuum, all tensors defined so far as well as eq. (1.9) hold also for manifolds of higher dimensionality. This is of particular interest since it allows us to consider space-times with an arbitrary number of extra spacelike and/or timelike dimensions and study them with the use of well understood mathematical tools of differential geometry. This freedom leaves a lot of room for new ideas to get integrated in the frame of classical General Relativity so as to create new universe models. The core concept of model-building in the frame of General Relativity is that of finding a novel solution of Einstein's equations. Given both eq. (1.9) and suitable equations for the matter considered, such a solution consists of finding a specific pseudo-Riemannian manifold (defined by giving the metric in suitable coordinates), and specific matter fields defined on it. Matter and geometry must, of course, satisfy Einstein's equations, thus the matter's energy-momentum tensor must be divergence-free, while the matter must also satisfy whatever additional equations were originally imposed on its properties. It was this feature that allowed Kaluza and Klein, only a few years after General Relativity was formulated, to postulate the existence of an extra dimension, in an attempt to unify the gravitational and the electromagnetic force, and to explicitly calculate the consequences of their idea thanks to the tensorial formulation of the theory [24, 25].

1.2 Introduction to brane world models

Interestingly enough, the question regarding the existence of extra spatial dimensions reemerged several decades after Kaluza and Klein's model, since they are a key demand of string theory. In the context of this theory five distinct $(1 + 9)$-dimensional superstring theories, all giving quantum theories of gravity, were formulated. Duality transformations relating these theories with the $(1 + 10)$-dimensional supergravity theory, led to the conjecture that all of these theories arise as different limits of a single theory, which goes under the name M theory. It is known that p-branes, which are extended objects of p spatial dimensions (strings for example are 1-branes), play a fundamental role in the theory. The most important subgroup of p-branes are the D-branes, on which open strings can end. Open strings describe the non-gravitational sector and their endpoints are firmly attached to branes. Closed strings, that describe the gravitational degrees of freedom, on the other hand, can propagate in the bulk. It has been proposed then that the observable Universe could be such a D-brane, that is a $(1+3)$-surface (referred to henceforth simply as the "brane") embedded in a $(1+3+n)$-dimensional space-time (the "bulk"), with Standard Model particles and fields trapped on the brane, while gravity is free to access the bulk. This is, in a nutshell, the central idea of the brane world models (see Fig. 1.2).

The main motivation for the formulation of brane world models is the attempt to find a solution to the hierarchy problem. That is the huge discrepancy between the electroweak scale (of order TeV) and the ordinary Planck scale, where quantum-gravitational effects arise (of order 10^{19} GeV), observed in 4 dimensions. In such models
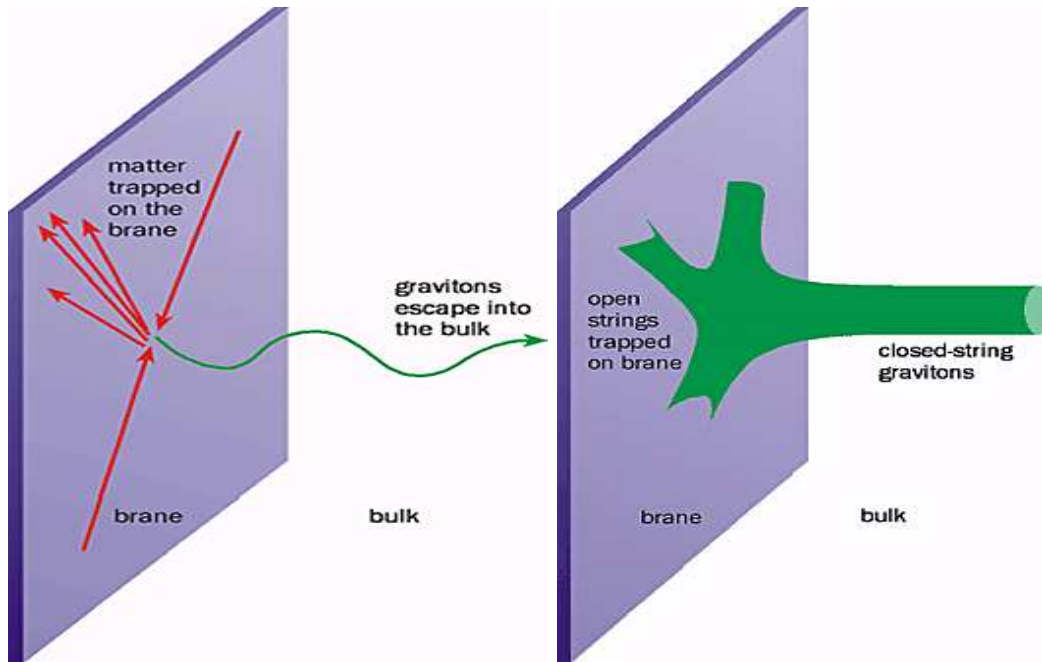
Figure 1.2: Diagrammatic representation of the brane world scenario, where our Universe is a 3-brane embedded in the bulk. **Left:** ordinary matter, consisting of Standard Model particle, is confined on the brane, while gravitons can propagate into the bulk. **Right:** the same fact in terms of string theory [27].

the additional freedom that stems from the existence of extra dimensions, allows for some more radical approaches to the problem. In general, the two scales are assumed to be of the same order, while the hierarchy problem is merely an artifact emerging on our brane, due to the non-trivial topology of the space-time as a whole. A very exciting prospect in this case is that the creation of black holes would become significantly easier and even possible at energies accessible by current experiments. Furthermore, other interesting ideas also were developed and embodied in the frame of brane world models that inspired many researchers to explore in detail various aspects of these models. We shall now move on to give a more detailed illustration of the two most famous such models.

1.2.1   The ADD model

The first model that incorporated the idea of extra spacelike dimensions of macroscopic size was proposed back in 1998 by N. Arkani-Hamed, S. Dimopoulos and G. Dvali (ADD) [28, 29, 30, 31]. They claimed that, since the validity of the inverse-square law for gravity was experimentally checked (by Cavendish-type experiments) only up to a few hundreds of μm (the current limit is down to just a few μm [32]), it is legitimate to imagine that extra spacelike dimensions even of that size, transverse to our 4-dimensional brane could also exist. Their number is an open-value parameter (with

$n \geq 2$ for consistency with experimental data) in the model and they are admitted to have a flat topology. As we cannot directly "see" them because, in principle, all Standard Model particles are confined strictly on the brane, they should indirectly manifest their existence by the modified gravitational potential one would measure when conducting experiments at appropriately short length scales. In their model the n extra spatial dimensions are allowed to be very large relative to the Planck scale[2]. The main consequence of this hypothesis is that then the fundamental gravity scale would be lowered, possibly even down to the electroweak (TeV) scale. The gravitational action in this case can be written as

$$S_{grav} = \frac{1}{2\kappa_{(4+n)}^2} \int d^4x \, d^n y \, \sqrt{-g_{(4+n)}} \left[R_{(4+n)} \right] , \qquad (1.21)$$

where x refers to the $(1+3)$ dimensions of our world, y stands for the extra dimensions, $\kappa_{(4+n)}^2$ is the gravitational coupling constant, $g_{(4+n)}$ is the determinant of the metric tensor and $R_{(4+n)}$ is the Ricci scalar all corresponding to the higher-dimensional model. The $(4+n)$-dimensional Poisson equation admits then the solution

$$V(r) \propto \frac{\kappa_{(4+n)}^2}{r^{1+n}}. \qquad (1.22)$$

The scale, where all these apply, depends on the scale L of the postulated large extra dimension. For scales $r \lesssim L$, the potential is $(4+n)$-dimensional, $V \propto r^{-(1+n)}$. On scales large relative to L the presence of extra dimensions does not induce measurable deviations from the 4-dimensional behavior, thus the potential becomes effectively 4-dimensional, that is $V \propto L^{-n} r^{-1}$. The usual Planck scale (M_P), therefore, can be encountered as merely an effective coupling constant suitable for treating gravity on scales much larger than the extra dimensions, that is related to the fundamental one ($M_{(4+n)}$) as

$$M_P^2 = M_{(4+n)}^{2+n} L^n. \qquad (1.23)$$

According to eq. (1.23) for L of order mm the M_{4+n} value would be as low as $\sim 1\text{TeV}$, which lies well inside the energy region that LHC is able to explore. This significantly lowered value for the (fundamental) Planck scale resolves then the hierarchy problem, since the higher-dimensional gravity scale and the electroweak scale are of the same order. We just see things differently only because up till now we used to perform experiments with not enough energy to "unlock" the extra dimensions and "reveal" the true Planck scale. In addition, a TeV-order gravity scale means that phenomena like the formation of black holes and manifestations of the unification of forces, can take place in the lab since these energy scales are now experimentally accessible.

The ADD model drew a great deal of attention since for the first time large extra dimensions were employed and predictions that could be actually get falsified through experiment were made. Even though there are some serious conceptual problems concerning the formulation of the model, one should always acknowledge that it was the

---

[2]Even though, in principle, they could be of different sizes, we usually take them all to be of the same size L.

one that brought in the foreground the hypothesis that extra dimensions could be significantly different than the compactified-to-Planck-scale ones, we used to consider up till then.

1.2.2   The Randall - Sundrum (RS) models

Shortly after the ADD scenario was proposed another brane world model was put forward by L. Randall and R. Sundrum. Actually they managed to built two, related but different models with distinct merits and problems [33, 34]. The trademark of the RS-models is the rather radical assumption concerning the existence of one additional spacelike dimension of infinite size transverse to our brane. The extra dimension doesn't have the trivial flat topology, though. Instead, it is characterized by the presence of a negative bulk cosmological constant Λ_5, that causes space-time to warp and acquire an ever increasing curvature as we move away from the brane of reference. The bulk space-time, therefore, is an anti-de-Sitter one with ℓ being its curvature radius related to Λ_5 as

$$\Lambda_5 = -\frac{6}{\ell^2}. \tag{1.24}$$

Another important property of the bulk is that Z_2-symmetry applies in it, which means that the space-time looks exactly the same when we move away from the brane by the same distance along the extra dimension, no matter to which direction we do so. The corresponding line-element is

$$ds^2 = e^{-2|y|/\ell}\,\eta_{\mu\nu}\,dx^\mu\,dx^\nu + dy^2, \tag{1.25}$$

with $\eta_{\mu\nu}$ being the Minkowski metric and the Z_2-symmetry being realized by the presence of $|y|$ in the exponent. The term $e^{-2|y|/\ell}$, usually called the "warp factor", stems from the existence of Λ_5 in the bulk and is the reason why gravity remains largely confined near the brane even though gravitons can, in principle, propagate throughout the entire (infinite) extra dimension. The brane per se $(y = 0)$ has a flat Minkowski topology and we ascribe a tension to it, that represents the brane self-gravity.

The RS-I model

The first version of the RS-models is an attempt to give an answer to the notorious hierarchy problem. In this we consider two branes lying at $y = 0$ and $y = L$ as far as their position along the fifth dimension, represented by y, is concerned. Because of Z_2-symmetry it holds that

$$y \leftrightarrow -y \quad \text{and} \quad L + y \leftrightarrow L - y. \tag{1.26}$$

The brane at $y = L$ is characterized as "visible" (or "weak" or "TeV brane"), has a negative tension $-\lambda$ and is supposed to represent our Universe, thus all Standard Model degrees of freedom are expected to be confined on it. The brane at $y = 0$, referred to as "hidden" (or "gravity" or "Planck brane"), has a positive tension λ and
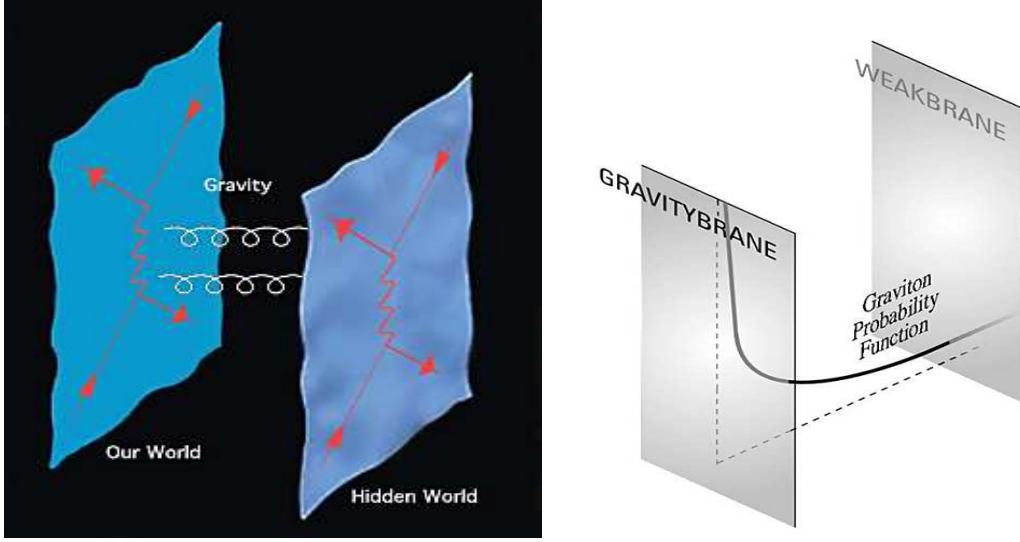
Figure 1.3: Randall - Sundrum two brane model (RS-I) [35, 36].

can only interact with our world through gravity. The tension λ is given by

$$\lambda = \frac{3M_5^2}{4\pi\ell^2},\tag{1.27}$$

where M_5 is the five-dimensional fundamental energy scale. The effective 4-dimensional fundamental scale on the hidden brane is admitted to be the ordinary Planck scale, which is connected to M_5 as

$$M_P^2 = M_5^3\,\ell\left[1 - e^{-2L/\ell}\right].\tag{1.28}$$

This is a very interesting result. It shows that the two scales are only weakly connected and thus, in principle, the size of the extra dimension could be arbitrarily large without any absurdities to occur. Exploiting this feature Randall and Sundrum were able to formulate a quite different and phenomenologically richer version of their model containing only one brane, that we shall present in the following subsection.

When we write down the action for the hidden and the visible brane we find that any energy parameter (masses, couplings, vev) m_0 on the hidden brane will be seen on the visible brane to have the significantly lower value

$$m = e^{-L/\ell}m_0,\tag{1.29}$$

because of the non-trivial warped geometry of the bulk. This inevitable warping effect on everything is the key to address the hierarchy problem in the context of this model.

The idea is that in reality there is no hierarchy problem in the context of the higher-dimensional theory. For an observer at the hidden brane (i.e. at $y = 0$) the the gravity and the electroweak scale are both of the same order. However, for an observer at the visible brane (at $y = L$) the effective electroweak scale (M_{EW}) is exponentially

smaller than the gravity scale, according to eq. (1.29), due to the warping caused by the bulk. Therefore, starting from $M_P \sim 10^{19}$GeV we can produce a $M_{EW} \sim$TeV scale for the "visible" brane by suitably choosing the ratio L/ℓ (a modest value of $L \sim 50\ell$ is sufficient to achieve the desired M_P/M_{EW} ratio). Then, an on-our-brane observer is expected to witness strong gravity phenomena at energies around 1TeV. Furthermore, because the branes are separated by a finite distance, the KK spectrum in this case is expected to be discrete. Nonetheless, at low energies we deal only with the 4-dimensional General Relativity as we know it, since no KK mode gets excited.

Interesting as it may be, the model is characterized by the need for some fine-tuning (equal and opposite brane tensions, suitably chosen L/ℓ ratio) and a (non-existing sofar) satisfactory mechanism, which would stabilize the inter-brane distance, in order to work. In addition, there are many unanswered questions about the interaction between the branes, mainly about the reflection on the visible brane of processes that take place on the hidden one, that, combined with the aforementioned shortcomings of the model, make the latter sound quite unnatural.

The RS-II model

Now we move to explore further the possibilities opened by the aforementioned model by sending the negative tension brane to infinity ($L \to \infty$), while considering that the remaining brane is the one that represents our Universe. The model this way becomes not only simpler and geometrically appealing, but at the same time is proven to provide a framework for AdS/CFT correspondence [38]. Furthermore, because of the warping, the volume outside the brane is not infinite, despite the infinite size of the extra dimension, rather it is of the order of the ℓ parameter. Then, for the 5-dimensional fundamental scale we can write that

$$M_P^2 = M_5^3 \, \ell. \tag{1.30}$$

Even though the hierarchy problem is not fully resolved, since M_5 can only be a few orders of magnitude lower than M_P because of the constraints regarding the value of ℓ, the model has some very interesting merits. The main result in this context is that even though the KK modes have a continuous spectrum, the impact of the $m \neq 0$ modes on the gravitational potential is quite small, because of the warp factor. Furthermore, the massless mode (that can be seen as the massless graviton) "sees" a potential of the form

$$V(y) = \frac{15k^2}{8(k|y| + 1)^2} - \frac{3k}{2}\delta(y), \tag{1.31}$$

where $k \equiv 1/\ell$ (see Fig. 1.4), that forces it to remain localized closely around the brane (thus we can speak about a bound state mode). The result of all these is that the 4-dimensional potential on the brane is written as

$$V(r) \approx \frac{GM}{r}\left(1 + \frac{1}{r^2 k^2}\right). \tag{1.32}$$

The first term (the usual Newtonian potential) is due to the bound state mode and dominates at low energies. The correction term, that reflects the impact of all the other
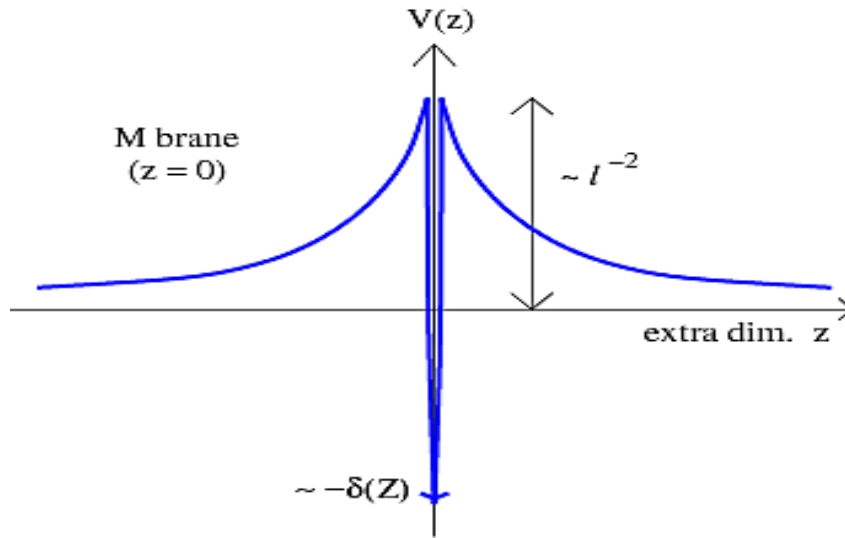
Figure 1.4: The "volcano" potential that causes the localization of the massless graviton in the frame of the RS-II model [37].

KK modes, becomes significant only for $r \to \ell$, so when experiments at appropriate energies would be conducted, the validity of the theory could be directly checked.

It is easy to understand the appeal of the model, when reflecting on the simplicity of the necessary assumptions and the specific predictions it makes. On the other hand, up till now no viable black hole solution in this frame has been found, which is a crucial (theoretical) test for the theory to pass.

1.3 Black hole physics

Black holes are the most extreme, imagination-capturing objects predicted to exist in the frame of General Relativity. Astrophysical black holes are formed as a result of the gravitational collapse of stars of sufficiently large mass[3]. Because of the extremely high contraction forces, the star mass eventually starts to get compressed in an ever decreasing volume. Since no mechanism is known sofar to be able to counterbalance the contraction process in the case of very massive stars, one has to accept that the entire mass gets squeezed inside a pointlike region of space-time. This dimesionless point, then, is admitted to be of infinite density and temperature, causing infinitely strong distortion of space-time around it as well. Because of these extreme properties, these points are characterized as space-time singularities and are considered to lay outside our ability of understanding, at least as long as quantum gravitational laws are yet to be found. What is also really interesting is that General Relativity doesn't introduce some generic lower bound for the actual mass of a black hole. This means

---

[3]The Tolman-Oppenheimer-Volkoff limit, which currently ranges from 1.5 to 3 solar masses as the maximum mass of a stable neutron star, means that a star has be quite more massive than this in order for a black hole to form at the end of its life.
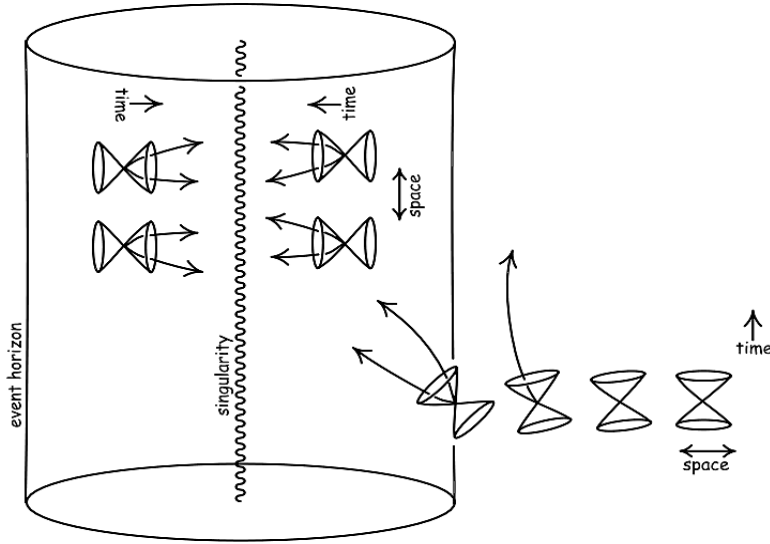
Figure 1.5: Light cones tilting towards the interior of the black hole with respect to the distance from the singularity [39].

that, on one hand, they can grow to become arbitrarily massive by attracting and swallowing matter. On the other hand, given that sufficient energy is available, one could, in principle, create a miniature black hole in ground-based experiments through the collision of highly energetic particles, that would approach each other at a distance smaller than the gravitational radius, which corresponds to the sum of their total energies. Then, instead of getting scattered, the particles would get trapped inside the horizon of the black hole.

The most important feature of black holes is the existence of an event horizon around them. The horizon represents a boundary in space-time beyond which events cannot affect an observer lying outside it. It is quite common to describe the horizon as the boundary, within which the escape velocity is greater than the speed of light, but this description is rather misleading as it fails to draw the attention to the fact that the emergence of such a boundary is due to the distortion of space-time caused by black holes. What actually happens is that, when coming closer to a black hole, the light cone gets tilted towards it and from a point on (the threshold being the event horizon), the cone gets so tilted that all light paths (and hence all possible paths of particles) point to the interior of the black hole (Fig. 1.5). Once a particle crosses the horizon, moving deeper into the black hole is as inevitable as moving forward in time (this is also implied by the change of the signs of the metric components)!

Furthermore, because of the extremely intense gravity close to black holes, gravitational time dilation plays a significant role when approaching the horizon. In other words, a clock near the black hole appears to run more slowly compared with an identical clock away from it. Because of this phenomenon, an object falling into a black hole appears to a distant observer to slow down as it approaches the event horizon, taking an infinite time to reach it. At the same time the observer records the light,

emitted by the object, to become redshifted (gravitational redshift) and dimmer as time elapses. Just before it reaches the event horizon, the falling object becomes so dim (and the radiation coming from it gets infinitely redshifted), that it can not be seen at the end. However, on the other hand, an observer falling into a black hole does not notice any of these effects as he crosses the event horizon. According to his own clock (that measures his proper time), he crosses the event horizon after a finite time without experiencing any absurd phenomena.

Another striking property of black holes is that they can be described by only three independent physical parameters: mass, electric charge and angular momentum. This fact is frequently expressed through the rather picturesque characterization of black holes having no hair. An observer outside a black hole is always able to measure them. Their total mass is calculated on the basis of the ADM technique[4] and/or observations concerning manifestations of their gravitational field such as microlensing effects, orbits of objects around them etc. The angular momentum can be measured from far away based on the frame dragging a spinning black hole causes in its neighborhood and the gravitomagnetic field produced as a consequence of this phenomenon. As for the charge, charged black holes repel and attract electric charges like any other charged object. The simplicity of their description also means that any two black holes that share the same values for these properties are indistinguishable according to classical mechanics, no matter what kind of objects were swallowed by them during their lifetimes. When an object falls into a black hole, any information about its shape or distribution of charge on it is lost to outside observers. The information that is lost includes every quantity that cannot be measured far away from the black hole horizon, including conserved quantum numbers such as the total baryon number and lepton number.

1.3.1 Black hole metrics

It must be clear by now that the main characteristic of black holes is the extreme deformation of space-time they cause. Consequently, their presence and impact can best be depicted by the metric, that describes the space-time geometry around them. The metric should encapsulate the three aforementioned parameters and be able to pass through the Einstein equations that, usually but not necessarily, correspond to an empty (other than the black hole itself) space-time. In what follows we shall present the metrics that represent the three most interesting black hole configurations for our study.

---

[4]The ADM formalism was developed in 1959 by Richard Arnowitt, Stanley Deser and Charles W. Misner [40]. ADM energy is a special way to define the energy in General Relativity, applicable to spacetimes that asymptotically approach a well-defined metric tensor at infinity. Then ADM is defined as a function of the deviation of the metric tensor from its prescribed asymptotic form. In other words, it is computed as the strength of the gravitational field at infinity. If the asymptotic metric is time-independent, thus respects the time-translational symmetry, then by Noether's theorem we infer that ADM energy is conserved.

The Schwarzschild metric

The Schwarzschild metric was discovered by Karl Schwarzschild in 1916 shortly after General Relativity was released [41]. It describes a geometry where an uncharged, non rotating black hole is present in an empty space-time. According to Birkhoff's theorem, the Schwarzschild solution is the most general spherically symmetric, vacuum solution of the Einstein field equations. The corresponding line element is written as

$$ds^2 = -\left(1 - \frac{2GM}{r}\right) dt^2 + \left(1 - \frac{2GM}{r}\right)^{-1} dr^2 + r^2\, d\theta^2 + r^2\, \sin^2\theta\, d\phi^2, \qquad (1.33)$$

where the speed of light was set equal to unity, M is the black hole mass and G is Newton's gravitational constant. The metric appears to have two ill behaved points, since for $r = 0$ the coefficient of dr^2 vanishes, while for $r = 2GM$ it blows up. However, in the second case the singularity is an artifact since it is a result of coordinate choice and doesn't represent a genuine "physical" singularity. This becomes evident when writing the same line element using a different coordinate system, e.g. Eddington-Finkelstein, Lemaître, Kruskal-Szekeres or Gullstrand-Painleve coordinates. Then the metric becomes regular at $r = 2GM$, while the singularity at $r = 0$ remains unaltered. Nevertheless, the value $r = 2GM$ is a special one since it marks the event horizon of the black hole[5]. In order to avoid similar deceptions due to technicalities, we turn to invariant gravitational qualities like R, $R_{\mu\nu}\, R^{\mu\nu}$ and $R_{\mu\nu\rho\sigma}\, R^{\mu\nu\rho\sigma}$. For the metric (1.33) we find that

$$R = 0, \quad R_{\mu\nu}\, R^{\mu\nu} = 0 \ \text{ and } \ R_{\mu\nu\rho\sigma}\, R^{\mu\nu\rho\sigma} = \frac{48G^2M^2}{r^6}, \qquad (1.34)$$

where it is evident that the only problematic point is $r = 0$, that corresponds to the singularity alleged to emerge at the center of the black hole as a result of the unstoppable gravitational collapse of matter. The 4-dimensional Schwarzschild metric (1.33) can easily be generalized to describe a non-rotating, non-charged black hole that lives in a D-dimensional space-time as

$$ds^2 = -\left(1 - \frac{\mu}{r^{d-3}}\right) dt^2 + \left(1 - \frac{\mu}{r^{d-3}}\right)^{-1} dr^2 + r^2 d\Omega_{d-2}^2, \qquad (1.35)$$

where we define the mass parameter μ as

$$\mu = \frac{16\pi\, G\, M}{(d-2)\, A_{d-2}}, \qquad (1.36)$$

with $d\Omega_{d-2}^2$ being the line element of a $(d-2)$-dimensional unit sphere S^{d-2} for which holds that

$$d\Omega_{d-2}^2 = d\theta_{d-3}^2 + \sin^2\theta_{d-3} d\theta_{d-4}^2 + \sin^2\theta_{d-3}\sin^2\theta_{d-4}d\theta_{d-5}^2 + ... + \sin^2\theta_{d-3}...\sin^2\theta_1 d\phi^2, \qquad (1.37)$$

where $0 < \phi < 2\pi$ and $0 < \theta_i < \pi$, while A_{d-2} is the area of that sphere given by $A_{d-2} = 2\pi^{(d-1)/2}/\Gamma[(d-1)/2]$. The metric (1.35) is known as the Schwarzschild-Tangherlini metric [**?**].

---

[5]This comes as no surprise as it is generic that horizons are determined through the values of r that cause the purely radial component g_{rr} to diverge with the event horizon, in particular, corresponding to the largest, positive, real such value.
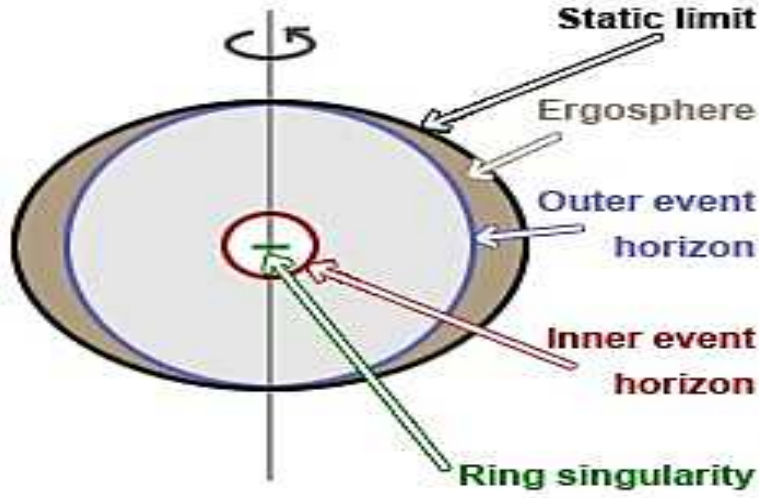
Figure 1.6: The Kerr black-hole structure [43].

The Kerr metric

Interesting and illuminating as it may be, the Schwarzschild metric corresponds to a rather idealized object. Since all objects in Nature from galaxies to subatomic particles appear to have angular momentum, a realistic black hole is expected to rotate in general, thus a metric capable of describing a rotating black hole is utterly necessary. Because Einstein's field equations are non-linear, it is far from trivial to find an exact solution satisfying all of them simultaneously, even when considering highly symmetric configurations. It wasn't until 1963 that Roy Kerr managed to discover a solution for an empty space-time around an axially-symmetric rotating black hole [42] having an event horizon, which is topologically a sphere. The Kerr metric for a black hole of mass M and angular momentum J in Boyer-Lindquist coordinates is then written as

$$ds^2 = -\left(1 - \frac{2M\,r}{\Sigma}\right)dt^2 - \frac{4M\,r\,\alpha\,\sin^2\theta}{\Sigma}\,dt\,d\phi + \frac{\Sigma}{\Delta}\,dr^2 + \Sigma\,d\theta^2 + \frac{A\,\sin^2\theta}{\Sigma}\,d\phi^2, \quad (1.38)$$

where we have introduced for brevity the quantities Σ, α, Δ and A defined as

$$\Sigma \equiv r^2 + \alpha^2\cos^2\theta, \quad \alpha \equiv \frac{J}{M},$$

$$\Delta \equiv r^2 - 2Mr + \alpha^2 \text{ and } A \equiv (r^2 + \alpha^2)^2 - \alpha^2\Delta\sin^2\theta.$$

A very distinctive property of these black holes is that they possess two horizons. These correspond to the values of r that cause the g_{rr} coefficient to diverge, which happens when $\Delta = 0$. From this condition we get two solutions that describe the outer and the inner horizon of the Kerr black hole. The outer one's radius is

$$r_{out} = M + \sqrt{M^2 - \alpha^2}. \quad (1.39)$$
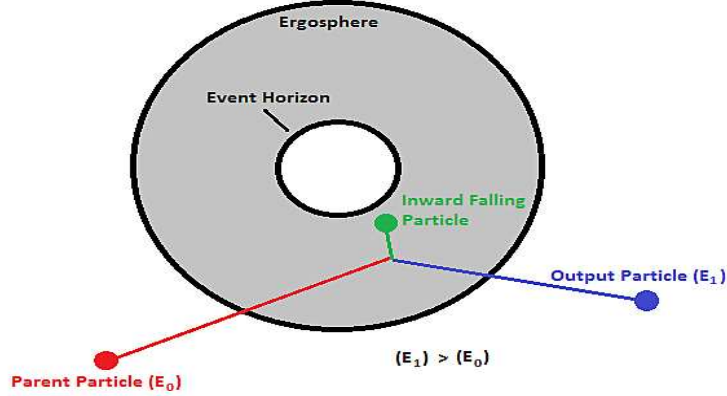
Figure 1.7: The Penrose process that can be used for controlled extraction of energy from a rotating black hole [47].

This spherically symmetric region is the event horizon of the rotating Kerr black hole in complete analogy with the horizon of the static Schwarzschild black hole. After all, the former reduces to the latter in the absence of rotation $\alpha \to 0$. The inner horizon, on the other hand, lies at

$$r_{in} = M - \sqrt{M^2 - \alpha^2}. \tag{1.40}$$

This one is also characterized as a Cauchy horizon, is important as far as the stability of the Kerr black hole is concerned and is invisible to distant observers, since it is inside the event horizon. From (1.39 and 1.40) we also obtain the constraint

$$M^2 \geq \alpha^2, \tag{1.41}$$

for the horizons to form. Another interesting feature of the metric (1.38) becomes evident when $\Sigma = 0$, in which case the g_{rr} component vanishes. This signifies the existence of a singularity, which, interestingly enough, is no longer point-like rather it is ring-shaped.

Finally, we turn our attention to the quantity

$$r_{erg} = M + \sqrt{M^2 - \alpha^2 \cos^2 \theta}. \tag{1.42}$$

This is the value of r for which the g_{tt} component of the metric, that determines the flow of time, vanishes. The meaning of this value is that it represents the boundary between the $r > r_{erg}$ region, where an object can be static (with some effort of course), and the $r_{out} < r < r_{erg}$ region, where it is unavoidable for all bodies to get dragged into rotation, regardless of their speed[6]. In the latter region the deformation of space-time is so strong there that the rotation of the black hole sets in motion the local Lorentz

---

[6]This is the reason why r_{erg} is also characterized as the static limit for the Kerr space-time.

reference frames, dragging them into rotation around its axis (frame-dragging effect)[7], so there is no way for someone to stand still with respect to some distant reference point. Note, however, that even when found at this region, which is called the *ergosphere*, it is still possible, in principle, for a body to escape from the gravitational field of the black hole and reach infinity (this is why r_{erg} is not an event horizon). The static limit lies beyond the event horizon in general and coincides with it only at the poles as shown in Fig. 1.6.

A very interesting consequence of the existence of the ergosphere is the theoretical possibility to extract energy from them (thus slowing them down) in a controlled way through what is known as the Penrose process. We know that, when a particle crosses the static limit, it is forced to rotate faster, because of the frame-dragging effect, and in this way it gains energy at the cost of the overall energy of the black hole. Then, if it escapes from the ergosphere (in the case that it has sufficiently high speed and a proper trajectory for that), it would take the extra energy away. This phenomenon is also called superradiance, in the sense that some objects actually go away from the black hole with energy greater than the one they had, while approaching it. Based on that, Penrose has formulated a Gedankenexperiment [48], which goes like this: A device is sent towards a rotating black hole. Once it enters the ergosphere, it splits into two pieces, by some internal mechanism. The momentum of the pieces can be arranged, in principle, in such a way that one of them escapes to infinity and the other one crosses the event horizon and gets lost into the black hole. Given the right initial conditions, it is possible the total energy of the escaping part to exceed the total energy of the original infalling device (see Fig. 1.7). The overall process results in a decrease in the angular momentum of the black hole with the corresponding rotational kinetic energy being transferred to the escaping body.

The Myers-Perry metric

The higher-dimensional generalization of the Kerr metric was discovered by Myers and Perry in 1986 [49]. Like the Kerr metric, the Myers-Perry metric has spherical horizon topology. The general solution for a D-dimensional black hole with arbitrary angular momentum in each of the $N = \frac{D-1}{2}$ independent rotational planes is

$$ds^2 = -dt^2 + (r^2 + \alpha_i^2)\left(d\mu_i^2 + \mu_i^2 d\phi_i^2\right) + \frac{\Pi F}{\Pi - \mu r^2}dr^2$$

$$+ \frac{\mu r^2}{\Pi F}(dt - \alpha_i \mu_i^2 d\phi_i)^2 \quad \text{for D being odd} \tag{1.43}$$

and

$$ds^2 = -dt^2 + (r^2 + \alpha_i^2)\left(d\mu_i^2 + \mu_i^2 d\phi_i^2\right) + \frac{\Pi F}{\Pi - \mu r}dr^2$$

$$+ \frac{\mu r}{\Pi F}(dt - \alpha_i \mu_i^2 d\phi_i)^2 + r^2 d\alpha^2 \quad \text{for D being even.} \tag{1.44}$$

---

[7]This effect holds also true in the case of weaker gravitational fields, where it is called the Lense-Thirring effect from the physicists first to predict it in 1918 [44, 45] and has been experimentally tested by the Gravity Probe B satellite [46].

In the above expressions summation over $i = 1 \ldots N$ is assumed, μ is the mass parameter defined earlier by (1.36), the parameters α_i are related to the different angular momenta as $J_i = \frac{2M}{D-2}\alpha_i$ and μ_i represent the directional cosines, for which the following conditions hold

$$\sum \mu_i^2 = 1 \text{ (for odd D)} \text{ and } \sum (\mu_i^2 + \alpha^2) = 1 \text{ (for even D).} \tag{1.45}$$

Furthermore, for every value of D we have that

$$F(r, \mu_i) = 1 - \frac{\alpha_i^2 \mu_i^2}{r^2 + \alpha_i^2} \text{ and } \Pi(r) = \prod_{i=1}^{N} (r^2 + \alpha_i^2), \tag{1.46}$$

whereas the horizon area is given by the relation

$$A = \frac{\Omega_{D-2}}{2\kappa} \mu \left(D - 3 - \frac{2\alpha_i^2}{r_0^2 + \alpha_i^2} \right). \tag{1.47}$$

In (1.47) r_0 is the event horizon radius, which we take to be the largest real root of g_{rr}^{-1}, that is

$$\Pi(r_0) - \mu r_0^2 = 0 \text{ (odd D)} \text{ and } \Pi(r_0) - \mu r_0 = 0 \text{ (even D)}, \tag{1.48}$$

while the surface gravity κ is found as

$$\kappa = \lim_{r \to r_0} \frac{\Pi' - 2\mu r}{2\mu r^2} \text{ (odd D)} \text{ and } \kappa = \lim_{r \to r_0} \frac{\Pi' - \mu}{2\mu r} \text{ (even D).} \tag{1.49}$$

The line element gets significantly simplified when considering a higher-dimensional black hole that rotates only in a single plane. Then all α_i parameters but one are set equal to zero and the metric takes the form

$$ds^2 = -dt^2 + \frac{\mu}{r^{D-5}\Sigma}(dt - \alpha \sin^2 \theta d\phi)^2 + \frac{\Sigma}{\Delta}dr^2$$
$$+ \Sigma d\theta^2 + (r^2 + \alpha^2)\sin^2 \theta d\phi^2 + r^2 \cos^2 \theta d\Omega_{D-4}^2, \tag{1.50}$$

where μ is the mass parameter of (1.36), $\alpha = (D-2)J/2M$ and for Σ and Δ we write

$$\Sigma = r^2 + \alpha^2 \cos^2 \theta \text{ and } \Delta = r^2 + \alpha^2 - \frac{\mu}{r^{D-5}}, \tag{1.51}$$

respectively. It is evident that for $D = 4$ we recover the usual Kerr metric.

The special (reduced) version (1.50) of the Myers-Perry metric has another merit apart from its simplicity. In particular, if one takes the rotation axis to be on the brane, then it would represent a higher-dimensional black hole, that we shall observe as rotating with angular momentum J. This is very important, since miniature black holes, that could possibly be created during on-ground experiments through the collision of highly energetic particles, are expected to have a single rotation axis parallel

to our brane[8], while being higher-dimensional objects. Thus, they would be described by the metric (1.50). Based on this metric we can perform an extensive analysis concerning the expected properties of the Hawking emission spectrum of such black holes, that an on-brane observer is expected to record, in relation with the dimensionality of space-time. In fact this is the objective of the work presented in chapter 2, that we shall discuss later on.

1.3.2   Hawking radiation from black holes

More than 30 years ago Hawking proved, using a semiclassical approximation, that black holes radiate because of the inevitable creation of pairs of particles due to quantum energy fluctuations at the vicinity of their horizon. Furthermore, he was able to show that this radiation is exactly thermal, that is no subtle or secret correlations exist between the emitted particles [50, 51].

The procedure may be pictured as follows (see Fig. 1.8). Just outside the event horizon of the black hole pairs of virtual particles are produced due to vacuum fluctuations – in the same way that virtual particle pairs are expected to form and annihilate everywhere. One of the particles has positive while the other has negative energy. The negative energy particle is initially in a (classically) forbidden region, that is our observable Universe, but there is no-zero probability it can tunnel its way to the black hole interior through the event horizon, where the Killing vector for time translations is spacelike. There the particle can exist as real, even though its energy relative to infinity is negative, in the sense of ADM energy (see footnote 4 in sec.1.3). The tunneling probability depends on the surface gravity κ, which shows how fast/easily the time translation Killing vector changes, when going from the one side of the horizon to the other. The other particle of the original pair, becomes also a real particle with positive energy (so there is no problem for it to propagate into our Universe), goes away from the black hole and becomes part of its radiation. In other words, the virtual particles come into (real) existence in the expense of the black hole total energy. The black hole experiences a flux of negative energy towards its interior, that causes its mass to decrease balancing this way the positive energy flux emitted to infinity.

This description of the Hawking mechanism is very useful in order for someone to get the general idea of the process, but one cannot rely on it to perform specific calculations. To do that, one has to go back to the semi-classical approach used by Hawking in [50], which crudely goes as follows: We consider a massless scalar field ϕ at past null infinity $(\mathcal{J}^-)$ living in a flat (Minkowski) space-time, which can be expressed as

$$\phi = \sum_i [f_i \hat{a}_i + \bar{f}_i \hat{a}_i^\dagger], \tag{1.52}$$

---

[8]It is evident that the collision itself can only take place on the brane, on which particles are confined by definition. Furthermore, the fact that the corresponding impact parameter is expected to be non-zero in general means that the particles will be engaged in a rotational move and acquire angular momenta. Because of the conservation of the system's total angular momentum, the latter will inevitably be transferred to the just-produced black hole.
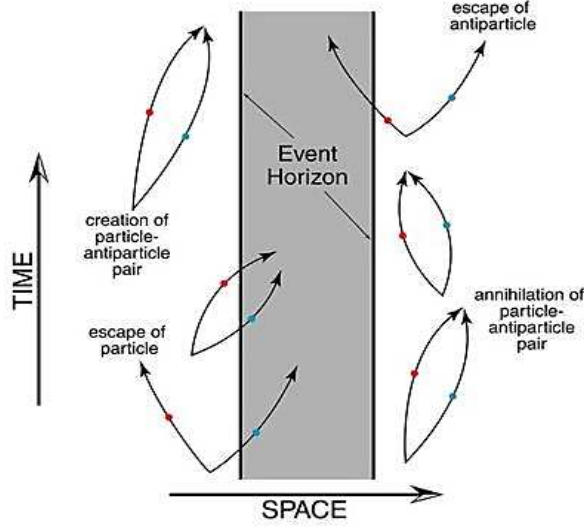
Figure 1.8: Pairs of particles emerging from vacuum fluctuations in the vicinity of the event horizon as the basis for the Hawking radiation emission by the black hole [52].

where f_i is a complete orthonormal family of complex solutions of the wave equation

$$\eta^{ab} f_{i;ab} \eta^{ab} = 0 \qquad (1.53)$$

containing only positive frequencies. Then the operators $\hat{a}_i$ and $\hat{a}_i^\dagger$ are the annihilation and creation operators respectively for the i-th state. The vacuum state is of course the one for which

$$\hat{a}_i \,|\, 0 \rangle = 0 \qquad (1.54)$$

holds. The scalar field is admitted to interact with a black hole, which forms at some point in the future, and, then, an observer at future null infinity ($\mathcal{J}^+$), lying in an asymptotically flat region, tries to describe it much in the same way as in the case of $\mathcal{J}^-$, that is by 1.52. The key remark is that the containing-only-positive-frequencies basis $f_{future\,i}$ for the last observer is different than the respective $f_{past\,i}$ basis the observer at $\mathcal{J}^-$ uses. This happens because the field propagates through a curved space-time region, when close to the black hole, before reaching $\mathcal{J}^+$. Since positive and negative frequencies have no invariant meaning in curved space-time, one cannot in general expect the original frequencies at $\mathcal{J}^-$ to smoothly evolve into the frequencies at $\mathcal{J}^+$ with one-to-one correspondence. All these also mean that the initial vacuum $|\, 0_{past} \rangle$ (defined by the constraint $\hat{a}_{past\,i} \,|\, 0_{past} \rangle = 0$) is different than the final vacuum $|\, 0_{future} \rangle$ (determined naturally by the demand $\hat{a}_{future;i} \,|\, 0_{future} \rangle = 0$) for which also holds that

$$\hat{a}_{past;i} \,|\, 0_{future} \rangle \neq 0. \qquad (1.55)$$

The interpretation of eq. (1.55) is that the gravitational field has provoked the creation of a number of scalar particles and this is the reason why the two vacuum states are not the same. Based on these conceptions, Hawking was able to explicitly show that

black holes radiate like black bodies of specific temperature T directly connected to their surface gravity κ through the relation

$$T = \frac{\kappa}{2\pi}, \tag{1.56}$$

which for the case of Schwarzschild black holes becomes

$$T = \frac{c^3 \hbar}{8\pi k_B G M}. \tag{1.57}$$

Or, in terms of the solar mass $M_\odot$,

$$T = 6.2 \times 10^{-8} \left(\frac{M_\odot}{M} \right) K. \tag{1.58}$$

This approach has the major advantage to be based on the use of well-defined field theoretical methods on Minkowski space-time, since only observers at flat or asymptotically flat regions were considered. Furthermore, the method can safely be considered valid as long as the black hole in question is massive enough to be described by the known metrics and the space-time curvature is not comparable to the Planck value 10^{66}cm^{-2} (fortunately this hold for the vast majority of the black holes). However, there is room for some objections since one could argue that when the scalar field is very near the event horizon, it gets redshifted to arbitrarily large frequencies and so (unknown) trans-Planckian phenomena have also to be considered, which the semiclassical approach simply ignores. Nevertheless, the approach is considered to be valid in general giving the right value for the black hole temperature.

Hawking radiation drew much attention since then as, for the very first time, physicists dealt with a procedure which results from the combination of a purely quantum mechanical process, such as particle creation from vacuum, with the dynamical properties of space-time, that are governed by the laws of General Relativity. Space-time is no longer considered as the passive background where quantum phenomena take place, but, on the contrary, its curvature and the existence of an event horizon are indispensable in order for a black hole to emit particles. Nevertheless, even quantum phenomena must abide by the energy conservation principle. Hence, when Hawking radiation escapes to infinity, we may safely conclude that it will carry energy away from the black hole, which must therefore shrink in mass. As the mass shrinks the surface gravity increases and with it the temperature. This is a self-catalyst process in which the entire mass evaporates away in a finite time. For Schwarzschild black holes this time is calculated to be of the order

$$\tau_{BH} \sim \left(\frac{M}{M_{pl}} \right) t_{pl} \sim \left(\frac{M}{M_\odot} \right)^3 10^{71} \text{sec} \tag{1.59}$$

where $M_{pl} \approx 10^{-5}\text{gr}$ is the Planck mass and $t_{pl} \approx 10^{-43}\text{sec}$ is the Planck time. All these mean that the estimated lifetime of a solar mass Schwarzschild black hole is 10^{53} times larger than the current age of our Universe, whose Hubble time is $t_H = H_0^{-1} \propto 10^{18}\text{sec}$. The duration of the process may seem extremely long for the evaporation of black

holes to have any practical impact on us, but one should notice that the lifetime of low mass black holes is so much shorter that primordial black holes could reach the end of their lives today (in a way that is far from being clear from the theoretical point of view) in front of our telescopes. On the other hand, miniature black holes with mass of few TeV, that could emerge during on-ground experiments should any large dimension scenario [28, 29, 30, 33, 34] hold true, are expected to be extremely short-lived. In any case, since we are talking about the very principles of Physics and the quest for the efficient combination of General Relativity with Quantum Mechanics, no time and/or energy scale can be regarded as extreme enough so as not to be worth considering.

1.3.3   Black hole thermodynamics

The discovery that black holes actually radiate, through the mechanism just analyzed, changed drastically our understanding about their nature. Originally, one expected them only to swallow matter without letting anything escape from their interior. Therefore, they were thought to have a temperature close to (if not exactly) absolute zero. Furthermore, questions regarding the validity of the second law of thermodynamics and the non-decreasing entropy were raised, since it appeared that the (classically expected) behavior of black holes would lead to the decrease of the overall entropy of the Universe. All these issues were put on a completely different basis after the discovery of Hawking radiation. Because of the latter, black holes are now considered to have a non-zero temperature and, consequently, thermodynamical properties. These are determined through a useful analogy between the first law of thermodynamics for ordinary systems and black hole physics.

First we consider an arbitrary black hole of mass M, angular momentum J and electric charge Q. Then its area A, when it reaches an equilibrium and becomes stationary, is given in relation with these parameters as

$$A = 4\pi \left(2M^2 - Q^2 + 2M\sqrt{M^2 - Q^2 - \frac{J^2}{M^2}} \right). \tag{1.60}$$

The internal energies of two stationary black hole with infinitesimal different values for their area (dA), angular momentum (dJ) and charge (dQ) differ by

$$dM = \frac{\kappa}{8\pi}\, dA + \Omega\, dJ + \Phi\, dQ, \tag{1.61}$$

where κ is the surface gravity

$$\kappa = 4\pi\sqrt{M^2 - Q^2 - J^2/M^2}\,/\,A,$$

Ω is the angular velocity

$$\Omega = 4\pi J\,/\,MA$$

and Φ the electric potential

$$\Phi = 4\pi Q(M + \sqrt{M^2 - Q^2 - J^2/M^2})\,/\,A$$
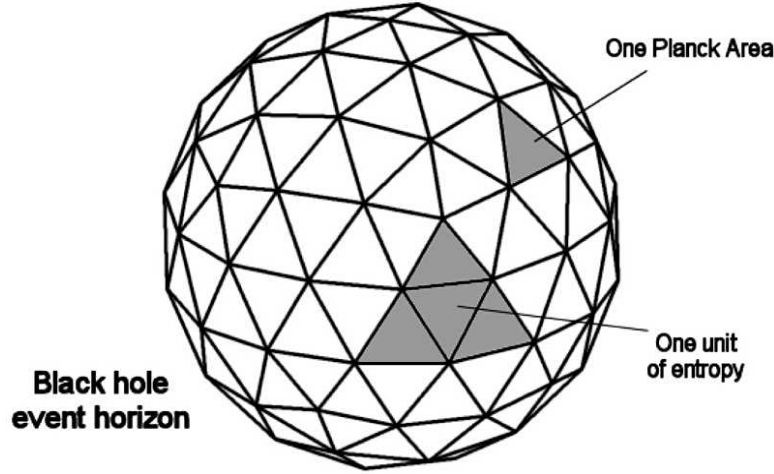
Figure 1.9: Diagrammatic representation of the event horizon as a spherical shell made of Planck-sized patches to emphasize the connection of the black hole entropy to its geometrical properties [53].

of the black holes. Relation (1.61) is in complete analogy with the first law of thermodynamics for an ordinary system, described by the same three properties, for which we write

$$dE = T\,dS + \Omega\,dJ + \Phi\,dQ. \tag{1.62}$$

Then it is quite straightforward[9] to assume that the following expressions hold in the case of black holes

$$E = M \quad \text{(internal energy)} \tag{1.63}$$

$$T_H = \frac{\kappa}{2\pi} \quad \text{(temperature)} \tag{1.64}$$

$$S_{bh} = \frac{A}{4} \quad \text{(entropy)} \tag{1.65}$$

in natural units, where $k_B = c = G = 1$.

Black hole thermodynamics is admitted to be governed by four fundamental laws, formulated by Bardeen, Carter and Hawking back in 1973 [54]. These are:

Zeroth law: The surface gravity κ of a stationary black hole is constant everywhere on the surface of the event horizon.

First law: When a black hole goes from a stationary state to another, its total mass changes by

$$dM = T\,dS + \Omega\,dJ + \Phi\,dQ. \tag{1.66}$$

---

[9]Actually based only on the analogy between 1.61 and 1.62 we cannot infer the exact expressions for T and S. The correct relation for T is provided through the study of particle creation (see sec.1.3.2). Then based on the aforementioned analogy we find a function for the entropy.

Second law: In any classical process, the area of the black hole and, hence its entropy S_{bh}, do not decrease:

$$\Delta S_{bh} \geq 0. \tag{1.67}$$

Third law: It is impossible by any procedure, no matter how idealized, to reduce the black hole temperature to zero by a finite sequence of operations.

Finally, in order to address issues concerning information, entropy and Hawking's area theorem, Bekenstein suggested [26, 55, 56] a generalized version of the second law of thermodynamics, namely:

Generalized Second Law: In any physical process, where a system that involves black holes is considered, the generalized entropy of it $\widetilde{S}$ does not decrease, i.e.

$$\Delta \widetilde{S} = \Delta S_{bh} + \Delta S_m \geq 0, \tag{1.68}$$

where S_{bh} is the entropy of the black holes and S_m is the entropy corresponding to the matter outside the black holes. The fact that the generalized second law includes, on an equal footing, the seemingly very different quantities S_m (which characterizes the "degree of chaos" in the structure of the physical matter) and S_{bh} (which is connected to a geometric characteristic of the black hole) is an indication of their profound similarity. In fact, the very possibility of this relation is rooted in Einstein's equations, which relate the physical characteristics of matter with geometric features of space-time [**?**].

1.3.4 Information paradox

The evaporation, that comes as a result of the emission of Hawking radiation, posed an unexpected question. Initially, the interior of black holes used to be considered as causally disconnected from the rest of the universe, so any kind of information, that gets inside a black hole, was believed to remain eternally trapped in it and, consequently, no physical or philosophical problems occurred. This not being the case, since black holes radiate, some amount of information eventually returns back to our universe. The major question, accompanying this observation, is whether, during the formation/evaporation process of a black hole, information is preserved or gets partially destroyed. Every scientist, that concerns him/herself with this issue, before anything else, always bumps into the question whether information is actually preserved or destroyed. Whatever the answer, the effort to support it gives rise to new questions and challenges. If information is conserved, then one should propose or invent some kind of a mechanism, which ensures this. Bearing in mind that we lose track of some amount of information in every ordinary process, why should black holes preserve it in the first place? If, on the other hand, one accepts the possibility that information can be destroyed, questions about when and why this happens should be addressed. Being it the case, what makes a black hole to abstain from destroying the whole of it and lose even its classical hair? And for the whole matter to get more complicated, unitarity, a key demand of Quantum Theory, appears to be violated in the context of the formation and evaporation of black holes since particles in pure state, that get absorbed by them, end up in mixed state as parts of Hawking radiation.

The "loss of history" issue

All these questions outline the celebrated information loss problem, which has been tantalizing physicists for more that three decades. This problem actually consists of two somehow different, but closely related, issues. The first one could be described as "loss of history" meaning that two black holes of the same mass, charge and angular momentum radiate exactly the same way, even though they probably have absorbed different objects during their lifetime. Therefore, we lose knowledge about the specific properties of whatever goes down a black hole apart from the three parameters mentioned above.

There are numerous papers, where theories about possible preservation mechanisms are presented by several scientists, since most of the physicists find the idea of information destruction and the subsequent breakdown of predictability to be unpalatable. The most significant ones have to do with the invention of some mechanism through which an enormous amount of information can either be encoded in Hawking radiation [57, 58, 59, 60, 61, 62] or is forced to remain trapped in the inaccessible interior of a black hole remnant [63]. Both of them, though, are still far from being considered as complete solution to the problem, since they have serious drawbacks. The existence of complicated but subtle correlations in the spectrum of Hawking radiation - possible as it may seem, meaning, of course, that the latter is nearly and not exactly thermal - constitutes a deviation from our present knowledge that also has to be explained. Furthermore, for the equilibrium between ingoing and outgoing information to hold, Hawking radiation should carry a really huge amount of all kinds of information and it is quite hard for one to see how this could be realized by these alleged correlations that, in any case, are assumed to be very feeble (for a convincing presentation of the arguments undermining the validity of such a solution see [64] and for a proposed way out see [65]). As far as black hole remnants are concerned, their existence is even more problematic as their abundance and total mass are calculated to be so large, that their gravitational impact on the known universe should have already been detected. Not to mention that only vague assumptions can be made about what kind of mechanism can stop the evaporation and save black holes from extinction by creating an extremely stable and long-lived remnant, that is left behind at the end [66, 67].

Quite a few other theories have been proposed over the years to address the problem, where information comes out massively once the black hole reaches the Planck size when the semiclassical approximation is no longer trustworthy [68], escapes into a baby-universe [69], is conserved in space-times of $1+1$ dimensions [70, 71], remains trapped inside the infinitely large interior of cornucopions (a variation of remnants) [72, 73, 74, 75], is stored in a topologically disconnected from our Universe region, created inside the black hole due to a topological change process that the horizon undergoes spontaneously, the latter being a fuzzy sphere in the first place [76] etc. Despite any virtues they may have, these theories suffer from very serious defects that make them least viable (see for example [77] for an extensive and thorough presentation and analysis of various theories both mainstream and exotic ones, and also [78]).

Significantly fewer papers appear in the literature to support the possibility of information destruction [77, 79], since the issue is not whether it can get lost for all

practical purposes, but if it can be destroyed in a way that is irreversible in principle. Most physicists seem reluctant to defend such a prospect, as one would have to answer why and how this could happen and what are the limitations of this procedure. Nevertheless, our present knowledge implies that this is probably the case even if this means that we should alter or expand some of our ideas concerning how nature works.

The unitarity violation issue

The second issue has to do with the apparent non-unitary evolution of particles that black holes seem to evoke, as stated earlier. More specifically, on the one hand one expects that particles, which get absorbed by the black hole during its lifetime, are in pure state (at least some of them, if not all). On the other hand, Hawking radiation has been calculated to be thermal [50, 51], that is black holes radiate like black bodies of temperature T, which means that all emitted particles are in mixed state and no correlations exist between them. All these lead us inevitably to the conclusion that particles originally in pure state end up in mixed state and, as a result of this evolution, a certain amount of information about the system gets lost in an irreversible way so it can never be recovered by any means. However, such an evolution is not predicted in the context of quantum physics. On the contrary, unitarity preservation, demanded by Quantum Theory, requires such a case never to occur!

Encountering the whole thing as a peculiar case of scattering, Hawking speculated that one could define an S-matrix capable of describing the process, which he named superscattering $ - matrix [79, 80]. This matrix, however, should be a very special one since it would cause the conversion of an ingoing particle in a pure state to an outgoing particle in mixed state and, therefore, it would be a non-unitary operator. For a matrix like this to be allowed to exist, we should change our view of quantum theory by introducing some new conjectures. However, such assumptions seem to create more problems than they solve and has been shown by the work of Banks, Susskind et al. [81] and Ellis, Hagelin et al. [82] that this cannot be the case.

As far as we know, unitarity violation that seems to occur during the formation and the evaporation of black holes, still remains an open issue whose answer is hoped to be found some time in the future, after scientists have discovered and understood the nature and the properties of the laws governing quantum gravity.

1.3.5   Higher-dimensional black holes

There is an outstanding and very interesting fact about the 4-dimensional black hole solutions. A series of theorems ensures that every static, uncharged black hole in 4 dimensions would be a Schwarzschild one (while Reissner-Nordström if charged), whereas a rotating, uncharged black hole would only be described by the Kerr metric (the Kerr-Newman if charged). These uniqueness theorems, though, do not apply, when considering space-times with more than 4 dimensions. This means that, in principle, the Schwarzschild-Tangherlini metric (as generalization of the Schwarzschild solution) given by (1.35) and the Myers-Perry metric (as generalization of the Kerr solution) given by (1.43 and 1.44) are not the only possible black hole solutions in

$(D > 4)$-dimensions. In fact, Emparan and Reall have found a black ring solution of the gravitational field equations in five dimensions (which got this name because of the $S^1 \times S^2$ topology of its event horizon) [83]. Gravity, therefore, appears to be richer in the presence of extra dimensions.

Apart from the additional freedom concerning the black hole topology, the existence of extra dimensions has also significant consequences regarding the strength of gravity itself and the energy scale needed for black hole formation, as analyzed earlier in sec. 1.2. In this context the fundamental energy scale (M_D) drops by several orders of magnitude from the usual $M_P \sim 10^{19}$GeV value, that holds for 4-dimensions. Since the gravitational constant is in general reversely proportional to the fundamental energy scale, we expect the higher-dimensional one (G_D) to be larger than the 4-dimensional Newton's constant. Even more, when considering phenomena that take place in the regime $r \ll L$, L being the characteristic size of the extra dimensions, Newton's inverse square law for gravitational interactions is also modified to become $\sim 1/r^{D-2}$, as we show in sec. 1.2. Thus, it is expected to be much easier for a black hole to form in this case. Note, however, that in the case where the horizon radius r_h is much larger than L, the produced black holes are effectively four-dimensional objects. If, on the other hand, $r_h \ll L$ then the extra dimensions "open up" for this small black hole, which is to be treated as a higher-dimensional object completely submerged into the extra-dimensional space-time. These black holes have significantly modified properties compared to a four-dimensional black hole with exactly the same mass M. They are larger, colder and, consequently, live longer compared to the latter.

To get an idea about the modifications caused we consider the case of a spherically symmetric (aka non-rotating), small enough black hole, for $r_h \ll L$ to hold, living in a space-time of $D = 4 + n$ dimensions. The corresponding metric is the Schwarzschild-Tangherlini one given by eq. (1.35). The horizon radius and the black hole mass M are related then as

$$r_h = \frac{1}{\sqrt{\pi} M_{4+n}} \left(\frac{M}{M_{4+n}} \right)^{\frac{1}{n+1}} \left(\frac{8\Gamma\left[\frac{n+3}{2}\right]}{n+2} \right)^{\frac{1}{n+1}} . \tag{1.69}$$

It is clear that, for $n \neq 0$, the relation between r_h and M is no longer linear. Furthermore, it is the new fundamental Planck scale M_* that appears in eq. (1.69), rather than the four-dimensional M_P, and this is the reason why these higher-dimensional black holes are larger and easier to create than the 4-dimensional ones. Assuming that $M_{4+n} = 1$ TeV and $M = 5$ TeV[10] we find the following values for the horizon radius with respect to n (Table 1.1).

The temperature of these black holes is given by [84]

$$T_H = \frac{(n+1)}{4\pi \, r_h} . \tag{1.70}$$

---

[10]M_{4+n} is chosen to be of order ~ 1 TeV because this is the energy regime our current experiments (namely the LHC) can explore, so that the results of our calculations would be falsifiable by potential observations. On the other hand, the black hole mass M is deliberately chosen to be a few times larger in order to be able to ignore quantum corrections. A mass of 5TeV makes it safe to use semi-classical methods for the study of the produced black holes [85].

n	1	2	3	4	5	6	7
r_h (10^{-4} fm)	4.06	2.63	2.22	2.07	2.00	1.99	1.99

Table 1.1: Horizon radii for a Schwarzschild-Tangherlini black hole for different values of the n parameter [84].

Using the values for r_h from Table 1.1 we can calculate the temperature of the produced higher-dimensional black hole (assuming again $M_{4+n} = 1$ TeV and $M = 5$ TeV) for different values of n, that we present in Table 1.2.

n	1	2	3	4	5	6	7
T_H (GeV)	77	179	282	379	470	553	629

Table 1.2: Expected temperature for Schwarzschild-Tangherlini black holes for different values of the n parameter [84].

Because of the radiation emission, they must decay and gradually evaporate. Their lifetime τ is calculated to be [84]

$$\tau \sim \frac{1}{M_{4+n}} \left(\frac{M}{M_{4+n}} \right)^{\frac{n+3}{n+1}} . \tag{1.71}$$

The values for τ are more or less of the same order (10^{-26}sec) for black hole masses in the area of few TeV and do not get significantly affected by the value of the n parameter.

With the expected temperature in the GeV regime and a lifetime within our current measuring abilities, Hawking radiation emission by this black hole type should be easily detected and recorded with great accuracy and detail. Actually, miniature higher-dimensional black holes are ideal objects from the observational point of view. The four-dimensional ones, on the contrary, pose great difficulties to any observation attempt. Astrophysical black holes have an ultra low temperature (for example a black hole with $M = 3M_\odot$ has a temperature $T_H \sim 20$ nK), which makes their emission spectrum virtually undetectable[11]. In addition, their lifetime is calculated to be much larger than the age of the Universe, therefore substantial changes in their properties due to Hawking radiation are expected to occur at time scales, that far exceed human measures. On the other hand, 4-dimensional black holes with mass of M_P would have a temperature approximately 26 orders of magnitude greater than the entries in Table 1.2. Thus, their lifetime would be of the order of Planck time ($t_P \sim 10^{-43}$sec), so no reliable measurements could be performed, if any measurement at all is possible, before they disappear.

---

[11]Since the temperature of the Cosmic Microwave Background is $T_{CMB} = 2.73$ K, this kind of ultra cold black holes actually absorb energy from their environment rather than emitting and, thus, no radiation signals coming from them can be recorded.

Higher-dimensional black holes emit Hawking radiation both in the bulk and on the brane. Of course, since only gravitons and (possibly) scalars are allowed to propagate into the bulk, these are the only degrees of freedom that can actually be emitted there. The on-brane emission is much richer and includes zero-mode scalars, fermions, gauge bosons and zero-mode gravitons as potential energy carriers away from the black hole. Brane-localized particles are the only ones that can be detected and studied, while the energy emission in the bulk would appear as "missing" energy, when considering the complete radiation spectrum of a black hole of specific mass, charge and angular momentum. The balance between the energy flux on the brane and the one towards the bulk is a very important feature of the spectrum. Depending on the number and the nature (e.g. flat or warped) of the extra dimensions this balance is modified, therefore, when determined (by the comparison of experimental results with the theoretically expected behavior) it would give direct evidence on the existence of the former.

To sum up, higher-dimensional black holes are easier to create, have a modest temperature, live long enough to be studied and are an excellent probe of the existence of extra spatial dimensions since their (observable) on-brane behavior is directly connected to the overall space-time geometry. No wonder, then, that their physics constitutes a very exciting and still active research area, which drew much attention during the last decade.

Chapter 2

Studying the Hawking radiation spectrum of higher-dimensional rotating black holes

It has been more than a decade since the introduction of the new theories postulating the existence of additional spacelike dimensions in nature. The large extra dimensions [28, 29, 30] and warped extra dimensions scenarios [33, 34] (that were presented in detail in Section 1.2 of the general introduction) have led to an intense research activity of the theoretical as well as the phenomenological consequences of that existence. The introduction of a new, significantly lower than the familiar four-dimensional Planck scale M_P, fundamental energy scale M_* for gravity (from now on we shall denote the higher-dimensional gravity scale as M_* rather than M_{4+n}) has created the expectation that the elusive quantum theory of gravity might manifest itself soon during high-energy particle collisions at ground-based accelerators. The products of these collisions will inevitably be manifestations of a strong gravity theory. One such strong-gravity effect could be the creation of higher-dimensional miniature black holes during the collision of ordinary Standard-Model particles localized on our brane – a (3+1)-dimensional hypersurface embedded in the $(4 + n)$-dimensional space-time, the bulk [86, 87, 88, 89, 90, 91, 92, 93, 94, 95, 96, 97].

These black holes would be rather elusive, extremely short-lived objects. Due to their small size, they will have a high temperature and will evaporate very quickly via Hawking radiation [50], i.e. the emission of ordinary particles with a thermal spectrum [84, 98, 99, 191, 100, 101, 102, 103, 105, 106, 192, 104]. Nevertheless they will be created and decay in a controlled environment and in front of our detectors, with the emission of Hawking radiation [50] being the main observable signature of their creation and, at the same time, a manifestation of the existence of additional spacelike dimensions in nature in the absence of which the creation of the former would not be possible.

It was only natural then, that the possibility of observing in the near future quantum-gravity effects has excited a lot of interest among high-energy physicists, both theorists and experimentalists, in the study of the radiation emission spectra from a higher-dimensional black hole in recent years (for some reviews, see [84, 98, 99, 100, 101, 102, 103, 104, 105, 106, 107]). As a result, the study of the emission of radi-

ation by higher-dimensional black holes has been the subject of an intensive research activity over the last years where the emission of zero and non-zero spin fields from both spherically-symmetric [113, 114, 115, 116, 117, 118, 119, 120, 121, 122, 123, 124, 125, 126, 127, 128, 129, 130, 131, 132] and rotating [119, 120, 121, 122, 123, 124, 133, 134, 135, 136, 137, 138, 141, 142, 143, 144, 145, 152, 151, 19, 178] black holes has been considered.

As we understand it today, black holes pass consequently through the *balding* [108, 109, 110, 111, 112], *spin-down*, and *Schwarzschild* phases [84, 98, 99, 100, 101, 102, 103, 104, 105, 106, 107] before reaching the so-called *Planck* phase. During the balding phase black holes radiate away all possible multipoles so that at the end of this phase they are left having only mass, charge and angular momentum (no hair then!). In addition, gravitational waves are expected also to be emitted throughout this period before the black hole settles down to the spin-down phase. During the latter, they emit preferably degrees of freedom that allow them to shed all their charge and angular momentum. Then we are left with a uncharged, non-rotating spherically-symmetric Schwarzschild (or Schwarzschild-like in the case of higher-dimensional space-times) black hole, which continues to shrink due to the Hawking mechanism until its temperature becomes comparable to the Planck scale. Then it enters the Planck phase, where ill-understood quantum-gravitational phenomena dominate, making any prediction about the evolution of this final stage at least precarious.

The emission of Hawking radiation is anticipated to take place during the two intermediate phases in the life of the black hole, the spin-down and the Schwarzschild phase. In the early days, the Schwarzschild phase was considered to be the longest and thus the most important. It was also the one with the simplest metric tensor describing the space-time around it, and therefore the first one to be exhaustively studied both analytically [113, 114, 193] and numerically [113, 114, 115, 116, 117, 118, 119, 120, 121, 122, 123, 124, 125, 126, 127, 128, 129, 130, 131, 132]. The results derived showed a strong dependence of the emission rates of all types of Standard Model particles on the brane on the number of spacelike dimensions existing transversely to the brane [1].

However, the most generic type of a black hole produced by the collision of two particles with a nonzero impact parameter is a rotating black hole. As a result, the interest was eventually turned to the study of the axially symmetric *spin-down* phase [119, 120, 121, 122, 123, 124, 133, 134, 135, 136, 137, 138, 141, 142, 143, 144, 145, 146] that was initially considered to be significantly shorter than and preceding the Schwarzschild phase. Moreover, a recent Monte Carlo simulation [147] (see also [148]) that has included the effect of rotation of the black hole, has found that the "spin-down" phase is not as short-lived as it was thought and that a separate Schwarzschild phase with no angular momentum might not exist at all.

The study of the spin-down phase is important for an additional reason: the question of the energy balance [149] between the "bulk" and "brane" channel during the Hawking radiation has not been answered yet. Studies of the Schwarzschild phase

---

[1] Variants of the spherically-symmetric Schwarzschild phase, where a cosmological constant [125] or the higher-curvature Gauss-Bonnet term [117] were introduced, were also studied with the spectrum exhibiting a dependence also on parameters related to these terms. In addition, the Schwarzschild phase of quantum-corrected black holes has been studied in [194].

[115, 116, 117, 118, 126, 127, 128, 129, 130, 131, 132] that included the emission of both scalar fields and gravitons have revealed that the brane channel is in most cases the dominant one, although at certain circumstances the bulk channel can be equally important at specific particle channels. Similar studies have also been performed in more recent years [119, 120, 121, 122, 123, 124, 152, 153, 154] for the emission of scalar fields during the spin-down phase, with the dominance of the brane channel still persisting.

One was thus led to hope that by detecting and studying the emission of Hawking radiation could not only shed light on aspects arising from the interplay between classical gravity and quantum physics but also give a quantitative answer to a century-old fundamental question, that of the dimensionality of space-time. To achieve this goal it is absolutely necessary to acquire a clear picture about what exactly should one expect to measure concerning the brane and bulk emission of miniature black holes (the latter would be "seen" as missing energy since we can conduct only on-brane experiments). Then by comparison of our models with potential experimental data we could end up with some safe conclusion.

2.1 Theoretical framework

In the work presented in this chapter, we will consider the case of a higher-dimensional, neutral, simply rotating black hole whose gravitational background is described by the following form of the Myers-Perry solution [49] as analyzed earlier in sec.1.3.1

$$ds^2 = -\left(1 - \frac{\mu}{\Sigma \, r^{n-1}}\right) dt^2 - \frac{2a\mu \sin^2 \theta}{\Sigma \, r^{n-1}} \, dt \, d\varphi + \frac{\Sigma}{\Delta} \, dr^2 + \Sigma \, d\theta^2$$

$$+ \left(r^2 + a^2 + \frac{a^2 \mu \sin^2 \theta}{\Sigma \, r^{n-1}}\right) \sin^2 \theta \, d\varphi^2 + r^2 \cos^2 \theta \, d\Omega_n^2, \qquad (2.1)$$

where

$$\Delta = r^2 + a^2 - \frac{\mu}{r^{n-1}}, \qquad \Sigma = r^2 + a^2 \cos^2 \theta, \qquad (2.2)$$

and $d\Omega_n^2(\theta_1, \theta_2, \ldots, \theta_{n-1}, \phi)$ is the line-element on a unit n-sphere. The above line-element is expected to describe black holes created by an on-brane collision of particles that acquire only one non-zero angular momentum component, parallel to our brane, since the colliding particles have a nonzero impact parameter only along the usual 3-space. As mentioned earlier, it is exactly this kind of black holes that would allow us to study the space-time properties in a direct way. The black hole's mass M and angular momentum J are then related to the parameters μ and a, respectively, as follows

$$M = \frac{(n+2)A_{n+2}}{16\pi G_D} \, \mu, \qquad J = \frac{2}{n+2} \, M \, a, \qquad (2.3)$$

with G_D being the $(4+n)$-dimensional Newton's constant, and A_{n+2} the area of a $(n+2)$-dimensional unit sphere given by

$$A_{n+2} = \frac{2\pi^{(n+3)/2}}{\Gamma\left(\frac{(n+3)}{2}\right)}. \qquad (2.4)$$

The black hole's horizon radius r_h follows from the equation $\Delta(r_h) = 0$, and may be written as

$$r_h^{n+1} = \frac{\mu}{1 + a_*^2},$$

(2.5)

where $a_* = a/r_h$. Furthermore, its temperature T_H is given by the expression

$$T_H = \frac{(n+1) + (n-1)a_*^2}{4\pi(1 + a_*^2)r_h}.$$

(2.6)

This metric apart from being the most reasonable choice, as just explained, carries a very important property for our goal to study higher-dimensional space-times. It has an explicit dependence on the number of extra spacelike dimensions, that is the value of the parameter n, which holds also in the case where one uses its reduced form, that describes our (3+1)-dimensional brane. This means that even though we can only conduct experiments on our 3-brane, these experiments can give us conclusive results, under some conditions, about the existence of extra dimensions, since we base our analysis on a metric that contains information about the total number of space-time dimensions, even if we cannot directly "see" them.

What we do, in short, is to determine the energy emission rate an observer is anticipated to measure, when witnessing the evaporation process of a black hole, with respect to the properties of the black hole and the space-time geometry. The differential emission rate for the energy is given in general by the relation

$$\frac{d^2E}{d\omega dt} = \frac{1}{2\pi} \sum_{j,\ell,m} \frac{\omega}{e^{\tilde{\omega}/T_H} - 1} N_\ell |\mathcal{A}_{j\ell m}|^2,$$

(2.7)

where ω and $\tilde{\omega}$ are parameters connected to the energy of the emitted particle, that will be analyzed in detail in the following sections, and T_H is the black hole temperature of eq. (2.6). In this relation N_ℓ denotes the multiplicity of particle modes emitted by the black hole every time, that is the number of different modes that have the same angular momentum quantum number ℓ. The term $\mathcal{A}_{j\ell m}$ is called the graybody factor and represents the fact that, even though black holes radiate like perfect black bodies, a distant observer will see a quite different picture. Because of the non-trivial topology of the region around the black hole (outside the event horizon, of course) a significant percentage of the emitted degrees of freedom fails to escape the gravitational attraction of the black hole and gets drawn back into the latter, while the more energetic part of the emitted radiation faces no such problems. Therefore, observers away from the black hole will ascribe to it an energy dispersion profile that resembles the one of black bodies, but at the same time can substantially deviate from that picture. This is encapsulated in the use of the term "gray-body radiation spectrum" one uses to characterize what the distant observer encounters, with the parameter $\mathcal{A}_{j\ell m}$ to be the one that deforms the black-body spectrum, originally emitted by the black hole, to become a gray-body type one. Note that the number of extra dimensions affects the values of the temperature, the multiplicity and the graybody factor. Further down, we will explicitly show how these parameters can be determined in the context of the specific cases considered.

In this chapter we will examine in detail the properties of the Hawking radiation spectrum in three different cases. First, we will focus on the emission of tensor-type gravitons by a higher-dimensional simply rotating black hole. Then we will present our work concerning the emission of massive scalars by the same object. Finally, we shall focus on the possibility to derive useful information by studying the angular profile of the fermion and boson emission spectra in the aforementioned space-time background.

2.2   Emission of tensor-type gravitons in the bulk

In order to give a final answer to the question of which exactly is the energy balance between the brane and the bulk emission by a higher-dimensional rotating black hole, we also need to include in our calculations the emission of gravitons during its spin-down phase. Until recently, the field equations of gravitational perturbations in a higher-dimensional, axially symmetric black-hole background were not known. Even today, we have at our disposal the field equations of specific gravitational modes in certain classes of axially symmetric gravitational backgrounds. The perturbation equations for tensorlike gravitational modes in the case of a higher-dimensional rotating black hole with $D \geq 7$ and equal angular-momentum components was derived in [155]. Later on, the corresponding equations for tensor-type gravitons for higher-dimensional black holes with one angular-momentum component and $D \geq 7$ were also derived following a different approach [156]. Then the stability and quasinormal modes of the considered tensor-type gravitational perturbations were investigated in [157]. Recently, in [158] perturbation equations were derived for particular scalar, vector and tensor-type gravitational modes for a five-dimensional rotating black hole with two equal angular-momentum components.

Here we present a study concerning the emission of Hawking radiation in the bulk in the form of tensor-type gravitational modes by a higher-dimensional black hole with one angular-momentum component. As just mentioned, the perturbation equations for gravitons in a higher-dimensional, rotating black-hole background have been derived in a limited number of cases. The geometrical background will be the one considered in [156] and we will therefore demand the existence of at least three additional spacelike dimensions. The line element of the higher-dimensional gravitational background is of the form

$$ds^2 = G_{MN}\, dz^M\, dz^N = g_{ab}\, dx^a\, dx^b + S^2(x)\, d\Omega_n^2, \qquad (2.8)$$

where $\{a, b\} = (0, 1, 2, 3)$ and $d\Omega_n^2$ stands for the line-element of an n-dimensional unit sphere S^n. The above line-element is a special $(4 + n)$-dimensional case of a more general class of gravitational backgrounds where the spacetime can be written as the warped product of an m-dimensional spacetime $\mathcal{N}$ and an n-dimensional space $\mathcal{K}$ of constant curvature [159, 160]. In these type of backgrounds, gravitational perturbations can be classified into tensor, vector and scalar types according to their transformation properties as tensors on the constant-curvature spacetime $\mathcal{K}$. It was this property that allowed for the derivation of perturbation equations for all types of gravitational modes

in the case of a maximally symmetric higher-dimensional black-hole background [161] where $m = 2$ and $\mathcal{K} = S^n$.

The Myers-Perry solution [49] that describes a D-dimensional black hole with $N = [(D-1)/2]$ independent angular-momentum parameters does not, in general, belong to the aforementioned class of line-elements. However, the line-element of a simply rotating black hole (2.1) constitutes a special case of the class of backgrounds considered in [159, 160], and more specifically of the class described by eq. (2.8) with $S(x) = r \cos \theta$. As first stated in [156] and later demonstrated in more detail in [162], the tensor-type gravitational perturbations for the line-element (2.1) – which exist only for $n \geq 3$, or $D \geq 7$ [156] – can be expanded in terms of a basis of transverse and traceless harmonic tensors $\mathbb{T}_{ij}^{(\ell,\alpha)}$ on the unit sphere S^n as follows:

$$\delta G_{ij} = 2S^2(x) \sum_{\ell,\alpha} H_T^{(\ell,\alpha)}(x) \, \mathbb{T}_{ij}^{(\ell,\alpha)}(y) \,, \tag{2.9}$$

where $\{i,j\}$ refer to the y coordinates along the sphere S^n, and $\mathbb{T}_{ij}^{(\ell,\alpha)}$ satisfy the eigenvalue equation

$$[\hat{\Delta} + \ell(\ell + n - 1) - 2] \, \mathbb{T}_{ij}^{(\ell,\alpha)} = 0. \tag{2.10}$$

In the above, $\hat{\Delta}$ is the Laplace-Beltrami operator on S^n, and $\ell = 2, 3, 4, \ldots$ an integer number that labels the corresponding eigenvalues. Finally, α is a label to distinguish harmonic tensors with the same eigenvalue.

Under the expansion (2.9), the (i,j) component of Einstein's equation in vacuum leads to the following second-order hyperbolic equation for the amplitude $H_T^{(\ell,\alpha)}(x)$ [162]

$$-\Box H_T - \frac{n}{r \cos \theta} \, g^{ab} \, \partial_a(r \cos \theta) \, \partial_b H_T + \frac{\ell(\ell + n - 1)}{r^2 \cos^2 \theta} \, H_T = 0, \tag{2.11}$$

where $\Box$ is the d'Alembertian operator for the metric $g_{ab}(x)$, and where, for simplicity, we have omitted the labels $\{\ell, \alpha\}$. Under the further factorization

$$H_T(x) = e^{-i\omega t} \, e^{im\varphi} \, R(r) \, Q(\theta) \tag{2.12}$$

the above partial differential equation reduces to a set of radial and angular equation, namely,

$$\frac{1}{r^n} \, \partial_r \left(r^n \Delta \, \partial_r R \right) + \left(\frac{K^2}{\Delta} - \frac{\ell(\ell + n - 1)a^2}{r^2} - \Lambda_{j\ell m} \right) R = 0 \,, \tag{2.13}$$

$$\frac{1}{\sin \theta \cos^n \theta} \, \partial_\theta \left(\sin \theta \cos^n \theta \, \partial_\theta Q \right)$$

$$+ \left(\omega^2 a^2 \cos^2 \theta - \frac{m^2}{\sin^2 \theta} - \frac{\ell(\ell + n - 1)}{\cos^2 \theta} + E_{j\ell m} \right) Q = 0 \,. \tag{2.14}$$

In the above, we have used the definitions

$$K = (r^2 + a^2) \, \omega - am \,, \qquad \Lambda_{j\ell m} = E_{j\ell m} + a^2\omega^2 - 2am\omega \,, \tag{2.15}$$

with $E_{j\ell m}$ being the separation constant of the two equations, and j a new quantum number that labels the eigenvalues of the angular function $Q(\theta)$.

In order to obtain the complete solution for the wave function of the tensor-type gravitational perturbations of the background (2.1) one needs to solve the above set of second-order ordinary differential equations (2.13)-(2.14) for R and Q. The same is, in principle, necessary for the computation of the energy emission rate for Hawking radiation in the form of tensor-type gravitational degrees of freedom: the radial equation will yield the expression for the absorption probability (or graybody factor) for the particular type of particles, with the angular equation providing the value of the separation constant $E_{j\ell m}$ that appears in the former equation. The above task can be performed either analytically, in the low-energy and low-angular-momentum limit, or numerically with no restriction on these two parameters. In the next two sections, we will follow both approaches to fulfill this task.

2.2.1 Analytic solution

As was noted before [156, 162] in the context of more general analyses, when the space-time background has the form of Eq. (2.8), the tensor-type gravitational perturbations are found to satisfy the same field equations that a massless scalar field obeys in the same background. In the present case, the same result also holds as the set of equations (2.13)-(2.14) are identical to the ones that follow from the scalar field equation

$$\frac{1}{\sqrt{-G}} \partial_M \left(\sqrt{-G} \, G^{MN} \partial_N \Phi \right) = 0 \,, \qquad (2.16)$$

if the following expansion of Φ in terms of the hyperspherical harmonics $\mathbb{Y}^{(\ell,\alpha)}(y)$ on S^n is used

$$\Phi(x,y) = e^{-i\omega t} e^{im\varphi} R(r) \, Q(\theta) \, \mathbb{Y}^{(\ell,\alpha)}(y) \,. \qquad (2.17)$$

Given the different nature of the scalar and gravitational degrees of freedom, the two sets of equations differ only in the allowed values of the angular-momentum number ℓ: whereas, in the scalar case, it satisfies the constraint $\ell \geq 0$ [164], this changes to $\ell \geq 2$ in the case of gravitons [156]. The decoupled set of equations for a massless scalar field propagating in the higher-dimensional background (2.1) first appeared in [164] and were further used in [152, 154] for the study of the energy emission rates for Hawking radiation emitted by the simply rotating Myers-Perry black hole in the form of scalar fields in the bulk.

The radial equation (2.13) was analytically solved for scalar fields propagating in the bulk in [152] in the low-energy and low-angular-momentum approximation. As the equation for tensor-type gravitons is identical, apart from the allowed range of values for ℓ, the analytic solution in this case follows along the same lines. For this reason, here we give only a brief account of the analysis and the results obtained for the absorption probability in the analytic approach, results that are compared with the exact numerical ones in the next section.

The analytic approach amounts to finding first the asymptotic solutions near the horizon of the black hole ($r \simeq r_h$), and far away from it ($r \gg r_h$) and matching the

two in an intermediate zone, to create an analytical solution for $R(r)$ over the whole radial regime.

In the near-horizon regime $(r \simeq r_h)$, eq. (2.13) can be rewritten in the form [152]

$$f(1-f)\frac{d^2R}{df^2} + (1-D_*f)\frac{dR}{df}$$

$$+ \left[\frac{K_*^2}{A_*^2 f(1-f)} - \frac{[\ell(\ell+n-1)a_*^2 + \Lambda_{j\ell m}](1+a_*^2)}{A_*^2(1-f)}\right]R = 0\,, \quad (2.18)$$

in terms of the new radial variable [144, 145]

$$r \rightarrow f(r) = \frac{\Delta(r)}{r^2+a^2} \tag{2.19}$$

and the insertion of the quantities

$$A_* = (n+1) + (n-1)a_*^2, \qquad K_* = (1+a_*^2)\omega_* - a_*m\,. \tag{2.20}$$

In the above, we have also defined $\omega_* \equiv \omega r_h$ and $D_* \equiv 1 - 4a_*^2/A_*^2$. Equation (2.18) is a hypergeometric differential equation whose general form is

$$f(1-f)\frac{d^2R}{df^2} + [c-(1+a+b)f]\frac{dR}{df} - abR = 0. \tag{2.21}$$

In order for the two expressions to coincide the indices $(a,\,b,\,c)$ are defined as $a \equiv \alpha + \beta + D_* - 1$, $b \equiv \alpha + \beta$, and $c \equiv 1 + 2\alpha$, while the parameters α and β are found to be

$$\alpha_\pm = \pm\frac{iK_*}{A_*} \qquad\qquad \text{and}$$

$$\beta_\pm = \frac{1}{2}\left[(2-D_*)\pm\sqrt{(D_*-2)^2 - 4\left[\frac{K_*^2 - [\ell(\ell+n-1)a_*^2 + \Lambda_{j\ell m}](1+a_*^2)}{A_*^2}\right]}\,\right]. \tag{2.22}$$

Then the general solution of eq. 2.18 can be written as [165]

$$R_{NH}(f) = A_- f^\alpha (1-f)^\beta F(a,b,c;f)$$

$$+ A_+ f^{-\alpha}(1-f)^\beta F(a-c+1, b-c+1, 2-c; f)\,, \tag{2.23}$$

where $A_\pm$ are integration constants. Using the convergence criterion for the hypergeometric functions

$$\Re(c-a-b) > 0 \tag{2.24}$$

we have to choose that $b = b_-$. Close to the horizon, the general solution (2.23) can be written as the sum of an incoming and an outgoing plane wave as

$$R_{NH}(f) \simeq A_- f^{\pm K_*/A_*} + A_+ f^{\mp K_*/A_*} = A_- e^{\pm iky} + A_+ e^{\mp iky}, \tag{2.25}$$

where

$$k \equiv \omega - m\Omega = \omega - \frac{ma}{r_h^2 + a^2}, \tag{2.26}$$

after employing a convenient transformation of the radial variable, namely,

$$y = r_h \frac{(1 + a_*^2) \ln(f)}{A_*}. \tag{2.27}$$

If we impose the boundary condition that no outgoing modes exist near the black hole's horizon, we can set either $A_- = 0$ or $A_+ = 0$, depending on the choice for the sign of α. The two choices are found to be equivalent, thus we choose $\alpha = \alpha_-$ and $A_+ = 0$. Then, the near-horizon solution acquires the form

$$R_{NH}(f) = A_- \, f^\alpha \, (1 - f)^\beta \, F(a, b, c; f). \tag{2.28}$$

On the other hand, in the far-field regime ($r \gg r_h$), eq. (2.13) can easily be brought into the form of a Bessel differential equation if we make the substitution [152]

$$R(r) = r^{-\left(\frac{n+1}{2}\right)} \tilde{R}(r) \tag{2.29}$$

and employ a new radial variable $z = \omega r$. Then we arrive at the equation

$$\frac{d^2 \tilde{R}}{dz^2} + \frac{1}{z} \frac{d\tilde{R}}{dz} + \left(1 - \frac{E_{j\ell m} + a^2 \omega^2 + \left(\frac{n+1}{2}\right)^2}{z^2}\right) \tilde{R} = 0. \tag{2.30}$$

If we further define for convenience the quantity $\nu = \sqrt{E_{j\ell m} + a^2 \omega^2 + \left(\frac{n+1}{2}\right)^2}$, the general solution in the far-field regime may be written as

$$R_{FF}(r) = \frac{B_1}{r^{\frac{n+1}{2}}} J_\nu(\omega r) + \frac{B_2}{r^{\frac{n+1}{2}}} Y_\nu(\omega r), \tag{2.31}$$

where J_ν and Y_ν are the Bessel functions of the first and second kind, respectively.

Before the two asymptotic solutions (2.28) and (2.31) can be matched, they both need to be expanded for intermediate values of the radial variable. To this end, the hypergeometric function appearing in (2.28) needs also to be shifted so that its argument changes from f to $1 - f$ by using the well-known relation [165, 152]

$$F(a, b, c; f) = \frac{\Gamma(c)\Gamma(c - a - b)}{\Gamma(c - a)\Gamma(c - b)} F(a, b, a + b - c + 1; 1 - f)$$

$$+ \quad (1 - f)^{c-a-b} \frac{\Gamma(c)\Gamma(a + b - c)}{\Gamma(a)\Gamma(b)} F(c - a, c - b, c - a - b + 1; 1 - f). \tag{2.32}$$

The reason for this argument shift is that we want to exploit a property of the hypergeometric functions, namely that

$$F(a, b, c; x) \to 1 \quad \text{when} \quad x \to 0. \tag{2.33}$$

Recalling what f stands for, (eq. 2.19), we can write for the $1 - f$

$$1 - f = \left(\frac{r_h}{r}\right)^{n-1} \frac{1 + a_*^2}{\left(\frac{r_h}{r}\right)^2 + a_*^2} \tag{2.34}$$

Then in the limit $r \gg r_h$ or, equivalently $1 - f \to 0$, the near-horizon solution takes the "stretched" form

$$R_{NH}(r) \simeq A_1 \, r^{-(n+1)\beta} + A_2 \, r^{(n+1)(\beta+D_*-2)} \,, \tag{2.35}$$

with A_1 and A_2 defined as

$$
\begin{aligned}
A_1 &= A_- \left[(1+a_*^2)\, r_h^{n+1}\right]^{\beta} \frac{\Gamma(c)\Gamma(c-a-b)}{\Gamma(c-a)\Gamma(c-b)}\,, \\
A_2 &= A_- \left[(1+a_*^2)\, r_h^{n+1}\right]^{-(\beta+D_*-2)} \frac{\Gamma(c)\Gamma(a+b-c)}{\Gamma(a)\Gamma(b)}\,.
\end{aligned}
\tag{2.36}
$$

Similarly, the far-field solution has to be "stretched" in order to describe what happens for small values of r. For that, we need the Bessel functions properties

$$J_\nu(z) \simeq \frac{(\frac{1}{2}z)^\nu}{\Gamma(\nu+1)} \quad \text{and}$$

$$Y_\nu(z) \simeq -\frac{1}{\pi} \frac{\Gamma(\nu)}{(\frac{1}{2}z)^\nu}\,, \tag{2.37}$$

when $z \to 0$. Then the far-field solution (2.31) in the limit of $r \to 0$ takes the polynomial form

$$R_{FF}(r) \simeq \frac{B_1 \left(\frac{\omega r}{2}\right)^\nu}{r^{\frac{n+1}{2}} \Gamma(\nu+1)} - \frac{B_2}{\pi \, r^{\frac{n+1}{2}}} \frac{\Gamma(\nu)}{\left(\frac{\omega r}{2}\right)^\nu}\,. \tag{2.38}$$

For the two stretched solutions to perfectly match, the power coefficients of r need to be the same. It can be easily shown that this is indeed the case in the limit of $a_* < 1$ and $\omega_* < 1$. Then, by ignoring terms of order $(\omega_*^2, a_*^2, a_*\omega_*)$ or higher in the expressions of β and ν, we find that

$$
\begin{aligned}
(n+1)\beta &\simeq -j, \tag{2.39} \\
\nu &\simeq j + \frac{n+1}{2} \qquad \text{and} \\
(n+1)(\beta+D_*-2) &\simeq -(j+n+1).
\end{aligned}
$$

By identifying the coefficients of the same powers of r, we finally obtain the constraint

$$\frac{B_1}{B_2} = -\frac{(2/\omega r_h)^{2j+n+1} \, \nu \, \Gamma^2(\nu)\, \Gamma(\alpha+\beta+D_*-1)\,\Gamma(\alpha+\beta)\,\Gamma(2-2\beta-D_*)}{\pi\,(1+a_*^2)^{\frac{2j+n+1}{n+1}} \, \Gamma(2\beta+D_*-2)\,\Gamma(2+\alpha-\beta-D_*)\,\Gamma(1+\alpha-\beta)}\,, \tag{2.40}$$

that guarantees the existence of a smooth, analytic solution for the radial part of the tensor-type graviton wave function for all r, valid for small a_* and ω_*.

Let us, at this point, clarify the expression for the eigenvalue $E_{j\ell m}$ that appears both in β and ν. This quantity does not exist in closed form, and can be found either numerically or in terms of a power series in the limit of small $a\omega$. We reserve the use of the first method for the next section - in the context of the present analysis, valid

in the low-energy and low-angular-momentum, we may use instead the analytic power
series expansion [166, 128, 129, 167]

$$E_{j\ell m} = \sum_{k=0}^{\infty} f_k \, (a\omega)^k \,. \tag{2.41}$$

For the accuracy of our analysis, we keep terms up to 4th order – the exact expressions[2]
of the coefficients f_k can be found in [166]. It is only in the expansion of the power
coefficients of r in the matching process that all terms beyond the first one are ignored;
in this case,

$$E_{j\ell m} \simeq f_0 = j(j + n + 1), \tag{2.42}$$

where $j \geq \ell + |m|$ and $\frac{j-(\ell+|m|)}{2} \in \{0, \mathbb{Z}^+\}$.

A quantity that determines, to a great extent, the Hawking radiation emission rate
of the black hole is the absorption probability $|\mathcal{A}_{j\ell m}|^2$ – or graybody factor, since it is
the reason for the deviation of the black-hole spectrum from a pure blackbody one, as
mentioned also earlier. We may derive it, by expanding the far-field solution (2.30) for
$r \to \infty$, in which case we obtain

$$R_{FF}(r) \simeq \frac{1}{r^{\frac{n+2}{2}}\sqrt{2\pi\omega}} \left[(B_1 + iB_2)\, e^{-i\left(\omega r - \frac{\pi}{2}\nu - \frac{\pi}{4}\right)} + (B_1 - iB_2)\, e^{i\left(\omega r - \frac{\pi}{2}\nu - \frac{\pi}{4}\right)} \right]. \tag{2.43}$$

The absorption probability is then easily determined via the amplitudes of the outgoing
and incoming spherical waves, namely,

$$|\mathcal{A}_{j\ell m}|^2 = 1 - |\mathcal{R}_{j\ell m}|^2 = 1 - \left|\frac{B_1 - iB_2}{B_1 + iB_2}\right|^2 = \frac{2i\,(B^* - B)}{BB^* + i\,(B^* - B) + 1}, \tag{2.44}$$

where $B \equiv B_1/B_2$ is given by eq. (2.40). The above result can be used to evaluate
the absorption probability for the emission of tensor-type gravitons in the bulk, from
a simply rotating black hole, in the low-energy and low-angular-momentum limit.

2.2.2 Numerical analysis

In this section, we use numerical analysis in order to solve both the angular and radial
equations for any value of the energy of the emitted particles and angular momentum
of the black hole. We start by presenting the main aspects of our numerical techniques,
and then we turn to the derivation of exact numerical results for the graybody factor
and energy emission spectrum for tensor-type gravitational modes in the bulk.

---

[2]For consistency, we should point out that in [166] the indices (j, ℓ) are interchanged compared to
the ones in this work, and the total sign of the f_2 coefficient should be reversed due to a typographical
error.

Numerical techniques

The angular equation (2.14), in terms of the new variable $x = \cos(2\theta)$, can be written in the following form

$$2(1-x^2)\, Q''(x) + [\, n - 1 - (n+3)x \,]\, Q'(x) \tag{2.45}$$

$$+ \left(\frac{E_{j\ell m} + a^2\omega^2}{2} + \frac{a^2\omega^2(x-1)}{4} + \frac{m^2}{x-1} - \frac{\ell(\ell+n-1)}{1+x} \right) Q(x) = 0\,.$$

The above differential equation has been solved in the literature before in different contexts and forms: for instance, its four-dimensional version (that follows for $\ell = n = 0$), in the presence of a positive cosmological constant, was solved in [168, 169]; in [166], the above higher-dimensional version was solved for scalar fields, i.e., for $\ell = 0, 1, 2, \ldots$; finally, for tensor-type gravitons living in a higher-dimensional space but in the presence of a negative cosmological constant, the corresponding equation was numerically solved in [162]. Thus, the numerical analysis demanded for solving eq. (2.45) for tensor-type gravitons living in a higher-dimensional asymptotically flat spacetime is a simplified case of the one presented in [162].

The differential equation (2.45) has three regular singular points, at $x = \pm 1$ and $x = \infty$. The angular function $Q(x)$ can be alternatively written as

$$Q(x) = (1-x)^{|m|/2}\,(1+x)^{\ell/2}\, y(z)\,, \tag{2.46}$$

where $x = 2z - 1$. Under further expansion of the rescaled function $y(z)$ in terms of an infinite series of Jacobi polynomials, supplemented by regularity conditions at $z = 0$ and $z = 1$, Eq. (2.45) takes the form of an algebraic equation – a three-term recurrence relation [162]

$$c_{k+1}\,\alpha_k + c_k\,\beta_k + c_{k-1}\,\gamma_k = 0 \tag{2.47}$$

for the coefficients c_k appearing in the expansion of $y(z)$. In the above relation, the coefficients α_k, β_k, and γ_k are constants depending on the fundamental parameters (ω_*, a_*, n) of the theory, the quantum numbers (ℓ, m), the angular eigenvalue $E_{j\ell m}$, and the new index $k = 0, 1, 2, \ldots$ that labels the power of the expansion.

The solution for the angular function $Q(\theta)$ is of limited physical importance for the calculation of the energy emission spectra for the simply rotating black hole. On the other hand, the computation of the eigenvalue $E_{j\ell m}$, that also appears in the radial equation (2.13) as a separation constant, is of paramount importance. The value of the separation constant can be obtained by applying the infinite continued fractions method [170] – which will be described in detail in sec. 2.4. The continued fraction equation [162] follows from the three-term recurrence relation (2.47) and involves ratios of successive terms of the coefficients α_k, β_k, and γ_k. This equation can be numerically solved in any desired accuracy for the value of $E_{j\ell m}$, for given values of ω_*, a_*, and n.

In the case of vanishing angular momentum of the black hole, the value of the separation constant can be found in a closed form by the requirement that the corresponding power series expansion of $y(z)$ with a finite number of terms converges [170]. In that case, we obtain [166, 162]

$$E_{j\ell m} = (2k + \ell + |m|)(2k + \ell + |m| + n + 1) \equiv j(j + n + 1)\,, \tag{2.48}$$

where, in the last part of the above equation, we have set $j \equiv 2k + \ell + |m|$. Under this alternative definition, the eigenvalue is labeled by a new quantum number with values $j = 2, 3, 4, \ldots$ and, at its lowest order, it coincides with the one for a $(n+2)$ sphere, in agreement with the discussion below eq. (2.41).

If the rotation parameter a of the black hole is non-vanishing, the eigenvalues $E_{j\ell m}$ are in principle non-integer and complex. In that case, we can find the value of $E_{j\ell m}(\omega_*, a_*)$, for any value of ω_* and a_*, by using the following procedure.

1. We start from the non-rotating black hole and find the exact value of $E_{j\ell m}$, for the corresponding j, according to eq. (2.48).

2. We increase the rotation parameter by a very small amount and search for the closest to the previously found solution for $E_{j\ell m}$.

3. We repeat the previous step until any required value of a_* is reached and all corresponding values of $E_{j\ell m}$ are found.

By following the aforementioned process, we are able to compute the values of the angular separation constant $E_{j\ell m}$, for any ω_* and a_*, and thus to proceed to the numerical integration of the radial equation (2.13).

Equation (2.13) can in turn be rewritten in an alternative form under the redefinition of the radial function $R(r) = r^{-n/2} (r^2 + a^2)^{-1/2} P(r)$ and the employment of the tortoise coordinate defined through the relation $dr_\star = (r^2 + a^2) dr / \Delta$. The new equation then reads

$$\frac{d^2 P(r_\star)}{dr_\star^2} + \left[\left(\omega - \frac{am}{r^2 + a^2} \right)^2 - \frac{\Delta}{(r^2 + a^2)^2} U(r) \right] P(r_\star) = 0, \qquad (2.49)$$

where

$$\begin{aligned} U(r) &= \Lambda_{j\ell m} + \frac{\ell(\ell + n - 1)a^2}{r^2} + \Delta \left[\frac{n(n+2)}{4r^2} + \frac{3a^2}{(r^2 + a^2)^2} \right] \\ &+ \left[\frac{(n+1)\mu}{r^{n-1}} - 2a^2 \right] \left(\frac{n}{2r^2} + \frac{1}{r^2 + a^2} \right) . \end{aligned} \qquad (2.50)$$

In this form it is straightforward to derive the asymptotic solutions at the horizon and spatial infinity. First, at the horizon, if we set $r \to r_h$ and $\Delta \to 0$, we easily obtain

$$P(r_\star) \simeq A_1 e^{i\tilde{\omega}r_\star} + A_2 e^{-i\tilde{\omega}r_\star}, \qquad (2.51)$$

where $A_{1,2}$ are integration constants, and

$$\tilde{\omega} \equiv \omega - m\,\Omega_h = \omega - \frac{am}{a^2 + r_h^2}, \qquad (2.52)$$

with Ω_h the rotation velocity of the black hole. Since no outgoing wave is allowed to classically exist outside the horizon of the black hole, the physically relevant solution of eq. (2.49) at the horizon is

$$P(r) = A_2 e^{-i\tilde{\omega}r_\star} \simeq (r - r_h)^{-i(\omega - m\,\Omega_h) \frac{r_h^2 + a^2}{\Delta'(r_h)}} (Z_h + \mathcal{O}(r - r_h)), \qquad (2.53)$$

where Z_h is a rescaled integration constant. As expected, the near-horizon solution (2.28), derived in Sec. 2.2.1, reduces to the same expression if we take the limit $f \to 0$, expand Δ in powers of $(r - r_h)$ and redefine the integration constant A_-.

For the purpose of our numerical analysis, we introduce close to the horizon the new function

$$z(r) = \left(1 - \frac{r_h}{r}\right)^{i\tilde{\omega}\,(r_h^2 + a^2)/\Delta'(r_h)} P(r). \tag{2.54}$$

Since $P(r)$ satisfies the asymptotic condition (2.53), $z(r)$ is regular at the event horizon. We may also fix the value of any undetermined integration constant, by setting

$$z(r_h) = 1. \tag{2.55}$$

If we then expand $z(r)$ near the event horizon as

$$z(r) = 1 + z'(r_h)\,(r - r_h) + \mathcal{O}\,(r - r_h)^2 \,, \tag{2.56}$$

and substitute into eq. (2.49), we find the value of $z'(r_h)$ which, together with eq. (2.55), are the boundary conditions for our eq. (2.49) at the horizon.

Next, at spatial infinity $(r \to \infty)$, the two linearly independent solutions of eq. (2.49) are

$$P_i(r) \sim e^{-i\omega r}, \qquad P_o(r) \sim e^{i\omega r}, \tag{2.57}$$

which describe the ingoing and outgoing wave, respectively. The functions $P_i(r)$ and $P_o(r)$ can be found analytically as series expansions for large r up to any order.

The numerical integration of eq. (2.49) then proceeds as follows: with the eigenvalue $E_{j\ell m}$ already numerically known for all values of ω_* and a_*, we start from the horizon, with the values of $z(r_h)$ and $z'(r_h)$ as boundary conditions, and move outwards by using the $NDSolve$ built-in function in $Mathematica$® for $r_h \leq r \leq r_f$, where $r_f \gg r_h$. After the function $P(r)$ is known numerically, we find a fit of this function by considering the superposition of the two solutions (2.57) in some region near r_f:

$$P(r) = Z_i\,P_i(r) + Z_o\,P_o(r). \tag{2.58}$$

The fitting procedure allows us to find the coefficients Z_i and Z_o. In order to check the precision of the coefficients we increase the internal precision of $NDSolve$, the value of r_f, and the number of terms in the series expansion for $P_i(r)$ and $P_o(r)$, making sure that the values of Z_i and Z_o do not change within the desired precision. The same shooting procedure, though for different boundary conditions, has been used recently in [163] for analysis of stability of higher-dimensional black holes.

Once this process is completed, the quantity Z_o/Z_i gives the ratio of the amplitudes of the outgoing and ingoing modes at a large distance from the black hole, and the absorption probability follows easily through the relation

$$|\mathcal{A}_{j\ell m}|^2 = 1 - |\mathcal{R}_{j\ell m}|^2 = 1 - |Z_o/Z_i|^2.$$
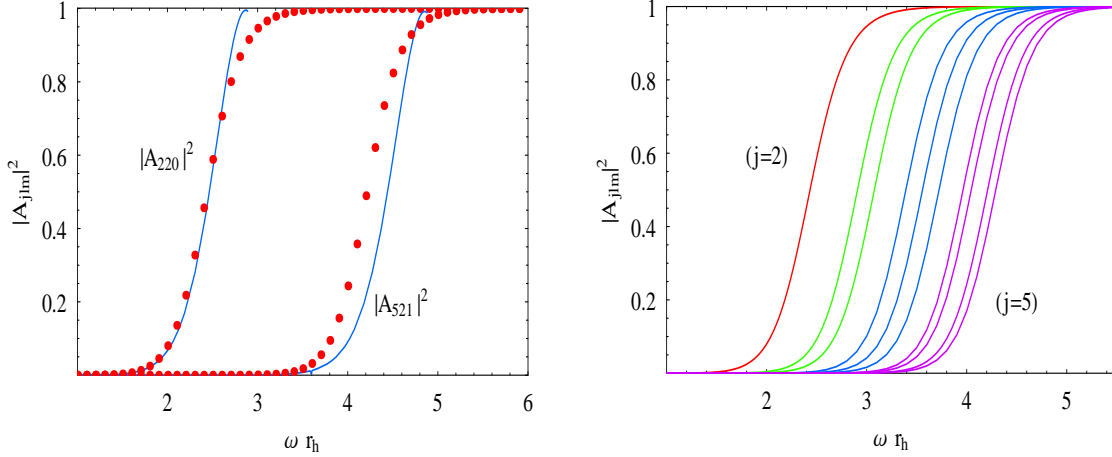
Figure 2.1: **(a)** Comparison between our analytical (solid lines) and numerical (data points) results for the graybody factor for the modes $(j = \ell = 2, m = 0)$ and $(j = 5, \ell = 2, m = 1)$, for $a = 0.5$ and $D = 7$. **(b)** Absorption probabilities for the sets of modes with $\ell = 2$, from left to right, $(j = 2, m = 0)$ (red line), $(j = 3, m = -1, 1)$ (green lines), $(j = 4, m = -2, 0, 2)$ (blue lines), and $(j = 5, m = -3, -1, 1, 3)$ (magenta lines), for $a = 0.5$ and $D = 7$.

Absorption probability

By following the two approaches described in Secs. 2.2.1 and 2.2.2, we have derived analytical approximate results as well as exact numerical ones for the absorption probability for gravitational tensor modes that propagate in the background of a higher-dimensional simply rotating black hole. The two sets of results ought to agree in the low-energy and low-angular-momentum limit, but we expect them to deviate once we move outside these regimes. In order to check the extent of the agreement of the two sets of results as well as its dependence on the particular mode studied, in Fig. 2.1(a) we depict these two sets for two indicative modes with $(j = 2, \ell = 2, m = 0)$ and $(j = 5, \ell = 2, m = 1)$: the analytical results are given by the solid lines whereas the numerical results are presented as data points - both sets of results correspond to the case with $D = 7$ (or $n = 3$) and $a = 0.5$ (in units of r_h). As expected, the agreement between the two sets is indeed very good in the low-energy and even intermediate-energy regime, but inevitably it breaks down as we move towards the high-energy one. The agreement is better for the lowest modes and it worsens for higher modes for which the graybody factor raises to a significant value and approaches unity at an increasingly higher value of the energy parameter ωr_h.

In Fig. 2.1(b), we examine the aforementioned behavior of the graybody factors for different tensor modes by using exact numerical results. We classify the modes primarily by the angular-momentum number j which can be considered as the total angular-momentum number of the mode, with ℓ denoting the angular-momentum along the compact space S^n and m the one in the plane of rotation of the black hole. As in the case of scalar fields [152, 154], a set of modes corresponds to each value of j:
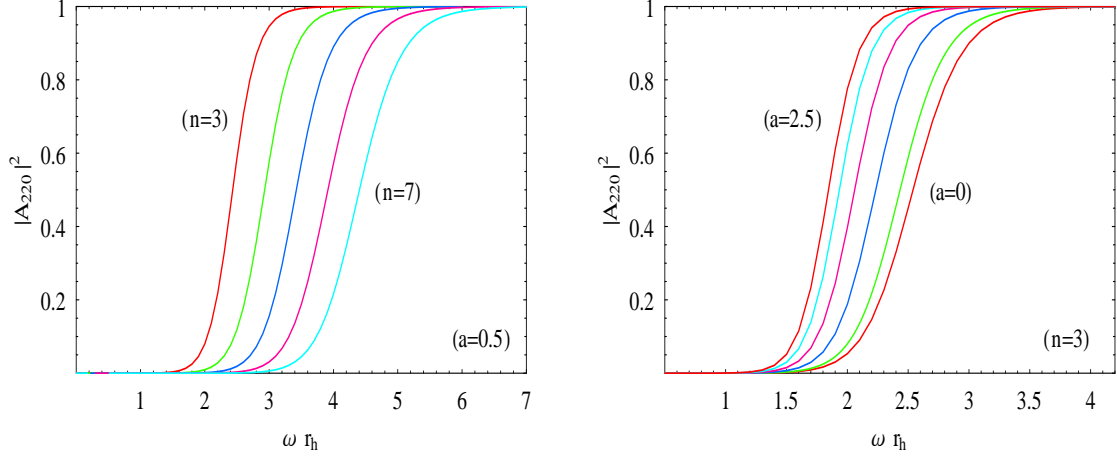
Figure 2.2: Absorption probabilities for the mode $(j = 2, \ell = 2, m = 0)$ as **(a)** a function of $n = 3, 4, 5, 6, 7$, for $a = 0.5$, and **(b)** a function of $a = 0, 0.5, 1, 1.5, 2, 2.5$, for $n = 3$.

the constraints $j \geq \ell + |m|$ and $\frac{j-(\ell+|m|)}{2} \in \{0, \mathbb{Z}^+\}$ [166] dictate that for each value of j, ℓ can take values in the range $[2, j]$ while, for given j and ℓ, m can take $j - \ell + 1$ values in total. In Fig. 2.1(b), we display the set of modes corresponding to the values $j = 2, 3, 4, 5$ - in order to keep the plot tidy, we fix $\ell = 2$ and present the graybody factors for the modes with the $j - \ell + 1$ allowed values of m in each case. We may clearly see that as either j or m increases, the corresponding graybody curve shifts to the right and to higher-energies – a similar behavior would have been observed if we also varied ℓ.

Next, we investigate the dependence of the gravitational tensorial graybody factors on the spacetime parameters of the theory, namely the number of additional spacelike dimensions n and the angular-momentum parameter of the black hole a. In Fig. 2.2(a), we display the absorption probabilities for the indicative mode $(j = 2, \ell = 2, m = 0)$ as n changes from 3 to 7, while keeping the angular-momentum parameter fixed at $a = 0.5$. The graybody factors for the gravitational modes in the bulk clearly decrease as the number of transverse-to-the-brane spacelike dimensions increases. For the same mode, in Fig. 2.2(b), we present the dependence of the graybody factors as a changes from 0 to 2.5, while keeping the dimensionality of spacetime fixed at $D = 7$. In this case, the graybody factors for tensorlike gravitons are clearly enhanced as the angular-momentum of the black hole increases. This behavior is in total agreement with the one observed for bulk scalar fields [152, 154] propagating in the same background.

Energy and angular-momentum emission rates

Having determined the exact value of the absorption probability, we can now proceed to compute the differential emission rates of energy and angular momentum from a higher-dimensional simply rotating black hole in the bulk in the form of tensor-type
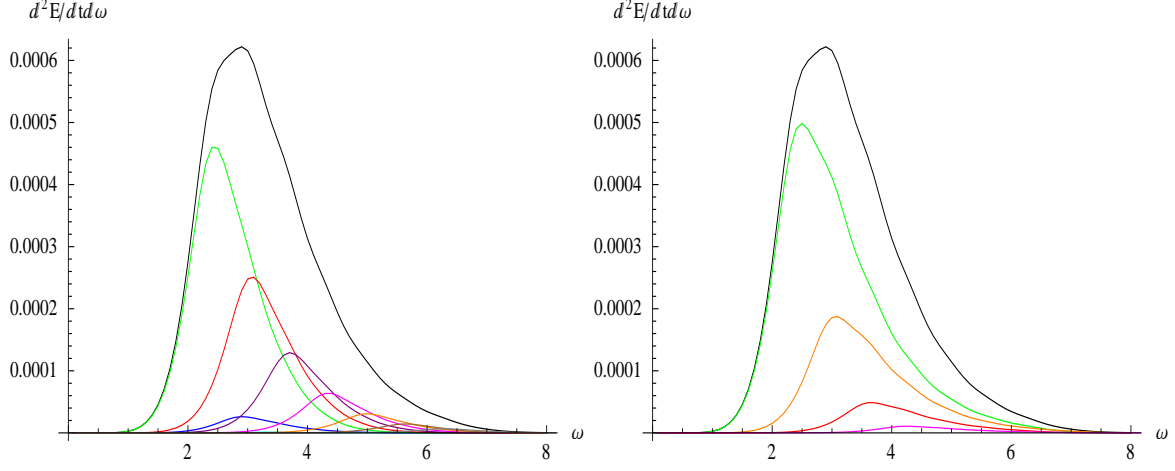
Figure 2.3: The energy emission of tensor-type gravitons for $D = 7$, $a_* = 0.5$ (black line) together with the contributions of different quantum numbers (color lines) are shown. In the left-hand figure: $m = -2$ (cyan line), $m = -1$ (blue line), $m = 0$ (green line), $m = 1$ (red line), $m = 2$ (purple line), $m = 3$ (magenta line), $m = 4$ (orange line), $m = 5$ (brown line), $m = 6$ (gray line). In the right-hand figure: $\ell = 2$ (green line), $\ell = 3$ (orange line), $\ell = 4$ (red line), $\ell = 5$ (magenta line). The largest contribution correspond to $m = 0$. Peaks of positive m contributions ($m = 1, 2, 3, 4, 5, 6$) lay to the right from the peak of $m = 0$ contribution.

gravitons. These are given by the following expressions,

$$\frac{d^2 E}{d\omega dt} = \frac{1}{2\pi} \sum_{j,\ell,m} \frac{\omega}{e^{\tilde{\omega}/T_H} - 1} N_{ST}^\ell(S^n) |\mathcal{A}_{j\ell m}|^2, \tag{2.59}$$

$$\frac{d^2 J}{d\omega dt} = \frac{1}{2\pi} \sum_{j,\ell,m} \frac{m}{e^{\tilde{\omega}/T_H} - 1} N_{ST}^\ell(S^n) |\mathcal{A}_{j\ell m}|^2, \tag{2.60}$$

where $\tilde{\omega}$ is defined in eq. (2.52) and the temperature T_H is given in eq. (2.6).

The quantity N_{ST}^ℓ is the multiplicity of the second-rank symmetric, traceless ($T^A{}_A = 0$) and divergence-free ($D_B T^{BA} = 0$) tensor harmonics T_{AB} that satisfy Eq. (2.10). Equivalently, it is the multiplicity of tensor modes on S^n that, under the aforementioned constraints, are described by the same angular-momentum number ℓ. This number was calculated by Rubin and Ordóñez in [171] and found to be

$$N_{ST}^\ell(S^n) = \frac{(n+1)(n-2)(n+\ell)(l-1)(n+2\ell-1)(n+\ell-3)!}{2(\ell+1)!(n-1)!}, \tag{2.61}$$

for the ℓth eigenvalue. The above formula was derived by expanding the tensor harmonics T_{AB} in terms of the harmonic functions $Y^\ell_{(m)}$ and utilizing the representation theory of $SO(n+1)$.

In order to compute the differential rates (2.59)-(2.60), we need to sum the contribution of all tensor modes labeled by the different values of the (j, ℓ, m) angular
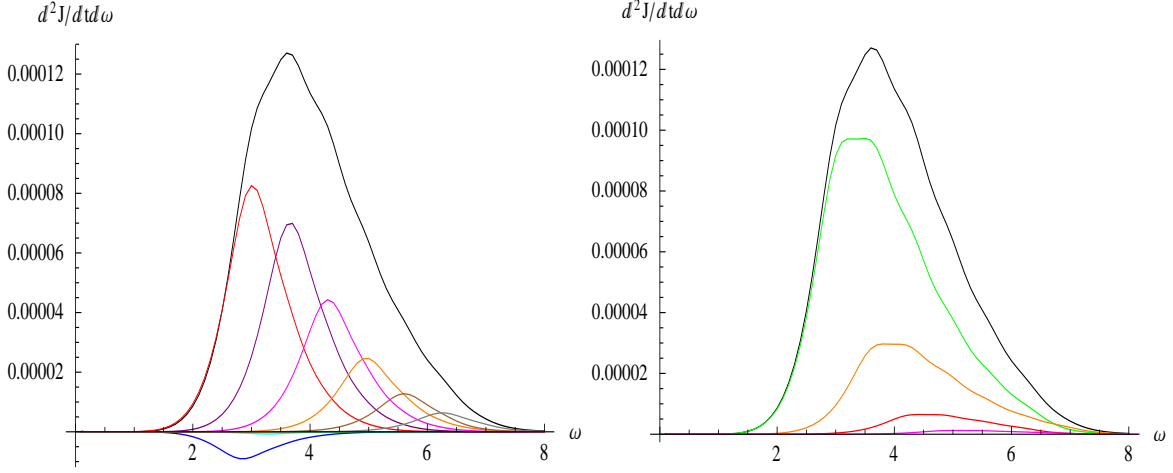
Figure 2.4: As above, for the angular-momentum emission of tensor-type gravitons (black line). In the left-hand figure: $m = -2$ (cyan line), $m = -1$ (blue line) $m = 0$ (green line), $m = 1$ (red line), $m = 2$ (purple line), $m = 3$ (magenta line), $m = 4$ (orange line), $m = 5$ (brown line), $m = 6$ (gray line). In the right-hand figure (from top to bottom): $\ell = 2$ (green line), $\ell = 3$ (orange line), $\ell = 4$ (red line), $\ell = 5$ (magenta line).
The largest contribution corresponds to $m = 1$. Peaks of other positive m contributions ($m = 2, 3, 4, 5, 6$) lay to the right from the peak of $m = 1$ contribution. The contributions of negative values of m are negative.

quantum numbers. In practice, the sums need to be truncated at an appropriate high value of each number in such a way that the derived values of the two rates are as close as possible to the real ones. To this end, we adopt the following procedure: we first fix one of the angular numbers and sum over the other two within this range – in this way we find the contribution of each value of the fixed parameter to the total sum. If the contribution of the highest considered value of an angular number is not small, we increase the particular value range. We repeat the described procedure for all angular numbers until the contribution to the energy and angular momentum emission rates of the highest considered multipole number becomes negligibly small.

As an indicative example, in Figs. 2.3(a,b) and 2.4(a,b) we display the contributions of the lowest m and ℓ tensor modes to the energy and angular-momentum emission rates, respectively, for $D = 7$ and $a = 0.5$. In all cases, we may observe the increasingly smaller contribution of the higher modes to the specific rate, and thus the convergence of the corresponding sum. This is due to the fact that, according to Fig. 2.1(b), the higher modes become important at a larger value of the energy parameter ωr_h, and this in practice takes place after the peak of the emission curves – determined by the temperature of the black hole – has been reached. As a result the higher modes contribute mostly to the "tail" of the emission curves. This is more clearly shown in Fig. 2.5 where the energy emission rate is presented, for $D = 7$ and $a = 1$, in terms of the contribution of the j modes: as the highest considered value of j increases, from
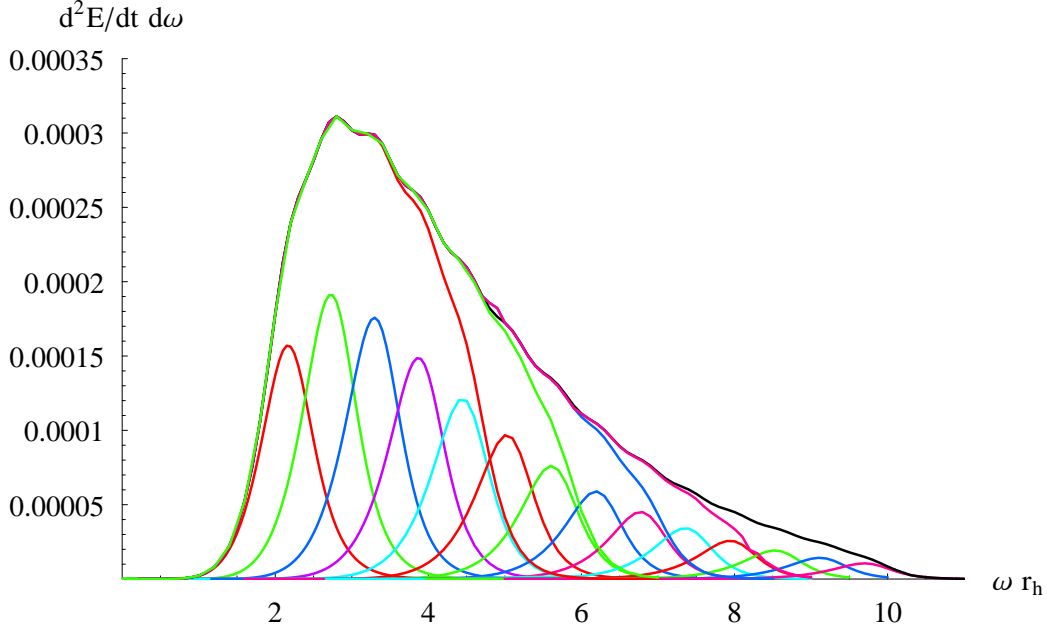
Figure 2.5: The energy emission of tensor-type gravitons for $D = 7$, $a_* = 1$. The different (upper) curves, from left to right, correspond to the highest value of j considered in the sum: $j = 6$ (red line), $j = 8$ (green line), $j = 10$ (blue line), $j = 12$ (magenta line), and $j = 15$ (black line).

$j = 5$ to $j = 8$, then to $j = 10$, $j = 12$, and finally to $j = 15$, the emission curve becomes wider and the slope of the tail decreases, whereas the low-energy behavior and the peak of the curve remain unchanged. As mentioned above, in all the cases studied in this work, care was taken so that the change in the emission curves would be negligibly small when a cutoff was imposed on the highest values of all angular numbers. In general, as either n or a_* increases, the number of modes that need to be summed increases, too – in order to obtain as accurate as possible emission spectra, we have summed up to $j = 22$, i.e., $m = 20$, in the cases considered.

Next, we turn to the dependence of the energy and angular-momentum emission rates of the black hole on the space-time parameters, namely, n and a_*. In Figs. 2.6(a,b), we illustrate the dependence of the energy spectrum on the number of additional spacelike dimensions and the angular momentum of the black hole, respectively. As in the case of scalar fields[3] [152, 154], the energy emission rate has a very strong dependence on n with an enhancement of almost two orders of magnitude as n changes from $n = 3$ to $n = 7$. This enhancement is present in all energy regimes with the emission curve becoming significantly taller and wider as n increases. The dependence of the energy spectrum on the angular momentum of the black hole is also nontriv-

---

[3]As a check of our numerical analysis, we have successfully reproduced the exact results for the energy emission rate of scalar fields in the bulk from a higher-dimensional simply rotating black hole [154] that were derived with an independent code.
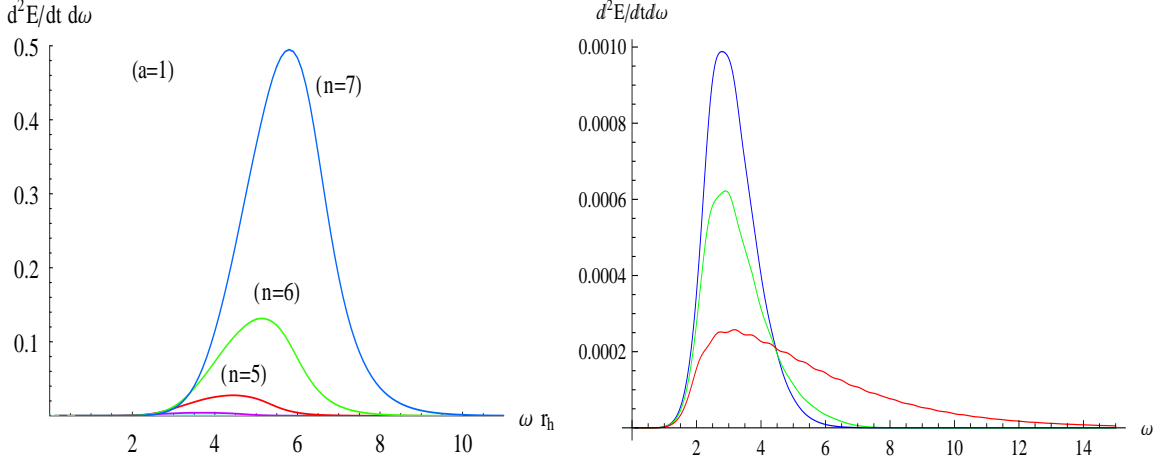
Figure 2.6: The energy emission rate for tensor-type gravitons in the bulk for **(a)** $a_* = 1$ and $n = 3, 4, 5, 6, 7$ (from bottom to top), and for **(b)** $n = 3$ and $a_* = 0$ (blue line, top), $a_* = 0.5$ (green line), $a_* = 1.2$ (red line, bottom).

ial, although of a smaller magnitude: for the case $n = 3$ depicted in Fig. 2.6(b), the increase of the angular-momentum parameter from $a_* = 0$ to $a_* = 1.2$ results into the emission of less energy per unit time in the low and intermediate regime and an enhancement in the emission of high-energy modes. As n gets larger, this dependence becomes milder, a feature which is again in accordance with the behavior of the bulk scalar fields emitted by the same black hole space=time.

In Figs. 2.7(a,b), we depict the dependence of the angular-momentum emission rate on the same spacelike parameters. As the number of extra dimensions increases, we observe again a significant enhancement in the rate of loss of angular momentum by the black hole. This enhancement reaches more than an order of magnitude and results in the emission of a higher number of modes in all energy regimes. Contrary to what happens in the energy spectrum, the increase in the rotation velocity of the black hole also increases the angular-momentum emission rate from the black hole. The enhancement is significant, although of a smaller magnitude than the one in terms of n, leads to the loss of angular momentum via the increased emission of modes in the whole energy spectrum, and manifests itself independently of the dimensionality of space-time.

Finally, in Fig. 2.8 one can see the total energy emission and angular-momentum emission for the tensor-type gravitons for $D = 9$ and a fixed $a_* = 1.2$ as well as contributions of different quantum numbers m, calculated by the accurate shooting method. In Table 2.1 the total emission power by the scalar field for $a_* = 1.0$ (taken from [154]) is given in comparison with the total emission power of tensor-type gravitons. There we can see that although at small number of space-time dimensions n the contribution of gravitons into the total radiation is tiny, it quickly increases with n and becomes dominant for large n.

Apart from its obvious theoretical interest, the calculation of the emission spectra
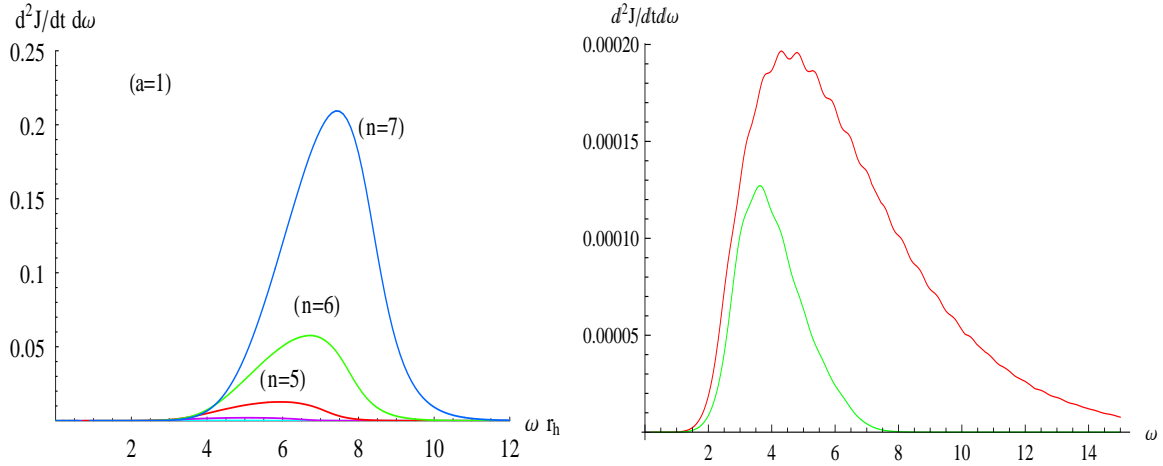
Figure 2.7: The angular-momentum emission rate for tensor-type gravitons in the bulk for **(a)** $a_* = 1$ and $n = 3, 4, 5, 6, 7$ (from bottom to top), and for **(b)** $n = 3$ and $a_* = 0.5$ (green line, bottom), $a_* = 1.2$ (red line, top).

n	Scalar field	Tensor-type gravitons	
3	0.1646	0.0013	0.8%
4	0.3808	0.0222	5.8%
5	0.7709	0.1853	24%

Table 2.1: Total emission power (mass loss rate, in units of $1/r_h^2$) by scalar field ($a_* = 1.0$ taken from [154]) and by tensor-type gravitons ($a_* = 1.2$).

of a higher-dimensional, simply rotating black hole in the form of gravitons in the bulk has a very important phenomenological interest in the exciting case of the creation of miniature black holes at ground-based accelerators. Previous studies [152, 154] have revealed that the bulk emission of the other species of particles allowed to propagate in the whole space-time, namely, the scalar fields, is subdominant compared to the emission that takes place in the form of brane-localized scalar fields. When this is combined with the fact that the total number of fermionic and gauge bosonic degrees of freedom of Standard Model are also restricted, and thus emitted, on the brane, the brane emission channel becomes even more dominant. Addressing the question of energy balance between the brane and bulk channel for the last species, i.e., the gravitons, is of paramount importance for the estimate of the percentage of the total energy of the black hole which is lost in the bulk, and thus of the chances for the potential detection of the produced black hole via the emitted Hawking radiation. The analysis and results presented in this work on the emission of tensor-type graviton modes in the bulk are the first necessary step towards this direction that will hopefully be soon complemented by a similar calculation for the vector and scalar gravitational modes.
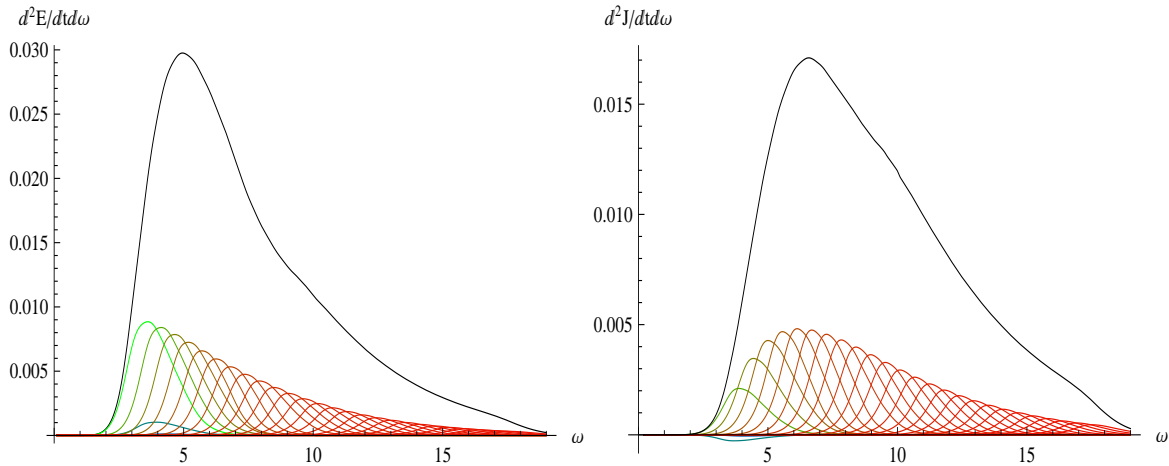
Figure 2.8: The energy emission (left) and angular-momentum emission (right) of tensor-type gravitons for $D = 9$, $a_* = 1.2$ (black line) together with the contributions of different quantum numbers m (color lines) are shown.

2.3   Bulk and brane emission of massive scalars

Scalars were the first particle species whose emission by black holes through the Hawking radiation mechanism was studied. This was a natural choice since, due to the absence of spin, the necessary calculations ought to be far less cumbersome to be done than the ones for fermions and/or bosons. In order to simplify the analysis, the emitted fields are assumed to be minimally-coupled to gravity but otherwise free as well as massless.

Later, in the context of the four-dimensional analysis [179] it was found that for certain particles and mass of the black hole, the particle mass can significantly (up to 50%) suppress the emission rate. Recently, a set of works [180, 181] has addressed the question of the role of the mass of the emitted field (as well as that of the charge) for emission on the brane by a higher-dimensional black hole. Here, we extend this analysis by considering the case of a higher-dimensional black hole with a non-vanishing angular momentum emitting massive scalar fields. We perform a comprehensive study of the absorption probability and energy emission rate for a range of values of the mass of the emitted field, number of extra dimensions, and angular momentum of the black hole. By integrating over the entire frequency range, we compute the total emissivities and obtain the suppression factors in each case. We also consider the cases of both bulk and brane emission, and pose the additional question of whether the presence of the mass of the emitted field can affect the bulk-over-brane energy ratio and threaten the dominance of the brane channel.

2.3.1 Emission of Massive Scalars in the Bulk

In this work, we will consider once again the case of a higher-dimensional, neutral, simply rotating black hole whose gravitational background is the one described by eq. (2.1) for all the reasons analyzed earlier.

A massive scalar field, with mass m_Φ, propagating in the gravitational background of a higher-dimensional simply rotating black hole (2.1) will satisfy the equation of motion

$$\frac{1}{\sqrt{-G}} \partial_M \left(\sqrt{-G} \, G^{MN} \partial_N \Phi \right) - m_\Phi^2 \Phi = 0 \,, \tag{2.62}$$

where G_{MN} the higher-dimensional metric tensor and G its determinant satisfying the relation

$$\sqrt{-G} = \Sigma \sin \theta \, r^n \cos^n \theta \prod_{i=1}^{n-1} \sin^i \theta_i \,. \tag{2.63}$$

Even in the presence of the mass term, the above equation can be separated [133, 182] by assuming the factorized ansatz

$$\Phi = e^{-i\omega t} e^{im\varphi} R(r) \, S(\theta) \, Y_{ln}(\theta_1, \ldots, \theta_{n-1}, \phi) \,, \tag{2.64}$$

where $Y_{ln}(\theta_1, \ldots, \theta_{n-1}, \phi)$ are the hyperspherical harmonics on the n-sphere that satisfy the equation [183, 164]

$$\sum_{k=1}^{n-1} \frac{1}{\prod_{i=1}^{n-1} \sin^i \theta_i} \partial_{\theta_k} \left[\left(\prod_{i=1}^{n-1} \sin^i \theta_i \right) \frac{\partial_{\theta_k} Y_{ln}}{\prod_{i>k}^{n-1} \sin^2 \theta_i} \right] +$$

$$\frac{\partial_{\phi\phi} Y_{ln}}{\prod_{i=1}^{n-1} \sin^2 \theta_i} + l(l+n-1) Y_{ln} = 0 \,. \tag{2.65}$$

The functions $R(r)$ and $S(\theta)$ in turn satisfy the following decoupled radial and angular equation

$$\frac{1}{r^n} \partial_r \left(r^n \Delta \, \partial_r R \right) + \left(\frac{K^2}{\Delta} - \frac{l(l+n-1)a^2}{r^2} - \tilde{\Lambda}_{j\ell m} - m_\Phi^2 r^2 \right) R = 0 \,, \tag{2.66}$$

$$\frac{1}{\sin \theta \cos^n \theta} \partial_\theta \left(\sin \theta \cos^n \theta \partial_\theta S \right) + \left(\tilde{\omega}^2 a^2 \cos^2 \theta - \frac{m^2}{\sin^2 \theta} - \frac{l(l+n-1)}{\cos^2 \theta} + \tilde{E}_{j\ell m} \right) S = 0 \,, \tag{2.67}$$

respectively. In the above,

$$K = (r^2 + a^2) \, \omega - am \,, \qquad \tilde{\Lambda}_{j\ell m} = \tilde{E}_{j\ell m} + a^2 \omega^2 - 2am\omega \,. \tag{2.68}$$

For the above decoupling to take place, the angular function $S(\theta)$ needs to satisfy a modified higher-dimensional spheroidal harmonics equation: compared to the massless case [166], it has the energy ω replaced by the momentum $\tilde{\omega} \equiv \sqrt{\omega^2 - m_\Phi^2}$. Then, the massive angular eigenvalue $\tilde{E}_{j\ell m}(a\tilde{\omega})$ is related to the massless one $E_{j\ell m}(a\omega)$ by merely a shift of its argument: $a\omega \to a\tilde{\omega}$. Here, we will employ the power-series

expression of the angular eigenvalue [166] in terms of the parameter $(a\omega)$ which, under the aforementioned shift and up to 5th order, takes the form

$$
\begin{aligned}
\tilde{E}_{jlm} =\ & j\,(j+n+1) - (a\tilde{\omega})^2\,\frac{\left[-1+2l(l-1)+2j(j+1)-2m^2+2n(j+l)+n^2\right]}{(2j+n-1)\,(2j+n+3)} \\
& +\ (a\tilde{\omega})^4\,\Bigg\{\frac{(l-j+|m|)(l+j-|m|+n-1)}{16(2j+n-3)(2j+n-1)^2}\Big[(2+l-j+|m|)(l+j-|m|+n-3) \\
& -\ 4(2j+n-3)\frac{[-1+2l(l-1)+2j(j+1)-2m^2+2n(j+l)+n^2]}{(2j+n-1)(2j+n+3)}\Big] \\
& -\ \frac{(l-j+|m|-2)(l+j+n-|m|+1)}{16(2j+5+n)(2j+n+3)^2}\Big[(l-j+|m|-4)(j+l+n-|m|+3) \\
& +\ 4(2j+n+5)\frac{[-1+2l(l-1)+2j(j+1)-2m^2+2n(j+l)+n^2]}{(2j+n-1)(2j+n+3)}\Big]\Bigg\} \\
& +\ \mathcal{O}\!\left((a\tilde{\omega})^6\right).
\end{aligned}
\tag{2.69}
$$

The analytic form of the angular eigenvalue was studied in detail in the context of previous works focusing on the emission of massless scalars [152, 151] and gravitons [19] in the bulk. It was found that its value, when terms up to 5th order or higher are kept, is remarkably close to the exact numerical value and that considerable deviations appear only for a very large angular momentum of the black hole or energy of the emitted particle, that lie beyond the range of values considered in this work. For this reason, the analytic form (2.69) of the angular eigenvalue will be employed in the derivation of the absorption probability in both an analytic and numerical method. We should still demand of course the convergence of the power series by imposing restrictions on the allowed values of the integer parameters (j,ℓ,m) that specify the emission mode: m, that denotes the angular momentum of the mode along our brane, may take any integer value while ℓ and j – the angular momentum number in the n-sphere and total angular momentum number, respectively – may take any positive or zero integer value provided [166] that $j \geq \ell + |m|$ and $\frac{j-(\ell+|m|)}{2} \in \{0, \mathbb{Z}^+\}$.

The Absorption Probability in the Bulk

For the derivation of the absorption probability $|\mathcal{A}_{j\ell m}|^2$ we need the solution for the radial function $R(r)$. We will first solve eq. (2.66) analytically by using an approximate method, and we will derive an analytic expression for the absorption probability which in principle is valid in the low-energy and low-angular-momentum limit. We will then solve the same equation numerically to derive the exact value of $|\mathcal{A}_{j\ell m}|^2$, that will subsequently be used to derive the Hawking radiation spectrum. The two sets of results will be compared, and the validity of the approximate method will be studied in terms of the value of the angular-momentum parameter a, number of extra dimensions n and mass of the emitted particle m_Φ.

The approximate analytic method amounts to solving the radial equation in the two asymptotic regimes, those of the black-hole horizon and far away from it, and

then matching them in an intermediate regime. Apart from the appearance of the mass parameter m_Φ, the analysis is very similar to the one for the emission of massless scalar fields in the bulk which has already appeared in the literature [152]. Therefore, here we briefly present the analysis and results giving emphasis to the differences arising due to the presence of the mass term.

In terms of the new radial variable [144, 145]

$$r \to f(r) = \frac{\Delta(r)}{r^2 + a^2},$$ (2.70)

the radial equation (2.66) near the horizon ($r \simeq r_h$) takes the form

$$f(1-f)\frac{d^2 R}{df^2} + (1 - D_* f)\frac{dR}{df} + \left[\frac{K_*^2}{A_*^2 f(1-f)} - \frac{C_*}{A_*^2(1-f)}\right] R = 0,$$ (2.71)

where

$$A_* \equiv (n+1) + (n-1)a_*^2 \qquad \text{and} \qquad D_* \equiv 1 - 4a_*^2/A_*^2,$$ (2.72)

while K_* and C_* are defined as

$$K_* = (1+a_*^2)\omega r_h - a_* m, \qquad C_* = \left[\ell(\ell+n-1)a_*^2 + \tilde{\Lambda}_{j\ell m} + m_\Phi^2 r_h^2\right](1+a_*^2),$$ (2.73)

respectively. By employing the transformation

$$R_{NH}(f) = f^\alpha (1-f)^\beta F(f)$$ (2.74)

eq. (2.71) takes the form of a hypergeometric differential equation [165] as long as

$$\alpha_\pm = \pm\frac{iK_*}{A_*}, \qquad \beta = \frac{1}{2}\left[(2 - D_*) - \sqrt{(D_*-2)^2 - 4\left(\frac{K_*^2 - C_*}{A_*^2}\right)}\right].$$ (2.75)

The radial function $R_{NH}(f)$ must satisfy the boundary condition that no outgoing modes exist near the black-hole horizon which then reduces the general solution of the hypergeometric equation to the physically acceptable one

$$R_{NH}(f) = A_- f^\alpha (1-f)^\beta F(a, b, c; f),$$ (2.76)

with $a = \alpha + \beta + D_* - 1$, $b = \alpha + \beta$, $c = 1 + 2\alpha$ and A_- an integration constant. Indeed, we may easily check that in the limit $r \to r_h$ (or equivalently $f \to 0$), and by making the choice $\alpha = \alpha_-$, we obtain

$$R_{NH}(f) \simeq A_- f^{-iK_*/A_*} = A_- e^{-iky}.$$ (2.77)

that has a form of an incoming plane-wave, as expected, in terms of a tortoise-like coordinate defined by $y = r_h(1 + a_*^2)\ln(f)/A_*$. In the above, k is given by

$$k \equiv \frac{K_*}{r_h(1+a_*^2)} = \omega - m\Omega_h = \omega - \frac{ma}{r_h^2 + a^2},$$ (2.78)

where Ω_h is the rotation velocity of the black hole.

In the far-field regime $(r \gg r_h)$, the substitution $R(r) = r^{-\left(\frac{n+1}{2}\right)} \tilde{R}(r)$ brings eq. (2.66) into the form of a Bessel equation [165]

$$\frac{d^2\tilde{R}}{dz^2} + \frac{1}{z}\frac{d\tilde{R}}{dz} + \left(1 - \frac{\tilde{E}_{j\ell m} + a^2\tilde{\omega}^2 + \left(\frac{n+1}{2}\right)^2}{z^2}\right)\tilde{R} = 0\,, \qquad (2.79)$$

in terms of $z \equiv \tilde{\omega}r$, with solution

$$R_{FF}(r) = \frac{B_1}{r^{\frac{n+1}{2}}}\,J_\nu\left(\tilde{\omega}r\right) + \frac{B_2}{r^{\frac{n+1}{2}}}\,Y_\nu\left(\tilde{\omega}r\right)\,. \qquad (2.80)$$

In the above, J_ν and Y_ν are the Bessel functions of the first and second kind, respectively, and $\nu = \sqrt{\tilde{E}_{j\ell m} + a^2\tilde{\omega}^2 + \left(\frac{n+1}{2}\right)^2}$.

We now need to smoothly match the two asymptotic solutions (2.76) and (2.80) in an intermediate regime in the same way as in the case of graviton emission. The near-horizon solution (2.76) must first be shifted, so that its argument changes from f to $(1-f)$, and subsequently expanded in the $r \gg r_h$ limit. Then, it takes the polynomial form

$$R_{NH}(r) \simeq A_1\,r^{-(n+1)\,\beta} + A_2\,r^{(n+1)\,(\beta+D_*-2)}\,, \qquad (2.81)$$

with A_1 and A_2 defined as

$$\begin{aligned} A_1 &= A_-\left[(1+a_*^2)\,r_h^{n+1}\right]^\beta\,\frac{\Gamma(c)\Gamma(c-a-b)}{\Gamma(c-a)\Gamma(c-b)}\,, \\[2mm] A_2 &= A_-\left[(1+a_*^2)\,r_h^{n+1}\right]^{-(\beta+D_*-2)}\,\frac{\Gamma(c)\Gamma(a+b-c)}{\Gamma(a)\Gamma(b)}\,. \end{aligned} \qquad (2.82)$$

The far-field solution (2.80) is in turn expanded to small values of r leading to

$$R_{FF}(r) \simeq \frac{B_1\left(\frac{\tilde{\omega}r}{2}\right)^\nu}{r^{\frac{n+1}{2}}\,\Gamma(\nu+1)} - \frac{B_2}{\pi\,r^{\frac{n+1}{2}}}\,\frac{\Gamma(\nu)}{\left(\frac{\tilde{\omega}r}{2}\right)^\nu}\,. \qquad (2.83)$$

The two polynomial forms match perfectly if we take the small a_* and $\tilde{\omega}_*$ limit in the power coefficients of r. In that case we can ignore terms of order $(\tilde{\omega}_*^2, a_*^2, a_*\tilde{\omega}_*)$ or higher, and obtain

$$\begin{aligned} (n+1)\,\beta &\simeq -j, & (2.84) \\[2mm] \nu &\simeq j + \frac{n+1}{2} & \text{and} \\[2mm] (n+1)\,(\beta+D_*-2) &\simeq -(j+n+1). \end{aligned}$$

We then demand the matching of the corresponding multiplicative coefficients, which leads to a constraint for the far-asymptotic integration constants B_1 and B_2, namely

$$B \equiv \frac{B_1}{B_2} = -\frac{1}{\pi}\left(\frac{2}{\tilde{\omega}r_h\,(1+a_*^2)^{\frac{1}{n+1}}}\right)^{2j+n+1}\sqrt{\tilde{E}_{j\ell m} + a^2\tilde{\omega}^2 + \left(\frac{n+1}{2}\right)^2}$$

$$\times\,\frac{\Gamma^2\left(\sqrt{\tilde{E}_{j\ell m} + a^2\tilde{\omega}^2 + \left(\frac{n+1}{2}\right)^2}\right)\Gamma(\alpha+\beta+D_*-1)\,\Gamma(\alpha+\beta)\,\Gamma(2-2\beta-D_*)}{\Gamma(2\beta+D_*-2)\,\Gamma(2+\alpha-\beta-D_*)\,\Gamma(1+\alpha-\beta)}\,, \qquad (2.85)$$

that guarantees the existence of a smooth, analytic solution for the radial part of the wavefunction for all r, valid in the low-energy and low-rotation limit. We stress that, in order to achieve a higher level of accuracy in our analysis, no expansion is performed in the arguments of the Gamma functions. This method has been used in the literature before to derive analytic solutions for brane [144] and bulk [152] massless scalar fields. In both cases, the analytic results were shown to be in excellent agreement with the exact numerical ones in the low-energy regime and quite often at the intermediate-energy regime too.

In the presence of the mass term, though, there is one more constraint that needs to be satisfied for the perfect match to take place. In the low-energy and low-angular-momentum limit, the expression for the parameter β, eq. (2.75), becomes

$$\beta \simeq \frac{1}{2} \left[1 - \frac{1}{(n+1)} \sqrt{(2j+n+1)^2 + 4m_\Phi^2 r_h^2} \right]. \tag{2.86}$$

For $j \geq 0$ and $n \geq 1$, we thus need to satisfy $m_\Phi r_h < 1$. In order to derive some quantitative results, let us assume that $M_* = 1$ TeV and $M = 5$ TeV. If we ignore for a moment the angular momentum of the black hole and use the mass-horizon radius relation for a higher-dimensional Schwarzschild black hole, we find $r_h \simeq (4-2)\,10^{-4}$ fm for $n = 1 - 7$, respectively [84, 98]. Then, the aforementioned constraint on the mass of the bulk scalar field translates to

$$m_\Phi < (0.5 - 1)\,\text{TeV}, \qquad \text{for} \quad n = 1 - 7. \tag{2.87}$$

If we reinstate the angular momentum of the black hole, then the value of the black-hole horizon, for the same mass, becomes smaller since $r_h^{n+1} = \mu/(1 + a_*^2)$; therefore, the upper bound on the mass of the scalar field increases further and becomes easier to satisfy.

In order to define the absorption probability, we finally expand the far-field solution (2.80) for $r \to \infty$, and obtain

$$\begin{aligned} R_{FF}(r) &\simeq \frac{1}{r^{\frac{n+2}{2}}\sqrt{2\pi\tilde{\omega}}} \left[(B_1 + iB_2)\,e^{-i\left(\tilde{\omega}r - \frac{\pi}{2}\nu - \frac{\pi}{4}\right)} + (B_1 - iB_2)\,e^{i\left(\tilde{\omega}r - \frac{\pi}{2}\nu - \frac{\pi}{4}\right)} \right] \\ &= A_{in}^{(\infty)}\frac{e^{-i\tilde{\omega}r}}{r^{\frac{n+2}{2}}} + A_{out}^{(\infty)}\frac{e^{i\tilde{\omega}r}}{r^{\frac{n+2}{2}}}, \end{aligned} \tag{2.88}$$

which readily leads to

$$|\mathcal{A}_{j\ell m}|^2 = 1 - \left| \frac{A_{out}^{(\infty)}}{A_{in}^{(\infty)}} \right|^2 = 1 - \left| \frac{B_1 - iB_2}{B_1 + iB_2} \right|^2 = \frac{2i\,(B^* - B)}{BB^* + i\,(B^* - B) + 1}. \tag{2.89}$$

The above expression, in conjunction with eq. (2.85), is our final analytic result for the absorption probability for massive scalar fields emitted in the bulk by a higher-dimensional, simply-rotating black hole. Summarizing all of the aforementioned assumptions, it is valid as long as the energy and mass of the emitted particle and the
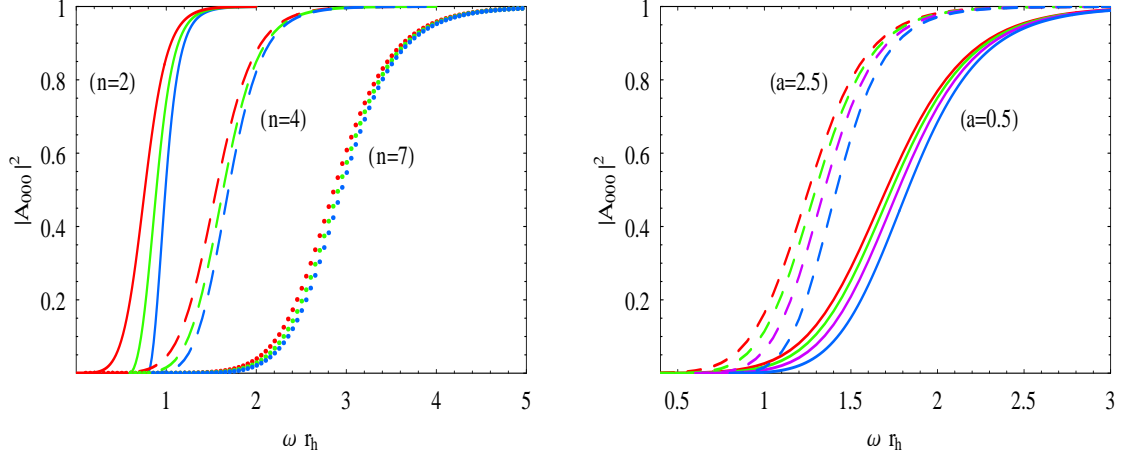
Figure 2.9: Absorption probabilities for the bulk scalar mode $j = \ell = m = 0$, for **(a)** $a_* = 1$, $m_\Phi = 0, 0.6, 0.8$ (from left to right) and various n, and **(b)** $n = 4$, $m_\Phi = 0, 0.4, 0.6, 0.8$ (from left to right) and various a_*.

angular-momentum of the black hole stay below unity (in units of r_h^{-1} and r_h, respectively). Its range of validity will be shortly investigated in terms of the values of the above parameters, as well as that of the number of extra dimensions n.

Equation (2.89) is also useful for studying analytically various aspects of the absorption probability such as its behavior in the superradiant regime and the asymptotic limit $\tilde\omega \to 0$. If we expand eq. (2.89) in the low-energy limit, a more convenient form may be derived for both purposes – a similar analysis was presented in all detail in [144] where the emission of massless scalar fields on the brane by the same type of black hole was studied. From eq. (2.85) we see that, in that limit, we obtain $B \propto 1/\tilde\omega^{2j+n+1}$, and therefore

$$|\mathcal{A}_{j\ell m}|^2 \simeq 2i \left(\frac{1}{B} - \frac{1}{B^*} \right) = \Sigma_1 \times \Sigma_2 \times \Sigma_3 \,, \tag{2.90}$$

where

$$\Sigma_1 = \frac{-2i\pi \, (\tilde\omega r_h/2)^{2j+n+1}}{(j + \frac{n+1}{2}) \, \Gamma^2(j + \frac{n+1}{2})} \frac{(1 + a_*^2)^{\frac{2j+n+1}{n+1}} \, \Gamma(2\beta + D_* - 2)}{\Gamma(2 - 2\beta - D_*)} \,, \tag{2.91}$$

$$\Sigma_2 = \frac{1}{|\Gamma(\alpha + \beta + D_* - 1)|^2 \, |\Gamma(\alpha + \beta)|^2} \,, \tag{2.92}$$

and

$$\begin{aligned} \Sigma_3 &= \Gamma(2 + \alpha - \beta - D_*) \, \Gamma(-\alpha + \beta + D_* - 1) \, \Gamma(1 + \alpha - \beta) \, \Gamma(-\alpha + \beta) - (cc) \\ &= \frac{-\pi^2 \, \sin(2\pi\alpha) \, \sin \pi(2\beta + D_*)}{\sin \pi(\alpha + \beta + D_*) \, \sin \pi(-\alpha + \beta + D_*) \, \sin \pi(\alpha + \beta) \, \sin \pi(-\alpha + \beta)} \,. \end{aligned} \tag{2.93}$$

The (cc) term above stands for the complex conjugate of the corresponding expression. As the energy of the emitted mode decreases, moving towards the asymptotic limit

$\tilde{\omega} \to 0$, for modes with $m > 0$, we meet the value $\omega = \omega_s \equiv m\Omega_h$. From eqs. (2.75) and (2.78), it is clear that for that value $\alpha \to 0$, in which case eq. (2.90) gets simplified to

$$|\mathcal{A}_{j\ell m}|^2 = \frac{4\pi \, (\tilde{\omega} r_h/2)^{2j+n+1} \, K_* \, \sin^2 \pi(2\beta + D_*) \, \Gamma^2(2\beta + D_* - 2) \, \Gamma^2(1-\beta) \, (2 - D_* - 2\beta)}{A_* \, (1 + a_*^2)^{-\frac{2j+n+1}{n+1}} \, (j + \frac{n+1}{2}) \, \Gamma^2(j + \frac{n+1}{2}) \, \Gamma^2(\beta + D_* - 1) \, \sin^2 \pi(\beta + D_*)} \, .$$
$$(2.94)$$

In the above expression, all terms are positive definite, including the $(2 - D_* - 2\beta)$ one, apart from K_* whose sign, as expected, defines the sign of the absorption probability: for $\omega < \omega_s$, $(\omega - m\,\Omega_h)$ takes a negative value signalling the occurrence of superradiance.

For modes with $m \leq 0$, there is no superradiance effect, and we may thus approach the asymptotic limit $\tilde{\omega} \to 0$. From the coefficient $(\tilde{\omega} r_h)^{2j+n+1}$ in the expression of Σ_1 it is clear that, in the massive case, too, it is the lowest partial modes that dominate the value of the absorption probability in the low-energy regime. We will therefore focus our attention on the dominant mode $j = \ell = m = 0$, and derive the behavior of the absorption probability in the above asymptotic limit. Although for massive modes with $m \leq 0$ the parameter α never becomes exactly zero, it acquires its smallest possible value as $\tilde{\omega} \to 0$. Equation (2.94) therefore remains approximately valid, and, for $j = \ell = m = 0$ and $\beta = 0 + \mathcal{O}(\tilde{\omega}^2)$, it is simplified further to give

$$|\mathcal{A}_{000}|^2 = \frac{4\pi(1 + a_*^2)^2(\tilde{\omega} r_h)^{n+1}\omega r_h}{A_* \, 2^n(n+1)\Gamma^2\left(\frac{n+1}{2}\right)(2 - D_*)} + \ldots \, . \tag{2.95}$$

We may also compute the absorption cross-section σ_{000} for the dominant massive scalar bulk mode in the asymptotic low-energy regime by using the formula [184, 185, 186, 152]

$$\sigma_{j\ell m}(\omega) = \frac{2^n}{\pi}\Gamma^2\left(\frac{n+3}{2}\right)\frac{A_H}{(\tilde{\omega} r_h)^{n+2}}\frac{N_\ell}{(1 + a_*^2)}|\mathcal{A}_{j\ell m}|^2 \, , \tag{2.96}$$

that relates the absorption cross-section with the absorption probability for a scalar mode propagating in the background of a higher-dimensional, simply rotating black hole. In the above

$$N_\ell = \frac{(2\ell + n - 1)(\ell + n - 2)!}{\ell! \, (n-1)!} \, , \qquad A_H = \frac{2\pi^{\frac{n+3}{2}} r_h^n \, (r_h^2 + a^2)}{\Gamma\left(\frac{n+3}{2}\right)} \tag{2.97}$$

are the multiplicity of the ℓ-th partial wave in the expansion of the wave function over the hyperspherical harmonics on the n-sphere [152], and the horizon area of the $(4 + n)$-dimensional rotating black hole, respectively. Substituting for the absorption coefficient, we obtain

$$\sigma_{000}(\omega) \simeq \frac{(n+1)(1 + a_*^2)A_H}{A_*(2 - D_*)}\left(\frac{\omega}{\tilde{\omega}}\right) + \ldots \, . \tag{2.98}$$

For $a_* = 0$ and $m_\Phi = 0$, the above reduces to the horizon area A_H of a higher-dimensional, spherically-symmetric black hole, as was found in [115]. For $a_* \neq 0$ and $m_\Phi = 0$, it was shown in [152, 119, 120, 121, 122, 123, 124] that the value of σ_{000}
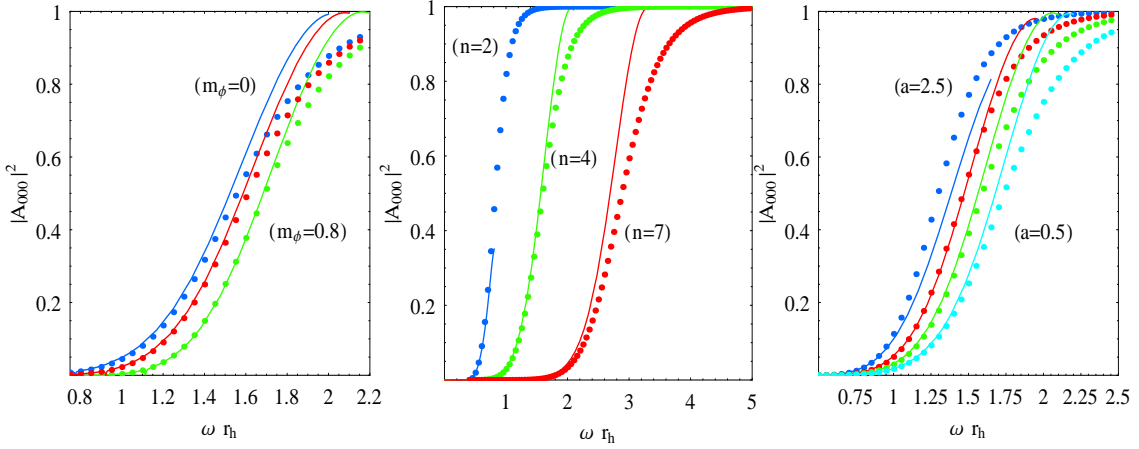
Figure 2.10: Comparison of the analytical (solid lines) and exact numerical (data points) results for the absorption probability for the bulk scalar mode $j = \ell = m = 0$, for **(a)** $a_* = 1$, $n = 4$ and $m_\Phi = 0, 0.5, 0.8$, **(b)** $a_* = 1$, $m_\Phi = 0.4$ and $n = 2, 4, 7$, and **(c)** $n = 4$, $m_\Phi = 0.4$ and $a_* = 0.5, 1, 1.5, 2.5$.

remains very close to the area of the corresponding rotating black hole as long as a_* is not large. For $m_\Phi \neq 0$, we observe significant deviations from this behavior as the value of the absorption cross-section for the lowest partial mode is not only energy-dependent but deviates as $\tilde{\omega} \to 0$ – this is in accordance with previous results derived in the cases of a massive field propagating in the background of a 4-dimensional Kerr [179] or of a $(4 + n)$-dimensional, spherically-symmetric black hole [119, 120, 121, 122, 123, 124]. This behaviour is observed only in the case of the lowest mode; higher modes have a $\tilde{\omega}^{2j+n+1}$ leading factor in their absorption probability, and a $\tilde{\omega}^{2j-1}$ dependence for their absorption cross-section – for $j \geq 1$, this leads to a vanishing value in the asymptotic limit $\tilde{\omega} \to 0$.

For the derivation of the value of the absorption probability, that would be valid for arbitrary values of the energy of the emitted particle and angular momentum of the black hole, we need to solve Eq. (2.66) numerically. To this end, a MATHEMATICA code was constructed that numerically solved for the value of the radial function $R(r)$ from the horizon outwards. The boundary conditions for the second order differential equation was the value of $R(r)$ and its first derivative at the horizon. The asymptotic solution (2.77) was used for that purpose, with the boundary conditions at $r \to r_h$ having the form

$$ R = 1, \qquad \frac{dR}{dr} = -ik \, \frac{dy}{dr} = -\frac{ik(1 + a_*^2)}{\Delta(r)} \,. \tag{2.99} $$

The first condition was imposed to ensure that $|A_-|^2 = 1$ since no outgoing mode is allowed to exist at the horizon. The second follows readily from the asymptotic solution (2.77) and the use of the first condition. The integration proceeds until we reach radial infinity (in practice, this happens for $r \simeq 1000 r_h$) where, according to eq. (2.88), the radial function is a superposition of incoming and outgoing modes. The corresponding

amplitudes are then isolated and the value of the absorption coefficient follows by use of the definition (2.89).

As a consistency check, we have successfully reproduced the numerical results presented in [151] for the case of massless scalar fields emitted in the bulk by a simply rotating black hole - the case with $m_\Phi = 0$ is also included in our plots for easy comparison with the massless case. In Fig. 2.9 we plot the absorption probability for the dominant mode $j = \ell = m = 0$ as a function of the three parameters, m_Φ, n and a, respectively. Figure 2.9(a) was drawn for fixed angular-momentum parameter $(a_* = 1)$, and depicts the dependence of $|\mathcal{A}_{000}|^2$ on the value of mass of the field and number of extra dimensions: we observe that as m_Φ increases the value of the absorption probability decreases as expected, since a larger amount of energy is necessary for the emission of an increasingly more massive field. This pattern holds independently of the value of n, nevertheless, the suppression with m_Φ becomes less important as the number of extra dimensions gets larger. Figure 2.9(a) reveals also that the suppression of the absorption probability with the number of extra dimensions, found previously for massless scalar fields in the bulk [152, 151], holds also for massive fields. In Fig. 2.9(b), we keep fixed the number of extra dimensions $(n = 4)$ and vary m_Φ and a_*: again the suppression with the mass of the field is evident - contrary to what happens with n, the suppression is more prominent as a_* increases, particularly in the low- and intermediate-energy regimes. The enhancement of the absorption probability as a_* itself increases, found again previously in [152, 151], persists also in the massive case.

It would be interesting to compare the exact numerical results for the value of the absorption probability with the ones following from the analytical expression (2.89) with B given by eq. (2.85). In Fig. 2.10 we plot both sets of results for a range of values of the parameters m_Φ, n and a_* – we consider again the dominant scalar bulk mode $j = \ell = m = 0$. Figure 2.10(a) reveals that the agreement between numerical and analytical results holds for a wide range of values of the mass parameter below unity (in units of r_h^{-1}), as indeed expected from the discussion below eq. (2.85) regarding the values of m_Φ. On the other hand, in terms of the number of extra dimensions, the agreement is case-dependent: as we see from Fig. 2.10(b), it is remarkably good for $n = 4$, for $n = 7$ it is limited in the lower part of the curves while for $n = 2$ it stops abruptly as the analytical result suffers from the existence of poles in the arguments of the Gamma functions that force the value of $|\mathcal{A}_{000}|^2$ to dip towards smaller values and eventually vanish. The expression for B, eq. (2.85), is clearly the result of an approximation method valid for small values of the angular-momentum parameter, and thus we expect the agreement between the two sets of results to become worse as the value of a_* increases gradually; however, in Fig. 2.10(c), we see that the agreement is actually improving as the angular-momentum parameter increases reaching values even beyond unity, a result that holds only in the presence of the mass term of the scalar field.

Let us finally comment on the behavior of the superradiance [187] on the parameters of the theory. In the context of the general suppression of the value of the absorption probability as the mass of the field increases, we expect that the effect of the superradiance will also be suppressed – this is indeed depicted in Fig. 2.11(a) where the value
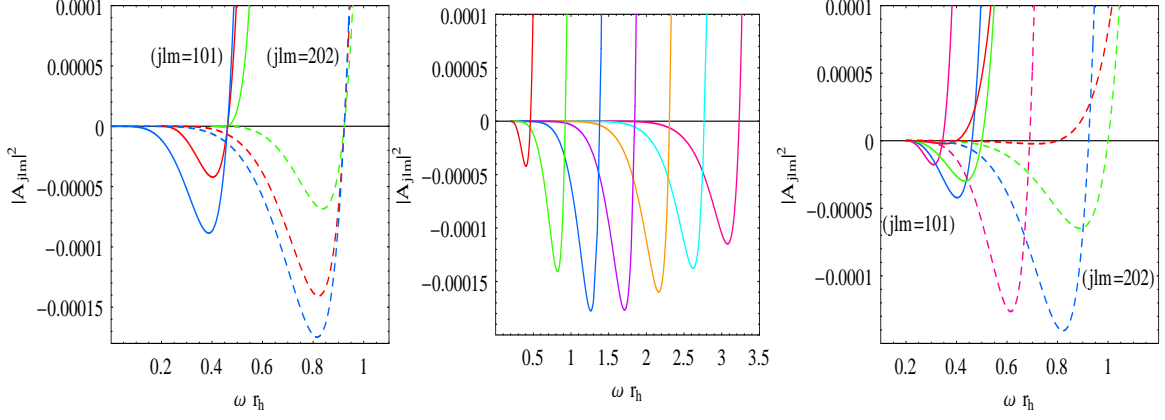
Figure 2.11: The dependence of superradiance for bulk massive scalar modes on **(a)** the mass, for $a_* = 1.5$, $n = 2$ and $m_\Phi = 0, 0.2, 0.4$ (from bottom to top), **(b)** on the angular momentum numbers, for $a_* = 1.5$, $n = 2$, $m_\Phi = 0.2$ and $j = m = 1, 2, 3, 4, 5, 6, 7$ (from left to right), and **(c)** on the angular momentum parameter, for $n = 2$, $m_\Phi = 0.2$ and $a_* = 0.5$ (red), 1 (green), 1.5 (blue), 2.5 (magenta).

of $|\mathcal{A}_{j\ell m}|^2$ is plotted for various values of m_Φ for the indicative modes $(j\ell m = 101)$ and $(j\ell m = 202)$. Despite the observed dominance of the superradiance effect for the mode $(j\ell m = 202)$ over the one for $(j\ell m = 101)$, this pattern does not hold indefinitely as the angular momentum numbers increase: in fact, from Fig. 2.11(b), where we plot the superradiant regime for the modes $j = m = 1, 2, ..., 7$ for $m_\Phi = 0.2$, $n = 2$ and $a_* = 1.5$, it is clear that the mode $j = m = 3$ is the dominant superradiant one, a result that was also found in the massless case [151]. The suppression of the superradiance with the number of extra dimensions observed in [151] for massless bulk scalar modes holds also in the massive case, and thus we do not comment further. A feature that has not been noted before is the non-monotonic behavior of both the magnitude of the superradiance effect and the extent of the superradiant regime in terms of the angular-momentum parameter a_*: in Fig. 2.11(c), we see that, as a_* increases from zero to 1.5, the superradiance effect is indeed enhanced, however, this behavior is reversed when a_* increases further. In addition, superradiance occurs for frequencies $m_\Phi < \omega < \omega_s = ma/(r_h^2 + a^2)$: the latter restriction is imposed by the vanishing of the value of the absorption probability; the former by the demand that its value is a real number, and signifies the fact that no particles of mass m_Φ can be created if energy less than that is available. Interestingly enough the width of the superradiance regime, $\delta\omega = ma/(r_h^2 + a^2) - m_\Phi$, does not monotonically grow with the increase of the angular momentum of the black hole, as one could instinctively expect. Indeed, its value reaches a maximum for a particular value of the angular-momentum parameter, namely $a = \pm r_h$, which is in fact independent of the mass and angular momentum numbers of the mode as well as of the number of extra dimensions [4]. For the case de-

---

[4]The monotonic behavior of the width and depth of the superradiance regime found in [152] is not
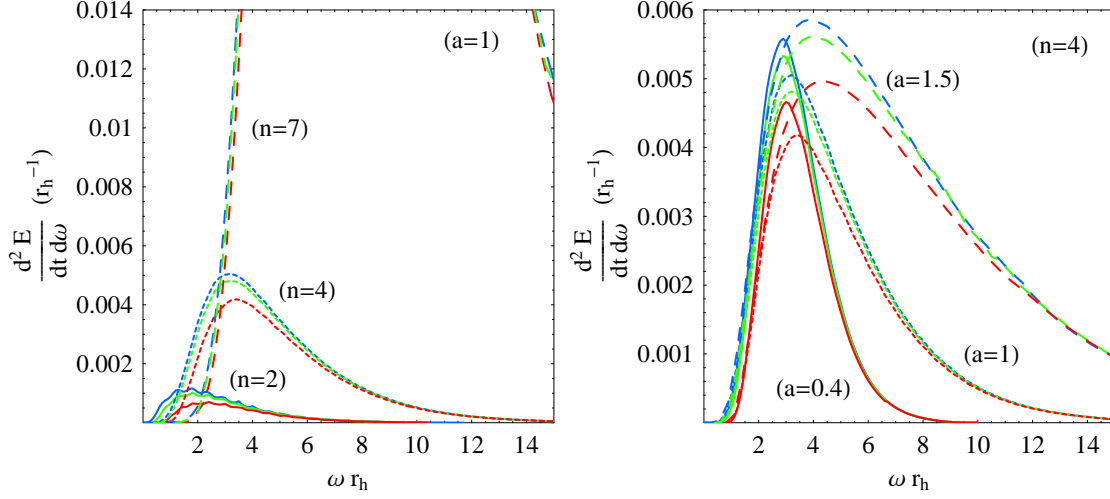
Figure 2.12: Energy emission rates for bulk scalar fields for: **(a)** for $a_* = 1$, $n = 2, 4, 7$ and $m_\Phi = 0, 0.4, 0.8$ (from top to bottom in each set of curves with fixed n), and **(b)** $n = 4$, $a_* = 0.4, 1, 1.5$ and $m_\Phi = 0, 0.4, 0.8$ (from top to bottom in each set of curves with fixed a_*).

picted in Fig. 2.11(c), where we have fixed the horizon value at $r_h = 1$ and considered only positive values of a_*, the superradiant regime takes its maximum value at $a_* = 1$, beyond which it starts to shrink, for both modes $(j\ell m = 101)$ and $(j\ell m = 202)$.

Energy Emission Rate in the Bulk

We will next compute the rate of energy emission in the bulk in the form of massive scalar fields by using the exact numerical results for the absorption probability found in the previous section. The emission of energy per unit frequency and unit time in the bulk is given by the expression [179, 152, 151]

$$\frac{d^2E}{dtd\omega} = \frac{1}{2\pi} \sum_{j,\ell,m} \frac{\omega}{\exp\left[k/T_H\right] - 1} N_\ell \left|\mathcal{A}_{j\ell m}\right|^2 . \tag{2.100}$$

The multiplicity of states N_ℓ from the expansion of the wavefunction of the field in the n-dimensional sphere is given in eq. (2.97) and the parameter k is defined in eq. (2.78). Finally, the temperature of the higher-dimensional, simply-rotating black hole (2.1) is the one given by eq. (2.6).

   Equation (2.100) is identical in form with the expression for the emission of massless scalar fields in the bulk, nevertheless, there are two major differences: the calculation of the spectrum starts from $\omega = m_\Phi$ instead of zero, and the value of the absorption

---

in contradiction with the results found here as only low values of the angular momentum of the black hole, lower than the turning points found here and in agreement with the low-a_* approximation used in [152], were considered in there.

probability depends, apart from the space-time parameters, on the characteristics of the emitted field including its mass.

In order to derive the energy emission spectrum, we need to sum over a significantly large number of partial waves labeled by the set of (j, ℓ, m) quantum numbers. For each value of n, a_* and m_Φ, we aimed at deriving the complete spectrum, i.e. to reach values of the energy parameter ωr_h where the corresponding value of the energy emission rate would be less than 10^{-6}. At the same time, the number of partial waves summed had to be large enough so that the derivation of the energy spectrum would be as close as possible to the real one – especially for the computation of the total emissivity presented in section 4. Taking all these constraints into account, we were able to sum the contribution of all bulk scalar modes up to $j = 30$, that brings the total number of summed modes to $N_{\mathrm{bu}} = 5456$. According to our estimates, the contribution of all modes higher than $j = 30$ should be less than 5%, for the higher values of parameters considered, namely $n = 7$ and $a_* = 1.5$, an error that falls below 0.001% for the lowest values considered, i.e. $n = 2$ and $a_* = 0.4$.

In Fig. 2.12, we depict the energy emission rate on the brane in the form of massive scalar fields in terms of the number of extra dimensions, value of the angular-momentum parameter, and mass of the emitted field itself. Thus, Fig. 2.12(a) shows the energy emission rate for fixed a_* ($a_* = 1$) and variable $n = 2, 4, 7$ and $m_\Phi = 0, 0.4, 0.8$, while Fig.2.12(b) plots the same quantity but for fixed n ($n = 4$) and variable $a_* = 0.4, 1, 1.5$. In terms of the space-time parameters n and a_*, these plots confirm the behavior found in the case of massless fields [152, 151]: the power spectrum is enhanced as the number of extra dimensions increases while its dependence on the angular momentum parameter is not monotonic but differs as n and/or ω varies. More detailed features, like the oscillatory pattern of the emission curves for low values of n and a_*, that are replaced by more smoother curves as the values of these parameters increase, are also recovered.

In terms of the mass of the scalar field, we observe the expected suppression of the emission rate, for fixed n and a_*, as m_Φ increases – the suppression is more prominent in the low- and intermediate-energy regimes whereas the effect of the mass becomes negligible at the high-energy regime. Compared to the case of the emission of masless scalar fields, the suppression in the low-energy regime becomes even more significant if the disappearance of the frequency range with $\omega < m_\Phi$ is taken into account. The magnitude of the suppression with m_Φ depends strongly on the particular value of n and a_* – the exact effect will be computed in section 4 where the total emissivities in bulk and brane will be calculated.

2.3.2   Emission of Massive Scalars on the Brane

In this section, we turn our attention to the emission of massive scalar fields by a higher-dimensional simply-rotating black hole on the brane. The analysis for the derivation of the absorption probability, both analytical and numerical, is quite similar to the one performed for the emission in the bulk; aspects of it have also been recently addressed in a set of publications [180, 181] that appeared while this work was still in progress. For the sake of comparison and completeness of the analysis, we will still present in

this section the most important points of our calculation on the brane and focus our discussion to aspects not covered before; these include, for example, the analytic study of the low-energy asymptotic behavior of the absorption probability and cross-section, the role of the angular momentum of the black hole, that was ignored in [180, 181], and the form of the energy emission spectrum, instead of the number flux that was studied in the same work.

Let us start with the form of the gravitational background that a massive scalar field sees as it propagates on the brane and its corresponding field equation. The 4-dimensional induced background will be the projection of the higher-dimensional one (2.1) onto the brane, and follows by fixing the values of the angular variables of the n-sphere. Then, the induced-on-the-brane line-element takes the form

$$ds^2 = \left(1 - \frac{\mu}{\Sigma\,r^{n-1}}\right) dt^2 + \frac{2a\mu\sin^2\theta}{\Sigma\,r^{n-1}}\,dt\,d\varphi - \frac{\Sigma}{\Delta}dr^2$$

$$- \Sigma\,d\theta^2 - \left(r^2 + a^2 + \frac{a^2\mu\sin^2\theta}{\Sigma\,r^{n-1}}\right)\sin^2\theta\,d\varphi^2\,, \tag{2.101}$$

which is very similar to the usual 4-dimensional Kerr one but carries an explicit dependence on the number of additional spacelike dimensions n. The field equation is still given by the covariant form (2.62) but with the higher-dimensional metric tensor G_{MN} replaced by the 4-dimensional one $g_{\mu\nu}$ defined above. The field factorization

$$\Phi(t, r, \theta, \varphi) = e^{-i\omega t}\,e^{im\varphi}\,P(r)\,T(\theta)\,, \tag{2.102}$$

leads again to the decoupling of variables and to the following set of radial and angular equations

$$\frac{d}{dr}\left(\Delta\frac{dP}{dr}\right) + \left(\frac{K^2}{\Delta} - \tilde{\Lambda}_{jm} - m_\Phi^2 r^2\right) P = 0\,, \tag{2.103}$$

$$\frac{1}{\sin\theta}\frac{d}{d\theta}\left(\sin\theta\frac{dT}{d\theta}\right) + \left(\tilde{\omega}^2 a^2\cos^2\theta - \frac{m^2}{\sin^2\theta} + \tilde{E}_{jm}\right)T = 0\,, \tag{2.104}$$

respectively. In the above, we have defined $\tilde{\Lambda}_{jm} = \tilde{E}_{jm} + a^2\omega^2 - 2am\omega$, while $\tilde{\omega}$ is again given by $\tilde{\omega} = \sqrt{\omega^2 - m_\Phi^2}$ and K by eq. (2.68). The angular function $T(\theta)$ satisfies again a modified spheroidal harmonics equation with $\omega \to \tilde{\omega}$. The corresponding massive eigenvalue $\tilde{E}_{jm}(a\tilde{\omega})$ is thus related to the massless one through the same shift, and in terms of a power series [188, 189, 190] is given by

$$\begin{aligned}
\tilde{E}_{jm} &= j\,(j+1) + (a\tilde{\omega})^2\,\frac{[2m^2 - 2j\,(j+1) + 1]}{(2j-1)\,(2j+3)} \\
&+ (a\tilde{\omega})^4\,\left\{\frac{2\,[-3 + 17j\,(j+1) + j^2(j+1)^2(2j-3)\,(2j+5)]}{(2j-3)\,(2j+5)\,(2j+3)^3(2j-1)^3}\right. \\
&+ \frac{4m^2}{(2j-1)^2(2j+3)^2}\left[\frac{1}{(2j-1)\,(2j+3)} - \frac{3j\,(j+1)}{(2j-3)\,(2j+5)}\right] \\
&+ \left.\frac{2m^4\,[48 + 5(2j-1)\,(2j+3)]}{(2j-3)\,(2j+5)\,(2j-1)^3(2j+3)^3}\right\} + \mathcal{O}\left((a\tilde{\omega})^6\right)\,, \tag{2.105}
\end{aligned}$$

The above form will be used in the computation of the absorption probability both analytically and numerically.

The Absorption Probability on the Brane

The approximation method employed in section 2.3.1 can again be used to solve the radial equation (2.103) analytically. The same change of variable $r \to f(r) = \Delta(r)/(r^2 + a^2)$, in the near-horizon regime $(r \simeq r_h)$, leads to an equation of the form (2.71) where now

$$D_* \equiv 1 + \frac{n\,(1 + a_*^2)}{A_*} - \frac{4a_*^2}{A_*^2}, \qquad C_* \equiv (\tilde{\Lambda}_{jm} + m_\Phi^2 r_h^2)\,(1 + a_*^2), \qquad (2.106)$$

while A_* and K_* are defined as in the bulk. The field redefinition $P(f) = f^\alpha(1 - f)^\beta F(f)$ reduces the above differential equation to a hypergeometric one with the physically acceptable solution in the near-horizon regime given by

$$P_{NH}(f) = A_-\, f^\alpha\,(1 - f)^\beta\, F(a, b, c; f). \qquad (2.107)$$

In the above, A_- is again an arbitrary integration constant, and $a = \alpha + \beta + D_* - 1$, $b = \alpha + \beta$, $c = 1 + 2\alpha$. The power coefficients α and β are given by the expressions in eq. (2.75), with D_* and C_* now taken their brane values. Under the choice $\alpha = \alpha_-$, that we will henceforth use, the above solution reduces, as expected, to an ingoing plane wave, $P_{NH} \simeq A_-\, f^{-iK_*/A_*} = A_-\, e^{-iky}$ with k defined in eq. (2.78).

In the far-field regime $(r \gg r_h)$, the radial equation (2.103), under the substitution $P(r) = \frac{1}{\sqrt{r}}\,\tilde{P}(r)$, takes again the form of a Bessel differential equation leading to the general solution

$$P_{FF}(r) = \frac{B_1}{\sqrt{r}}\, J_\nu\,(\tilde{\omega}r) + \frac{B_2}{\sqrt{r}}\, Y_\nu\,(\tilde{\omega}r), \qquad (2.108)$$

where now $\nu = \sqrt{\tilde{E}_{jm} + a^2\tilde{\omega}^2 + 1/4}$.

The process of the matching proceeds as in the case of bulk emission. The near-horizon solution (2.107), after it is shifted, is expanded in the limit $r \gg r_h$, while the far-field one (2.108) is expanded in the $r \to 0$ limit. Both reduce to polynomial forms similar to those in eqs. (2.81) and (2.83). If we again ignore terms of order $(\tilde{\omega}_*^2, a_*^2, a_*\tilde{\omega}_*)$ or higher in the power coefficients, we obtain $-(n + 1)\beta \simeq j$, $(n + 1)(\beta + D_* - 2) \simeq -(j + 1)$, and $\nu \simeq j + 1/2$. These simplifications hold provided that the mass of the scalar field on the brane does not exceed an upper value: following a similar argument to the case of the bulk emission, this constraint is found to be $m_\Phi < (250 - 500)\,\text{GeV}$ for $n = 1 - 7$ – note that the upper value of the mass on the brane is reduced by a factor of two compared to the one in the bulk. Then, the matching of the corresponding multiplicative in the coefficients, leads to the constraint

$$B \equiv \frac{B_1}{B_2} = -\frac{1}{\pi}\left(\frac{2}{\tilde{\omega}r_h\,(1 + a_*^2)^{\frac{1}{n+1}}}\right)^{2j+1} \sqrt{\tilde{E}_{jm} + a^2\tilde{\omega}^2 + 1/4}$$

$$0.1cm \quad \times \quad \frac{\Gamma^2\left(\sqrt{\tilde{E}_{jm} + a^2\tilde{\omega}^2 + 1/4}\right)\Gamma(\alpha + \beta + D_* - 1)\,\Gamma(\alpha + \beta)\,\Gamma(2 - 2\beta - D_*)}{\Gamma(2\beta + D_* - 2)\,\Gamma(2 + \alpha - \beta - D_*)\,\Gamma(1 + \alpha - \beta)} \qquad (2.109)$$
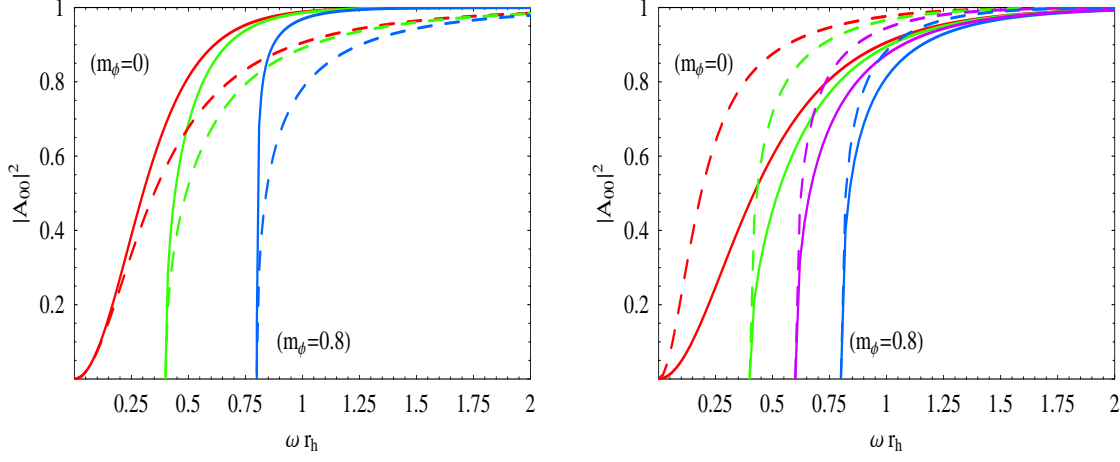
Figure 2.13: Absorption probabilities for the brane scalar mode $j = m = 0$, for **(a)** $a_* = 1$, $m_\Phi = 0, 0.4, 0.8$ and $n = 2$ (solid lines) and 7 (dashed lines), and **(b)** $n = 4$, $m_\Phi = 0, 0.4, 0.6, 0.8$ and $a_* = 0.5$ (solid lines) and 2.5 (dashed lines).

The above completes the derivation of the analytic solution for the radial part of the massive scalar field on the brane. By expanding the far-field solution (2.108) at asymptotic infinity, we recover again a superposition of spherical waves

$$ P_{FF}(r) \simeq \frac{1}{\sqrt{2\pi\tilde{\omega}}} \left[\frac{(B_1 + iB_2)}{r} e^{-i\left(\tilde{\omega}r - \frac{\pi}{2}\nu - \frac{\pi}{4}\right)} + \frac{(B_1 - iB_2)}{r} e^{i\left(\tilde{\omega}r - \frac{\pi}{2}\nu - \frac{\pi}{4}\right)} \right] (2.110) $$

The absorption probability for the brane emission $|\mathcal{A}_{jm}|^2$ is then given again by the right-hand-part of Eq. (2.89) with B in this case defined in eq. (2.109).

At the very low-energy regime, we may again derive a simplified, compact expression for the absorption probability. Following the same analysis as in the case of bulk emission, we obtain $|\mathcal{A}_{jm}|^2 = \Sigma_1 \times \Sigma_2 \times \Sigma_3$, where

$$ \Sigma_1 = \frac{-2i\pi \ (\tilde{\omega}r_h/2)^{2j+1}}{(j + \frac{1}{2}) \, \Gamma^2(j + \frac{1}{2})} \frac{(1 + a_*^2)^{\frac{2j+1}{n+1}} \, \Gamma(2\beta + D_* - 2)}{\Gamma(2 - 2\beta - D_*)}, \qquad (2.111) $$

while Σ_2 and Σ_3 are given by the corresponding bulk equations (2.92) and (2.93) but with the parameters α, β and D_* now taken their brane values. For modes with $m > 0$, the limit $\alpha \to 0$, will give us the behavior of the absorption probability at the upper boundary of the superradiance regime which is given by

$$ |\mathcal{A}_{jm}|^2 = \frac{4\pi \, (\tilde{\omega}r_h/2)^{2j+1} \, K_* \, \sin^2 \pi(2\beta + D_*) \, \Gamma^2(2\beta + D_* - 2) \, \Gamma^2(1 - \beta) \, (2 - D_* - 2\beta)}{A_* \, (1 + a_*^2)^{-\frac{2j+1}{n+1}} \, (j + \frac{1}{2}) \, \Gamma^2(j + \frac{1}{2}) \, \Gamma^2(\beta + D_* - 1) \, \sin^2 \pi(\beta + D_*)}. $$
$$ (2.112) $$

As expected it is again the sign of K_* that defines the sign of the absorption probability in this energy regime since $K_* = r_h(1 + a_*^2)(\omega - m\Omega_h)$. By setting $j = m = 0$ and expanding further in the limit $\omega \to 0$, eq. (2.112) can also give us the asymptotic value

of $|\mathcal{A}_{00}|^2$ for the dominant scalar mode, which is

$$|\mathcal{A}_{00}|^2 = \frac{4\,\omega\tilde{\omega}r_h^2\,(1 + a_*^2)}{A_*\,(1 + a_*^2)^{-1/(n+1)}\,(2 - D_*)} + \dots.$$

(2.113)

Equation (2.96) may also provide the relation between the absorption cross-section and the absorption probability for a massive scalar field living on the brane. By setting $n = 0$ and $N_\ell = 1$, since the brane modes do not 'see' the n-sphere, we obtain the 4-dimensional formula

$$\sigma_{00} = \frac{\pi}{\tilde{\omega}^2}\,|\mathcal{A}_0|^2 = 4\pi\,\left(\frac{\omega}{\tilde{\omega}}\right)(r_h^2 + a^2)\,\frac{(1 + a_*^2)^{1/(n+1)}}{[(n + 1) + (n - 1)\,a_*^2]\,(2 - D_*)} + \dots.$$

(2.114)

Again, for $m_\Phi = 0$ and $a_* = 0$, the value of the absorption cross-section reduces to the area $4\pi r_h^2$ of the 4-dimensional Schwarzschild black hole, as expected [113, 114, 115]; for $a_* \neq 0$, it approaches the area $4\pi(r_h^2 + a^2)$ of the 4-dimensional rotating black hole for small values of the angular-momentum parameter [144]. However, as soon as the mass of the scalar field becomes larger than zero, the aforementioned constant values of σ_{00} are replaced by diverging ones for both rotating and non-rotating black holes – in the latter case, this is again in accordance with previous analyses [179, 119, 120, 121, 122, 123, 124]. As in the case of the bulk scalar field, and due to the $\tilde{\omega}^{2j+1}$ factor in eq. (2.112), all higher modes with $j \geq 1$ have a vanishing asymptotic value as $\tilde{\omega} \to 0$.

The derivation of the complete energy spectrum demands once again the calculation of the value of the absorption probability by numerical means. The asymptotic behavior of the brane massive scalar field close to and far away from the black hole horizon is similar to the one of a bulk field: it is an incoming plane wave in the near-horizon regime, as discussed below eq. (2.107), and a spherical wave at radial infinity according to eq. (2.108). The numerical integration of the radial differential equation (2.103) on the brane is performed by using the same method as in the bulk: the integration starts very close to the black-hole horizon with boundary conditions given again by eq. (2.99) and proceeds until we reach radial infinity, where the amplitudes of the incoming and outgoing modes are isolated to compute the value of the absorption probability $|\mathcal{A}_{jm}|^2$.

Therefore, in Fig. 2.13, we depict the exact numerical results for the value of the absorption probability of the dominant mode $j = m = 0$. In Fig. 2.13(a), the value of $|\mathcal{A}_{00}|^2$ is plotted for fixed angular momentum $(a_* = 1)$ and variable m_Φ, equal to 0, 0.4, 0.8 (from left to right), and for two different values of the number of extra dimensions, $n = 2$ (solid lines) and $n = 7$ (dashed lines). As expected, the value of the absorption probability is suppressed with the number of extra dimensions, as noted before in the literature [136, 141, 144]. The suppression becomes significantly more important as the value of the mass of the brane scalar field increases – this is also in agreement [5] with the results derived recently in [180, 181], therefore, we do not comment on this further.

_____

[5]The agreement is mainly qualitative as our results are derived for non-vanishing angular momentum parameter a_* while in [180, 181] the effect of the rotation of the black hole was ignored and the role of the mass and charge of the brane field was studied instead. Nevertheless, there is a general agreement between the two sets of results in terms of both the number of extra dimensions and the value of the mass of the brane scalar field.
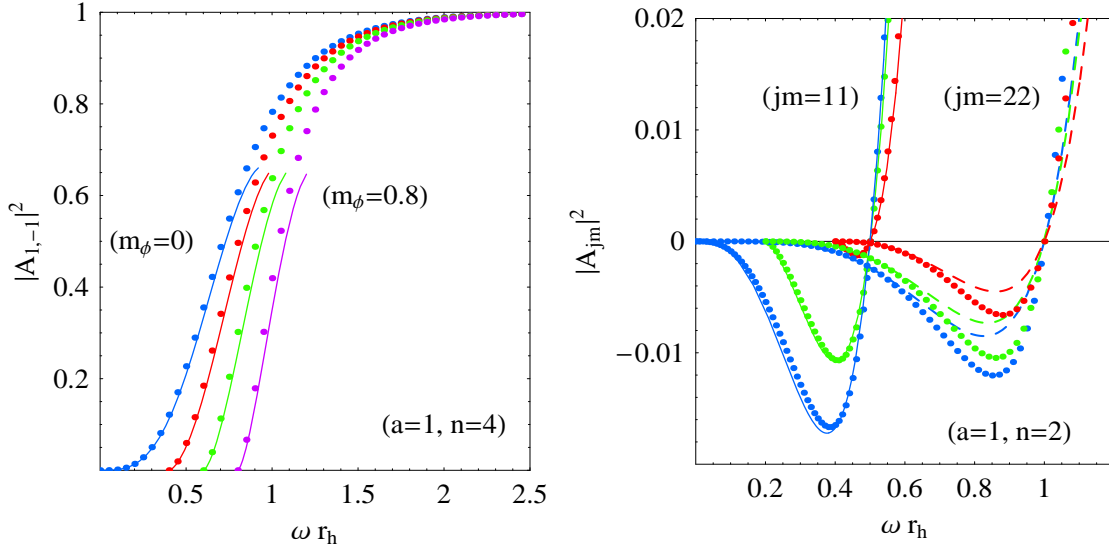
Figure 2.14: Comparison of the analytical (solid lines) and exact numerical (data points) results for the absorption probability for: **(a)** the brane scalar mode $(j,m) = (1,-1)$, for $a_* = 1$, $n = 4$ and $m_\Phi = 0, 0.4, 0.6, 0.8$, and **(b)** the superradiant brane scalar modes $(j,m) = ((1,1),(2,2))$ for $a_* = 1$, $n = 2$, and $m_\Phi = 0, 0.2, 0.4$ (from bottom to top).

On the other hand, Fig. 2.13(b) depicts the dependence of $|\mathcal{A}_{00}|^2$ on the angular-momentum parameter, that takes the values $a_* = 0.5$ and $a_* = 2.5$, while n remains fixed $(n = 4)$ and m_Φ changes from 0 to 0.8 (from left to right again). For $m_\Phi = 0$, the absorption probability increases as a_* increases, too, in accordance again with the literature [136, 141, 144] - the same behavior is observed as the mass of the scalar field becomes larger but with the enhancement becoming increasingly less significant. For the purpose of the analysis presented in section 2.3.3, where the bulk and brane energy spectra are compared, let us note here that both effects, the suppression with n and the enhancement with a_*, are much more prominent for massive bulk scalar fields than for brane fields of the same type.

As in the case of the emission in the bulk, we would like to investigate the validity of the analytic method used above to derive the value of the absorption probability for the emission of massive scalar fields on the brane, and how this is affected by the value of the mass and angular-momentum numbers of the emitted field, the number of extra dimensions and the magnitude of the angular momentum of the black hole. To this end, in Fig. 2.14(a), we plot both the analytical (solid lines) and numerical (data points) results for the absorption probability of the indicative mode $(j,m) = (1,-1)$, for fixed angular-momentum parameter $(a_* = 1)$ and number of extra dimensions $(n = 4)$ and $m_\Phi = 0, 0.4, 0.6, 0.8$. We observe that the agreement between the two sets of results remains particularly good even well beyond the low-energy regime. The solid lines terminate again due to the existence of poles in the arguments of the Gamma functions
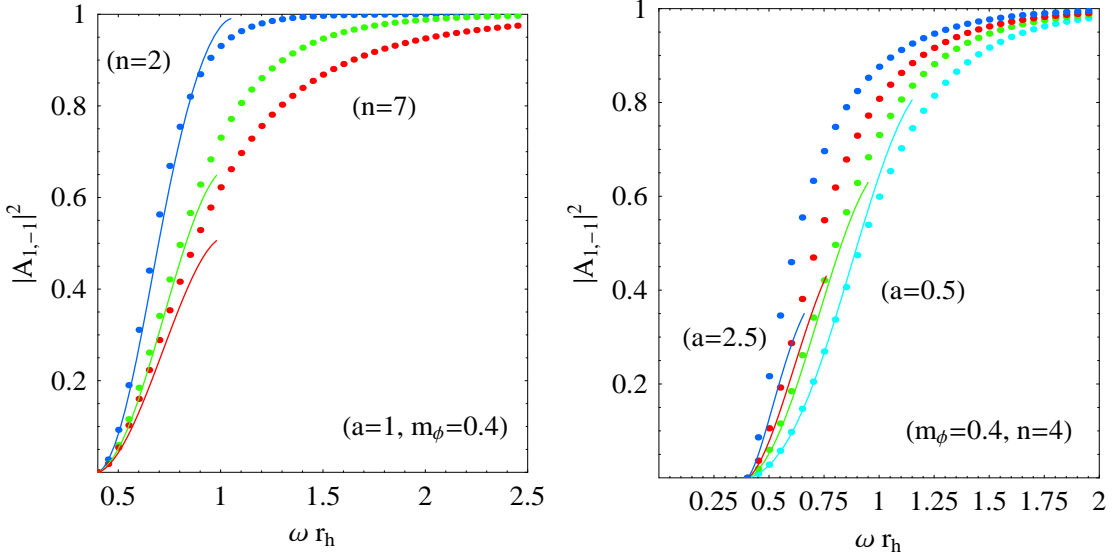
Figure 2.15: Comparison of the analytical (solid lines) and exact numerical (data points) results for the absorption probability for the brane scalar mode $(j, m = 1, -1)$, for **(a)** $a_* = 1$, $m_\Phi = 0.4$ and $n = 2, 4, 7$, and **(b)** $m_\Phi = 0.4$, $n = 4$ and $a_* = 0.5, 1, 1.5, 2.5$.

in the analytic expression of the absorption coefficient. We find that the appearance of the poles, for modes with given j, takes place much earlier for the modes with $m = 0$ than for $m > 0$, while for the ones with $m < 0$ this happens at much higher values of the energy, a fact which significantly extends the range of validity of the analytic results in the latter case as is clear from Fig. 2.14(a). In Fig. 2.14(b), we focus on the low-energy regime of two superradiant modes, $(j, m) = (1, 1)$ and $(j, m) = (2, 2)$: in agreement with results drawn in the massless case [144], we find that the analytic results for the value of the absorption probability start to deviate from the exact numerical ones as the angular-momentum numbers of the mode increase; this is due to the shift of the curve towards higher values of the energy – note that the range of agreement extends well beyond the value $\omega r_h = 0.6$ for both modes, however, for the $(j, m) = (2, 2)$ mode this covers only a part of the superradiant regime contrary to what happens for the $(j, m) = (1, 1)$ mode. It deserves to be noted that the value of the mass of the emitted field affects the relative values of the absorption probability of different superradiant modes: while for $m_\Phi = 0$, the $(j, m) = (1, 1)$ mode dominates over the $(j, m) = (2, 2)$ one, this radically changes as soon as the mass of the scalar field exceeds the value $m_\Phi = 0.2$.

Let us finally comment on the range of validity of the analytic results in terms of the parameters of the higher-dimensional space-time. In Fig. 2.15(a), we plot both sets of results for the mode $(j, m = 1, -1)$ for fixed angular-momentum parameter $(a_* = 1)$ and mass of the field $(m_\Phi = 0.4)$ while the number of extra dimensions takes the values $n = 2, 4, 7$. From the plot, it is clear that the agreement between the

analytic and numerical results is excellent for low values of n while it quickly worsens as the number of extra dimensions increases. Figure 2.15(b) plots the two sets of results for the same mode for fixed mass ($m_\Phi = 0.4$) and number of extra dimensions ($n = 4$), but variable angular-momentum parameter ($a_* = 0.5, 1, 1.5, 2.5$). Again, the agreement extends well beyond the intermediate-energy regime for low values of a_* while it is gradually restricted in the low-energy regime as the value of a_* increases. The observed behavior is in agreement with the one found in the massless case [144] and stems from the fact that several of our approximations in the analytic method become less accurate as either n or a_* increases.

Energy Emission Rate on the Brane

The exact value of the absorption probability $|\mathcal{A}_{jm}|^2$ for massive scalar fields on the brane, as this followed after the numerical integration of the radial equation of the wavefunction, will now be used for the computation of the corresponding energy emission rate. The higher-dimensional, simply-rotating black hole emits massive scalar particles on the brane with a rate given by the expression [134, 136, 137, 138, 141]

$$\frac{d^2E}{dtd\omega} = \frac{1}{2\pi} \sum_{j,m} \frac{\omega}{\exp\left[k/T_\mathrm{H}\right] - 1} \, |\mathcal{A}_{jm}|^2 \, . \tag{2.115}$$

In the above, k is defined in eq. (2.78) as before, while the temperature for the emission on the brane is that of the higher-dimensional black hole given in eq. (2.6). As in the case of bulk emission, the formula of the emission rate for massive fields is the same as the one for massless, with the effect of the mass being encoded in the value of the absorption probability and the frequency range of the emission.

As in the case of the bulk emission, for the derivation of the energy emission spectrum on the brane we need to sum over a significantly large number of partial waves labeled by the (j, m) quantum numbers. The absence of the 'internal' quantum number ℓ, that further characterizes the bulk modes, makes the brane summation easier, nevertheless the process remained significantly time-consuming [6]. We summed the contribution of all modes up to $j = 40$, that brings the total number of brane modes to $N_{br} = 1681$, and computed the spectrum up to the value of energy where the power rate dropped again below 10^{-6}. According to our estimates, the error in our results by leaving out the higher modes is less than 5%, for the higher values of n and a_* considered, and below 0.001% for the lowest.

In Fig. 2.16, we plot the energy emission rate on the brane in the form of massive scalar fields in terms of the number of extra dimensions, value of the angular-momentum parameter, and mass of the emitted field – we have kept the same values of these parameters as in the case of bulk emission for easier comparison. Figure 2.16(a) shows the energy emission rate for fixed a_* ($a_* = 1$) and variable $n = 2, 4, 7$ and $m_\Phi = 0, 0.4, 0.8$, while in Fig. 2.16(b) we keep n fixed ($n = 4$) and vary $a_* = 0.4, 1, 1.5$.

---

[6]For the largest values of the parameters considered, i.e. $n = 7$, and $a_* = 1.5$, the derivation of the complete spectrum for each value of the mass m_Φ lasted more than 4 days - this is to be contrasted with the corresponding summation in the bulk where a single run lasted more than 6 days.

t
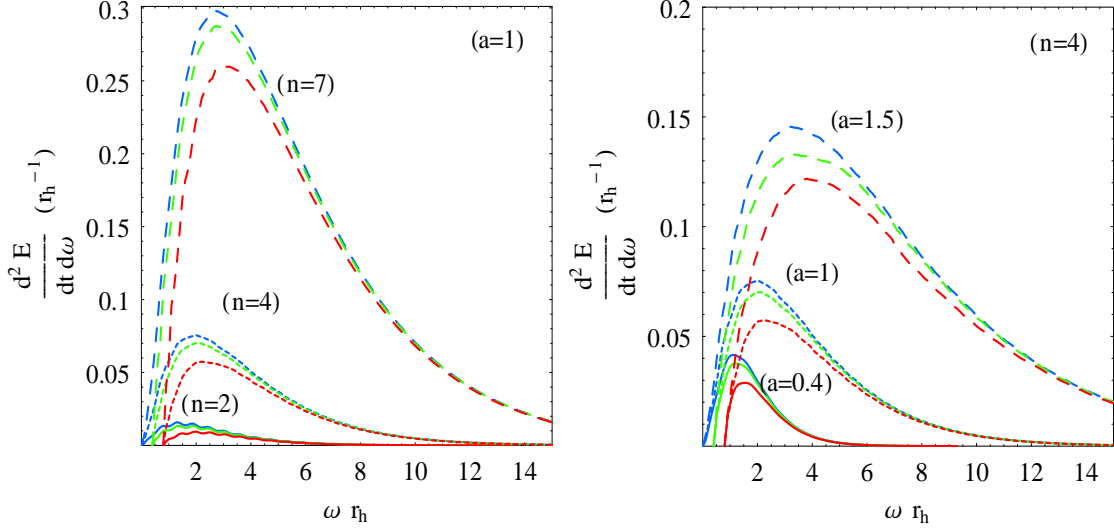
Figure 2.16: Energy emission rates for brane scalar fields for: **(a)** for $a_* = 1$, $n = 2, 4, 7$ and $m_\Phi = 0, 0.4, 0.8$ (from top to bottom in each set of curves with fixed n), and **(b)** $n = 4$, $a_* = 0.4, 1, 1.5$ and $m_\Phi = 0, 0.4, 0.8$ (from top to bottom in each set of curves with fixed a_*).

Again, our results reproduce successfully the behavior found in the case of massless fields [136, 141, 152], and demonstrate that the enhancement of the emission spectrum as either the number of extra dimensions or the angular momentum of the black hole increases persists even for non-vanishing values of the mass of the emitted field. The mass of the scalar field causes again the suppression of the spectrum in all energy regimes, apart from the very high-energy one where its effect becomes negligible. The suppression is again strongly dependent on the particular value of n and a_*. By comparing Figs. 2.12 and 2.16, we see that the brane emission is larger than the bulk emission by more than an order of magnitude - accordingly, we expect the suppression with m_Φ to be larger on the brane than in the bulk. The exact role of m_Φ in the total emissivity of the black hole, in conjunction with the parameters (n, a_*) and the type of emission channel (brane or bulk), will be investigated in the next section.

2.3.3 Bulk and Brane Total Emissivities

Although the global properties of the absorption probability and energy spectra do not change when the mass of the scalar field is introduced, important variations in their values appear which differ as the value of m_Φ, together with that of either n or a_*, changes. For this reason, we expect that differences will appear when the spectra for the emission of massive and massless fields are compared. These differences may be evident at particular energy regimes or range of values of the parameters (n, a_*),

		$a_* = 0.4$	$a_* = 1.0$	$a_* = 1.5$
$n = 2$	$m_\Phi = 0$	1.00	1.54	3.46
	$m_\Phi = 0.4$	0.84	1.34	3.05
	$m_\Phi = 0.8$	0.52	0.95	2.46
$n = 4$	$m_\Phi = 0$	6.29	9.57	19.22
	$m_\Phi = 0.4$	5.97	9.13	18.61
	$m_\Phi = 0.8$	5.12	7.99	16.74
$n = 7$	$m_\Phi = 0$	131.47	202.48	327.37
	$m_\Phi = 0.4$	128.56	197.27	322.87
	$m_\Phi = 0.8$	121.57	188.58	310.18

Table 2.2: Total energy emissivities for massive scalar fields in the bulk

and may significantly affect the total energy emissivities. The modifications in the spectrum may also be different when bulk or brane emission is considered, therefore, in this section we compute the total emissivities for both emission channels and compare them.

To this end, we have integrated the differential energy rates per unit time and unit frequency, computed in sections 2.3.1 and 2.3.2, over the entire frequency range of emission. In Tables 2.2 and 2.3, we present the corresponding total emissivities for bulk and brane emission, respectively, for some indicative values of the number of extra dimensions ($n = 2, 4, 7$), angular-momentum parameter of the black hole ($a_* = 0.4, 1, 1.5$) and mass of the emitted field ($m_\Phi = 0, 0.4, 0.8$). The values of the total emissivities are normalized to the one for $n = 2$, $a_* = 0.4$ and $m_\Phi = 0$, in each case, for easy comparison.

The entries of both tables confirm the enhancement of the total emissivities as either n or a_* increases and the suppression with m_Φ. As it was anticipated from the plots, the suppression is strongly dependent not only on m_Φ but also on both n and a_*. We observe that, as either n or a_* increases, the suppression of the total emissivity with the mass of the scalar field decreases in magnitude. Starting from the bulk channel (Table 2.2), we see that for a fixed, low value of n, i.e. $n = 2$ the total emission for a scalar field with mass $m_\Phi = 0.8$ drops to 52% of the emission for a massless field, if $a_* = 0.4$, but to 71% if $a_* = 1.5$. The suppression is even more limited when the value of n takes a much higher value: thus, for $n = 7$, the emission for a $m_\Phi = 0.8$ scalar field in the bulk drops only to the 92% of the massless value if $a_* = 0.4$ and to 95% if $a_* = 1.5$. It seems that both the number of extra dimensions and the rotation of the black hole subsidize the emission of massive scalar fields.

The same behavior is observed for emission on the brane (Table 2.3) although here the suppression is larger: for $n = 2$ the total emission for a brane scalar field with mass $m_\Phi = 0.8$ drops to 39% of the emission for a massless field, if $a_* = 0.4$, but to 72% if $a_* = 1.5$; for $n = 7$, the emission for a $m_\Phi = 0.8$ scalar field on the brane drops to the 80% of the massless value if $a_* = 0.4$ and to 91% if $a_* = 1.5$.

Since the suppression of the total emissivities between brane and bulk emission

		$a_* = 0.4$	$a_* = 1.0$	$a_* = 1.5$
$n = 2$	$m_\Phi = 0$	1.00	3.37	13.18
	$m_\Phi = 0.4$	0.75	3.10	11.98
	$m_\Phi = 0.8$	0.39	2.16	9.51
$n = 4$	$m_\Phi = 0$	6.56	25.73	89.89
	$m_\Phi = 0.4$	5.73	23.75	84.18
	$m_\Phi = 0.8$	4.14	19.51	83.39
$n = 7$	$m_\Phi = 0$	36.75	144.53	483.83
	$m_\Phi = 0.4$	34.48	138.86	471.08
	$m_\Phi = 0.8$	29.28	126.53	440.77

Table 2.3: Total energy emissivities for massive scalar fields on the brane

differ, it is imperative to calculate the relative emissivities to find out whether the mass of the emitted field changes the energy balance in the bulk-brane channels. These, derived by dividing the actual values of the bulk and brane emissivities for each set of values (n, a_*, m_Φ), are displayed in Table 2.4. Our results confirm and extend the ones of [151] where the emission of massless scalar fields was studied. In there, it was found that the bulk emission channel was becoming increasingly sub-dominant as the value of the rotation parameter increased from $a_* = 0$ to $a_* = 1$ - here, we show that this behavior persists for higher values of the angular momentum parameter. Also, we confirm that the bulk-over-brane ratio take its lower value for an intermediate value of the number of extra dimensions (a result that was found in the case of both rotating [151] and non-rotating [115] black holes) but starts increasing again as $n > 4$.

Overall, it is clear that the brane channel remains the dominant one over the bulk channel, during the emission of both massless and massive fields. Nevertheless, we find that the presence of the mass gives a considerable boost to the bulk-over-brane energy ratio, especially for low values of the angular momentum parameter. The boost depends also on the number of extra dimensions: for $n = 2$, the mass of a $m_\Phi = 0.8$ scalar field increases the bulk-over-brane energy ratio of a black hole with $a_* = 0.4$ by 33%, while for $n = 7$ the increase is 16%. We thus conclude that, when the effect of the mass of the emitted field is taken into account, it is the fast-rotating black holes living in a space-time with a fairly large number of extra dimensions that lose the smallest part of their energy into invisible bulk emission.

Let us finally note that the results presented in this work not only extend previous analyses for massless fields, but also improve those, too. For instance, our results for the total bulk emissivities when $m_\Phi = 0$ agree in the first or second decimal point (depending on the value of n and a_*) with those derived in [151] - the agreement is reassuring as a different numerical code was used. Small deviations between our results may be due to the fact that, in the calculation of the total emissivities, we have not imposed any cut-off on the frequency but instead tried to obtain the complete spectrum by keeping a realistically large number of scalar modes.

In conclusion, in this work we have performed a comprehensive study of the emission

		$a_* = 0.4$	$a_* = 1.0$	$a_* = 1.5$
$n = 2$	$m_\Phi = 0$	0.180	0.076	0.0451
	$m_\Phi = 0.4$	0.202	0.078	0.0458
	$m_\Phi = 0.8$	0.24	0.079	0.0466
$n = 4$	$m_\Phi = 0$	0.173	0.067	0.038
	$m_\Phi = 0.4$	0.188	0.069	0.039
	$m_\Phi = 0.8$	0.223	0.074	0.040
$n = 7$	$m_\Phi = 0$	0.645	0.253	0.122
	$m_\Phi = 0.4$	0.673	0.256	0.124
	$m_\Phi = 0.8$	0.749	0.269	0.127

Table 2.4: Bulk-over-brane relative energy emissivities for massive scalar fields

of massive scalar fields by a higher-dimensional, simply rotating black hole both in the bulk and on the brane. We have studied the dependence of the absorption probabilities and energy emission rates on all parameters of the theory, and compared analytic and numerical methods for the computation of their value. We have confirmed the importance of the emission of a higher-dimensional black hole both in the bulk and on the brane, and demonstrated that properties of the emitted field, such as its mass which was up to now largely ignored, can play a significant role in the bulk-over-brane energy balance.

2.4 Angular profile of the particle emission on the brane

As mentioned earlier, at the beginning of this chapter, before reaching the Schwarzschild phase rotating black holes pass through the axially-symmetric spin-down phase. The gravitational background around a simply-rotating black hole – one of the very few cases where the equations of motion of the propagating particles can be decoupled and solved – depends not only on the black hole mass but also on the angular-momentum parameter a of it. According to the results existing in the literature [136, 141, 142, 143, 134, 137, 138, 144, 145, 133, 135, 153, 146, 152, 154, 156, 160, 172, 19, 124, 150, 180, 181, 20], the latter dependence is carried over in the form of the radiation emission spectra and is, in fact, found to be similar to the effect that the number of additional space-like dimensions n has on them. To complicate things more, simulations of black hole events [147, 148] have revealed that the spin-down phase is not a short-lived one, as previously thought, and that the rotation of the black hole remains significant for most of its lifetime.

The fact that the dependence of the radiation spectra on the number of extra dimensions n for all types of particles is entangled with the dependence on the angular-momentum parameter a means that measuring both of these parameters is extremely

difficult. The only way out was to employ another observable that would strongly depend on only one of these two parameters while being insensitive to the other. Upon determination of that particular parameter, the second could then be determined from the radiation spectra. One characteristic feature of the emission spectra coming from the spin-down phase is the non-isotropic emission, in contrast to the one coming from the Schwarzschild phase where the emitted particles are evenly distributed over a 4π solid angle. It has therefore been suggested [195, 178] that this non-isotropy can serve as the additional observable necessary to disentangle the n and a-dependence of the spectra. Indeed, it was demonstrated [178] that the angular profile of the emitted radiation depends extremely weakly on the number of additional dimensions n while it may provide valuable information on the angular momentum of the black hole (see, for example, [180, 181]). More specifically, under the combined effect of the centrifugal force exerted on the emitted particles and the spin-rotation coupling for particles with non-zero spin (an analytical explanation of the latter is given in [197]), the orientation of the emitted radiation depends strongly on the energy channel in which the particles are emitted and on how fast the black hole rotates. If we look specifically at the low-energy channel, then we observe that gauge bosons and fermions have a distinctly different behavior: the emitted gauge bosons remain aligned to the rotation axis of the black hole independently of the angular-momentum parameter; fermions, on the other hand, form an angle with the rotation axis whose value strongly depends on the value of a. As a result, the orientation of gauge bosons can serve as a good indicator of the rotation axis of the black hole [178] and the orientation of fermions can then provide a measurement of the value of the angular momentum of the black hole [195, 178]. The aforementioned results presented in [195, 178] were derived by means of a very complicated and time-consuming process that involved the numerical integration of both the radial and angular part of the equation of motion of each emitted particle as well as additional challenges such as the numerical calculation of the angular eigenvalue itself, which does not exist in closed form for a rotating background, and the summation of a very large number of partial modes.

The purpose of the work presented next is to provide an alternative way of deriving the angular profile of the emitted radiation without resorting to complicated numerical calculations. This is facilitated by the fact that all valuable information that may be derived from the angular spectra is restricted in the low-energy regime where the radial equations for all types of particles have been analytically solved [144, 145]. In addition, analytical formulae, in the form of power series, for the angular eigenfunction and eigenvalue exist in the literature. By combining all the above in a constructive way, we investigate which contributions are the dominant ones, that predominantly determine the angular profile of the emitted radiation. In this way, we formulate simple constraints involving a finite number of terms and partial modes that successfully reproduce all the features of the anisotropic emission, namely the value of the angle where the emission becomes maximum and the corresponding value of the energy emission rate.

2.4.1   Theoretical framework

The most generic type of a black hole in a higher-dimensional space-time is the one that rotates around one or more axes. The gravitational field around such a black hole is described by the Myers-Perry solution [49]. However, it is only for particular configurations of the angular-momentum components that the equation of motion of a particle propagating in the higher-dimensional space-time can be decoupled into an angular and a radial part. The case of a simply-rotating black hole, where the black hole possesses only one angular-momentum component that lies on a plane parallel to our brane, corresponds to one of these configurations and the one that has been mostly considered in the literature. The corresponding line-element then is the one of eq. (2.1). Nevertheless, in this work we will study effects that take place strictly on our brane, namely the emission of Hawking radiation by the higher-dimensional, rotating black hole in the form of non-zero-spin Standard-Model fields. Therefore, we have to consider the induced-on-the-brane 4-dimensional projection of the general Myers-Perry solution given by eq. (2.101) [84, 98, 99, 191]

The derivation of the field equations that the brane-localized Standard-Model fields satisfy in the above background follows the analysis performed originally by Teukolsky in 4 dimensions [198, 199, 200]. The method demands the use of the Newman-Penrose formalism and results in a 'master' partial differential equation that scalars, fermions and gauge bosons obey on the brane. If we use a factorized ansatz for the field perturbation Ψ_h of the form

$$\Psi_h(t, r, \theta, \varphi) = \sum_\Lambda {}_h a_\Lambda \, {}_h R_\Lambda(r) \, {}_h S_\Lambda(\theta) \, e^{-i\omega t} \, e^{im\varphi} \,, \tag{2.116}$$

the aforementioned "master" equation separates, in the background of eq. (2.101), into two decoupled ordinary differential equations, a radial

$$\Delta^{-h} \frac{d}{dr}\left(\Delta^{h+1} \frac{d_h R_\Lambda}{dr}\right) + \left[\frac{K^2 - ihK\Delta'(r)}{\Delta} + 4ih\omega r + h(\Delta''(r) - 2)\delta_{h,|h|} - {}_h\lambda_\Lambda\right] {}_h R_\Lambda = 0 \,, \tag{2.117}$$

and an angular one

$$\frac{d}{dx}\left[(1 - x^2)\frac{d_h S_\Lambda(x)}{dx}\right] + \left[a^2\omega^2 x^2 - 2ha\omega x - \frac{(m + hx)^2}{1 - x^2} + h + {}_h A_\Lambda\right] {}_h S_\Lambda(x) = 0 \,. \tag{2.118}$$

In the above, h is the spin-weight, $h = (-|s|, +|s|)$, of the given field that distinguishes its radiative components, and $\Lambda = \{lm\omega\}$ denotes the set of 'quantum numbers' of each mode. We have also defined the quantities $K \equiv (r^2 + a^2)\omega - am$ and $x \equiv \cos\theta$. Finally, ${}_h A_\Lambda$ is the eigenvalue of the spin-weighted spheroidal harmonics ${}_h S_\Lambda(x)$ - as we will shortly comment, the value of this constant does not exist in closed form. This quantity also determines the separation constant between the radial and angular equations with ${}_h\lambda_\Lambda \equiv {}_h A_\Lambda - 2ma\omega + a^2\omega^2$.

The above set of equations has been used in the literature in order to study the emission of Hawking radiation, in the form of an arbitrary spin-s field, from a higher-dimensional, simply-rotating black hole on the brane [136, 141, 142, 134, 137, 138]. The

resulting differential energy emission rate per unit time, energy and angle of emission is given by the expression [136, 141, 142]

$$\frac{d^3 E}{d(\cos\theta)\, dt\, d\omega} = \frac{1 + \delta_{|s|,1}}{4\pi} \sum_{l,m} \frac{\omega}{\exp(\tilde{\omega}/T_H) \pm 1} \mathbf{T}_\Lambda \left({}_{-h}S_\Lambda^2 + {}_{h}S_\Lambda^2 \right) . \qquad (2.119)$$

The radiation spectrum of the black hole resembles those of a black body with a temperature

$$T_H = \frac{(n+1) + (n-1)a_*^2}{4\pi \left(1 + a_*^2\right) r_h} . \qquad (2.120)$$

At the same time, however, the spectrum is significantly modified compared to the black-body one: in the exponent, the combination $\tilde{\omega} = \omega - am/(a^2 + r_h^2)$, includes the effect of the rotation of the black hole; also, the quantity $\mathbf{T}_\Lambda$, the transmission probability (or, graybody factor), determines the number of particles that eventually overcome the gravitational barrier of the black hole and reach asymptotic infinity. If eq. (2.119) is integrated over all angles of emission θ, we obtain the power rate in terms of unit time and energy

$$\frac{d^2 E}{dt\, d\omega} = \frac{1 + \delta_{|s|,1}}{2\pi} \sum_{l=|s|}^{\infty} \sum_{m=-l}^{+l} \frac{\omega}{\exp(\tilde{\omega}/T_H) \pm 1} \mathbf{T}_\Lambda . \qquad (2.121)$$

The derivation of the integrated-over-all-angles power spectra, for all species of brane-localized fields – scalars, fermions and gauge bosons, was performed both analytically [144, 145] and numerically [136, 141, 142, 134, 137, 138]. According to these results, the energy emission rate – as well as the particle and angular-momentum emission rates – are significantly enhanced as both the number of additional, spacelike dimensions and the angular-momentum of the black hole increase. The enhancement factor was of order $\mathcal{O}(100)$ when n varied between 1 and 6, and of order $\mathcal{O}(10)$ as a_* increased from zero towards its maximum value $a_*^{max} = (n+2)/2$.

In contrast to the case of the spherically-symmetric Schwarzschild phase, the emission of particles during the rotating phase of the life of the black hole is not isotropic. The axis of rotation introduces a preferred direction in space and the emitted radiation exhibits an angular variation as θ ranges from 0 to π. It was found [136, 141, 142, 134, 137, 138] that a centrifugal force is exerted on all species of particles, that becomes stronger as either ω or a increases and forces the particles to be emitted along the equatorial plane ($\theta = \pi/2$). In addition, for particles with non-vanishing spin, an additional force, sourced by the spin-rotation coupling, aligns the emitted particles parallel or antiparallel to the rotation axis of the black hole – this effect is more dominant the smaller the energy and larger the spin of the particle is. If the form (2.119) of the power spectrum is used where both helicities appear, the spectrum is symmetric over the two hemispheres, $\theta \in [0, \pi/2]$ and $[\pi/2, \pi]$. If a modified form, in which only one of the helicities appear each time, is used instead, then the angular profile is asymmetric with particles with positive helicity (corresponding to ${}_{-|s|}S_\Lambda^2$) being emitted in the upper hemisphere and particles of negative helicity (corresponding to ${}_{+|s|}S_\Lambda^2$) being emitted in the lower one. This angular variation in the Hawking radiation spectra is considered

to be one of the main observable effects on the brane of a higher-dimensional, rotating, decaying black hole.

One would ideally like to deduce the values of both space-time parameters, n and a, from the predicted forms of the Hawking radiation spectra. However, the fact that both parameters affect the integrated-over-all-angles spectra in a similar way impose a great obstacle. The resolution of this problem would demand the existence of an observable that depends strongly on only one of the two parameters while being (almost) insensitive to the other. That observable was shown [195, 178] to be the angular variation of the spectra discussed above. Particularly, in the low-energy channel, the alignment of the gauge bosons along the rotation axis can reveal the orientation of the angular-momentum of the black hole. Then, it was demonstrated that the angle of emission of fermions, in the same energy channel, is very sensitive to the value of the angular-momentum of the black hole: the larger the a parameter is, the larger the value of θ, around which the emission is peaked, becomes. Remarkably, the behavior of gauge bosons and fermions alike remains unaltered as the dimensionality of space-time changes.

2.4.2 Analytical forms of the radial and angular functions

The results on the angular profile of the emitted fields with non-zero spin on the brane, discussed above, were derived by numerically integrating both the radial (2.117) and the angular (2.118) equation: the latter in order to find the angular eigenvalue $_hA_\Lambda$ and eigenfunction $_hS_\Lambda$, and the former in order to determine the graybody factor $\mathbf{T}_\Lambda$ through the radial function $_hR_\Lambda$. The numerical manipulation of the radial and angular differential equations is necessary for the derivation of the exact solutions for $_hR_\Lambda$ and $_hS_\Lambda$, respectively, and subsequently of the complete Hawking radiation spectra. However, when it comes to the spectra of gauge bosons and fermions revealing information about the orientation of axis and value of the angular momentum of the black hole, the range of interest is the low-energy one. Thus, in what follows we will focus on the low-energy channel, and attempt to derive analytically information about the angular profile of non-zero-spin fields emitted on the brane. To this end, we will henceforth ignore the single-component scalar fields and concentrate our study on brane-localized fields with spin 1/2 and 1.

Under the assumption of low-energy of the emitted field and low-angular-momentum of the black hole, the radial equation (2.117) was analytically solved in [144, 145] for all species of particles. A well-known approximation method was used in which the radial equation was solved first near the horizon, then at asymptotic infinity, and the two were finally matched at an intermediate regime to construct the complete solution for $_hR_\Lambda$. The transmission probability $\mathbf{T}_\Lambda$ for fermions was defined as the ratio of the flux of particles at the black-hole horizon over the one at infinity, with the flux being determined through the conserved particle current. For gauge bosons, where no conserved particle current exists, a radial function redefinition and a simultaneous change of the radial coordinate conveniently change the corresponding gravitational potential to a short-range one - then, the amplitudes of the outgoing and incoming plane waves at infinity can easily determine the transmission probability. For fermions and gauge

bosons, $\mathbf{T}_\Lambda$ comes out to have the form [145]

$$\mathbf{T}_\Lambda^{(1/2)} = 1 - \frac{4\omega^2}{\frac{1}{2}A_\Lambda + 1 + a^2\omega^2} \left| \frac{Y_{\frac{1}{2}}^{(out)}}{Y_{\frac{1}{2}}^{(in)}} \right|^2 , \qquad (2.122)$$

and

$$\mathbf{T}_\Lambda^{(1)} = 1 - \frac{16\omega^4}{(_1 A_\Lambda + 2 + a^2\omega^2)^2} \left| \frac{Y_1^{(out)}}{Y_1^{(in)}} \right|^2 , \qquad (2.123)$$

respectively, where

$$\frac{Y_h^{(out)}}{Y_h^{(in)}} = \frac{\Gamma\left(1+Z\right)\Gamma\left(\frac{1}{2}+h+\frac{Z}{2}\right)}{(2i\omega)^{2h}\,\Gamma\left(\frac{1}{2}-h+\frac{Z}{2}\right)\left[\Gamma\left(1+Z\right)e^{i\pi\left(\frac{1}{2}-h+\frac{Z}{2}\right)}+B\,\Gamma\left(\frac{1}{2}+h+\frac{Z}{2}\right)\right]} \qquad (2.124)$$

and

$$B \equiv \frac{\Gamma(Z)}{\Gamma(\frac{1}{2}-h+\frac{Z}{2})}\,\frac{\Gamma(c-a-b)\Gamma(a)\Gamma(b)}{\Gamma(c-a)\Gamma(c-b)\Gamma(a+b-c)}\,\frac{\left[(1+a_*^2)\,r_h^{n+1}\right]^{2\beta+|s|+B_*-2}}{(2i\omega)^Z}. \qquad (2.125)$$

In the above, the quantity Z, defined by

$$Z = \sqrt{(2|s|-1)^2 + 4(_h A_\Lambda + 2|s| + a^2\omega^2)}, \qquad (2.126)$$

appears in the solution of the radial equation in the asymptotic infinity that is expressed in terms of the Kummer functions M and U. Similarly, the coefficients $(a,\,b,\,c)$, given by

$$a = \alpha + \beta + D_* - 1, \qquad b = \alpha + \beta, \qquad c = 1 - |s| + 2\alpha, \qquad (2.127)$$

are the coefficients of the hypergeometric function F in terms of which the solution of the radial equation is written near the black-hole horizon. Finally, the following definitions hold [145]

$$D_* \equiv 1 - |s| + \frac{2|s| + n\left(1 + a_*^2\right)}{A_*} - \frac{4a_*^2}{A_*^2}, \qquad \alpha = \frac{|s|}{2} - \left(\frac{iK_*}{A_*} + \frac{h}{2}\right), \qquad (2.128)$$

$$\beta = \frac{1}{2}\left[(2-|s|-D_*) - \sqrt{(D_*+|s|-2)^2 - \frac{4K_*^2 - 4ihK_*A_*}{A_*^2} - \frac{4(4ih\omega_* - _h\tilde{\lambda}_\Lambda)\left(1+a_*^2\right)}{A_*^2}}\right]. \qquad (2.129)$$

supplemented by the following ones: $A_* = n + 1 + (n-1)a_*^2$, $K_* = K/r_h$ and $_h\tilde{\lambda}_\Lambda = {}_h\lambda_\Lambda + 2|s|$.

For scalar fields, the transmission probability is again defined from the amplitudes of the outgoing and ingoing spherical waves at infinity [144]

$$\mathbf{T}_\Lambda^{(0)} = 1 - \left|\frac{B-i}{B+i}\right|^2 = \frac{2i\left(B^* - B\right)}{BB^* + i\left(B^* - B\right) + 1}, \qquad (2.130)$$

where B now is given by the expression

$$B = -\frac{1}{\pi} \frac{Z\, 2^{2l}}{\left[\omega r_h \,(1 + a_*^2)^{\frac{1}{n+1}}\right]^{2l+1}}$$

$$\times\; \frac{\Gamma^2\,(Z/2)\,\Gamma(\alpha + \beta + D_* - 1)\,\Gamma(\alpha + \beta)\,\Gamma(2 - 2\beta - D_*)}{\Gamma(2\beta + D_* - 2)\,\Gamma(2 + \alpha - \beta - D_*)\,\Gamma(1 + \alpha - \beta)}. \quad (2.131)$$

We note that the angular eigenvalue $_hA_\Lambda$ makes its appearance in the above analytic results both in eq. (2.126) and eq. (2.129). As already mentioned in the previous section, in the case of a rotating black hole, this quantity does not exist in closed form. For arbitrary large values of the energy of the emitted particle and angular momentum of the black hole, its value can be determined only via numerical means - that was the method applied in [136, 141, 142] where the complete spectra for scalars, fermions and gauge bosons were derived. However, for low ω and low a, the angular eigenvalue of the spin-weighted spheroidal harmonics can be expressed as a power series with respect to $a\omega$ [200, 189, 188, 190, 166]

$$_hA_\Lambda = \sum_{k=0}^{\infty} f_k \,(a\omega)^k. \quad (2.132)$$

By using the above power-series form for the angular eigenvalue and keeping terms up to fourth order, the analytically derived formulae for the transmission probabilities (2.122) and (2.123) for fermions and gauge bosons - as well as the one for scalar fields - were shown in [144, 145] to be in excellent agreement with the exact numerical ones derived in [136, 141, 142]. The power-series expansion of the angular eigenvalue is quite cumbersome and, up to the sixth order, can be found in [200, 189, 188, 190, 166]. It is worth giving here, some particularly simple formulae we have derived, for the needs of our analysis, for the eigenvalues of fermions and gauge bosons up to second order, namely

$$_{\frac{1}{2}}A_\Lambda = l(l+1) - \frac{3}{4} - \frac{m\,(a\omega)}{2l(l+1)} + \left\{\frac{\mathcal{A}_{1/2}^2 + \mathcal{B}_{1/2}^2}{2l(l+1)} - \frac{1}{2} + \frac{m^2}{8}\left[\frac{1}{(l+1)^3} - \frac{1}{l^3}\right]\right\}(a\omega)^2 + ... \quad (2.133)$$

and

$$_1A_\Lambda = l(l+1) - 2 - \frac{2m\,(a\omega)}{l(l+1)} + \left\{2(\mathcal{A}_1^2 + \mathcal{B}_1^2)\left[1 - \frac{3}{l(l+1)}\right]\right.$$

$$\left. -\; 2m^2\left[\frac{3(l+2)}{(l+1)^3} - \frac{2l+3}{l^3(l+1)^2}\right] + (3 - 2l - 2l^2)\right\}\frac{(a\omega)^2}{(2l+3)(2l-1)} + ... \quad (2.134)$$

where

$$\mathcal{A}_h = \max\,(|m|, |s|), \qquad \mathcal{B}_h = \frac{mh}{\max\,(|m|, |s|)}. \quad (2.135)$$

In the above, we have given the values of the angular eigenvalues for the positive helicities $h = 1/2$ and $h = 1$, respectively. The angular eigenvalues exhibit a well-known symmetry [170, 166] according to which, if $_{|s|}A_\Lambda$ is the eigenvalue for the positive-helicity component of a given field, then the one for the negative helicity $_{-|s|}A_\Lambda$ readily

follows from the relation $_{-|s|}A_\Lambda = {}_{|s|}A_\Lambda + 2|s|$. For completeness, we add here a similar formula for the angular eigenvalue of scalar fields that first appeared in [104]:

$$_0 A_\Lambda = l(l+1) + \left[\frac{1 - 2l - 2(l^2 - m^2)}{(2l-1)\,(2l+3)} \right] (a\omega)^2 + \dots . \tag{2.136}$$

Let us now turn to the angular equation (2.118). Leaver [170] found an analytic solution for the angular eigenfunction $_h S_\Lambda(x)$ that may be expressed as a series of the following form

$$_h S_\Lambda(x) = e^{a\omega x} (1+x)^{k_-} (1-x)^{k_+} \sum_{p=0}^{\infty} a_p (1+x)^p , \tag{2.137}$$

where $x = \cos\theta$ and $k_\pm \equiv |m \pm h|/2$. The expansion coefficients a_p can be found through a three-term recursion relation

$$\alpha_0 a_1 + \beta_0 a_0 = 0 , \tag{2.138}$$

$$\alpha_p\, a_{p+1} + \beta_p\, a_p + \gamma_p\, a_{p-1} = 0 , \qquad (p = 1, 2, ...) \tag{2.139}$$

In the above, the coefficients $(\alpha_p,\, \beta_p,\, \gamma_p)$ are in turn determined by the relations

$$
\begin{aligned}
\alpha_p &= -2(p+1)(p+2k_-+1) , \\
\beta_p &= p(p-1) + 2p(k_- + k_+ + 1 - 2a\omega) - [a^2\omega^2 + h(h+1) + {}_h A_\Lambda] \\
&\quad - [2a\omega(2k_- + h + 1) - (k_- + k_+)(k_- + k_+ + 1)] , \\
\gamma_p &= 2a\omega(p + k_- + k_+ + h) .
\end{aligned}
\tag{2.140}
$$

The above analytic form determines the angular eigenfunction up to a constant that can be fixed by imposing the normalization condition $\int_{-1}^{1} |_h S_\Lambda(x)|^2 dx = 1$. According to [166], an excellent approximation to the exact solution is obtained by keeping ~ 10 terms in the expansion of (2.137).

2.4.3   Analytical description of the angular profile

In this section, we will attempt to study the angular profile of the emitted Hawking radiation on the brane by employing semi-analytic techniques. Our starting point will be eq. (2.119) that determines the angular profile of the emitted radiation as a function of $x = \cos\theta$. By using the analytical formulae presented in the previous section, we will compute the value of the angle θ where the emission of particles becomes maximum. Since the emission of positive and negative helicity components is symmetric under the change $\theta \to \pi - \theta$ [178], in what follows we consider only the emission of positive helicity components, $h > 0$.

In eq. (2.119), the dependence on the angle θ is restricted in the angular eigenfunction $_h S_\Lambda(x)$. One may then naively try to extremize this equation to find a constraint

that will determine the desired value of $\theta_{\max}$, defined as the value of the angle where the differential rate of emission takes its maximum value. We then obtain

$$\frac{d}{dx}\left(\frac{d^3E}{dx\,dt\,d\omega}\right) = \frac{1+\delta_{|s|,1}}{4\pi}\sum_{l,m}\frac{\omega}{\exp(\tilde{\omega}/T_H)\pm 1}\mathbf{T}_\Lambda\left(2\,_hS_\Lambda\frac{d\,_hS_\Lambda}{dx}\right) = 0\,. \qquad (2.141)$$

By employing the analytical expression (2.137) for the angular eigenfunction $_hS_\Lambda(x)$ and evaluating the derivative, we obtain the following constraint

$$\sum_{l,m}\,_hW_\Lambda(1+x)^{2k_-}\,(1-x)^{2k_+}\sum_{p=0}^{\infty}a_p\,(1+x)^p\sum_{q=0}^{\infty}a_q\,(1+x)^q\left(a\omega+\frac{k_-+q}{1+x}-\frac{k_+}{1-x}\right) = 0\,.$$
$$(2.142)$$

In the above, we have defined the "weight factor" $_hW_\Lambda$ as

$$_hW_\Lambda \equiv \frac{\omega}{\exp[(\omega-m\Omega)/T_H]\pm 1}\,\mathbf{T}_\Lambda\,. \qquad (2.143)$$

The analytical evaluation of the constraint (2.142) in full is not possible. As mentioned above, the sum over p (and q), originating from the analytic form of the angular eigenfunction, may be truncated at a finite value, but care must be taken so that the truncated series remains close to the exact solution and the value of $\theta_{\max}$ is not affected. The constraint contains two additional sums: one with respect to l, the total angular-momentum number ranging from $|s|$ to ∞, and one over m, the azimuthal angular-momentum number that takes values in the range $[-l, +l]$. None of these sums can be discarded: all of the quantities involved, the coefficients $k_\pm$, a_p (and a_q), as well as the weight factor $_hW_\Lambda$, depend on both angular-momentum numbers in a non-trivial manner. It is, therefore, the combined contributions of all, in principle, partial modes that determines the angular profile of the emitted radiation. Finally, these contributions do not enter on an equal footing: each mode carries a weight factor $_hW_\Lambda$ – defined in eq. (2.143) in terms of the 'thermal/statistics' function and the graybody factor $\mathbf{T}_\Lambda$ – that determines the magnitude of its contribution to the angular profile.

In what follows, we will attempt to shed light to the important contributions to eq. (2.142) that determine the value and location, in terms of the angle θ, of the maximum emission rate for fermions and gauge bosons. As the interesting phenomena take place in the low-energy regime, we will use purely analytic expressions for all quantities involved, namely the angular eigenvalue, the angular eigenfunctions and the graybody factor. Having been established in the literature [178] that the orientation of the emission of fermions and gauge bosons is not affected by the value of the number of extra dimensions introduced in the model, we will keep fixed the value of n and, henceforth, set $n = 2$.

Emission of Fermions

We will start with the most phenomenologically interesting case, the emission of fermions. Our strategy will be the following: by using the most complete analytic forms, we will investigate when a particular contribution to the angular profile becomes so small that is irrelevant and can thus be ignored. We will therefore use the
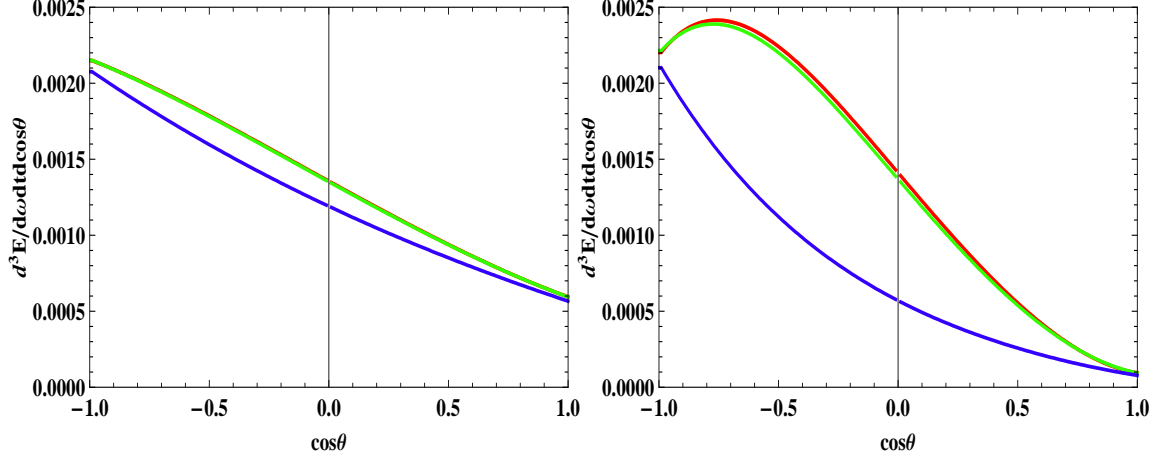
Figure 2.17: The differential energy emission rate (2.119) in terms of $\cos\theta$, for $n = 2$, $\omega_* = 0.5$, and (a) $a_* = 0.5$ (left plot) and (b) $a_* = 1.5$ (right plot). The different curves correspond to the emission rate when partial modes up to $l = 1/2$, $l = 3/2$, $l = 5/2$ and $l = 7/2$ (from bottom to top) have been summed up.

power series expansion (A.1) for the angular eigenvalue up to fourth order in $(a\omega)$, the analytic form of the angular eigenfunction given in (2.137) by keeping terms [7] up to $p = 10$, and, at the beginning, allow the angular-momentum numbers (l, m) to vary over their full range.

In Figs. 2.17(ab), we depict the differential emission rate (2.119) per unit time, unit frequency and angle of emission in terms of $\cos\theta$, for the case $\omega_* = 0.5$ and $a_* = 0.5$ (left plot) and $a_* = 1.5$ (right plot). The different curves correspond to the derived spectrum where modes up to a certain value of l (and all values of m in the range $[-l, +l]$) have been summed up: the lower (blue) curve includes only the $l = 1/2$ modes, the next (green) one modes up to $l = 3/2$, the subsequent (red) one modes up to $l = 5/2$ and the last (orange) one modes up to $l = 7/2$. We observe that the $l = 7/2$ curve is not even visible as it is completely covered by the $l = 5/2$ one – the same happens for all higher modes. As a matter of fact, the difference between the $l = 5/2$ and $l = 3/2$ curves is also quite small: for the maximum value of the angular momentum considered, $a_* = 1.5$, the difference in the value of the emission rate at its maximum and of $\theta_{\max}$ is of the order of only 1%; for smaller values of a_*, the errors reduce even more: for $a_* = 0.5$, the difference in the value of the emission rate at its maximum drops at the level of 0.08% while $\theta_{\max}$ is not affected at all. We may thus conclude, that the sum over l in (2.142) can be safely truncated at $l = 3/2$. The reason for this significant truncation is the weight factor $_hW_\Lambda$: although the thermal/statistics factor gives a boost to modes with large and positive m, the significant suppression of the graybody factor $\mathbf{T}_\Lambda$ in the low-energy regime as l increases ensures that higher

---

[7]We have confirmed that, by keeping terms up to $p = 10$ in this expansion, the derived values of the angular eigenfunction agree extremely well with the exact numerical ones – as a consistency check, we have successfully reproduced the plots of the angular eigenfunctions appearing in [166, 142].
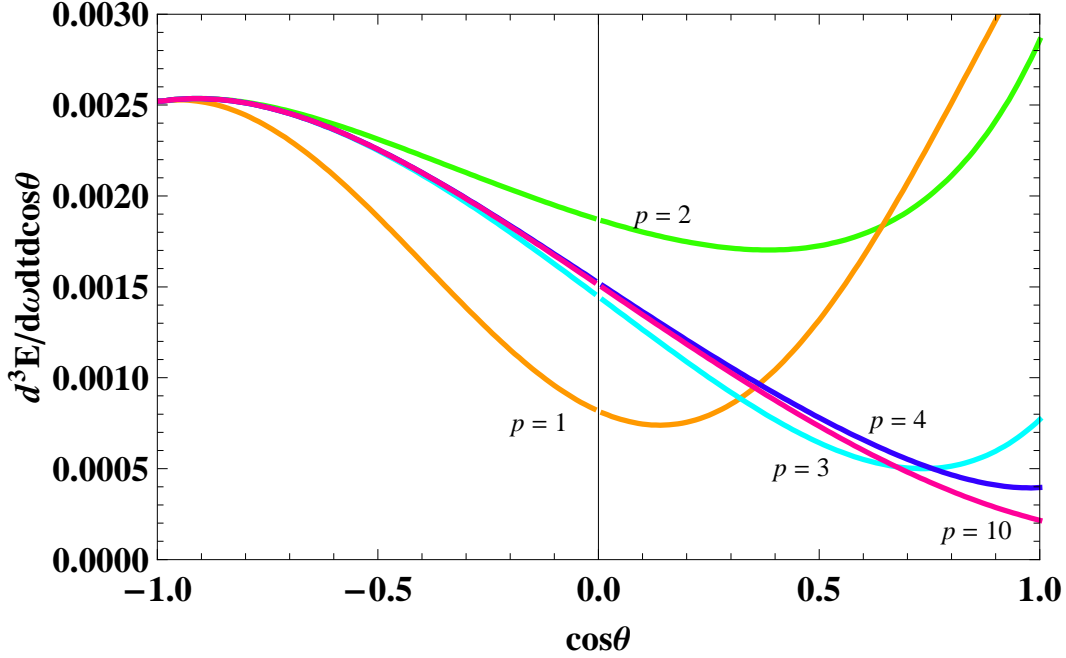
Figure 2.18: Energy emission rate per unit time, unit frequency and angle of emission in terms of $\cos\theta$, for $n = 2$, $\omega_* = 0.5$ and $a_* = 1$, and terms in the series expansion of the angular eigenfunction summed up to $p = 1$, $p = 2$, $p = 3$, $p = 4$ and $p = 10$.

modes can be safely ignored.

As a next step in our study, we investigate whether the sum in the series expansion of the eigenfunction can also be truncated. To this end, we have computed the differential energy emission rate (2.119), for $\omega_* = 0.5$ and $a_* = 1$, by keeping modes up to $l = 5/2$ for extra safety, and gradually increasing the maximum value of the sum index p. The behavior of the corresponding results for the emission rate as a function again of $\cos\theta$ is plotted in Fig. 2.18, where the different curves correspond to the maximum value of p kept in the sum, $p = 1, 2, 3, 4$ and 10. We observe that the correct value of the emission rate at its maximum is obtained fairly soon, when terms only up to $p = 2$ are included in the sum; the value of $\theta_{\max}$, on the other hand, needs one more term in the expansion ($p = 3$) to acquire its actual value. Our results are not in contradiction with [166] where the value of $p = 10$ was defined as the one that accurately reproduces the exact form of the eigenfunction. Indeed, higher terms included in the sum up to $p = 10$ do change the behavior of the eigenfunction, however, these changes are restricted in the area away from the angle of maximum emission, as Fig. 2.18 clearly shows. The value of the angular momentum of the black hole strongly affects the value of $p_{\max}$: for $a_* = 1.5$, the correct value of θ is obtained when terms up to $p = 4$ are included; in contrast, for $a_* = 0.5$, no terms higher than $p = 1$ are needed in the sum.

Let us comment at this point on the expression of the angular eigenvalue that was used in our calculations. As noted above, we initially employed the power series form of eq. (A.1) with terms up to the fourth order in $(a\omega)$. However, we have found that

the expression (2.133), with terms up to second order only, is more than adequate to lead to accurate results. Although including higher-order terms cause, at times, a significant change in the value of the angular eigenvalue itself, that change hardly affects any aspects of the angular profile of the emitted radiation. For example, for the mode $l = 1/2$ and $m = -1/2$, the difference in the value of the eigenvalue, when terms up to second and third order, respectively, are kept, is of the order of 10%, the effect in the value of the coefficient β_p appearing in eq. (2.140) is only 0.2% which leaves the angular profile virtually unchanged.

One may simplify further the analysis by considering more carefully the partial modes that dominate the energy emission spectrum. According to the results above, the sum over l can be safely truncated at the value $l = 3/2$, and thus we need to sum over the following six modes: $(l, m) = [(\frac{1}{2}, \frac{1}{2}), (\frac{1}{2}, -\frac{1}{2}), (\frac{3}{2}, \frac{3}{2}), (\frac{3}{2}, \frac{1}{2}), (\frac{3}{2}, -\frac{1}{2}), (\frac{3}{2}, -\frac{3}{2})]$. However, not all of the above modes have the same contribution to the angular variation of the energy spectrum. In Fig. 2.19(a), we display the angular eigenfunctions of the four most dominant modes out of the aforementioned six, for $n = 2$, $\omega_* = 0.5$ and angular momentum $a_* = 0.5$ (left plot). It is clear that, for small values of a_*, the two $l = 1/2$ modes dominate over the $l = 3/2$ ones. This dominance is further enhanced when the corresponding weight factors are taken into account, with the ones for the $l = 3/2$ modes being at least one order of magnitude smaller than the ones for the $l = 1/2$ modes. But even the contribution of the two dominant modes, $(\frac{1}{2}, \pm\frac{1}{2})$, is not of the same magnitude: when the weight factors and the difference in magnitude of the angular eigenfunctions are taken into account, the $(\frac{1}{2}, \frac{1}{2})$ mode is found to have at least five times bigger contribution than the $(\frac{1}{2}, -\frac{1}{2})$ one. As a result, the angular pattern of the emitted radiation at the low-energy channel, for small values of the angular momentum parameter, is predominantly defined by the $(\frac{1}{2}, \frac{1}{2})$ mode. Then, the constraint (2.142) takes the simplified form [8]

$$\sum_{q=0}^{3} a_q \, (1 + x)^q \left(a\omega + \frac{q}{1 + x} - \frac{1}{2(1 - x)} \right) = 0 \,, \tag{2.144}$$

and more particularly

$$\left(a\omega - \frac{1}{2(1 - x)} \right) \left[a_0^{(1/2)} + a_1^{(1/2)}(1 + x) + a_2^{(1/2)}(1 + x)^2 + a_3^{(1/2)}(1 + x)^3 \right]$$

$$+ a_1^{(1/2)} + 2a_2^{(1/2)}(1 + x) + 3a_3^{(1/2)}(1 + x)^2 = 0 \,. \tag{2.145}$$

In the above, we have used that $k_- = 0$ and $k_+ = 1/2$ for the mode $(\frac{1}{2}, \frac{1}{2})$, and the superscript $\{1/2\}$ denotes that the set of coefficients $a_p^{(1/2)}$ for this particular mode should be used here. In Appendix B.1, we list the results for the angular eigenvalue, as this follows from eq. (2.133), the values of the $(\alpha_p, \beta_p, \gamma_p)$ coefficients, according to the definitions (2.140), and finally the relations between the first four sum coefficients

---

[8]In what follows, we will adopt the value $p = 3$ as the maximum value of the sum index needed to accurately reproduce the behavior of the fermionic eigenfunction around the angle of maximum emission.
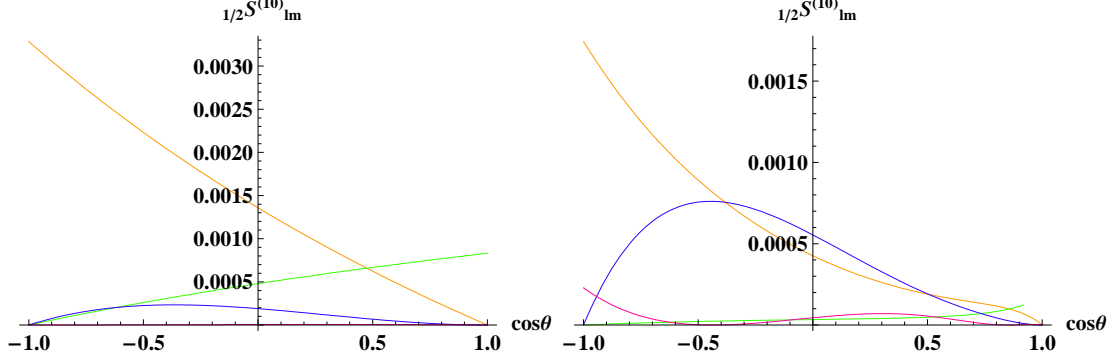
Figure 2.19: The fermionic angular eigenfunction $_{1/2}S_{lm}^{(10)}$ as a function of $\cos\theta$, for $n = 2$, $\omega_* = 0.5$ and: a) $a_* = 0.5$ (left plot) and $(l, m) = [(\frac{1}{2}, \frac{1}{2}), (\frac{1}{2}, -\frac{1}{2}), (\frac{3}{2}, \frac{3}{2}), (\frac{3}{2}, \frac{1}{2})]$ (from top to bottom), b) $a_* = 1.5$ (right plot) and $(l, m) = [(\frac{1}{2}, \frac{1}{2}), (\frac{3}{2}, \frac{3}{2}), (\frac{3}{2}, \frac{1}{2}), (\frac{1}{2}, -\frac{1}{2})]$ (from top to bottom).

a_p, given by the three-term recursion relations (2.138)-(2.139). A simple numerical analysis, then, shows that eq. (2.145) does not have any roots in the range $x \in (-1, +1)$ for $a\omega < 0.52$, with the global maximum located at $x = -1$ and the global minimum at $x = 1$. Therefore, if we fix the energy channel at e.g. $\omega_* = 0.5$, the angular eigenfunction of the $(\frac{1}{2}, \frac{1}{2})$-mode does not show any extrema up to $a_* \simeq 1$; as a result, the energy emission rate takes its maximum value at $\theta = \pi$ in accordance with the exact numerical results derived in [195, 178].

Nevertheless, as a_* increases, the $(\frac{3}{2}, \frac{3}{2})$-mode becomes important – this may be clearly seen in Fig. 2.19(b). Let us examine the behavior of this mode on its own. Its extremization constraint is given now by

$$\left(a\omega + \frac{1}{2(1 + x)} - \frac{1}{(1 - x)}\right) \left[a_0^{(3/2)} + a_1^{(3/2)}(1 + x) + a_2^{(3/2)}(1 + x)^2 + a_3^{(3/2)}(1 + x)^3\right]$$

$$+ a_1^{(3/2)} + 2a_2^{(3/2)}(1 + x) + 3a_3^{(3/2)}(1 + x)^2 = 0, \qquad (2.146)$$

where we have used that, for this mode, $k_- = 1/2$ and $k_+ = 1$. By making use of the relations between the first four $a_p^{(3/2)}$ coefficients, as these are found again in Appendix B.1, and performing a simple numerical analysis, we arrive at the following results: for $a\omega = 0$, all a_i with $i \geq 1$ vanish, and the constraint (2.146) reveals the existence of a sole extremal point at $x = -1/3$; this extremum is a local maximum – as a_* increases, the local maximum becomes gradually more important and slowly moves to the left, thus competing with the maximum of the $(\frac{1}{2}, \frac{1}{2})$-mode at $x = -1$ to create a global maximum for the energy emission rate in the range $(-1, -1/3)$ with the exact location depending on the value of a_*.

Thus, summarizing the above results, for an arbitrary value of a_*, the angular variation of the emitted fermions is mainly determined by the contribution of the
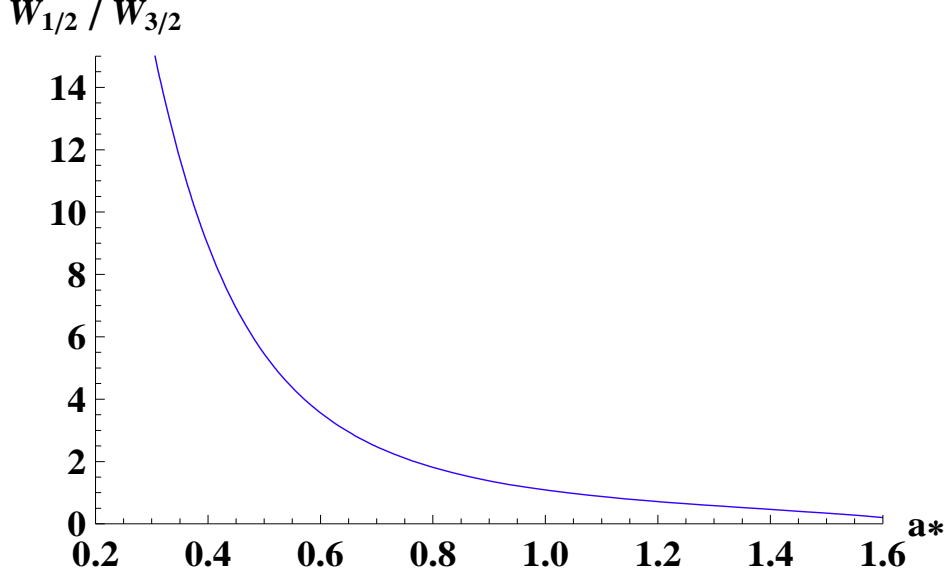
Figure 2.20: The relative weight factor $W_{rel} = W_{1/2}/W_{3/2}$ in terms of the angular-momentum parameter a_*, for the particular case of $\omega_* = 0.6$.

$(\frac{1}{2}, \frac{1}{2})$ and $(\frac{3}{2}, \frac{3}{2})$ modes, and thus the constraint (2.142) may take the final form

$$W_{rel} \sum_{p=0}^{3} a_p^{(1/2)} (1+x)^p \sum_{q=0}^{3} a_q^{(1/2)} (1+x)^q \left(a\omega + \frac{q}{1+x} - \frac{1}{2(1-x)} \right)$$

$$+(1-x^2) \sum_{p=0}^{3} a_p^{(3/2)} (1+x)^p \sum_{q=0}^{3} a_q^{(3/2)} (1+x)^q \left(a\omega + \frac{1/2+q}{1+x} - \frac{1}{1-x} \right) = 0 . \quad (2.147)$$

We have also defined the relative "weight factor" $W_{rel} = W_{1/2}/W_{3/2}$ whose value de-pends strongly on the angular parameter a_* – this dependence is shown in Fig. 2.20. For small values of a_*, W_{rel} takes large values and the extremization constraint is dom-inated by the $(\frac{1}{2}, \frac{1}{2})$-mode causing the emitted fermions to be aligned with the rotation axis. As a_* increases, W_{rel} decreases reaching the value one for approximately $a_* = 1$ – now, both modes contribute equally and $\theta_{\max}$ is pushed away from the $\theta = \pi$ value. For even larger values of a_*, the $(\frac{3}{2}, \frac{3}{2})$-mode starts dominating with the angle of maximum emission moving further away.

In support of our argument, that the $(\frac{1}{2}, \frac{1}{2})$ and $(\frac{3}{2}, \frac{3}{2})$ modes predominantly de-termine the angular variation of the fermionic spectrum, in Table 2.5 we display the values of the energy emission rate at the angle of maximum emission as well as the value of the corresponding angle $\theta_{\max}$, for various values of the energy parameter ω_* and angular-momentum parameter a_*. In each case, we display two values: the first one follows by taking into account the contribution of the two aforementioned modes and keeping terms only up to $p = 3$ in the sum of the angular eigenfunction (or, up to $p = 4$ for $a_* \geq 1$); the second follows by keeping all terms up to $p = 10$ and all partial

	$\omega_* = 0.5$		$\omega_* = 0.6$		$\omega_* = 0.7$		$\omega_* = 0.8$	
	approx.	full	approx.	full	approx.	full	approx.	full
$a_* = 0.50$	2.078	2.150	1.956	2.053	1.545	1.657	1.028	1.132
	-0.99	-0.99	-0.99	-0.99	-0.99	-0.89	-0.87	-0.74
$a_* = 0.75$	2.316	2.406	2.054	2.168	1.693	1.827	1.232	1.402
	-0.99	-0.99	-0.82	-0.81	-0.66	-0.64	-0.57	-0.52
$a_* = 1.00$	2.444	2.535	2.170	2.282	1.809	1.970	1.303	1.552
	-0.91	-0.91	-0.68	-0.67	-0.56	-0.54	-0.51	-0.46
$a_* = 1.25$	2.488	2.567	2.090	2.205	1.590	1.784	1.019	1.338
	-0.81	-0.81	-0.61	-0.60	-0.52	-0.50	-0.46	-0.43
$a_* = 1.50$	2.347	2.415	1.715	1.831	1.038	1.248	$-$	0.098
	-0.76	-0.76	-0.57	-0.56	-0.41	-0.42	$-$	-0.40

Table 2.5: The approximated and full values of the energy emission rate (2.119) at the angle of maximum emission, in units of $10^{-3}/r_h$, and the corresponding values of $\cos(\theta_{\max})$ for fermions.

modes up to $l = 7/2$. The values of the energy parameter ω_* have been chosen to lie in the low-energy regime and, at the same time, to display a non-trivial angular variation of the spectrum - it is worth mentioning that for all values smaller than $\omega_* = 0.5$, the angle of maximum emission is constantly located at $\theta = \pi$. On the other hand, the angular-momentum parameter a_* scans a fairly broad range from $a_* = 0.5$ to $a_* = 1.5$.

For the energy channel $\omega_* = 0.5$, the agreement between the two sets of results is extremely good: the error in the value of the energy emission rate at its maximum reaches the magnitude of 3.5% at most, while the agreement in the value of $\theta_{\max}$ is perfect. In agreement with the exact numerical results [178] where this energy channel was studied, for small values of a_*, the emitted radiation remains very close to the rotation axis and only for values close to $a_* = 1.0$ the emission starts showing a maximum at a gradually smaller angle. For $\omega_* = 0.6$, the errors in the value of the emission rate and $\theta_{\max}$ are at the level of 5% and 3% respectively, with the emission being peaked at an angle away from the horizon axis for $a_* \geq 0.75$. For $\omega_* = 0.7$, the error in the value of $\theta_{\max}$ is still quite small [9] ranging between 3% and 4%, whereas the error in the value of the emission rate at its maximum is now taking large values (7%-17%). Finally, for completeness, we show the energy channel of $\omega_* = 0.8$: although we have probably exceeded the range of validity of our approximation, the error in the value of $\theta_{\max}$ remains less than 10%.

The above comparison demonstrates that, for low values of the parameters ω_* and a_* where our semi-analytic approximation is valid, the use of the two modes, the $(\frac{1}{2}, \frac{1}{2})$

---

[9]The error in the value of $\theta_{\max}$ is indeed quite small for all values of $a_* \geq 0.75$. For $a_* = 0.5$, we observe a significant deviation of $\theta_{\max}$ from its actual value for the energy channels $\omega_* = 0.7$ and $\omega_* = 0.8$. This is due to the fact that, for these specific values of the energy parameter and angular momentum , the mode $(\frac{1}{2}, -\frac{1}{2})$ that we have ignored in our approximation is of the same order of magnitude as the $(\frac{3}{2}, \frac{3}{2})$ that we have taken into account.

and $(\frac{3}{2}, \frac{3}{2})$ ones, and the constraint (2.147) can provide realistic results for the angular variation of the fermionic spectrum. This can consequently help to determine the value of the angular momentum of the black hole according to the proposal of [195, 178]. The results displayed in Table 2.5 confirm the behavior found numerically for the energy channel $\omega_* = 0.5$ [178], extend the set of values that could be used for comparison with experiment to additional low-energy values of ω_* and, finally, provide a very satisfactory semi-analytic approximation in terms of only two partial modes.

Emission of Gauge Bosons

Let us now address the emission of gauge bosons on the brane by the simply-rotating black hole. We will again focus on the low-energy regime as this is the energy channel at which the emission of gauge bosons is polarized along the rotation axis of the black hole. We will attempt to determine the main factors that contribute to this behavior and, if possible, provide analytical arguments that justify it.

Following a similar strategy as in the case of fermions, we first investigate whether the infinite sum over the partial modes, characterized by (l, m), in eq. (2.142) can be truncated. By gradually increasing the value of l (and summing over all corresponding values of m), we looked for that value beyond which any increase in l makes no difference to the value of the energy emission rate at its maximum and of the corresponding angle. It turns out that, at the low-energy regime, this value is reached very quickly – this behavior is clearly displayed by the entries of Table 2.6. In the upper part of the Table, we present the energy emission rate (2.119) at its maximum and the corresponding angle as we increase l from 1 to 3 and vary a_* from 0.5 to 1.5 in a random low-energy channel ($\omega_* = 0.3$). We observe that the value of the angle of maximum emission for positive-helicity ($h = 1$) gauge bosons is indeed $\theta = \pi$, i.e. anti-parallel to the angular-momentum vector of the black hole, and that this value is not affected at all by adding any partial modes beyond the ones with $l = 1$. The energy emission rate also varies very little: its value at the angle of maximum emission is already reached for $l = 2$ and the difference from its value when only the $l = 1$ modes are taken into account is of the order of 0.1% independently of the value of the angular-momentum of the black hole. We may thus conclude that the angular profile of the emission of gauge bosons at the low-energy regime is determined almost exclusively by the lower $l = 1$ modes: the sum over l, therefore, in eq. (2.142) can be replaced by the contribution of only its first term.

We performed a similar analysis regarding the value of p in the sum in the expression for the angular eigenfunction, and we have found similar results displayed in the lower part of Table 2.6. The value of the angle of maximum emission is again not affected as terms beyond the first one ($p = 0$) are added. The actual value of the energy emission rate at the maximum angle is also very loosely dependent on p: as p goes from 1 to 2, the difference is of the order of 10^{-3}%, while the difference between the cases with $p = 0$ and $p = 1$ is again very small, of the order of 0.5%. While, according to the above, the sum over p can be clearly truncated even at $p = 0$, to increase the validity of the subsequent analysis, we will also keep terms with $p = 1$, and thus write the

	$a_* = 0.5$		$a_* = 1.0$		$a_* = 1.5$	
$l_{\max}$	Rate	$\cos(\theta_{\max})$	Rate	$\cos(\theta_{\max})$	Rate	$\cos(\theta_{\max})$
$l = 1$	0.017866	-0.99	0.028779	-0.99	0.066357	-0.99
$l = 2$	0.017883	-0.99	0.028817	-0.99	0.066440	-0.99
$l = 3$	0.017883	-0.99	0.028817	-0.99	0.066440	-0.99
$p_{\max}$	Rate	$\cos(\theta_{\max})$	Rate	$\cos(\theta_{\max})$	Rate	$\cos(\theta_{\max})$
$p = 0$	0.017948	-0.99	0.029051	-0.99	0.067319	-0.99
$p = 1$	0.017866	-0.99	0.028778	-0.99	0.066353	-0.99
$p = 2$	0.017866	-0.99	0.028779	-0.99	0.066357	-0.99
$p = 3$	0.017866	-0.99	0.028779	-0.99	0.066357	-0.99

Table 2.6: The differential energy emission rates at the maximum angle of emission and the corresponding angle for gauge bosons, for $\omega_* = 0.3$ and $n = 2$, in terms of the angular-momentum number l and sum index p, and for three indicative values of a_*.

analytic expression (2.137) of the angular eigenfunction as

$$
{}_1S_\Lambda(x) = e^{a\omega x} (1 + x)^{k_-} (1 - x)^{k_+} [a_0 + a_1 (1 + x)] . \tag{2.148}
$$

A final point that needs to be addressed is the contribution of the different m-modes. For $l = 1$, we have three modes with $m = +1, 0, -1$ that have, nevertheless, a different weight factor and thus a different contribution to the constraint (2.142). A numerical evaluation of the weight factor (2.143), with $\mathbf{T}_\Lambda$ given in eq. (2.123), for these three modes, in conjunction with the value of the angular eigenfunction in each case, reveals that the contribution of the $m = 1$ mode to the constraint (2.142) is almost two orders of magnitude larger than the one of the $m = 0$ mode, and that in turn is larger by two orders of magnitude than the contribution of the $m = -1$ mode. Therefore, it is the $l = m = 1$ mode that effectively determines the angular profile of the emitted radiation.

Then, the constraint (2.142) can take a particularly simple form. For $l = m = 1$ and $h = 1$, we obtain $k_- = 0$ and $k_+ = 1$, which then leads to the condition

$$
a_0 \left(a\omega - \frac{1}{1 - x} \right) + a_1 (1 + x) \left(a\omega + \frac{1}{1 + x} - \frac{1}{1 - x} \right) = 0 . \tag{2.149}
$$

The above can be written as a quadratic polynomial in x, with solutions

$$
x_{\mathrm{ex}} = - \left(\frac{a_0}{2a_1} + \frac{1}{a\omega} \right) \pm \sqrt{1 + \frac{1}{(a\omega)^2} + \frac{a_0}{a_1} + \frac{a_0^2}{4a_1^2}} . \tag{2.150}
$$

If the above values correspond to extremal points in the regime $x \in (-1, 1)$, then they should satisfy the inequality $|x_{\mathrm{ex}}| < 1$. This in turn imposes constraints on the coefficients a_0 and a_1. As in the case of fermions, these coefficients, for a given set of numbers (h, l, m), are given solely in terms of the parameter $a\omega$. In Appendix B.2, we

present the main steps for the derivation of the relations between the sum coefficients a_p in the case of gauge bosons. There, it is found that, for the mode $h = l = m = 1$,

$$\frac{a_1^{(1)}}{a_0^{(1)}} = -\frac{a\omega}{2}\left(3 + \frac{9a\omega}{20}\right). \tag{2.151}$$

We substitute the above ratio into eq. (2.150), and demand that $-1 < x_{\mathrm{ex}} < 1$. While the left-hand-side inequality is automatically satisfied for all values of $a\omega$, the right-hand-side translates to $9(a\omega)^2 + 60a\omega - 20 > 0$ that leads to the constraint $a\omega > 0.32$.

Therefore, for $a\omega < 0.32$ no extremal points for the differential energy emission rate exist in the range $x \in (-1, 1)$. This quantity is thus monotonic and has global extremal points at the end points $x = -1$ and $x = +1$. Substituting $k_- = 0$ and $k_+ = 1$ in eq. (2.148), it is easy to see that, for $x = +1$, the angular eigenfunction vanishes, while, for $x = -1$, it takes its maximum value $2a_0 e^{-a\omega}$. As a result, the positive-helicity component of the gauge field is perfectly aligned in an anti-parallel direction to the angular-momentum vector of the black hole ($\theta = \pi$), in agreement with the exact numerical results [178]. If $a\omega$ exceeds the value 0.32, a local maximum develops at an internal point of the range $(-1, 1)$, however, this remains subdominant to the global maximum at $x = -1$ up to the value $a\omega \simeq 0.85$. Therefore, if we fix the energy channel to $\omega_* = 0.5$, the maximum of the emitted radiation in the form of gauge fields remains aligned in an antiparallel direction to the angular-momentum of the black hole for all values of a_* up to 1.7, in agreement again with the exact numerical results [178].

Emission of Scalars

We finally address the case of the emission of scalar fields on the brane by a simply-rotating black hole. Although no useful information regarding the angular momentum of the black hole can be derived in this case, for completeness, we briefly discuss the main characteristics of the angular pattern of the scalar emission and the main contributing factors.

In order to investigate whether it is possible again to truncate the sums over l and p, that appear in the constraint (2.142), we construct Table 2.7. The left-hand-side of the table displays the energy emission rate at the angle of maximum emission and the corresponding angle in terms of the angular-momentum number l. The energy channel $\omega_* = 0.3$ has been chosen as an indicative case, the number of extra dimensions has been again fixed to $n = 2$, and the angular-momentum parameter is taken to be $a_* = 1.5$ – this is the highest value of a_* considered in this analysis, and the one for which the convergence of the sums over l and p is the most difficult to achieve. We observe that all modes beyond $l = 2$ add a contribution of order 0.01%, and thus can be safely ignored. But the difference between the values of the emission rate when all modes up to $l = 1$ and $l = 2$ have been, respectively, summed up is also very small, of the order of 1%. The value of $\theta_{\max}$ has also been stabilized to $\pi/2$ when $l_{max} = 1$. Therefore, in the context of our semi-analytic approach, the sum over l can be indeed truncated at $l = 1$ with no significant error.

$l_{\max}$	Rate	$\cos(\theta_{\max})$	$p_{\max}$	Rate	$\cos(\theta_{\max})$
$l = 0$	0.00052329	± 1	$p = 1$	0.00438439	± 1
$l = 1$	0.00137162	0	$p = 2$	0.00165378	± 0.67
$l = 2$	0.00139658	0	$p = 3$	0.00135215	± 0.05
$l = 3$	0.00139688	0	$p = 4$	0.00137489	0
$l = 4$	0.00139688	0	$p = 5$	0.00137122	0
$l = 5$	0.00139688	0	$p = 6$	0.00137167	0

Table 2.7: The differential energy emission rates at the maximum angle of emission and the corresponding angle, for $\omega_* = 0.3$, $n = 2$ and $a_* = 1.5$, in terms of the angular-momentum number l and sum index p for scalar fields.

On the right-hand-side of Table 2.7, we keep all partial modes up to $l = 2$ for extra accuracy, and examine the convergence of the sum over p. The change in the value of the energy emission rate at the angle of maximum emission between the cases with $p = 4$ and $p = 5$ is of the order of 0.3%, while all higher contributions are an order of magnitude smaller. The value of $\theta_{\max}$ has also taken the exact value of $\pi/2$, therefore this sum can be safely truncated at $p = 4$.

An exhaustive analysis of the values of the weight factors of the contributing partial modes $(l, m) = \{(0,0), (1,-1), (1,0), (1,1)\}$ for a variety of energy channels, $\omega_* \in (0.2 - 0.8)$ and angular-momentum of the black hole, $a_* \in (0.5 - 1.5)$, reveals that the two most dominant modes are the $(0,0)$ and $(1,1)$ with the contributions of the other two being always two orders of magnitude smaller. Therefore, combining all the above results, the extremization constraint (2.142) for the case of scalar fields, takes the simplified form:

$$W_{rel} \sum_{p=0}^{4} a_p^{(00)} (1+x)^p \sum_{q=0}^{4} a_q^{(00)} (1+x)^q \left(a\omega + \frac{q}{1+x} \right)$$

$$+ \sqrt{1-x^2} \sum_{p=0}^{4} a_p^{(11)} (1+x)^p \sum_{q=0}^{4} a_q^{(11)} (1+x)^q \left(a\omega + \frac{1/2+q}{1+x} - \frac{1}{2(1-x)} \right) = 0. \quad (2.152)$$

In the above, we have used that for the $(0,0)$-mode, $k_- = k_+ = 0$, while for the $(1,1)$-mode, $k_- = k_+ = 1/2$. Also, in this case, the relative weight factor is defined as $W_{rel} \equiv W_{00}/W_{11}$. The expressions of the sum coefficients $a_p^{(00)}$ and $a_p^{(11)}$ for the two modes can be found at the Appendix B.3.

Let us consider individually the two dominant modes. Starting from the $l = m = 0$ mode, we write its extremization constraint as

$$\sum_{p=0}^{3} [a\omega\, a_p + (p+1)\, a_{p+1}] (1+x)^p + a\omega\, a_4(1+x)^4 = 0. \quad (2.153)$$

This is a polynomial of fourth degree that in principle has four roots and, therefore, four potential extremal points. However, if we use the expressions of the a_p coefficients for

the $l = m = 0$ mode listed in Appendix B.3, we find that two of these roots are complex conjugates and one lies outside the range $[-1, 1]$. Thus, the angular wavefunction of the $l = m = 0$ mode has only one extremal point with respect to $x = \cos\theta$. This extremum is a minimum located at $x = 0$ ($\theta = \pi/2$) for small values of $a\omega$ that moves to positive values of x as $a\omega$ increases. However, the latter effect is actually an artifact of the truncation of the sum in the expression of the angular eigenfunction at a finite value of p. Even in our approximation where terms up to $p = 4$ are kept, we may see that the constant term of the polynomial (2.153) is given by a particular combination of the a_p coefficients that due to multiple cancelations quickly tends to zero, namely

$$\sum_{p=0}^{3} \left[a\omega\, a_p + (p + 1)\, a_{p+1} \right] + a\omega\, a_4 \simeq -\frac{(a\omega)^4}{72} + \mathcal{O}(a\omega)^5 \,. \tag{2.154}$$

Had we kept all terms in the series expansions of the angular eigenvalue and eigenfunction, every subsequent term in the sum of (2.154) would cancel part of the remain of all previous ones all the way to infinity, thus ensuring that the $x = 0$ is always an extremum of the $l = m = 0$ mode. A simple numerical analysis then shows that this local extremum is the only one in the range $(-1, 1)$ and corresponds to a minimum. Due to the fact that $k_+ = k_- = 0$, the $l = m = 0$ mode reaches the same maximum value at the boundary points $x = \pm 1$.

Moving to the next dominant mode $l = m = 1$, its extremization constraint reads

$$\sum_{p=0}^{4} a_p (1 + x)^p \left[a\omega (1 - x^2) - x(p + 1) + p \right] = 0 \,. \tag{2.155}$$

This is a polynomial of sixth degree whose six roots are potential extremal points. Substituting the a_p coefficients for this mode from Appendix B.3 and performing a simple numerical analysis, one may see that the four roots are two pairs of complex conjugate numbers and one lies outside the range $[-1, 1]$ leaving again only one root that may indeed correspond to a local extremal point of the angular eigenfunction of the $l = m = 1$ scalar mode with respect to $x = \cos\theta$. As in the case of the $l = m = 0$ mode, the extremum is located at $x = 0$ and moves towards positive values of x as the parameter $a\omega$ increases. We have again confirmed that the constant term of the above polynomial tends again to zero very quickly, i.e.

$$\sum_{p=0}^{4} (a\omega + p)\, a_p \simeq -\frac{(a\omega)^4}{375} + \mathcal{O}(a\omega)^5 \,, \tag{2.156}$$

signalling the fact that the $x = 0$ is always an extremum of the angular eigenfunction of the $l = m = 1$ mode. The difference from the case of the $l = m = 0$ mode lies in the fact that now this extremum is a global maximum instead of a minimum with the angular eigenfunction of the $l = m = 1$ mode vanishing at the boundary points $x = \pm 1$ since $k_+ = k_- = 1/2$. Let us briefly add here that a similar analysis of the remaining two scalar modes, $l = 1, m = 0$ and $l = -m = 1$, shows that these follow the behavior of the $l = m = 0$ and $l = m = 1$ modes, respectively.

The exact numerical analysis of the emission of scalar fields on the brane by a simply-rotating higher-dimensional black hole [136, 141] has revealed that the corresponding spectrum shows no angular variation for low values of the energy parameter ω_* and of the angular-momentum number a_*. Clearly, for $a_* = 0$, the constraint (2.153) is trivially satisfied and the $l = m = 0$ mode shows no extremal points – note that, for the mode $l = m = 1$, the constraint (2.155) still leads to a maximum at $x = 0$ even at $a_* = 0$. For low values of ω_*, a careful analysis reveals that it is the $l = m = 0$ mode that dominates over the others, therefore, for low a_*, the spectrum remains spherically-symmetric. As a_* starts increasing, the $l = m = 0$ also develops an extremum at $x = 0$ – it turns out that there is always a low-energy regime where the minima of the $l = m = 0$ and $l = 1, m = 0$ modes exactly cancel the maxima of the $l = m = 1$ and $l = -m = 1$ modes leading again to a spherically symmetric spectrum, however, this energy regime becomes gradually more narrow. If we allow the energy parameter ω_* to increase, too, then fairly quickly the $l = m = 1$ mode starts dominating causing the spectrum to exhibit maximum emission at $x = 0$, i.e. on the equatorial plane ($\theta = \pi/2$), in agreement with the exact numerical results [136, 141].

Closing, we should stress that the aspects of the particular problem studied here, i.e. the angular profile of the emission of Standard Model particles on the brane by a higher-dimensional black hole, could not be performed only by means of 4-dimensional tools: the particles emitted propagate on a brane embedded in a higher-dimensional space-time, and this is reflected in the expressions of the graybody factors that determine to a great extent the weight factors of the individual partial modes. It is therefore the combination of both traditional 4-dimensional and brane techniques that has allowed us to analytically reproduce the angular distribution of energy emission, and hopefully provide the means for the determination of the angular momentum and axis of rotation of the produced black hole.

Chapter 3

Quest for localized 4-D black holes in brane worlds: a no-go result

The novel theories that postulated the existence of additional spacelike dimensions in nature [28, 29, 30, 33, 34] changed dramatically the way scientists perceive today our 4-dimensional world, as emphasized many times so far in this dissertation. Our Universe is considered as a 4-dimensional hypersurface, a brane, embedded in a higher-dimensional spacetime, the bulk. This proposal has led to an intensive research activity that studies its implications on gravity, particle physics and cosmology. Gravity, in particular, has seen one of the most important pillars of the General Theory of Relativity, the concept of 4-dimensional spacetime, being modified in order to accommodate the potential existence of extra spacelike dimensions. This inevitably led to the reviewing of all known solutions and predictions of 4-dimensional gravity, with the most-studied one being the black-hole solutions. In the context of the Large Extra Dimensions scenario [28, 29, 30], where the extra dimensions were assumed to be flat, the study of black holes was straightforward since higher-dimensional versions of the Schwarzschild [201] and Kerr solutions [49] were known for decades. However, in the context of the Warped Extra Dimensions Scenario [33, 34], the task to derive a black hole on a brane embedded in a curved 5-dimensional background has proven to be unexpectedly difficult (for reviews, see [202, 105, 203, 99, 204]).

The first attempt to derive a brane-world black-hole solution appeared in [205] where the 4-dimensional Minkowski line-element in the Randall-Sundrum metric was substituted by the Schwarzschild solution, i.e.

$$ds^2 = e^{2A(y)} \left[-\left(1 - \frac{2M}{r} \right) dt^2 + \left(1 - \frac{2M}{r} \right)^{-1} dr^2 + r^2 \left(d\theta^2 + \sin^2 \theta \, d\varphi^2 \right) \right]. \quad (3.1)$$

The above line-element satisfies the 5-dimensional Einstein's field equations of the Randall-Sundrum model since the Schwarzschild solution, just like the Minkowski one, is a vacuum solution. However, it was demonstrated that the above ansatz does not describe a regular black hole localized on the brane since the solution is characterized by a string-like singularity extended along the fifth dimension. This becomes manifest

in the expression of the 5-dimensional curvature invariant quantity

$$R^{MNRS}R_{MNRS} \propto \frac{48e^{-4A(y)}M^2}{r^6} \, . \tag{3.2}$$

For $A(y) = -ky$, where k is the AdS curvature radius, as in the Randall-Sundrum model, or for any other, decreasing away from the brane, warp function, the above quantity blows up at y-infinity; more importantly, it reveals the existence of a singularity at $r = 0$ at every slice $y = const.$ of the 5-dimensional AdS spacetime. The above solution was therefore a black-string, rather than a black-hole, solution and was soon proven to be plagued by the Gregory-Laflamme instability [206, 207].

In the years that followed, other attempts to derive a regular black-hole solution in a warped 5-dimensional background proved how tricky the nature of the problem was: no analytical solution that would satisfy the 5-dimensional field equations and describe a 4-dimensional black hole on the brane was found, despite the several different approaches that were used (for some of them, see [208, 209, 210, 211, 212, 213, 214, 215, 216, 217]). One of those approaches [211] was to assume that the black-hole mass has a non-trivial y-profile along the extra dimension: if M in eq. (3.1) is not a constant quantity but a function of y, then, upon a convenient choice, the expression on the r.h.s. of eq. (3.2) could die out at a finite distance from the brane. However, the line-element inside the square brackets in (3.1) with $M = M(y)$ is not anymore a vacuum solution. A bulk matter distribution must be introduced for the 5-dimensional line-element to satisfy the field equations. The corresponding energy-momentum tensor was found [210, 211] to describe a shell-like distribution of matter engulfing the brane with a stiff-fluid equation of state that satisfied all energy conditions on the brane and vanished, as expected, away from the brane. Unfortunately, no field configuration, in the context of scalar or gauge field models, was found that could support such an energy-momentum tensor.

Numerical solutions were found [218, 219, 220] in the context of five- and six-dimensional warped models that exhibited the existence of black-hole solutions with horizon radius smaller than or at most of the order of the AdS length $\ell = 1/k$. No larger black-hole solutions were found, and that led to arguments of non-existence of large, classical, static black-hole solutions on the brane [221, 222, 223, 224, 225, 226] as well as to counter-arguments [227, 228, 229, 230]. Even, in the case of small black holes, no closed analytic solutions, that would allow us to study their topological and physical properties in a complete way, were ever found - in addition, the existence itself of the numerical solutions describing small vacuum black holes was put into question in recent works [231, 232]. However, additional numerical solutions employing novel numerical techniques have been presented [233, 234] that describe both small and large black holes in the context of the RS model: the solutions have been constructed starting from an AdS_5/CFT_4 solution with an exact Schwarzschild metric at the AdS infinite boundary; the boundary background is then rewritten in a more general way and expanded along the bulk to derive a RS brane at a finite proper distance whose induced metric is a perturbed Schwarzschild metric.

It is an intriguing fact that, contrary to the findings of the numerical works [218, 219, 220], all analytical attempts to derive a 5-dimensional regular black hole localized on the brane have been forced to introduce some form of matter in the theory, either in

the bulk [210, 211, 213, 230] or on the brane [215, 216, 217, 229, 235], or even higher-order geometrical terms [209, 236]. It is clear that the localization of the black-hole topology close to the brane demands support from some additional form of matter and cannot be realized by itself. For this reason, here, we shall turn again to the approach of [210, 211] in order to investigate potential field-theory models that could yield the well-behaved energy-momentum tensor that supported a regular, localized black hole. The mass of the black hole will be assumed again to have a non-trivial profile along the extra dimension: this will be motivated primarily by the need to eliminate the singular term of eq. (3.2) and turn the singular black-string spacetime to a regular AdS one at a finite distance from the brane; in addition, as the question of whether a purely Schwarzschild line-element should be recovered on the brane still remains open, this y-dependence will keep the model general enough to accommodate solutions that either resemble the Schwarzschild line-element on the brane or deviate from it. In addition, a time-dependence will be introduced in the line-element in an attempt to investigate whether the outcome of the gravitational collapse can be indeed static or not.

3.1 Theoretical Framework

As mentioned above, the factorized metric ansatz (3.1) leads to a black-string solution rather than a black-hole one. Therefore, one has to consider a non-factorized metric with a y-dependence in the 4-dimensional part of the line-element and more specifically in the mass parameter M. The obvious choice, to substitute the constant M in eq. (3.1) by a function of the fifth coordinate, however, leads to the appearance of an additional singularity in the 5-dimensional spacetime at the location of the horizon [210]. In [211], it was demonstrated that this is due to the non-analyticity of the 4-dimensional line-element: employing an analytic ansatz, i.e. a 4-dimensional line-element without a horizon, leads to a 5-dimensional spacetime without additional singularities.

Therefore, in what follows, we will consider the following analytic Vaidya-type line-element

$$ds^2 = e^{2A(y)} \left[-\left(1 - \frac{2m(v, y)}{r}\right) dv^2 + 2\epsilon dv dr + r^2 \left(d\theta^2 + \sin^2 \theta d\varphi^2\right) \right] + dy^2 . \quad (3.3)$$

For a constant value of y, the line-element inside the square brackets is a non-static Vaidya metric that can be used to describe the dynamical process of a collapsing ($\epsilon = +1$) or an expanding ($\epsilon = -1$) shell of matter. If we ignore also the v-dependence, the 4-dimensional static Vaidya metric is related to the Schwarzschild one by a mere coordinate transformation. Although we will be interested in final states that describe a static black hole (thus, we set $\epsilon = +1$), during this work, we will keep the v-dependence as we would like to investigate whether static configurations can exist at all or whether some type of dynamical evolution is necessary to exist in the model even after the formation of the black hole - as a matter of fact, it was Vaidya-types of metric that were used in some of the original works addressing this question [221, 222].

The modified, due to the assumed y-dependence, Vaidya-type line-element (3.3) was also shown to exhibit some attractive characteristics in the quest of localized black

holes [211]. Not only is the necessary bulk energy-momentum tensor fairly simple, but also the structure of the 5-dimensional spacetime resembles the one of the factorized spacetime of the black-string solution - indeed, the 5-dimensional curvature invariant quantities for the ansatz (3.3) have the form

$$R = -20A'^2 - 8A'' \,, \qquad R_{MN}R^{MN} = 4\left(20A'^4 + 16A'^2A'' + 5A''^2\right) \,, \qquad (3.4)$$

$$R_{MNRS}\,R^{MNRS} = 8\left(5A'^4 + 4A'^2A'' + 2A''^2 + \frac{6e^{-4A}\,m^2(v,y)}{r^6}\right) \,, \qquad (3.5)$$

and are formally identical to the ones for the metric (3.1) with no extra terms appearing due to the assumed y-dependence – a behavior not observed for any other choice of non-factorized line-elements. On the other hand, the assumed scaling of the mass function with y can in principle eliminate the last singular term of eq. (3.5) and restore the finiteness of the 5-dimensional spacetime at a moderate distance from the brane - indeed, any function decreasing faster than the square of the warp factor could achieve the localization of the black-hole singularity.

Thus focusing on the line-element (3.3), we derive the components of the Einstein tensor G_{MN} which, in mixed form, are found to be

$$G^v{}_v = G^r{}_r = G^\theta{}_\theta = G^\phi{}_\phi = 6A'^2 + 3A'' \,, \qquad (3.6)$$

$$G^r{}_v = \frac{2}{r^2}\,e^{-2A}\,\partial_v m - \frac{1}{r}\left(\partial_y^2 m + 4A'\,\partial_y m\right) \,, \qquad (3.7)$$

$$G^y{}_v = e^{2A}\,G^r{}_y = \frac{1}{r^2}\,\partial_y m \,, \qquad (3.8)$$

$$G^v{}_r = G^y{}_r = G^v{}_y = 0 \,, \qquad (3.9)$$

$$G^y{}_y = 6A'^2 \,. \qquad (3.10)$$

The Einstein's field equations in the bulk will follow by equating the above components of G^M_N with the corresponding ones of the energy-momentum tensor T^M_N. The latter will be determined once the bulk Lagrangian is defined, in the next section. However, the form of the above equations allows us to make some basic observations. The assumed y-dependence of the mass function introduces off-diagonal, non-isotropic pressure components. The dependence on v does not by itself introduce a new pressure component but contributes to one of the non-isotropic ones. In [211], the assumption was made that the warp factor has the form of the Randall-Sundrum model, $A(y) = -ky$, which is supported by the bulk cosmological constant. In that case, the diagonal components (3.6) and (3.10) are trivially satisfied and no energy density or diagonal pressure components are necessary in the bulk. However, here, we will assume that the warp factor has a general form $A(y)$ in order to allow for less restricted field configurations that, in general, generate both diagonal and off-diagonal components. Since it holds that $G^v{}_v = G^r{}_r = G^\theta{}_\theta = G^\phi{}_\phi$, the bulk energy-momentum tensor will satisfy, by construction, a stiff equation of state.

In the following sections, we will study a variety of field theory models in an attempt to find the one that could support the aforementioned line-element (3.3). It

is already known [210] that the desired Vaidya-type metric cannot be supported by conventional forms of matter (realized by either scalar or gauge fields). Motivated by previous considerations of non-ordinary scalar field theories, that aimed to produce additional pressure components necessary for the stabilisation of brane-world models [237, 238, 239, 240, 241], we will focus our attention on scalar fields and consider a variety of models. These will include one or more minimally-coupled scalar fields with a general Lagrangian, admitting non-canonical kinetic terms, derivative interactions, mixing terms or the presence of ghosts, as well as a scalar field conformally-coupled with gravity with a general conformal coupling function.

Once a consistent solution in the bulk is found, a single brane will then be introduced in the model that in general contains a localized energy-momentum tensor $S_{\mu\nu}$. The spacetime will be assumed to be invariant under the mirror transformation $y \rightarrow -y$. The bulk equations will then be supplemented by the junction conditions [242]

$$[K_{\mu\nu} - h_{\mu\nu} K] = -\kappa_5^2 S_{\mu\nu} , \qquad (3.11)$$

relating the extrinsic curvature $K_{\mu\nu}$, the induced metric tensor $h_{\mu\nu}$ and the energy-momentum tensor $S_{\mu\nu}$ on the brane - the brackets denote the discontinuity across the brane. The discontinuity of the l.h.s. of the above equation will be a function of the warp factor $A(y)$, the mass function $m(v,y)$ and their derivatives with respect to y. With the help of the bulk solution, if existent, the above equation will give us the necessary matter content of the brane for its consistent embedding in the 5-dimensional warped spacetime.

3.2   A Field Theory with minimally-coupled Scalars

In this section, we focus on the case of models with minimally-coupled scalar fields with a general form of Lagrangian. The action functional of the gravitational theory therefore reads

$$\mathcal{S} = \int d^4x \, dy \, \sqrt{-g} \left(\frac{R}{2\kappa_5^2} - \mathcal{L}_{sc} - \mathcal{L}_m \right) , \qquad (3.12)$$

where g_{MN} and R are the metric tensor and Ricci scalar, respectively, of the 5-dimensional spacetime described by (3.3), and $\kappa_5^2 = 8\pi G_N$ the 5-dimensional gravitational constant. The action contains in addition the general Lagrangian $\mathcal{L}_{sc}$, associated with one or more scalar fields, and $\mathcal{L}_m$ stands for any other form of matter or energy in the theory - throughout this work, we will assume that this term describes the distribution of a uniform, negative energy-density and thus $\mathcal{L}_m = \Lambda_B$, where Λ_B the bulk cosmological constant. The field equations resulting from the aforementioned action have the form

$$R_{MN} - \frac{1}{2} g_{MN} R = \kappa_5^2 (T_{MN} - g_{MN} \Lambda_B) , \qquad (3.13)$$

with T_{MN} being the energy-momentum tensor associated with the scalar fields

$$T_{MN} = \frac{2}{\sqrt{-g}} \frac{\delta(\sqrt{-g} \, \mathcal{L}_{sc})}{\delta g^{MN}} . \qquad (3.14)$$

In the following subsections, we consider particular choices for $\mathcal{L}_{sc}$, and we examine the existence of a viable solution of the field equations in the bulk.

3.2.1   A Single Scalar Field with a non-canonical kinetic term

As a fist step, we consider the following theory of a single scalar field with a non-canonical kinetic term

$$\mathcal{L}_{sc} = \sum_{n=1} f_n(\phi) \left(\partial^M \phi \, \partial_M \phi\right)^n + V(\phi)\,, \tag{3.15}$$

where $f_n(\phi)$ are arbitrary, smooth functions of the scalar field ϕ. The components of the corresponding energy-momentum tensor follow from the expression

$$T^A_{\ B} = 2 \sum_{n=1} n f_n(\phi) \left(\partial^M \phi \, \partial_M \phi\right)^{n-1} \partial^A \phi \, \partial_B \phi - \delta^A_B \left[\sum_{n=1} f_n(\phi) \left(\partial^M \phi \, \partial_M \phi\right)^n + V(\phi)\right]. \tag{3.16}$$

The off-diagonal components $T^v_{\ r}$, $T^y_{\ r}$ and $T^v_{\ y}$ of the energy-momentum tensor must trivially vanish since the corresponding components of the Einstein tensor (3.9) do the same. These conditions however impose strict constraints on the form of the scalar field: the vanishing of the $T^v_{\ r}$ component, for instance,

$$T^v_{\ r} = 2 \sum_{n=1} n f_n(\phi) \left(\partial^M \phi \, \partial_M \phi\right)^{n-1} (\partial_r \phi)^2 \, e^{-2A} \tag{3.17}$$

demands that the scalar field is not a function of the radial coordinate, $\partial_r \phi = 0$. But then it is not possible to satisfy the remaining Einstein's equations: assuming that $\phi = \phi(v, y)$[1], the expression of the non-vanishing off-diagonal component $T^y_{\ v}$, when combined with the corresponding component of the Einstein tensor (3.8), leads to the equation

$$\frac{\partial_y m}{r^2} = 2\kappa_5^2 \sum_n n f_n(\phi) \left(\partial_y \phi\right)^{2n-1} \partial_v \phi\,. \tag{3.18}$$

An incompatibility problem arises immediately: the field ϕ and, therefore, the right-hand-side of the above equation is independent of r but the left-hand-side has an explicit dependence on that coordinate. As a result, the case of a single, minimally-coupled scalar field, even with a general non-canonical kinetic term, does not lead to a solution.

3.2.2   Two interacting scalar fields

We are thus forced to consider a multi-field model. We will study first the case of two scalar fields ϕ and χ whose dynamics and interactions are described by the Lagrangian

$$\mathcal{L}_{sc} = f^{(1)}(\phi, \chi) \, \partial^M \phi \, \partial_M \phi + f^{(2)}(\phi, \chi) \, \partial^M \chi \, \partial_M \chi + V(\phi, \chi)\,, \tag{3.19}$$

---

[1]Throughout this work, and in order to preserve the spherical symmetry of any potential solution, we assume that the scalar fields do not depend on the angular coordinates θ and ϕ.

where $f^{(1,2)}$ are arbitrary smooth functions of the two fields. The energy-momentum tensor now reads:

$$T^A_{\ B} = 2f^{(1)}(\phi, \chi)\,\partial^A\phi\,\partial_B\phi + 2f^{(2)}(\phi, \chi)\,\partial^A\chi\,\partial_B\chi - \delta^A_{\ B}\,\mathcal{L}_{sc}\,. \tag{3.20}$$

The vanishing of the off-diagonal components $G^v_{\ r}$, $G^y_{\ r}$ and $G^v_{\ y}$ implies again the vanishing of the corresponding components of the energy-momentum tensor, which now results in the following two constraints[2] on the fields:

$$f^{(1)}(\phi, \chi)\,(\partial_r\phi)^2 + f^{(2)}(\phi, \chi)\,(\partial_r\chi)^2 = 0\,, \tag{3.21}$$

$$f^{(1)}(\phi, \chi)\,\partial_r\phi\partial_y\phi + f^{(2)}(\phi, \chi)\,\partial_r\chi\partial_y\chi = 0\,. \tag{3.22}$$

From the constraint (3.21), it is clear that if one of the fields were not to depend on r, neither would the other one. Although, in this case, both of the constraints would be trivially satisfied, the same incompatibility problem associated with the (yv)-component of the field equations, that now has the form

$$\frac{\partial_y m}{r^2} = 2\kappa_5^2 \left[f_1^{(1)}(\phi, \chi)\partial_y\phi\partial_v\phi + f_1^{(2)}(\phi, \chi)\partial_y\chi\partial_v\chi\right]\,, \tag{3.23}$$

would again arise with the r.h.s. being necessarily r-independent and the l.h.s. a function of r. Similarly, the constraint (3.22) implies that if one of the fields were not to depend on y, neither would the other one. But this case is also excluded since, through eq. (3.23), the mass of the black hole would then necessarily loose the assumed y-dependence.

The constraints (3.21)-(3.22) are supplemented by a third one following from the diagonal components of the Einstein's field equations along the brane. By using the expression (3.20) and applying the constraint (3.21), the corresponding components of the energy-momentum tensor are found to have the form:

$$T^v_{\ v} = T^r_{\ r} = 2e^{-2A}\left[f^{(1)}(\phi, \chi)\,\partial_r\phi\partial_v\phi + f^{(2)}(\phi, \chi)\,\partial_r\chi\partial_v\chi\right] - \mathcal{L}_{sc}\,, \tag{3.24}$$

$$T^\theta_{\ \theta} = T^\varphi_{\ \varphi} = -\mathcal{L}_{sc}\,. \tag{3.25}$$

The components of the Einstein tensor along the brane (3.6) satisfy the relation $G^v_{\ v} = G^r_{\ r} = G^\theta_{\ \theta} = G^\phi_{\ \phi}$, therefore the aforementioned components of T^M_N should also be equal. This holds if the additional constraint on the field configurations is imposed

$$f^{(1)}(\phi, \chi)\,\partial_r\phi\partial_v\phi + f^{(2)}(\phi, \chi)\,\partial_r\chi\partial_v\chi = 0\,. \tag{3.26}$$

From the above constraint, we may again conclude that if one of the fields were not to depend on v, neither would the other one. As a matter of fact, we note from eq. (3.23), that, in order for a solution with a non-trivial profile of the mass distribution, i.e. $m = m(y)$, along the extra dimension to exist, the fields must necessarily depend on v; therefore, if such a solution exists, the matter distribution around such a black

---

[2] $T^v_{\ y} = g^{vr}\,T^y_{\ r}$, and as a result there are only two independent constraints.

hole owes to be dynamical and not static, with this demand holding even if the mass of the black hole itself is not time-evolving and thus independent of v.

Coming back to the existence of the solution and assuming that $\phi = \phi(v, r, y)$ and $\chi = \chi(v, r, y)$, we proceed as follows: we solve the new constraint (3.26) for the coupling function $f^{(2)}(\phi, \chi)$, and then substitute it into the (yv)-component (3.23) to obtain the following alternative form for that equation

$$\frac{\partial_y m}{r^2} = 2\kappa_5^2 \, f^{(1)}(\phi, \chi) \frac{\partial_v \phi}{\partial_r \chi} \left(\partial_y \phi \partial_r \chi - \partial_y \chi \partial_r \phi \right). \tag{3.27}$$

However, a similar rearrangement of eq. (3.21) and substitution into the constraint (3.22) leads to

$$\partial_y \phi \partial_r \chi - \partial_y \chi \partial_r \phi = 0, \tag{3.28}$$

that unfortunately causes the r.h.s. of eq. (3.27) to be zero and thus to loose the desired y-dependence of the mass function. We note that the absence of the solution holds independently of the signs of the coupling functions $f^{(1,2)}(\phi, \chi)$ – i.e. of whether the two scalar fields are normal or tachyonic – or of the form of the potential $V(\phi, \chi)$ that determines the interaction between the two fields.

3.2.3   Two interacting scalar fields with general kinetic terms

We now combine the two previous models considered to construct a Lagrangian of two scalar fields interacting through an arbitrary potential $V(\phi, \chi)$ and admitting general kinetic terms. The Lagrangian of the scalar fields then reads

$$\mathcal{L}_{sc} = \sum_{n=1} f_n^{(1)}(\phi, \chi) \left(\partial^M \phi \partial_M \phi \right)^n + \sum_{n=1} f_n^{(2)}(\phi, \chi) \left(\partial^M \chi \partial_M \chi \right)^n + V(\phi, \chi), \tag{3.29}$$

while the energy momentum tensor assumes the form:

$$\begin{aligned} T^A_{\ B} &= 2 \sum_{n=1} f_n^{(1)}(\phi, \chi) \, n \left(\partial^M \phi \partial_M \phi \right)^{n-1} \partial^A \phi \partial_B \phi \\ &\quad + 2 \sum_{n=1} f_n^{(2)}(\phi, \chi) \, n \left(\partial^M \chi \partial_M \chi \right)^{n-1} \partial^A \chi \partial_B \chi - \delta^A_{\ B} \, \mathcal{L}_{sc}. \end{aligned} \tag{3.30}$$

Working as in the previous subsection, from the vanishing of the off-diagonal components $G^v_{\ r}$, $G^v_{\ y}$ and $G^y_{\ r}$, we derive the following two constraints on the fields

$$\sum_{n=1} n \left[f_n^{(1)}(\phi, \chi) \left(\partial^M \phi \partial_M \phi \right)^{n-1} (\partial_r \phi)^2 + f_n^{(2)}(\phi, \chi) \left(\partial^M \chi \partial_M \chi \right)^{n-1} (\partial_r \chi)^2 \right] = 0, \tag{3.31}$$

$$\sum_{n=1} n \left[f_n^{(1)}(\phi, \chi) \left(\partial^M \phi \partial_M \phi \right)^{n-1} \partial_r \phi \partial_y \phi + f_n^{(2)}(\phi, \chi) \left(\partial^M \chi \partial_M \chi \right)^{n-1} \partial_r \chi \partial_y \chi \right] = 0 \tag{3.32}$$

Also, the equality of the diagonal components of the Einstein tensor along the brane results into the additional constraint

$$\sum_{n=1} n \left[f_n^{(1)}(\phi, \chi) \left(\partial^M \phi \partial_M \phi \right)^{n-1} \partial_r \phi \partial_v \phi + f_n^{(2)}(\phi, \chi) \left(\partial^M \chi \partial_M \chi \right)^{n-1} \partial_r \chi \partial_v \chi \right] = 0, \tag{3.33}$$

while the (yv)-component of the Einstein's field equations now has the form

$$\frac{\partial_y m}{r^2} = 2\kappa_5^2 \sum_{n=1} n \left[f_n^{(1)}(\phi,\chi) \left(\partial^M \phi \partial_M \phi\right)^{n-1} \partial_y \phi \partial_v \phi + f_n^{(2)}(\phi,\chi) \left(\partial^M \chi \partial_M \chi\right)^{n-1} \partial_y \chi \partial_v \chi \right].$$
(3.34)

The following observation makes the attempt to find a viable solution in the context of this model obsolete: if we define the following functions

$$\tilde{f}^{(1)}(\phi,\chi) = \sum_{n=1} n f_n^{(1)}(\phi,\chi) \left(\partial^M \phi \partial_M \phi\right)^{n-1}, \tag{3.35}$$

$$\tilde{f}^{(2)}(\phi,\chi) = \sum_{n=1} n f_n^{(2)}(\phi,\chi) \left(\partial^M \chi \partial_M \chi\right)^{n-1}, \tag{3.36}$$

then, Eqs. (3.31-3.34) reduce to Eqs. (3.21), (3.22), (3.26), and (3.23), respectively, with the $f^{(1,2)}(\phi,\chi)$ coupling functions being replaced by $\tilde{f}^{(1,2)}(\phi,\chi)$. As a result, upon a similar rearrangement of the three constraints, the r.h.s. of the (yv)-component vanishes, a result that eliminates again the y-dependence of the mass function.

3.2.4   Two interacting scalar fields with mixed kinetic terms

We now increase the complexity of the model by allowing the scalar fields to have mixed kinetic terms and thus consider the following generalized form of the scalar Lagrangian

$$\mathcal{L}_{sc} = f^{(1)}(\phi,\chi)\,\partial^M \phi \partial_M \phi + f^{(2)}(\phi,\chi)\,\partial^M \chi \partial_M \chi + f^{(3)}(\phi,\chi)\,\partial^M \phi \partial_M \chi + V(\phi,\chi). \tag{3.37}$$

Then, the energy-momentum tensor reads:

$$\begin{aligned} T^A_{\ B} &= 2f^{(1)}(\phi,\chi)\,\partial^A \phi \partial_B \phi + 2f^{(2)}(\phi,\chi)\,\partial^A \chi \partial_B \chi \\ &\quad + f^{(3)}(\phi,\chi) \left[\partial^A \phi \partial_B \chi + \partial^A \chi \partial_B \phi\right] - \delta^A_{\ B}\,\mathcal{L}_{sc}. \end{aligned} \tag{3.38}$$

The vanishing of the off-diagonal components $G^v_{\ r}$, $G^v_{\ y}$ and $G^y_{\ r}$ imposes again the vanishing of the corresponding components of the energy-momentum tensor, which in this case results in the following two constraints

$$f^{(1)}(\phi,\chi)\,(\partial_r \phi)^2 + f^{(2)}(\phi,\chi)\,(\partial_r \chi)^2 + f^{(3)}(\phi,\chi)\,\partial_r \phi \partial_r \chi = 0, \tag{3.39}$$

$$2f^{(1)}(\phi,\chi)\,\partial_r \phi \partial_y \phi + 2f^{(2)}(\phi,\chi)\,\partial_r \chi \partial_y \chi + f^{(3)}(\phi,\chi)\,[\partial_r \phi \partial_y \chi + \partial_y \phi \partial_r \chi] = 0. \tag{3.40}$$

From the first of the above two equations, it is clear that both fields must simultaneously depend, or not, on the radial coordinate r. If they are both independent of r, then the two constraints are satisfied but the non-vanishing off-diagonal (yv)-component, that now takes the form

$$\frac{\partial_y m}{r^2} = \kappa_5^2 \left[2f^{(1)}\,\partial_v \phi \partial_y \phi + 2f^{(2)}\,\partial_v \chi \partial_y \chi + f^{(3)}\,(\partial_v \phi \partial_y \chi + \partial_y \phi \partial_v \chi) \right], \tag{3.41}$$

becomes inconsistent due to the explicit r-dependence on its l.h.s.. Equation (3.41) seems to allow for certain combinations of the partial derivatives $(\partial_y \phi, \partial_y \chi, \partial_v \phi, \partial_v \chi)$

to vanish. However, to proceed, we will assume the most general case, i.e. that $\phi = \phi(r, v, y)$ and $\chi = \chi(r, v, y)$, and we will comment on the more special cases at the end of this subsection.

We now turn to the diagonal components of the Einstein's field equations. The diagonal components of the Einstein tensor along the brane are equal, and thus the same must hold for the components of the energy-momentum tensor, that now have the form

$$T^v_{\ v} = T^r_{\ r} = e^{-2A} \left[2f^{(1)} \partial_r \phi \partial_v \phi + 2f^{(2)} \partial_r \chi \partial_v \chi + f^{(3)} \left(\partial_r \phi \partial_v \chi + \partial_r \chi \partial_v \phi \right) \right] - \mathcal{L}_{sc} \quad (3.42)$$

$$T^\theta_{\ \theta} = T^\varphi_{\ \varphi} = -\mathcal{L}_{sc} \,. \quad (3.43)$$

Demanding the equality of the above expressions, the following additional constraint is obtained

$$2f^{(1)}(\phi, \chi) \, \partial_r \phi \partial_v \phi + 2f^{(2)}(\phi, \chi) \, \partial_r \chi \partial_v \chi + f^{(3)}(\phi, \chi) \left(\partial_r \phi \partial_v \chi + \partial_r \chi \partial_v \phi \right) = 0 \,. \quad (3.44)$$

Let us now consider the system of constraints (3.39), (3.40) and (3.44): it is a homogeneous system of linear equations for $f^{(1)}$, $f^{(2)}$ and $f^{(3)}$ – the necessary condition for this system to possess a solution other than the trivial one is the vanishing of the determinant of the matrix of coefficients:

$$\begin{vmatrix} (\partial_r \phi)^2 & (\partial_r \chi)^2 & \partial_r \phi \partial_r \chi \\ 2\partial_r \phi \partial_y \phi & 2\partial_r \chi \partial_y \chi & \partial_r \phi \partial_y \chi + \partial_y \phi \partial_r \chi \\ 2\partial_r \phi \partial_v \phi & 2\partial_r \chi \partial_v \chi & \partial_r \phi \partial_v \chi + \partial_v \phi \partial_r \chi \end{vmatrix} = 0 \,. \quad (3.45)$$

One may easily check that the above condition indeed holds, therefore the system may be solved to yield the values of two coupling functions in terms of the third one. Making the arbitrary choice of $f^{(2)}$ being the undetermined one, we find the following expressions for the other two coupling functions:

$$f^{(1)} = f^{(2)} \frac{(\partial_r \chi)^2}{(\partial_r \phi)^2} \,, \qquad f^{(3)} = -2f^{(2)} \frac{\partial_r \chi}{\partial_r \phi} \,. \quad (3.46)$$

If we then use the above relations in the expression of the (yv)-component (3.41), we obtain the alternative form

$$\frac{\partial_y m}{r^2} = \frac{2\kappa_5^2 f^{(2)}}{(\partial_r \phi)^2} \left(\partial_v \phi \partial_r \chi - \partial_r \phi \partial_v \chi \right) \left(\partial_y \phi \partial_r \chi - \partial_r \phi \partial_y \chi \right) \,. \quad (3.47)$$

We observe that, contrary to what happens in the previous two models considered, the rearrangement of the three constraints (3.39), (3.40) and (3.44) in this model does not by itself cause the vanishing of the r.h.s. of the above equation. Clearly, as the Lagrangian of the model becomes more complex, the system of field equations becomes more flexible.

The remaining independent off-diagonal component that we have not considered yet follows by combining the $G^r_{\ v}$ component (3.7) of the Einstein tensor with the

corresponding component of the energy-momentum tensor. Then, we obtain the field equation

$$\frac{2\partial_v m}{r^2} - \frac{e^{2A}}{r}\left(\partial_y^2 m + 4A'\partial_y m\right) = 2\kappa_5^2\left[f^{(1)}\left(\partial_v\phi\right)^2 + f^{(2)}\left(\partial_v\chi\right)^2 + f^{(3)}\partial_v\phi\partial_v\chi\right]. \quad (3.48)$$

Similarly, if we use the relations (3.46) in the above equation, this may be rewritten as

$$\frac{2\partial_v m}{r^2} - \frac{e^{2A}}{r}\left(\partial_y^2 m + 4A'\partial_y m\right) = 2\kappa_5^2\frac{f^{(2)}}{(\partial_r\phi)^2}\left(\partial_v\phi\partial_r\chi - \partial_r\phi\partial_v\chi\right)^2. \quad (3.49)$$

Finally, the last diagonal component, the one along the extra dimension, assumes the form

$$6A'^2 = \kappa_5^2\left[-\Lambda_B + 2f^{(1)}(\partial_y\phi)^2 + 2f^{(2)}(\partial_y\chi)^2 + 2f^{(3)}\partial_y\phi\partial_y\chi - \mathcal{L}_{sc}\right]. \quad (3.50)$$

At this point we will need the explicit expression of the Lagrangian $\mathcal{L}_{sc}$. By making use of the constraints (3.39) and (3.44), this turns out to be

$$\mathcal{L}_{sc} = f^{(1)}(\partial_y\phi)^2 + f^{(2)}(\partial_y\chi)^2 + f^{(3)}\partial_y\phi\partial_y\chi + V(\phi,\chi). \quad (3.51)$$

If we use the above expression, then eq. (3.50) and the diagonal components of the field equations along the brane reduce to the following two independent differential equations

$$6A'^2 = \kappa_5^2\left[-\Lambda_B + f^{(1)}(\partial_y\phi)^2 + f^{(2)}(\partial_y\chi)^2 + f^{(3)}\partial_y\phi\partial_y\chi - V(\phi,\chi)\right] \quad (3.52)$$

$$6A'^2 + 3A'' = \kappa_5^2\left[-\Lambda_B - f^{(1)}(\partial_y\phi)^2 - f^{(2)}(\partial_y\chi)^2 - f^{(3)}\partial_y\phi\partial_y\chi - V(\phi,\chi)\right] \quad (3.53)$$

respectively. As usually, if we subtract the first of the above equations from the second, the latter may be substituted by the simpler form

$$3A'' = -2\kappa_5^2\left[f^{(1)}(\partial_y\phi)^2 + f^{(2)}(\partial_y\chi)^2 + f^{(3)}\partial_y\phi\partial_y\chi\right] = -\frac{2\kappa_5^2 f^{(2)}}{(\partial_r\phi)^2}\left(\partial_y\phi\partial_r\chi - \partial_r\phi\partial_y\chi\right)^2,$$
$$(3.54)$$

where, in the last part, we have used again the relations (3.46). If we now take the square of eq. (3.47) and combine it with Eqs. (3.49) and (3.54), we obtain a differential equation for the mass function with no dependence on the fields and their coupling functions, namely

$$\frac{(\partial_y m)^2}{r^3} = 3A''\left[-\frac{2\partial_v m}{r} + e^{2A}\left(\partial_y^2 m + 4A'\partial_y m\right)\right]. \quad (3.55)$$

Unfortunately, this equation is again inconsistent as it involves an explicit dependence on the radial coordinate on which the mass function is assumed not to depend.

Even in the case where the mass function is assumed to have an r-dependence, this model fails again to lead to a viable solution due to the restrictions that the field equations impose on the field configurations: as the warp factor is solely a function of the y-coordinate, then through Eqs. (3.54) and (3.52), the potential $V(\phi,\chi)$ should also be a function of y. Assuming that the potential depends on both fields, and that these are general functions of the (r, v, y) coordinates, $V(\phi,\chi)$ ought to have a particular form so that its dependence on the (r, v) coordinates vanishes. These forms could be:

- $V(\phi, \chi) = F(\chi^n + \phi^n)$, where n an arbitrary integer and F an arbitrary function of the combination $\chi^n + \phi^n$. For the latter to be a function of y, we should also have: $\chi^n = \chi_1(y) + \chi_2(r, v)$ and $\phi^n = \phi_1(y) + \phi_2(r, v)$, with $\phi_2(r, v) = -\chi_2(r, v)$. But then, one may easily show that

$$\partial_r \chi \partial_v \phi - \partial_r \phi \partial_v \chi = \frac{(\chi\phi)^{1-n}}{n^2} \left(\partial_v \chi_2 \partial_r \chi_2 - \partial_r \chi_2 \partial_v \chi_2 \right) = 0, \qquad (3.56)$$

  in which case the r.h.s. of the (yv)-component (3.47), and the assumed dependence of the mass function on y, vanishes.

- $V(\phi, \chi) = G(\chi^{n_1} \phi^{n_2})$, where G an arbitrary function of the combination $\chi^{n_1} \phi^{n_2}$, and (n_1, n_2) arbitrary integers. In this case, we should have: $\chi = \chi_1(y) \chi_2(r, v)$ and $\phi = \phi_1(y) \phi_2(r, v)$, with $\phi_2(r, v) = c\chi_2(r, v)^{-n_1/n_2}$ and c a constant. Once again, the combination $(\partial_r \chi \partial_v \phi - \partial_r \phi \partial_v \chi)$ is easily found to be zero.

Let us finally investigate whether more special assumptions on the form of the fields or the potential are allowed. Clearly, the case where the potential V depends only on one of the two fields, i.e. $V = V(\chi)$, is excluded: χ must necessarily depend on r, as discussed below Eqs. (3.39)-(3.40), and the presence of ϕ in the expression of the potential is imperative in order for this r-dependence to cancel. The same argument excludes the case where only one of the two fields depend on the time-coordinate v, as in that case $V(\chi, \phi)$ would carry this v-dependence. The case where none of the two fields depend on v is also rejected since then the r.h.s. of eq. (3.47) would be zero - the same holds if we assume that both fields are not functions of the extra coordinate. The assumption that only one of the two fields may depend on y is the only one allowed with Eqs. (3.47), (3.52) and (3.54) assuming then simpler, yet non-trivial forms – nevertheless, this assumption does not alter the arguments presented above regarding the form of the potential and thus fails to lead to a viable solution.

The analysis presented in this subsection may be easily generalized to allow for more general kinetic terms along the lines of subsection 3.3. Then, the Lagrangian would read

$$\mathcal{L}_{sc} = \sum_{n=1} \left[f_n^{(1)}(\phi, \chi) \left(\partial^M \phi \partial_M \phi \right)^n + f_n^{(2)}(\phi, \chi) \left(\partial^M \chi \partial_M \chi \right)^n \right.$$

$$\left. + f_n^{(3)}(\phi, \chi) \left(\partial^M \phi \partial_M \chi \right)^n \right] + V(\phi, \chi). \qquad (3.57)$$

Although the expressions of all constraints and non-vanishing field equations would become more complicated, one may again show that these, upon conveniently redefining the coupling functions, reduce to the ones presented in this subsection. As the same arguments regarding the restrictions on the potential and form of fields would still hold, no viable solution would emerge in the context of this model either.

3.3 A Field Theory with a conformally-coupled Scalar

Let us now turn to the case of a conformalLy-coupled scalar field present in the bulk. We consider the following general form of the action

$$\mathcal{S} = \int d^4x \, dy \, \sqrt{-g} \left[\frac{f(\Phi)}{2\kappa_5^2} R - \frac{1}{2}(\nabla\Phi)^2 - V(\Phi) - \Lambda_B \right] , \tag{3.58}$$

where $f(\Phi)$ is an arbitrary, smooth, positive-definite function of the scalar field Φ, and g_{MN} is the five-dimensional metric given again by eq. (3.3). The equations of motion resulting from the aforementioned action have the form

$$f(\Phi)\left(R_{MN} - \frac{1}{2} g_{MN} R\right) = \kappa_5^2 \left(-g_{MN} \Lambda_B + \mathbb{T}_{MN}^{(\Phi)}\right), \tag{3.59}$$

with $\mathbb{T}_{MN}^{(\Phi)}$ being the generalized energy-momentum tensor of the scalar field defined as

$$\mathbb{T}_{MN}^{(\Phi)} = \nabla_M\Phi\nabla_N\Phi - g_{MN}\left[\frac{1}{2}(\nabla\Phi)^2 + V(\Phi)\right] + \frac{1}{\kappa_5^2}\left[\nabla_M\nabla_N f(\Phi) - g_{MN}\nabla^2 f(\Phi)\right] \tag{3.60}$$

In order to derive the explicit form of the above field equations, we need to combine the non-vanishing components of the energy-momentum tensor with those of the Einstein tensor G_{MN} presented in Eqs. (3.6)-(3.10). First, the off-diagonal components $\mathbb{T}^y{}_r$, $\mathbb{T}^v{}_r$, $\mathbb{T}^y{}_v$, $\mathbb{T}^r{}_v$ lead, respectively, to the following four equations:

$$(1 + f'') \, \partial_y\Phi \, \partial_r\Phi + f' \, \partial_y\partial_r\Phi - A'f' \, \partial_r\Phi = 0 , \tag{3.61}$$

$$(1 + f'') \, (\partial_r\Phi)^2 + f' \, \partial_r^2\Phi = 0 , \tag{3.62}$$

$$(1 + f'') \, \partial_y\Phi \, \partial_v\Phi + f' \, \partial_y\partial_v\Phi - A'f' \, \partial_v\Phi - \frac{\partial_y m}{r} f' \, \partial_r\Phi = f \frac{\partial_y m}{r^2} , \tag{3.63}$$

$$(1 + f'') \, (\partial_v\Phi)^2 + f' \, \partial_v^2\Phi - \frac{m}{r^2} f' \, \partial_v\Phi - \frac{\partial_v m}{r} f' \, \partial_r\Phi + e^{2A} \frac{\partial_y m}{r} f' \, \partial_y\Phi +$$

$$(1 - \frac{2m}{r})\left[(1 + f'') \, \partial_v\Phi \, \partial_r\Phi + f' \, \partial_v\partial_r\Phi\right] = f\left[\frac{2}{r^2} \, \partial_v m - \frac{e^{2A}}{r} \, (\partial_y^2 m + 4A'\partial_y m)\right] \tag{3.64}$$

In the above, f' and f'' denote the first and second, respectively, derivative of the coupling function f with respect to Φ, and, for simplicity, κ_5^2 has been set to unity. Also, note that the off-diagonal components of the energy-momentum tensor $\mathbb{T}^v{}_y$ and $\mathbb{T}^r{}_y$ are not independent and their corresponding equations reduce again to Eqs. (3.61) and (3.63).

Furthermore, the diagonal components provide us with three additional equations:

$$e^{-2A}\left[(1 + f'') \, \partial_v\Phi \, \partial_r\Phi + f' \, \partial_v\partial_r\Phi + \frac{m}{r^2} f' \, \partial_r\Phi\right] + A'f' \, \partial_y\Phi$$

$$-(\mathcal{L}_\Phi + \Box f + \Lambda_B) = 3f\left(2A'^2 + A''\right), \tag{3.65}$$

$$\frac{e^{-2A}}{r}\, f' \Big[\partial_v \Phi + \big(1 - \frac{2m}{r}\big)\partial_r \Phi\Big] + A' f' \partial_y \Phi - (\mathcal{L}_\Phi + \Box f + \Lambda_B) = 3f\,(2A'^2 + A'') \,, \quad (3.66)$$

$$(1 + f'')\,(\partial_y \Phi)^2 + f'\,\partial_y^2 \Phi - (\mathcal{L}_\Phi + \Box f + \Lambda_B) = 6f\,A'^2\,. \tag{3.67}$$

The above equations contain the complicated expressions of $\mathcal{L}_\Phi$ and $\Box f$, which are given by

$$\mathcal{L}_\Phi \equiv \frac{1}{2}(\nabla \Phi)^2 + V(\Phi) = \frac{e^{-2A}}{2}\Big[2\,\partial_v \Phi\,\partial_r \Phi + \big(1 - \frac{2m}{r}\big)(\partial_r \Phi)^2\Big] + \frac{1}{2}\,(\partial_y \Phi)^2 + V(\Phi)\,, \quad (3.68)$$

and

$$\Box f = e^{-2A}\,\partial_v \partial_r f + \frac{e^{-2A}}{r^2}\,\partial_r \Big[r^2 \partial_v f + r^2\big(1 - \frac{2m}{r}\big)\,\partial_r f\Big] + e^{-4A}\partial_y\big(e^{4A}\,\partial_y f\big)\,, \quad (3.69)$$

respectively, and are thus cumbersome to use. However, the combination of Eqs. (3.65) and (3.66) results to a simpler and more useful condition, namely

$$(1 + f'')\,\partial_v \Phi\,\partial_r \Phi + f'\,\partial_v \partial_r \Phi = \frac{f'}{r}\,\Big[\partial_v \Phi + (1 - \frac{3m}{r})\,\partial_r \Phi\Big]\,. \tag{3.70}$$

In the above analysis, we have assumed that the scalar field Φ, and consequently the coupling function f, does not depend on the angular coordinates θ and ϕ in order to preserve the spherical symmetry of the solutions on the brane. We have nevertheless retained their dependence on all remaining coordinates (r, v, y). It is easy to see that any simpler ansatz fails to pass the field equations: if we assume that the scalar field Φ depends only on the bulk coordinate y, then eq. (3.63) leads to the result $\partial_y m = 0$ – the same equation is inconsistent due to its explicit r-dependence in the case where Φ is assumed to be only a function of the time-coordinate v; finally, if the field depends only on the radial coordinate r, then eq. (3.61) demands that $f' = 0$ - but this takes us back to the minimal-coupling case that has already been excluded [211].

The above arguments clearly indicate that the scalar field Φ must depend at least on a pair of coordinates. However, even such an assumption does not satisfy the field equations, since:

- if $\Phi = \Phi(v, y)$ and thus $\partial_r \Phi = 0$, eq. (3.70) leads to either $\partial_v \Phi = 0$ (excluded above) or $f' = 0$ - but the latter option again reduces eq. (3.63) to an inconsistent equation.

- if $\Phi = \Phi(v, r)$ and thus $\partial_y \Phi = 0$, eq. (3.62) demands, for $\partial_r \Phi \neq 0$, $f' = 0$ - then, eq. (3.70) leads to $\partial_v \Phi = 0$ which is in contradiction with our assumption.

- if $\Phi = \Phi(r, y)$ and thus $\partial_v \Phi = 0$, eq. (3.70) demands, for $\partial_r \Phi \neq 0$, $f' = 0$ - then, eq. (3.62) leads to $\partial_y \Phi = 0$ which is again in contradiction with our assumption.

Therefore, we conclude that any attempted simplification in the form of the scalar field does not conform with the field equations, and this, interestingly enough, holds regardless of the form of the coupling function $f(\Phi)$. We are thus led to consider

whether the only remaining possibility $\Phi(r, v, y)$, in conjunction with an appropriate choice of $f(\Phi)$, could support the existence of a solution with a mass function $m = m(v, y)$ that would perhaps localize a black hole together with its singularity close to the brane. Therefore, in what follows we consider a number of natural choices for the coupling function $f(\Phi)$ and investigate whether these can lead to any viable solutions.

3.3.1 The $f(\Phi) = a\,\Phi$ case

Postulating that $f(\Phi) = a\,\Phi$, with a being a constant, gives $f'(\Phi) = a$ and $f''(\Phi) = 0$, which significantly simplifies the field equations. Looking for a solution for $\Phi(v, r, y)$, we immediately see that a purely factorized form, e.g. $\Phi(v, r, y) = U(v)R(r)Y(y)$, or any other form in which at least one of the coordinates is factorized out, are excluded as they fail to satisfy the field equations.

As a matter of fact, for the particular choice of the coupling function f, eq. (3.62) can be analytically integrated to determine the form of Φ. For $f(\Phi) = a\,\Phi$, it takes the form

$$\frac{\partial_r^2 \Phi}{(\partial_r \Phi)^2} = -\frac{1}{a}\,, \tag{3.71}$$

and, upon integrating twice, it yields the general solution

$$\Phi(v, r, y) = a\,\ln\left[r + aB(v, y)\right] + C(v, y)\,, \tag{3.72}$$

where $B(v, y)$ and $C(v, y)$ are arbitrary functions. However, the above solution fails again to satisfy the condition (3.70): this takes the form $a\,\partial_v B + B\,\partial_v C + 1 - 3m/r = 0$ that cannot be satisfied due to the explicit dependence on r. This result therefore excludes the particular choice for the coupling function.

3.3.2 The $f(\Phi) = a\,\Phi^2$ case

Also in this case, upon substituting $f'(\Phi) = 2a\Phi$ and $f''(\Phi) = 2a$, where a is again a constant, eq. (3.62) takes the form

$$-\frac{(1 + 2a)}{2a}\frac{\partial_r \Phi}{\Phi} = \frac{\partial_r^2 \Phi}{\partial_r \Phi}\,. \tag{3.73}$$

This can be analytically integrated twice to yield the general solution for Φ, namely

$$\Phi(v, r, y) = \left[B(v, y)\,r + C(v, y)\right]^{2a/(1+4a)}\,, \tag{3.74}$$

where again $B(v, y)$ and $C(v, y)$ are arbitrary functions. Interestingly enough, the above form of the scalar field together with the assumption $f(\Phi) = a\,\Phi^2$ manage to satisfy all off-diagonal equations (3.61)-(3.64), with the latter providing constraints that determine the unknown functions $B(v, y)$ and $C(v, y)$ in terms of the warp factor $A(y)$ and the mass function $m(v, y)$. However, the diagonal equations (3.65)-(3.67) are more difficult to satisfy with the constraint (3.70) proving the particular configuration of f and Φ once again inconsistent by taking the form $\partial_v C + B(1 - 3m/r) = 0$ and thus demanding the trivial result $B(v, y) = 0$.

3.3.3   The $f(\Phi) = a\,\Phi^n$ case

In this case, we have $f'(\Phi) = an\,\Phi^{n-1}$ and $f''(\Phi) = an(n-1)\,\Phi^{n-2}$, and eq. (3.62) takes the form

$$-\frac{1}{an}\left[\Phi^{1-n} + \frac{an(n-1)}{\Phi}\right]\partial_r\Phi = \frac{\partial_r^2\Phi}{\partial_r\Phi}\,. \tag{3.75}$$

Integrating the above, we obtain

$$\partial_r\Phi(v,r,y) = b(v,y)\,\Phi^{1-n}\,\exp\left[\frac{\Phi^{2-n}}{an(n-2)}\right], \tag{3.76}$$

where $b(v,y)$ an arbitrary function. Unfortunately, the solution of the above first-order differential equation for $n \geq 3$ cannot be written in a closed form, however, the following integral form

$$\int d\Phi\,\Phi^{n-1}\,\exp\left[-\frac{\Phi^{2-n}}{an(n-2)}\right] = b(v,y)\,r + c(v,y)\,, \tag{3.77}$$

where $c(v,y)$ is another arbitrary function, will prove to be more than adequate for our purpose. Although an explicit form for the scalar field Φ cannot be found, differentiating both sides of the above equation with respect to v yields

$$\partial_v\Phi(v,r,y) = \Phi^{1-n}\,\exp\left[\frac{\Phi^{2-n}}{an(n-2)}\right]\,[\partial_v b(v,y)\,r + \partial_v c(v,y)]\,. \tag{3.78}$$

Differentiating also eq. (3.76) with respect to v yields $\partial_v\partial_r\Phi$ and upon substitution of the relevant quantities in eq. (3.70), we obtain once again the, condemning for our ansatz, constraint $\partial_v c + b(1 - 3m/r) = 0$.

It is worth noting that the case where the coupling function $f(\Phi)$ is a linear combination of different powers of Φ, i.e. $f(\Phi) = \sum_{k=0}^{n} a_k\,\Phi^k$, was also considered [3]. For $n = 1$ and $n = 2$, the analyses followed closely the ones for the cases with $f(\Phi) = a\Phi$ and $f(\Phi) = a\Phi^2$, respectively, leaving no space for a viable solution. For $n = 3$, eq. (3.62) could be again integrated once to yield the result

$$\partial_r\Phi(v,r,y) = \frac{b(v,y)}{a_1 + 2a_2\Phi + 3a_3\Phi^2}\,\exp\left[-\frac{1}{\lambda}\,\arctan\left(\frac{a_2 + 3a_3\Phi}{\lambda}\right)\right], \tag{3.79}$$

where $\lambda = \sqrt{3a_1a_3 - a_2^2}$. Integrating once more, we obtain again an integral equation. Following a similar analysis as above, we arrive again, from eq. (3.70), at the constraint $\partial_v c + b(1 - 3m/r) = 0$ and the trivial result $b(v,y) = 0$. For $n \geq 4$, our set of equations could not give a closed form even for $\partial_r\Phi$.

---

[3]This particular choice for the coupling function of a conformally-coupled bulk scalar field was considered in [243] in the context of a brane-world cosmological solution that could produce accelerated expansion on the brane at late times.

3.3.4 The $f(\Phi) = e^{k\Phi}$ case

We finally consider the case of an exponential coupling function for which $f'(\Phi) = k\, e^{k\Phi}$ and $f''(\Phi) = k^2\, e^{k\Phi}$, where k is a constant – note than an arbitrary constant multiplying the exponential function can be absorbed into the value of Φ and thus is set to unity. Then, eq. (3.62) takes the form

$$-\frac{1}{k}\left(e^{-k\Phi} + k^2\right)\partial_r\Phi = \frac{\partial_r^2\Phi}{\partial_r\Phi}\,, \tag{3.80}$$

with solution

$$\partial_r\Phi(v,r,y) = b(v,y)\, e^{-k\Phi}\, \exp\left[\frac{e^{-k\Phi}}{k^2}\right]. \tag{3.81}$$

Integrating once more, we obtain

$$\int d\Phi\, e^{k\Phi}\, \exp\left[-\frac{e^{-k\Phi}}{k^2}\right] = b(v,y)\, r + c(v,y)\,. \tag{3.82}$$

Deriving, from Eqs. (3.81) and (3.82), the expressions for $\partial_v\partial_r\Phi$ and $\partial_v\Phi$, respectively, and substituting them together with $\partial_r\Phi$ in eq. (3.70), we obtain again the constraint $\partial_v c + b(1 - 3m/r) = 0$, that clearly excludes the exponential ansatz as well.

3.3.5 A general no-go argument

The failure of finding a viable solution, after a variety of forms for the coupling function $f(\Phi)$ have been considered, seem to hint that perhaps the particular form of metric assumed, given in eq. (3.3), is altogether inconsistent with the realization of the additional bulk matter in terms of a conformally-coupled scalar field. In that case, one should be able to develop a general argument that would exclude the emergence of a solution independently of the form of the coupling function $f(\Phi)$.

To this end, we bring eq. (3.62) to the form

$$1 + f''(\Phi) = -f'(\Phi)\,\frac{\partial_r^2\Phi}{(\partial_r\Phi)^2}\,, \tag{3.83}$$

which we can replace into eq. (3.61) to obtain

$$A' = \partial_r\left(\frac{\partial_y\Phi}{\partial_r\Phi}\right). \tag{3.84}$$

The above differential equation can be integrated with respect to r to give

$$\partial_y\Phi = \partial_r\Phi\left[A'(y)\, r + F(v,y)\right]. \tag{3.85}$$

Similarly, eq. (3.70) can be brought to the following form

$$\left(\partial_r - \frac{1}{r}\right)\frac{\partial_v\Phi}{\partial_r\Phi} = \frac{1}{r}\left(1 - \frac{3m}{r}\right), \tag{3.86}$$

which upon integration with respect to r yields

$$\partial_v \Phi = \partial_r \Phi \left[-1 + \frac{3m}{2r} + D(v,y)\, r \right].$$
(3.87)

The functions $F(v,y)$ and $D(v,y)$ appearing in Eqs. (3.85) and (3.87) are arbitrary, and at the moment, unrelated functions. To proceed, we differentiate eq. (3.85) with respect to v and eq. (3.87) with respect to y to obtain

$$\partial_v \partial_y \Phi = \partial_v F(v,y)\, \partial_r \Phi + (A'r + F)\, \partial_r \partial_v \Phi\,,$$
(3.88)

$$\partial_y \partial_v \Phi = r \partial_y D(v,y)\, \partial_r \Phi + \left(-1 + \frac{3m}{2r} + D(v,y)\, r \right) \partial_r \partial_y \Phi\,.$$
(3.89)

Equating the right-hand sides of the above two equations, we arrive at the relation

$$\partial_v F(v,y)\, \partial_r \Phi + (A'r + F)\, \partial_r \partial_v \Phi = r \partial_y D(v,y)\, \partial_r \Phi + \left(-1 + \frac{3m}{2r} + D(v,y)\, r \right) \partial_r \partial_y \Phi\,.$$
(3.90)

Taking finally the derivatives of eqs. (3.85) and (3.87) with respect to r, these yield the expressions of the double derivatives $\partial_r \partial_y \Phi$ and $\partial_r \partial_v \Phi$ that appear above. Substituting and simplifying leads to the final constraint

$$-\frac{3m}{2r^2}\, F(v,y) - \frac{3m}{r} \left(A' + \frac{\partial_y m}{2m} \right) + \partial_v F(v,y) + A' + F(v,y)D(v,y) - r \partial_y D(v,y) = 0\,.$$
(3.91)

However, the above is catastrophic for the existence of the desired solution. The only way the above relation can hold is if the coefficients of all powers of r identically vanish. This leads to the result that $F(v,y) = 0$, that subsequently demands that $A'(y) = 0$ which is clearly in contradiction with our assumption as it eliminates the warp factor from the model. In addition, the desired dependence of the mass term on the extra coordinate y is also forced to vanish, once we assume that $A'(y) = 0$, that destroys the localization of the black-hole singularity.

Although of a secondary importance, let us finally note that even if the function $A(y)$ was not forced to be trivial, the constraint following from the second term of eq. (3.91) would lead to the result $m(v,y) \sim e^{-2A(y)}$ – thus, for a decreasing warp factor, the mass term would have to increase away from the brane thus invalidating the idea of the localization of black hole. Therefore, a viable field-theory model owes not only to support a non-trivial profile of the mass function of the black hole but also a profile that could localize the black hole close to the brane.

In previous related works, configurations involving also gauge fields were studied; the arguments however that excluded the existence of a viable solution were identical to the ones used for the case of scalar models. Although here we have restricted our study in scalar field-theory models, we anticipate that similar results would follow even in the case of non-ordinary gauge field-theory models. Finally, one should note that all of the above observations are independent of the sign of the parameter ϵ that appears in our metric ansatz, and thus hold not only for the creation of a brane-world black hole but also for any expanding distribution of matter in a brane-world set-up.

Our analysis is by no means exhaustive. Nevertheless, in our attempt to generate the bulk energy-momentum tensor necessary for the localization of the black-hole topology close to the brane, we have considered a general selection of non-ordinary scalar field-theory models with a high degree of flexibility, and reached a negative result in each case. We have also considered a particular non-factorized metric ansatz – no matter how well motivated this choice was, we cannot exclude the possibility that the 5-dimensional line-element assumes a different form that may perhaps be related to the Schwarzschild black-hole metric on the brane in a more subtle way.

Chapter 4

Issues concerning information in the presence of black holes

It is quite common to consider the formation/evaporation process of a black hole as analogous to the scattering by it of particles coming from past null infinity ($\mathcal{J}^-$), which get measured at future null infinity ($\mathcal{J}^+$) by an observer living in an asymptotically flat region of spacetime. One should note though that the term scattering is used in a quite extended sense. What is actually meant is that particles coming from $\mathcal{J}^-$ merge and form a black hole, undergo a series of unknown processes in its interior and, eventually, get observed at $\mathcal{J}^+$. The simplicity of this analogy makes it a useful tool for someone to grasp the general idea of how black holes interact with the rest of the Universe. Nevertheless, as we have also argued in a recent work [17], one should always bear in mind the limitations of this analogy, when using it. Indeed, because of our current ignorance about the laws of quantum gravity, it is not possible to take under consideration that, in reality, particles spend a part of their life interacting with the singularity through these yet unknown laws and, therefore, the aforementioned analogy is, at least, incomplete. This is the reason why the alleged equivalence of the two processes leads to the emergence of the celebrated information paradox.

As analyzed earlier in section 1.3.4, the main problem with this procedure is the apparent non-unitary evolution of the particles, which causes an irreversible destruction of the information load of every system, that gets swallowed by the black hole, thus resulting to the emergence of the "loss of history" issue. From that analysis, it must be evident that the information loss paradox cannot be encountered in a conventional way.

We argue that any viable resolution of the paradox should be based on a combination of well-known and established theories with some innovative idea that would allow us to go a step further. Two such ideas [17, 18] are presented in the following sections in an attempt to address the unitarity violation and "loss of history" conundrums in order to fully understand and efficiently describe what really happens during the formation/evaporation process of black holes.

4.1 A new approach to information loss (no) problem

4.1.1 Classes of information

The new approach proclaimed by the title is heavily based on the notion of "information classification". In the context of this idea, we postulate that all kinds of information, in general, about a physical system fall into two categories. Let's call them Π1 and Π2 (Π is the first letter of the greek word that stands for information). Π1 class contains the most fundamental information that defines a particle, such as the mass, the electric and magnetic charge and its angular momentum. The much larger Π2 category includes information about how particles mingle with each other and the properties that arise from their combinations. A book, for example, contains a vast number of Π1-info about the aforementioned conserved quantities, of the elementary particles it consists of, and an even larger number of Π2-info about how these particles unite to form different nucleons, atoms and molecules including also the way all these combine to form letters and words that mean something.

There is a variety of well-known conservation laws that impose the preservation of Π1-info by any physical system. Black holes satisfy this requirement by emitting all kinds of particles that carry away exactly this type of information. It should be pointed out here that whether information about leptonic and baryonic numbers or any fermionic degrees of freedom, in general, should be considered as Π1 type is an open question. Although we know that black holes have no well-defined leptonic or baryonic number [244, 245, 246, 247, 248, 249, 250, 251], we cannot tell yet if they behave in a way that results to the conservation of fermionic quantum numbers or some combination of them. As for the Π2 category, there are no such laws to prevent this information from extinction and, consequently, different processes destroy different amounts of it. Actually, we conjecture that the various kinds of Π2-info resist their destruction to different degrees. In general, more violent procedures destroy more of them, but not in a proportional way. For instance, going back to the book example, tearing it apart leads to some Π2-info loss, like the meaning of the sentences and the words written in it. By burning it, we destroy much more Π2-info, since now words and letters disappear and no paper or ink survives, but the atoms, it was made of, are still there. Because all usual phenomena are confined to a low energy scale, not even all Π2-info gets destroyed during them. This means that in every day life we get to observe the loss of only a part of the total Π2 category practically in every process, which leads to an increase of the total entropy, as dictated by the second law of thermodynamics and no paradoxes occur. However, the case of black holes is somewhat different in that, being the most extreme objects in the Universe, the matter, they absorb, undergoes impacts of arbitrarily large violence, that destroy all Π2-info ruthlessly and, as a result, their entropy adds up to enormous values. Meanwhile Π1-info remains intact even in this case.

In a few words, we argue that the concept of information loss as the physical basis of the second law of thermodynamics [252] should be completed with the limitation

that this loss can only concern Π2-info, no matter how easy or difficult it is to be destroyed. Furthermore, black holes are postulated to be the most efficient Π2-info destroyers in the Universe and no such info can survive after having crossed their horizon. Rephrasing a well known aphorism by R. Price [253, 254], "any Π2 type piece of information that could be destroyed by a black hole, will be destroyed".

4.1.2 Confronting the paradox

Taking under consideration the idea of information classification, we gain a more incisive perception of the behavior of black holes, which has significant advantages and almost no flaws. To be more specific there are six arguments in favor of the new idea.

First, information, as far as the subset Π1 of fundamental importance is concerned, is never lost and, therefore, no paradox rises at this level.

Second, because information does get destroyed by the black hole, even if it can only be of Π2 category, the absorption and incorporation of matter by the black hole is a thermodynamically favored procedure, as expected by the fact that this is what always happens in reality.

Third, since black holes interact with the rest of the universe via their horizon, the rate they absorb matter and, consequently, destroy the information contained in it, must be proportional to their surface A. This observation provides us with a possible explanation of why black hole entropy is directly analogous to their surface, as explicitly shown by the famous Bekenstein - Hawking formula

$$S = \frac{A}{4} \quad \text{with} \quad c = G = \hbar = 1 \tag{4.1}$$

and not to their volume, as could one instinctively assume accounting black holes to be some sort of ordinary thermodynamical systems.

Fourth, everything we know so far about the behavior of black holes and the laws governing it, like the Generalized Second Law, remain intact and valid since no revision of them is necessary in the context of our theory.

Fifth, it provides us with some mechanism capable of explaining why black hole entropy generally takes enormous values, as we can ascribe it to the complete and irreversible destruction of all Π2-info.

Sixth, the fact that less information contributes to the creation of the entropy of black holes, since they destroy only Π2-info, even though Π2 class constitutes the greater part of the total information load of incoming matter, can help us deal with the problematic current estimation that the entropy of ordinary black holes is almost equally large as the entropy of the Universe. More specifically, the latter is approximately equal to the number of relativistic particles whose number, within a Hubble radius, is calculated to be $S_U = 10^{88}$. On the other hand, black hole entropy measured in Planck units is equal to the 1/4 of their surface and converting this quantity into astrophysical units we find the Bekenstein - Hawking entropy to have the huge value

$$S_{BH} \sim 10^{90} \left(\frac{M}{10^6 M_\odot} \right)^2. \tag{4.2}$$

This equation means that a single million solar mass black hole has more entropy than the whole known universe. At the same time, General Relativity certainly allows for the existence of such supermassive objects and astronomical observations imply that they must exist in the centre of almost every galaxy, so another paradox rises. A possible way out is that the idea of information classification also means that the way black hole entropy is calculated should be reconsidered on the basis of Π1 and Π2 information classes in order to express the fact that only Π2-info gets destroyed. The refined calculation should result to an entropy value several orders of magnitude smaller than the one mentioned above, resolving the new paradox.

Finally, the information classification proposition is quite appealing in that, while predicting some kind of information conservation, avoids any assumptions about remnants or exotic encoding in the spectrum of Hawking radiation or other even more radical but least possible alternatives. Its simplicity should be seen as an extra advantage of it, if one is to trust Occam and his famous razor [1].

4.2 The question of unitarity and the possibility to extract information from the black hole interior

We shall now move on to address the issue of the apparent unitarity violation, that emerges during the formation and the subsequent evaporation, through the emission of Hawking radiation, process of black holes. We should note here that Hawking radiation is substantially different from the radiation emitted, e.g., by a burning piece of coal. In the latter case, the emitted quanta stem from the burning material itself so, once created, they bounce off the atoms still remaining in the coal and then carry away the information left behind in these atoms. So, at the end, all quanta collected at infinity are entangled with themselves and manage to carry all information existed in the initial piece of coal. However, in the case of black holes, the quanta rise from vacuum at a considerable spatial distance from where all matter is, therefore one should indispensably address the question about the mechanism capable of transferring information from the singularity to the outgoing quanta [64]. We argue that one has to consider the role of the Einstein - Podolsky - Rosen (EPR) phenomenon [255] in order to overcome the paradox that renders the scattering approach to the aforementioned process incomplete and unsatisfactory, if not invalid.

Reflecting on the semiclassical approximation for particle creation by a black hole at the vicinity of its horizon [50], the way it is presented in section 1.3.2, it becomes evident that the particles of each pair are entangled to each other and in a mixed state from the very first moment they come into existence. While being entangled, the particle with negative energy E_1, with respect to infinity, propagates in the interior of the black hole all the way down to the singularity, whereas the one with positive energy E_2 goes away from the horizon, being the famous Hawking radiation, which

---

[1]Occam's razor: philosophical argument stating that among all theories, capable of explaining a phenomenon, the one with the simplest conjectures is most probably the correct one.

at this point is still thermal. Here comes into play the EPR phenomenon. That is the existence of a special correlation between particles that interacted with each other sometime and became entangled, which holds even if the particles are separated at infinitely large distances. Because of it each particle can "feel" any change in the state of the other and react instantaneously to it [255].

To better understand this phenomenon, let's consider for simplicity, without losing any of the physics involved, a Bohmian biparticle two-state system, where each particle can be found either in the $| + \rangle$ or in the $| - \rangle$ state, no matter what they stand for in specific as long as they are complementary with each other [256]. When created, the wavefunction of the system is a superposition of its two possible eigenstates, that is:

$$\Psi = \frac{1}{\sqrt{2}}(\phi_+ \otimes \psi_- - \phi_- \otimes \psi_+), \tag{4.3}$$

where $\phi_\pm$ and $\psi_\pm$ are the corresponding eigenstates for the first and the second particle respectively. This description holds as long as no measurement on either particle is made, even though the particles can be spatially separated by large distances. Once an observer performs a measurement on the first particle, he/she would find it to be in the ϕ_+ or ϕ_- state. This means that the original wavefunction has collapsed to become $\phi_+ \otimes \psi_-$ or $\phi_- \otimes \psi_+$ respectively. Therefore, the observer instantly infers with certainty that the second particle is in the ψ_- or ψ_+ state based on the fact that these states are (anti)correlated, acquiring this way information about the distant particle without in any way getting in direct contact with it.

The aforementioned standard Bohmian example can be straightforwardly generalised to arbitrary dimensional systems [257]. Let $\mathcal{H}_1$ and $\mathcal{H}_2$ be two Hilbert spaces of finite dimension N corresponding to two subsystems S_1 and S_2 and $(\phi_i)_{1 \leq i \leq N}$ and $(\psi_i)_{1 \leq i \leq N}$ be orthonormal bases in these spaces respectively. Then for the wavefunction of the overall system we write

$$\Psi = \frac{1}{\sqrt{N}} \sum_{i=1}^{N} \phi_i \otimes \psi_i. \tag{4.4}$$

It follows from this, as in the Bohm example, that if $\mathcal{O}_1$ is any observable with N distinct values in the S_1 system, then there is an equally large observable $\mathcal{O}_2$ in the S_2 system, whose values can be predicted with certainty if we know the values of $\mathcal{O}_1$ by direct measurements on the S_1 system and vice versa.

Bearing the above analysis in mind, we go back to apply it to the case of particle creation by black holes. We shall focus our study to Schwarzschild black holes for simplicity, since our main results remain unaltered in essence for any kind of black holes. We appoint the following wavefunction to the black hole

$$| \Psi_0 \rangle = | n_1, n_2, ..., n_N \rangle, \tag{4.5}$$

where $(n_i)_{1 \leq i \leq N}$ are the quantum numbers that correspond to the values of the N parameters necessary to fully describe the black hole state. Since particles emerge in pairs from vacuum in the vicinity of the horizon their properties have to be complementary

and, therefore, their wavefunctions are expected to be (anti)correlated. With respect to the N parameters mentioned before, we write the wavefunctions for the first pair of particles created as

$$| 1 \rangle_1 = | a_1^1, a_2^1, ..., a_N^1 \rangle \quad \text{and} \quad | 2 \rangle_1 = | b_1^1, b_2^1, ..., b_N^1 \rangle \tag{4.6}$$

with $| 1 \rangle_1$ and $| 2 \rangle_1$ symbolizing the state of the first and the second particle of the first pair respectively and $(a_i^1)_{1 \leq i \leq N}$ and $(b_i^1)_{1 \leq i \leq N}$ being the set of the values of the N observables corresponding to them. Note that the aforementioned complementarity of the states imposes the condition

$$a_i^1 + b_i^1 = 0 \quad \text{with} \quad 1 \leq i \leq N. \tag{4.7}$$

The wave function of the pair as a whole is, of course, a superposition of all possible eigenstates that emerge from the combination of the allowed values for a_i^1 and b_i^1.

As it is well understood, the ingoing particle (let it be the first particle of every pair) will inevitably reach the singularity and this should happen at a finite time. To get an idea about the magnitude of the time interval required, we use the so-called Lemaître reference frame, which is suitable to describe the spacetime within the Schwarzschild radius [258]. The metric in the frame of freely falling particles has the form

$$ds^2 = -c^2 dT^2 + \frac{dR^2}{B} + B^2 r_h^2 (d\theta^2 + sin^2\theta d\phi^2), \tag{4.8}$$

where T is the proper time of the particle,

$$B = \left[\frac{3}{2r_h}(R - cT) \right]^{\frac{2}{3}}, \tag{4.9}$$

and R is the new radial coordinate. One finds, then, that the time needed for a particle to get to the singularity starting from the vicinity of the horizon is

$$t_{r_h \to 0} = \frac{4GM}{3c^3} \sim 10^{-5} \frac{M}{M_\odot} \text{ sec.} \tag{4.10}$$

When the E_1^1-particle (the particle of the first pair with negative energy) arrives there, the interaction with the singularity forces its wavefunction to collapse into one of its possible eigenstates. It is as if the singularity performs a kind of measurement on the ingoing particle. Then, because of the EPR-type connection between the two entangled particles, the one with $E_2^1 > 0$, that has freely propagated away from the black hole in the meantime, instantaneously falls into the complementary eigenstate, therefore in a pure state. All these mean that the thermal nature of the Hawking radiation disappears shortly after its emission. Thus, whenever it gets to be measured by an observer living in an asymptotically flat region of the universe, the latter would record it being in a pure state (in the sense that the particle is already in an eigenstate before the observer's measurement is performed). Finally, the black hole state becomes

$$| \Psi_1 \rangle = | n_1 + a_1^1, n_2 + a_2^1, ..., n_N + a_N^1 \rangle \tag{4.11}$$

and the second particle is found to be in an specific eigenstate that can be measured to give us the specific values of b_i^1 that characterize it.

Furthermore, when the next pair of $E_1^2(< 0)$ and $E_2^2(> 0)$ particles is created, E_1^2 falls into the black hole, reaches the singularity, that has been already modified by its earlier interaction with the E_1^1-particle and therefore EPR-ly correlated with the E_2^1-particle, and interacts with it modifying once more its overall state, which now becomes

$$| \Psi_2\rangle =| n_1 + a_1^1 + a_1^2, n_2 + a_2^1 + a_2^2, ..., n_N + a_N^1 + a_N^2\rangle. \qquad (4.12)$$

Then, again due to the EPR phenomenon, the E_2^2-particle collapses to an eigenstate, gets correlated with the singularity and indirectly with the E_2^1-particle as well. This way all quanta emitted at early times are correlated with the singularity and these correlations are then transferred to the quanta emitted at later times. This process continues in the same way as more and more particles get created and emitted by the black hole. Therefore, after the emission of the k-th particle the black hole wavefunction takes the form

$$| \Psi_k\rangle =| n_1 + \sum_{j=1}^{k} a_1^j, n_2 + \sum_{j=1}^{k} a_2^j, ..., n_N + \sum_{j=1}^{k} a_N^j\rangle. \qquad (4.13)$$

The aforementioned procedure allows us, as external observers, to extract information from the black hole interior. Every emitted particle, that gets measured, provides us with an elementary piece of information regarding the internal states of the black hole, reducing our ignorance about them. Recalling that the entropy of a system is considered to be directly correlated to our lack of knowledge about it, the gain of information about the black hole state should lead to a decrease of its entropy. On the other hand, emission of Hawking radiation results to the shrinking of the black hole mass and, consequently, its surface area A, which is proven to be connected to its entropy through the famous Bekenstein - Hawking formula $S = \frac{A}{4}$ (use of natural units, A measured in planckian units). We argue that this concordance of predictions about the entropy, derived by two quite different starting points, is not incidental and should be seen as an extra argument in favor of our analysis.

At the end, all emitted quanta are correlated with each other so the whole of the information emerges gradually as the black hole slowly evaporates. At these late times, after having emitted an ensemble of Z particles, the black hole can eventually disappear completely (that is $| \Psi_{final}\rangle =| 0, 0, ..., 0\rangle$) without any overall loss of information to occur. It is obvious that we come up with the following system of N equations

$$n_i + \sum_{j=1}^{Z} a_i^j = 0, \qquad 1 \leq i \leq N. \qquad (4.14)$$

By direct measurements on every emitted degree of freedom we get a specific set of values corresponding to all $(b_i^j)_{1\leq i\leq N, 1\leq j\leq Z}$ parameters. Based on the (anti)correlation relation (4.7) we can infer with certainty the values of the $(a_i^j)_{1\leq i\leq N, 1\leq j\leq Z}$ parameters.

Then from eq. (4.14) we get full knowledge of $(n_i)_{1 \leq i \leq N}$, that is the complete set of parameters describing the initial black hole state. Thus, the whole of the information is retrieved from black hole interior, presumably the total of $\Pi 1$-info in accordance to the ideas presented in **??**.

One could argue, though, that measurements of time scale of order $t_{r_h \to 0}$ are well within the abilities of current experiments and, consequently, if measured at $t < t_{r_h \to 0}$ the black hole radiation will be found to be thermal and we would be confronting a non-unitary evolution of the system. Fortunately, there is a way out in the sense that in such a case the outgoing particles would be at a distance $r \leq \frac{5}{3} r_h$ from the singularity, therefore, at a region that is far from being considered as flat. Unitarity, however, results from the key demand of quantum mechanics for asymptotic completeness, which has been established in asymptotically flat spacetime in the first place. Therefore, it is legitimate to conjecture that in curved spacetime a deviation from unitarity could be allowed to occur, as long as the system finally settles down in some finite time to such a situation, that any observer at infinity would only record its overall evolution as unitary. This way the proposed use of the EPR phenomenon, as the underlying mechanism that transfers information from the interior of the black hole to the outgoing quanta, seems to work well in any case without leading to paradoxes. This is a crucial assumption for the whole idea to hold, therefore, it needs to be further analysed. As pointed out in [259] the scattering matrix, that connects the *in* and *out* states, cannot be a well-defined operator on the Hilbert space of states, when considering effects that take place in curved spacetimes. The general lack of Poincaré invariance in curved spacetimes means that there is a substantial bluriness in our understanding of the evolution of physical processes there. All these imply that there is room for a rapidly self-decaying and effectively non-observable deviation from unitarity to occur, when it comes to curved spacetimes.

It is also worth noting that, according to a calculation by Wald [260], observers near infinity should see a black hole radiate for all times t, such that $t - t_0 >> t_D$, where t_0 denotes the time of black hole creation, as defined in [261], and the dynamical time scale t_D to be

$$t_D \sim \frac{GM}{c^3} \sim 10^{-5} \frac{M}{M_\odot} \sec. \qquad (4.15)$$

Therefore, in all cases there is enough time for the ingoing particle to reach the singularity, collapse into a pure state and provoke the corresponding transition of the outgoing particle to the complementary pure state, before the latter could be observed at the asymptotically flat infinity.

We should mention here that even though the explanation of the EPR connection remains highly controversial for over 70 years, since it was first established theoretically, its existence is undoubted as it has also been experimentally observed [262, 263, 264, 265]. The violation of Bell's inequalities [266], that was proven beyond doubt by these experiments, establishes the non-local nature of the phenomenon and it is exactly this non-locality that allows us to postulate that the EPR connection between particles is insensitive to the non-trivial topology of space-time near the black hole, as to the very existence of the horizon itself. Bearing all the above in mind, the concept of

approaching the black-hole formation/evaporation as a multiparticle scattering process changes substantially. Particles in a pure state $\mid i \rangle$ come from $\mathcal{J}_-$, merge to form a black hole, reemerge in the vicinity of its horizon, get scattered and end up at $\mathcal{J}_+$ being in a pure state $\mid f \rangle$. Therefore, at least in principle, we are able to define an S-matrix that can describe this procedure having the very important property to be unitary for all observers located near infinity, as it ultimately predicts the evolution of a pure initial state into a pure final state. The matrix elements

$$\langle i \mid S \mid f \rangle \tag{4.16}$$

can, obviously, only be determined *a posteriori*, should we ever be able to observe the complete creation and evaporation process of a black hole in a fairly known and controlled environment (hopefully at the LHC, if any theory predicting the Planck scale to be as low as few TeV [28, 29, 30, 33, 34] is proven to be right [2]). This limitation, however, is inherent in the study through scattering of every system, for which we lack a complete microscopic description, and should not be seen as a fatal flow of our approach. Even though the determination of the matrix elements would probably be very difficult in practice (also because of the arbitrarily large number of dimensions that it needs to have in the case of massive black holes), the important thing is that this matrix can be defined in the first place and sought for.

---

[2]In this case we would be able to produce a multitude of mini black holes using conveniently prepared particles and record a detailed evaporation profile of them. Then, our measurements would provide us with the transition amplitudes associated with this procedure and the validity of our approximation could be tested against the experimental results.

Chapter 5

Conclusions and discussion

Black holes are indeed the most celebrated class of solutions arising in the context of General Relativity as well as by higher-dimensional generalizations of the latter. However, at the same time they remain the most mysterious objects with some of their properties, both at classical and quantum level, being only partially understood.

In the framework of this dissertation, an effort has been made to adress some of the questions regarding the nature of black holes. In this last chapter we shall make a comprehensive review of the main results of our research and share some thoughts concerning them. As mentioned several times so far, in the case where theories postulating the existence of large extra spacelike dimensions (and consequently a lower fundamental energy scale for gravity) are proven to be valid, the exciting possibility rises that black holes could actually be created in the lab. Then we would witness their evaporation just before our detectors and observe their emission in great detail. But for the observations to give us reliable information about the space-time structure, we should have a clear knowledge about the connection of the Hawking emission spectrum features with the characteristics of the space-time geometry. With this motivation we conducted a research programme focused on the Hawking-type emission by higher-dimensional rotating black holes. In particular, we studied first the emission of tensor-type gravitons by such a black hole. Then we turned our attention to the emission of massive scalar degrees of freedom in the same background. In both cases we were able to solve the corresponding equations of motion, to determine the graybody factor of the modes considered and finally find an expression giving the differential energy and angular momentum emission rate with respect to the number of the extra dimensions. These calculations were done analytically as well as numerically. The analytic approach was based on a commonly used and widely accepted technique for the study of Hawking radiation. Since the equations of motion are too complicated for one to find a single closed-form solution, we attacked the problem in an indirect way. First we solved them in the near horizon regime, imposing the boundary condition that no outgoing solutions should exist for $r \to r_h$. Then we solved them for $r \gg r_h$ (far field solution). In addition, at some intermediate region the two solutions are expected to describe the same phenomena and, thus, we demanded that they completely match (at least in the low energy limit). Furthermore, the far-field solution was written as a combination of ingoing and outgoing spherical waves for $r \to \infty$. The absorption

probability then was easily found via the ratio between the wave amplitudes. The final step was to sum all modes emitted to find the energy and angular momentum flux away from the black hole. At this point, a more detailed review of our study is in order.

In sec. 2.2 the work concerning the tensor-graviton emission was presented. Because of the complexity of the analysis demanded for the derivation of the perturbed gravitational equations in the background of a higher-dimensional non-spherically-symmetric black hole, the emission of Hawking radiation in the form of gravitational modes from such a space-time has been up to now an uncharted territory[1]. We have used the results of a previous analysis [156] according to which the derivation of the field equations for tensor-type gravitational perturbations is indeed possible under the assumption that the space-time manifold is the warped product of two submanifolds with its line-element having the form of eq. (2.8). This class of space-times includes not only the previously studied higher-dimensional spherically symmetric black-hole backgrounds but also the case of a $(4+n)$-dimensional rotating black hole with a single angular-momentum component along the $(3+1)$-dimensional brane. In addition, it was further shown that these equations, upon the use of tensor harmonics as a basis, can lead to a set of decoupled ordinary differential equations with respect to the space-time coordinates.

The derived equations for the tensor-type gravitons propagating in the bulk are found to be identical in form with the ones satisfied by bulk scalar fields. We were thus able to analytically study the problem of the computation of the absorption probability by using techniques employed previously for the emission of scalar fields by the same type of black hole, under proper modifications to allow for the different values of the angular-momentum quantum numbers that characterize the graviton modes. This study led to an analytical expression for the absorption probability for tensor-type bulk gravitons valid in the limit of low-energy emitted modes and low-angular-momentum of the black hole.

In order to derive the complete emission spectra, for arbitrary values of the energy of the emitted mode and angular momentum of the black hole, we also performed an exact numerical analysis to solve both the angular and radial part of the graviton's field equation. In the process, the value of the angular eigenvalue, that appears in and connects the two equations and which does not exist in closed form, was also computed. Having all the above exact results at our disposal, we were thus able to find the value of the absorption probability, or graybody factor, for tensor-type graviton modes in the specific background.

The exact form of the absorption probability in terms of the energy parameter ωr_h was studied in detail as well as its dependence on the particular graviton mode considered. A comparison between the approximate analytical and exact numerical results for its value was performed, and it was found that, for the lowest graviton modes, the agreement of the two sets of results is remarkably good and extends up to the high-energy regime; as higher modes are considered, the analytical result deviates from the exact one at an increasingly smaller value of the energy. The dependence of

---

[1]While the calculations presented here were being executed, a complementary work was also in progress concerning the emission of tensor-type gravitons in the bulk by a simply rotating black hole, which was published almost at the same time as our work [172].

the graybody factor on the space-time parameters, namely the number of additional spacelike dimensions and angular momentum of the black hole, was also investigated. According to our results, the absorption probability for tensor-type gravitons decreases with the number of transverse-to-the-brane dimensions but increases as the black hole rotates faster - this behavior is similar to the one found for bulk scalar fields in previous analyses [152, 154].

We next moved to the computation of the emission spectra, namely the energy and angular-momentum ones. The value of the corresponding differential emission rates strongly depends on the number of modes – characterized by the set of (j, ℓ, m) angular-momentum numbers – that are considered in the sum. For this reason, we performed a careful study of the convergence of our results before imposing a cutoff on the three quantum numbers. In all cases studied, we made sure that the effect of all the higher modes left out of the sum was always negligible. In addition, a technical calculation was performed for the derivation of the multiplicity of tensor modes characterized by the same set of angular-momentum numbers – this number is distinctly different from the one for bulk scalar fields and affects the value of the differential emission rates.

Combining the above, the energy and angular-momentum emission spectra were finally computed. Both spectra exhibit a very strong dependence on the number of additional spacelike dimensions with the increase in the rate of emission of either energy or angular momentum reaching even 2 or 1 orders of magnitude, respectively. The dependence on the angular momentum of the black hole is more particular: while the angular-momentum emission is clearly enhanced, the differential energy emission rate displays either an enhancement of the high-energy modes and suppression of the other frequencies, for low values of n, or a rather mild dependence of the spectrum on a_*, for high values of n.

In sec. 2.3, we have moved towards the direction of considering the emission of realistic particle states by a higher-dimensional, simply rotating black hole. We have studied the emission of massive scalar fields both in the bulk and on the brane, and investigated the role that the mass of the field plays in the corresponding energy spectra profiles and in the bulk-over-brane energy ratio.

The emission of Hawking radiation in the bulk in the form of massive scalar fields was the first to be studied. The radial part of the field equation was first solved analytically, and an expression for the absorption probability was found that helped us investigate low-energy aspects of the emission. Next, by using numerical analysis, the exact value of the absorption probability was determined and its dependence on the mass of the emitted field, in conjunction with the number of extra dimensions and angular-momentum of the black hole, was studied. As expected, the presence of the mass term caused the suppression of the absorption probability as additional energy is required for the emission of a massive field. Our numerical and analytical results were directly compared, and found to be in excellent agreement in the low and intermediate energy regimes for scalar fields with a mass smaller than (0.5-1) TeV.

The exact numerical value of the absorption probability was subsequently used to derive the differential emission rate per unit time and unit frequency in the bulk. Particular care was taken so that a large enough number of scalar modes ($N_{bu} \simeq 5500$)

was summed up in our computation of the energy spectra. The mass term caused the suppression of the energy spectra in the low and intermediate-energy regimes, compared to the massless case: for low values of n and a_* and $m_\Phi = 0.8$, the suppression is of the order of 50%, while it becomes smaller in magnitude as either n or a_* increases.

The same task was performed for the emission of massive scalar fields on the brane. The value of the absorption probability was again found both analytically and numerically, and it was shown that the two sets of results are in very good agreement, in the lowest part of the spectrum, up to masses of order (250-500) GeV. The exact profile of the energy spectra on the brane was found next in terms of the parameters (m_Φ, n, a_*), with the mass term causing again a significant suppression in their value. The suppression was larger than the one in the bulk decreasing the value of the energy emission rate to approximately 40% of that in the massless case, for low values of n and a_* and for $m_\Phi = 0.8$. As in the case of bulk emission, a considerable number of modes ($N_{br} \simeq 1700$) was summed up in our calculation so that the computed spectra are as close as possible to the real ones.

The role of the mass of the emitted field in the bulk-over-brane energy ratio was also investigated. The total energy emissivities of bulk and brane emission were derived and directly compared. In agreement with previous analyses [149, 115, 151] – that we have generalized by considering a larger range of parameters of both n and a_* – we found that the bulk channel remains sub-dominant to the brane one; nevertheless, the bulk-over-brane ratio takes a considerable value especially for a large number of extra dimensions and a slowly rotating black hole. We further found that the presence of the mass of the emitted field increases the percentage of energy which is spent by the black hole in the bulk. For a small number of extra dimensions and a low value of the angular-momentum of the black hole, the enhancement of the bulk channel over the brane one can reach the value of 33% if $m_\Phi = 0.8$.

In section 2.4 a quite different problem, concerning once again the emission spectrum of a decaying black hole, was considered. We know from previous studies that during the study of the spherically-symmetric Schwarzschild phase, the radiation spectra of higher-dimensional black holes – even if we focus on the part of the emission that takes place on the brane where ourselves, the observers, are located – show a strong dependence on the number of additional spacelike dimensions that exist transversely to our brane. Therefore, the expectation was formed that the detection of the Hawking radiation spectra could lead to the determination of the number of extra spacelike dimensions in nature. However, if the angular-momentum of the black hole is taken into account – which generically is non-zero and seems to dominate almost all of the life of the black hole – this dependence on n is entangled with the dependence on the angular-momentum parameter a. Furthermore during the spin-down phase of the black hole, the emission exhibits, among other features, a strong angular variation in the radiation spectra with respect to the rotation axis of the black hole. It has been suggested then [195, 178] that this angular variation is the observable that could disentangle the dependence of the radiation spectra on n and a as it depends strongly on the latter while being (almost) insensitive to the former. It was found that, in the low-energy channel, the emitted gauge bosons become aligned to the rotation axis of

the produced black hole while fermions form an angle with the rotation axis whose exact value depends on the angular-momentum of the black hole.

Attacking the problem of the angular variation of the Hawking radiation spectra in an exact way, and for all values of the parameters of the theory, is extremely challenging. It demands the numerical determination of both the radial and angular eigenfunction of the emitted fields as well as the numerical calculation of the angular eigenvalue that connects the corresponding equations. In addition, the angular pattern of the emitted spectra is formed from the contribution of an, in principle, infinite number of partial modes, numbered by the pair of angular-momentum numbers (l, m), each entering in the expression of the emission rate with its own weight (thermal and graybody) factor. Therefore, the use of the formal extremization constraint, that we have derived and which should determine the angles of maximum emission of all species of particles, seems rather unrealistic.

Nevertheless, as the exact numerical analyses [195, 178] have shown, all the valuable information that we should deduce from the angular spectra are restricted in the low-energy regime. In this regime, one may use approximate techniques to solve the radial equation and thus determine the weight-factor of each contributing partial mode [144, 145]. In addition, analytic formulae for the angular eigenvalue and eigenfunction exist [200, 189, 188, 190, 166, 170] that allow us to study the problem of the angular variation of the spectra without resorting to complex numerical techniques. Combining the above tools in a constructive but critical manner, we were able to study the angular variation of the Hawking radiation spectra of fermions, gauge bosons and scalar fields in a semi-analytic way.

Starting from the case of fermionic fields, the use of the analytic form of the gray-body factor allowed us to compute the weight factor of each contributing partial mode. This, combined with a power series form for both the angular eigenvalue and eigen-function, led to the isolation of the partial modes that predominantly determine the angular pattern of the corresponding radiation spectra in the low-energy regime. Also, by demanding that the errors associated to the elimination of all higher-order terms were small, we were able to truncate the infinite sums in both the expressions of the angular eigenvalue and eigenfunction. At the end, we demonstrated that the contribution of only two partial modes, the $(\frac{1}{2}, \frac{1}{2})$ and $(\frac{3}{2}, \frac{3}{2})$, was more than adequate to provide approximate results for the value of the angle of maximum emission and of the corresponding emission rate that were within a range of 5% accuracy of the full results. Our study was completed by the derivation of the values of the above quantities, both in an exact and approximate way, for a variety of values of the energy parameter ω_* of the emitted fermionic field and angular-momentum parameter a_* of the black hole, that could in principle be used for the determination of the angular momentum upon the observation of such a radiation spectrum.

Whereas the angular variation of the radiation spectra of the emitted fermions is very sensitive to the value of the angular-momentum of the black hole – the larger the a parameter is, the larger the value of $\theta_{\max}$ – the orientation of the gauge bosons emitted in the low-energy regime was found, by the exact numerical analyses, to be constantly aligned to the rotation axis of the black hole. Thus although it seems

that no further information can be deduced from the study of the gauge bosons, we nevertheless performed the same analysis in an attempt to justify analytically the predicted behavior. We demonstrated, by using a similar strategy as in the case of fermions, that a single mode, the $l = m = 1$, mainly determines the angular profile of the emitted gauge bosons. As its angular eigenfunction exhibits no extremal points up to $a\omega = 0.32$, and even then these extrema remain subdominant to the global maximum at $\theta = 0, \pi$ (for helicities $h = \mp 1$, respectively) up to $a\omega = 0.85$, it is thus confirmed that the emission of gauge bosons in the low-energy regime will remain aligned to the rotation axis of the black hole for a wide range of the angular-momentum parameter. For example, gauge bosons emitted in the energy channel $\omega_* = 0.5$ will remain mostly parallel or antiparallel to the rotation axis up to the value of $a_* = 1.7$, however, they will start deviating significantly from this behavior for values of the angular momentum parameter of the black hole larger than this.

For completeness, we have finally studied the case of the emission of scalar fields on the brane by a simply-rotating black hole. In this case, the exact numerical analyses have shown that the emission remains spherically-symmetric for low values of ω and a and then, as either of the two parameters increases, the emission starts concentrating on the equatorial plane. One could thus assume that by looking at the emission of scalar fields, the equatorial plane, and thus the rotation axis of the black hole, could again be determined. Our analysis has shown that the angular profile of the radiation spectra of scalars in the low-energy regime is mainly determined by two modes, the $l = m = 0$ and $l = m = 1$, the first having a minimum at $\theta = \pi/2$ and the second a maximum at the same point. For small values of ω_* and a_*, we have confirmed that the combination of these two modes creates indeed a "spherically-symmetric zone" in the emission where the two extrema exactly cancel each other. As either ω_* and a_* increases further, it is the $l = m = 1$ mode that starts dominating pushing the bulk of the emitted scalars towards the equatorial plane. Nevertheless, this transition becomes gradually and is finally realized for values of the parameters of the theory where our approximate techniques are not valid any more.

As a closing remark, let us note that our analysis in this work was based on the study of aspects, such as the existence of extremal points and relative magnitudes, of the spin-weighted spheroidal harmonics. These functions arise in a variety of problems, both in four dimensions as well as in the context of brane models, whenever the study of spin-s fields in a 4-dimensional space-time with one angular-momentum component is performed. We thus envisage that the properties of the angular eigenfunctions revealed in this analysis as well as the analytic expressions of the angular eigenvalues and a_p coefficients for fermions, gauge bosons and scalar fields presented in the Appendices A and B will be of use in a variety of problems.

In chapter 3 we deal with a still unanswered question. Namely, to find a metric representing a realistic black hole in the context of the Randall-Sundrum one brane model. Despite an intensive research activity over a period of almost fifteen years, an analytical solution, in closed form, that describes a 5-dimensional regular black hole localized on a brane is still missing. Numerical solutions have appeared in the literature that reassure us of their existence, however, the way to proceed in order to derive a

complete analytical solution remains unclear. As almost all of those numerical solutions rely on the presence of some type of matter, either on the brane or in the bulk, in this work, we turned to a previous idea that a type of bulk matter can help to localize the extended black-string singularity close to the brane and thus restore the finiteness of the 5-dimensional AdS space-time at a small distance from the brane. We allowed the warp factor to have an arbitrary form, with the only restriction to be y-dependent and no kind of fine-tuning was presupposed between bulk and brane parameters. However, all the models studied were proven unable to support the desired behavior.

Our analysis has, nevertheless, confirmed that such a localization demands the synergetic action of both the bulk and the brane part of space-time. The chosen metric ansatz introduces in the bulk, apart from an energy-density and an isotropic diagonal pressure that satisfy a stiff equation of state, additional off-diagonal, non-isotropic pressure components. The dependence of the mass function on both the fifth- and the time-coordinate contributes to these. It becomes therefore clear that gravitational degrees of freedom tend to leak from the brane – similarly to the black-hole singularity – and, although the models considered in specific in this work have failed to localize them, a mechanism must exist that will achieve this. Another important point that has emerged from our analysis is the necessity of the time-dependence of the field configurations in all the models we studied - even when the mass parameter is assumed to be time-independent; according to our findings, a static black-hole configuration may indeed exist, however, the associated field configuration itself has to be dynamic.

However, the metric ansatz that would describe a 5-dimensional space-time of this form had to be carefully constructed. The black-string space-time was associated to a factorized metric ansatz, therefore, the localization of the extended singularity would be realized only through a non-factorized ansatz, in which the 4-dimensional part would exhibit dependence on the fifth coordinate. Previous attempts [210, 211] had shown that such line-elements characterized by the presence of a horizon in their 4-dimensional part led to space-times with additional singularities apart from the extended black-string one. A modified Vaidya-type 4-dimensional line-element was finally chosen and embedded in a 5-dimensional warped space-time. Being analytic in 4 dimensions, this metric ansatz was free from any additional singularities. Moreover, with its mass being a function of both the fifth and the time-coordinate, it provided a reasonable ansatz for a perturbed Schwarzschild background on the brane, ideal for investigating both the localization of the black-hole singularity and the existence of a static solution.

With the gravitational part of our model decided, we then turned to the determination of the field theory model that would support such a space-time. Previous attempts to find such a model based on ordinary theories of scalar or gauge fields had led to a negative result [210]. Therefore, in this work, we decided to study instead a variety of field theories that could be characterized as non-ordinary – for simplicity, we focused on the case of scalar field theories. In Section 3.2, we examined the case of a field theory with one or more scalar fields minimally-coupled to gravity but otherwise described by a general Lagrangian. The cases studied included a single scalar field with a non-canonical kinetic term and two interacting scalar fields with either canonical, non-canonical or mixed kinetic terms. Our analysis allowed for general forms of

potentials as well as the case where one or both of the scalar fields were ghosts. In Section 3.3, we turned to the field theory of a single scalar field conformally-coupled to gravity, and studied the cases where its conformal coupling function was a power-law of the field, a polynomial, an exponential function, or of a completely arbitrary form.

In order to avoid any unreasonable restrictions on the field configurations, we allowed the warp factor to assume a y-dependent, but otherwise, arbitrary form. We also imposed no fine-tunings between bulk and brane parameters. A viable bulk solution, if emerged, would be subsequently used, to determine, through the junction conditions, the brane content. Nevertheless, our analysis never reached that point: all the field theory models studied, no matter how general, were shown not to be able to support the assumed gravitational background. Considering only the set of gravitational equations in the bulk, we were able to demonstrate that in each and every case, the scalar field-theory model chosen was not compatible with the basic assumptions for the metric ansatz necessary for the localization of the black-string singularity. Our results demonstrate how difficult, if possible at all, the construction of a localized 5-dimensional black hole may be in the context of a well-defined field-theory model.

Finally, in chapter 4 a very different aspect of black holes attracted our attention. In particular, we deal with the so-called information loss paradox. In a nutshell, the paradox is about the fate of information in the presence of a black hole, since the latter is expected at some point to evaporate away, through the emission of thermal Hawking-type radiation. Questions like whether black holes actually destroy information or how can they force a quantum system, originally in a pure state, to evolve into a mixed state (as our picture about their formation/evaporation process suggests) are far from being clearly answered. The information loss conundrum then is a still open issue that indicates the limits of the 20th century physics and waits for its solution to be found, hopefully, in the 21st century. Several efforts have been made so far to resolve it, but all of them have such serious drawbacks that hardly any can be considered constituting the base of a definitive answer. Here we present two ideas that could help us confront the paradox or at least to serve as the basis for the formulation of a successful resolution of the paradox.

The first is based on a differentiation in the way we perceive the notion of information, namely that not all kinds of information are equally important to nature. We argue that some of them are of fundamental and others of secondary importance, that are characterized as Π1 and Π2 respectively, on the basis that the first ones are protected by a series of conservation laws against destruction, while the latter ones are allowed to be destroyed with different degrees of ease. Postulating that black holes radiate away all Π1 information through Hawking radiation and, at the same time, they destroy all of the Π2 one, we manage to avoid any paradoxes, while their behavior remains compatible with the second law of thermodynamics.

The second idea deals with the apparent unitarity violating phenomenon, where a particle in a pure state can evolve into some mixed state during the formation/evaporation process of a black hole, which also means that information about the system gets lost for ever. It is proposed that the combination of the semiclassical approximation for particle creation by black holes, as presented by Hawking, with the EPR connection

between entangled particles, as established by Einstein, Podolsky and Rosen, can provide us with a viable explanation of what really happens during the evaporation of a black hole, without assuming that unitarity can be violated against all requirements of quantum theory. It is only enough the EPR phenomenon to hold also in the case of black holes and there is no apparent reason why it shouldn't do so. Then, all particles will evolve into some pure state soon after their creation due to the influence of the singularity on them both directly (by contact) and indirectly (through the EPR correlation). Any observer away from the black hole would measure them to find that they all are already in a pure state and, on top of that, entangled with each other in such a way that we can extract information from the black hole interior. In this sense unitarity remains safe and no paradox occurs to undermine the credibility of our quantum mechanical understanding of nature.

Concluding this review, let us emphasize the importance of studying the black hole properties. As purely gravitational objects, their formation, topology and evaporation are affected by the overall space-time structure. Therefore, they can serve as probes of this geometry providing us with evidence of the existence, the number and the geometry of extra dimensions. Furthermore, they are the only objects for the description of which gravitational and quantum mechanical phenomena can be equally important, provided they have the right mass. In this sense their behavior could also give us some hints about the long sought-for quantum gravitational laws. In addition, when dealing with black holes, complicated issues concerning entropy, information and the statistical approach to thermodynamics rise, challenging our understanding of them and potentially marking the limitations of our knowledge. Even more, the acquaintance with novel algebraic techniques, unconventional ideas and radical suggestions and the deeper understanding of General Relativity one develops during the study of black hole physics is the valuable legacy one is left with to employ in the quest to understand the Cosmos.

Appendix A

Angular eigenvalue of spin-weighted spheroidal harmonics

The quantity $_hA_\Lambda$ is the eigenvalue of the spin-weighted spheroidal harmonics $_hS_\Lambda(x)$. It also determines the separation constant between the radial (2.117) and the angular (2.118) equations to which the general "master" equation, governing the emission of particles by a black hole, decouples. In the case of a rotating black hole, this quantity does not exist in closed form. However, for low ω and low a, the angular eigenvalue of the spin-weighted spheroidal harmonics can be expressed as a power series with respect to $a\omega$ [200, 189, 188, 190, 166]

$$_hA_\Lambda = \sum_{k=0}^{\infty} f_k \, (a\omega)^k \, . \tag{A.1}$$

Defining

$$
\begin{aligned}
\frac{1}{2}(\alpha + \beta) &= \max(|m|, |s|), \\
\frac{1}{2}(\alpha - \beta) &= \frac{ms}{\max(|m|, |s|)} \qquad \text{and}
\end{aligned}
\tag{A.2}
$$

$$h(l) = \frac{\left[l^2 - \frac{1}{4}(\alpha + \beta)^2\right] \left[l^2 - \frac{1}{4}(\alpha - \beta)^2\right] (l^2 - s^2)}{2\left(l - \frac{1}{2}\right) l^3 \left(l + \frac{1}{2}\right)} \, , \tag{A.3}$$

we have for the first coefficients

$$f_0 = l(l+1) - s(s+1) \,, \tag{A.4}$$

$$f_1 = -\frac{2ms^2}{l(l+1)} \,, \tag{A.5}$$

$$f_2 = h(l+1) - h(l) - 1 \,, \tag{A.6}$$

$$f_3 = \frac{2h(l)ms^2}{(l-1)l^2(l+1)} - \frac{2h(l+1)ms^2}{l(l+1)^2(l+2)} \,, \tag{A.7}$$

$$f_4 = m^2 s^4 \left(\frac{4h(l+1)}{l^2(l+1)^4(l+2)^2} - \frac{4h(l)}{(l-1)^2 l^4(l+1)^2} \right)$$
$$- \frac{(l+2)h(l+1)h(l+2)}{2(l+1)(2l+3)}$$
$$+ \frac{h^2(l+1)}{2(l+1)} + \frac{h(l)h(l+1)}{2l^2+2l} - \frac{h^2(l)}{2l} + \frac{(l-1)h(l-1)h(l)}{4l^2-2l} \,, \tag{A.8}$$

$$f_5 = m^3 s^6 \left(\frac{8h(l)}{l^6(l+1)^3(l-1)^3} - \frac{8h(l+1)}{l^3(l+1)^6(l+2)^3} \right)$$
$$+ ms^2 h(l) \left(-\frac{h(l+1)(7l^2+7l+4)}{l^3(l+2)(l+1)^3(l-1)} - \frac{h(l-1)(3l-4)}{l^3(l+1)(2l-1)(l-2)} \right)$$
$$+ ms^2 \left(\frac{(3l+7)h(l+1)h(l+2)}{l(l+1)^3(l+3)(2l+3)} - \frac{3h^2(l+1)}{l(l+1)^3(l+2)} + \frac{3h^2(l)}{l^3(l-1)(l+1)} \right) \tag{A.9}$$

$$f_6 = \frac{16m^4 s^8}{l^4(l+1)^4} \left(\frac{h(l+1)}{(l+1)^4(l+2)^4} - \frac{h(l)}{l^4(l-1)^4} \right) + \frac{4m^2 s^4}{l^2(l+1)^2}$$
$$\times \left(-\frac{(3l^2+14l+17)h(l+1)h(l+2)}{(l+1)^3(l+2)(l+3)^2(2l+3)} + \frac{3h^2(l+1)}{(l+1)^3(l+2)^2} - \frac{3h^2(l)}{l^3(l-1)^2} \right)$$
$$+ \frac{4m^2 s^4}{l^2(l+1)^2}$$
$$\times \left(\frac{(11l^4+22l^3+31l^2+20l+6)h(l)h(l+1)}{l^3(l-1)^2(l+1)^3(l+2)^2} + \frac{(3l^2-8l+6)h(l-1)h(l)}{l^3(l-2)^2(l-1)(2l-1)} \right)$$
$$+ \frac{h(l+1)h(l+2)}{4(l+1)(2l+3)^2}$$
$$\times \left(\frac{(l+3)h(l+3)}{3} \frac{l+2}{l+1} \left((l+2)h(l+2) - (7l+10)h(l+1) + \frac{(3l^2+2l-3)h(l)}{l} \right) \right)$$
$$+ \frac{h^3(l+1)}{2(l+1)^2} - \frac{h^3(l)}{2l^2} + \frac{h(l)h(l+1)}{4l^2(l+1)^2}$$
$$\times \left((2l^2+4l+3)h(l) - (2l^2+1)h(l+1) - \frac{(l^2-1)(3l^2+4l-2)h(l-1)}{(2l-1)^2} \right)$$
$$+ \frac{h(l-1)h(l)}{4l^2(2l-1)^2} \left((l-1)(7l-3)h(l) - (l-1)^2 h(l-1) - \frac{l(l-2)h(l-2)}{3} \right) \,. \tag{A.10}$$

Based on these general relations we were able to derive the formulae given by eq. (2.133), eq. (2.134) and eq. (2.136) to determine the eigenvalue up to second order in the case of fermion, boson and scalar emission respectively.

Appendix B

Spin-weighted spheroidal harmonics expansion coefficients

According to Leaver [170] the angular eigenfunction $_hS_\Lambda(x)$ may be expressed as a series of the following form

$$_hS_\Lambda(x) = e^{a\omega x} (1+x)^{k_-} (1-x)^{k_+} \sum_{p=0}^{\infty} a_p (1+x)^p, \qquad (\text{B.1})$$

where $x = \cos\theta$ and $k_\pm \equiv |m \pm h|/2$.

The three-term recursion relations (2.138)-(2.139) can be used to determine the coefficients a_p that appear in the expansion of the spin-weighted spheroidal harmonics $_hS_\Lambda$. For instance, for the first five expansion coefficients, we obtain

$$a_1 = -\frac{\beta_0}{\alpha_0} a_0, \qquad a_2 = -\frac{\beta_1}{\alpha_1} a_1 - \frac{\gamma_1}{\alpha_1} a_0 = \left(\frac{\beta_1\beta_0}{\alpha_1\alpha_0} - \frac{\gamma_1}{\alpha_1} \right) a_0, \qquad (\text{B.2})$$

$$a_3 = -\frac{\beta_2}{\alpha_2} a_2 - \frac{\gamma_2}{\alpha_2} a_1 = \left(-\frac{\beta_2\beta_1\beta_0}{\alpha_2\alpha_1\alpha_0} + \frac{\beta_2\gamma_1}{\alpha_2\alpha_1} + \frac{\gamma_2\beta_0}{\alpha_2\alpha_0} \right) a_0, \qquad (\text{B.3})$$

$$a_4 = -\frac{\beta_3}{\alpha_3} a_3 - \frac{\gamma_3}{\alpha_3} a_2 = \left(\frac{\beta_3\beta_2\beta_1\beta_0}{\alpha_3\alpha_2\alpha_1\alpha_0} - \frac{\beta_3\beta_2\gamma_1}{\alpha_3\alpha_2\alpha_1} - \frac{\beta_3\gamma_2\beta_0}{\alpha_3\alpha_2\alpha_0} - \frac{\gamma_3\beta_1\beta_0}{\alpha_3\alpha_1\alpha_0} + \frac{\gamma_3\gamma_1}{\alpha_3\alpha_1} \right) a_0. \tag{B.4}$$

The $(\alpha_p, \beta_p, \gamma_p)$ coefficients are given by eqs. (2.140) and must be evaluated for each specific partial mode.

B.1   Fermions

For the needs of our analysis, we determine the above coefficients for the fermionic modes $(\frac{1}{2}, \frac{1}{2})$ and $(\frac{3}{2}, \frac{3}{2})$. First, for the $(\frac{1}{2}, \frac{1}{2})$-mode, eq. (2.133) leads to the following result for the corresponding eigenvalue $(h = 1/2)$

$$_{\frac{1}{2}}A_{\frac{1}{2}\frac{1}{2}} = -\frac{a\omega}{3} - \frac{11}{27} (a\omega)^2, \qquad (\text{B.5})$$

where we have used that, for this mode, $k_- = 0$ and $k_+ = 1/2$. Then, the $(\alpha_p, \beta_p, \gamma_p)$ coefficients take the form

$$\alpha_p^{(1/2)} = -2(p+1)^2, \quad \beta_p^{(1/2)} = p\,(p+2) - 4a\omega\,(p+\frac{2}{3}) - \frac{16}{27}\,(a\omega)^2, \quad \gamma_p^{(1/2)} = 2a\omega(p+1). \tag{B.6}$$

Then, the recursion relations (2.138)-(2.139) lead to the following relations between the first four sum coefficients

$$\frac{a_1^{(1/2)}}{a_0^{(1/2)}} = -\frac{4}{3}\,a\omega\left(1 + \frac{2a\omega}{9}\right), \qquad \frac{a_2^{(1/2)}}{a_0^{(1/2)}} = (a\omega)^2\left(1 + \frac{28a\omega}{81}\right) + \dots, \tag{B.7}$$

$$\frac{a_3^{(1/2)}}{a_0^{(1/2)}} = -\frac{392}{729}\,(a\omega)^3\left(1 + \frac{187}{441}\,a\omega\right) + \dots. \tag{B.8}$$

The superscript $(1/2)$ denotes that the above expressions hold for the case of the $(\frac{1}{2}, \frac{1}{2})$ partial mode. We have also given only the relations between the first four expansion coefficients since, as shown in section 2.4.3, in the case of fermions, it suffices to consider only terms up to $p = 3$ in the sum of eq. (2.137).

For the mode $(\frac{3}{2}, \frac{3}{2})$, using the fact that now $k_- = 1/2$ and $k_+ = 1$, we arrive at the following result for the angular eigenvalue

$$_{\frac{1}{2}}A_{\frac{3}{2}\frac{3}{2}} = 3 - \frac{a\omega}{5} - \frac{29}{125}\,(a\omega)^2. \tag{B.9}$$

In turn, the $(\alpha_p, \beta_p, \gamma_p)$ coefficients take the form

$$\alpha_p^{(3/2)} = -2(p+1)(p+2), \quad \beta_p^{(3/2)} = p(p+4) - 4a\omega(p+\frac{6}{5}) - \frac{96}{125}\,(a\omega)^2, \quad \gamma_p^{(3/2)} = 2a\omega(p+2). \tag{B.10}$$

Finally, the above result into the following relations between the first four sum coefficients

$$\frac{a_1^{(3/2)}}{a_0^{(3/2)}} = -\frac{6}{5}\,a\omega\left(1 + \frac{4a\omega}{25}\right), \qquad \frac{a_2^{(3/2)}}{a_0^{(3/2)}} = \frac{4}{5}\,(a\omega)^2\left(1 + \frac{34a\omega}{125}\right) + \dots, \tag{B.11}$$

$$\frac{a_3^{(3/2)}}{a_0^{(3/2)}} = -\frac{716}{1875}\,(a\omega)^3\left(1 + \frac{1588}{4475}\,a\omega\right) + \dots. \tag{B.12}$$

B.2   Gauge Bosons

We now turn to the case of gauge bosons, and more particularly to the dominant mode with $h = l = m = 1$. Employing eq. (2.134) and (2.140), we find the following results for the angular eigenvalue

$$_1A_{11} = -a\omega - \frac{11}{20}\,(a\omega)^2, \tag{B.13}$$

and the $(\alpha_p, \beta_p, \gamma_p)$ coefficients

$$\alpha_p = -2(p+1)^2\,, \qquad \beta_p = p(p+3) - a\omega(4p+3) - \frac{9(a\omega)^2}{20}\,, \qquad \gamma_p = 2a\omega(p+2)\,. \quad \text{(B.14)}$$

We may then compute the relations between the different sum coefficients a_p - although for our analysis we need only the relation between a_1 and a_0, for completeness, we display again the relations between the first four coefficients

$$\frac{a_1^{(1)}}{a_0^{(1)}} = -\frac{a\omega}{2}\left(3 + \frac{9a\omega}{20}\right)\,, \qquad \frac{a_2^{(1)}}{a_0^{(1)}} = (a\omega)^2\left(\frac{6}{5} + \frac{9a\omega}{32}\right) + ...\,, \qquad \text{(B.15)}$$

$$\frac{a_3^{(1)}}{a_0^{(1)}} = -\frac{(a\omega)^3}{32}\left(\frac{65}{3} + \frac{1247}{200}\,a\omega\right) + ...\,. \qquad \text{(B.16)}$$

B.3 Scalar Fields

We finally study the case of scalar fields $(h = 0)$. For our analysis, we will need the sum coefficients a_p for the modes $l = m = 0$ and $l = m = 1$. We start with the case with $l = m = 0$: employing again eq. (2.136) and (2.140), we find the following results for the angular eigenvalue

$$_0A_{00} = -\frac{(a\omega)^2}{3}\,, \qquad \text{(B.17)}$$

and the $(\alpha_p, \beta_p, \gamma_p)$ coefficients

$$\alpha_p = -2(p+1)^2\,, \qquad \beta_p = p(p+1) - a\omega(4p+2) - \frac{2(a\omega)^2}{3}\,, \qquad \gamma_p = 2a\omega p\,, \quad \text{(B.18)}$$

that, in turn, lead to the following relations between the first five sum coefficients a_p

$$\frac{a_1^{(00)}}{a_0^{(00)}} = -a\omega\left(1 + \frac{a\omega}{3}\right)\,, \qquad \frac{a_2^{(00)}}{a_0^{(00)}} = \frac{(a\omega)^2}{3}\left(2 + a\omega + \frac{(a\omega)^2}{12}\right)\,, \qquad \text{(B.19)}$$

$$\frac{a_3^{(00)}}{a_0^{(00)}} = -\frac{(a\omega)^3}{3}\left(1 + \frac{65a\omega}{108}\right) + ...\,, \qquad \frac{a_4^{(00)}}{a_0^{(00)}} = \frac{(a\omega)^4}{108}\left(\frac{115}{8} + \frac{29a\omega}{3}\right) + ...\,. \quad \text{(B.20)}$$

For the mode $l = m = 1$, a similar analysis leads to the following results for the eigenvalue

$$_0A_{11} = 2 - \frac{(a\omega)^2}{5}\,, \qquad \text{(B.21)}$$

the $(\alpha_p, \beta_p, \gamma_p)$ coefficients

$$\alpha_p = -2(p+1)(p+2)\,, \qquad \beta_p = p(p+3) - 4a\omega(p+1) - \frac{4(a\omega)^2}{5}\,, \qquad \gamma_p = 2a\omega(p+1)\,,$$
$$\text{(B.22)}$$

and the first five sum coefficients a_p

$$\frac{a_1^{(11)}}{a_0^{(11)}} = -a\omega\left(1 + \frac{a\omega}{5}\right), \qquad \frac{a_2^{(11)}}{a_0^{(11)}} = \frac{(a\omega)^2}{5}\left(3 + a\omega + \frac{(a\omega)^2}{15}\right), \qquad \text{(B.23)}$$

$$\frac{a_3^{(11)}}{a_0^{(11)}} = -\frac{(a\omega)^3}{15}\left(4 + \frac{103a\omega}{60}\right) + ..., \qquad \frac{a_4^{(11)}}{a_0^{(11)}} = \frac{(a\omega)^4}{300}\left(\frac{571}{20} + \frac{43a\omega}{3}\right) + ... \quad \text{(B.24)}$$

Appendix C

MATHEMATICA codes

Here we state some indicative codes that we used to calculate the absorption probabilities, the differential energy and angular momentum emission rates and the angular distribution of the emitted energy at various stages of our work.

C.1 Graviton emission

C.1.1 Absorption probability

Code for calculating the graybody factor for the graviton mode $j, l, m = 2, 2, 0$ in the case of a 7-dimensional $(n = 3)$ rotating black hole with angular momentum parameter $a = 0.5$, both numerically (f_1) and analytically (f_2).

```
n = 3;
rh = 1;
j = 2;
l = 2;
m = 0;
a = 0.5;
far = 1000;
near = rh + 0.00001;
a$ = a/rh;

nh1[x_, w_] := 1
nh2[x_, w_, m_] := -\[ImaginaryI]*(w - (m*a)/(rh^2 + a^2))*(1 + a^2/x^2)/
(1 + a^2/x^2 - (1 + a^2/rh^2)*(rh/x)^(n + 1))

A$ = (n + 1) + (n - 1)*a$^2
D$ = 1 - (4*a$^2)/A$^2
K$[w_] := (1 + a$^2)*w*rh - a$*m
Ejlm[w_] :=
 j*(j + n +
     1) - (a*w)^2*((-1 + 2*l*(l - 1) + 2*j*(j + 1) - 2*m^2 +
```

```
          2*n*(l + j) + n^2)/((2*j + n - 1)*(2*j + n + 3))) + (a*
       w)^4*((((l - j + Abs[m])*(l + j - Abs[m] + n - 1))/(
       16*(2*j + n -
           3) (2*j + n -
           1)^2)*((2 + l - j + Abs[m])*(j + l - Abs[m] + n - 3) -
        4*(2*j + n -
           3)*(-1 + 2*l*(l - 1) + 2*j*(j + 1) - 2*m^2 + 2*n*(l + j) +
            n^2)/((2*j + n - 1)*(2*j + n + 3))) - ((l - j + Abs[m] -
         2)*(l + j - Abs[m] + n + 1))/(
       16*(2*j + n +
          5)*(2*j + n +
          3)^2)*((l - j + Abs[m] - 4)*(l + j - Abs[m] + n + 3) +
        4*(2*j + n +
           5)*(-1 + 2*l*(l - 1) + 2*j*(j + 1) - 2*m^2 + 2*n*(l + j) +
            n^2)/((2*j + n - 1)*(2*j + n + 3)))))
Ljlm[w_] := Ejlm[w] + a^2*w^2 - 2*a*m*w

(w = 0.05; Label[w - loop];
 s = NDSolve[{r^4*(1 + (a/r)^2 - (1 + (a/rh)^2)*(rh/r)^(n + 1))*
        D[r^n*r^2*(1 + (a/r)^2 - (1 + (a/rh)^2)*(rh/r)^(n + 1))*R'[r],
        r] + r^n*(r^2*((r^2 + a^2)*w - a* m)^2 - (l*(l + n - 1)*a^2 +
           Ljlm[w]*r^2)*
         r^2*(1 + (a/r)^2 - (1 + (a/rh)^2)*(rh/r)^(n + 1)))*R[r] ==
     0,
    R[near] == nh1[near, w],
    R'[near] == nh2[near, w, m]},
   R[r], {r, far - 1, far + 5}, MaxSteps -> Infinity,
   AccuracyGoal -> Infinity];
 Rff[r] = R[r] /. s[[1]];
 R1[r] = r^((n + 2)/2)*Rff[r];
 R2[r] = D[r^((n + 2)/2)*Rff[r], r];
 Aout = 1/2*
    Exp[-\[ImaginaryI]*w*r]*(R1[r] - \[ImaginaryI]*R2[r]/w) /.
   r -> far;
 Ain = 1/2*Exp[\[ImaginaryI]*w*r]*(R1[r] + \[ImaginaryI]*R2[r]/w) /.
   r -> far;
 Absorption = 1 - Abs[Aout^2/Ain^2];
 Do[{w, Absorption} >>> j2l2m0.dat];
 Print[w, Absorption];
 If[w < 4.0, {w = w + 0.05, Goto[w - loop]}];)

 data = Import["C:\Users\user\Documents\j2l2m0.dat", "Table"]

f1 = ListPlot[data, PlotStyle -> {PointSize[0.015], Hue[0.2]}]
```

%%

```
\[Alpha][w_] := -K$[w]/A$*I
\[Alpha]\[Sigma]\[Upsilon]\[Zeta][w_] := K$[w]/A$*I
\[Beta][w_] :=
 1/2*((2 - D$) -
    Sqrt[(D$ - 2)^2 -
      4*(1/A$^2 (K$[
            w]^2 - (l*(l + n - 1)*a$^2 + Ljlm[w])*(1 + a$^2)))])

G1[w_] := Gamma[Sqrt[Ejlm[w] + a^2*w^2 + (n + 1)^2/4]]
G2[w_] := Gamma[\[Alpha][w] + \[Beta][w] + D$ - 1]
G2\[Sigma]\[Upsilon]\[Zeta][w_] :=
 Gamma[\[Alpha]\[Sigma]\[Upsilon]\[Zeta][w] + \[Beta][w] + D$ - 1]
G3[w_] := Gamma[\[Alpha][w] + \[Beta][w]]
G3\[Sigma]\[Upsilon]\[Zeta][w_] :=
 Gamma[\[Alpha]\[Sigma]\[Upsilon]\[Zeta][w] + \[Beta][w]]
G4[w_] := Gamma[2 - 2*\[Beta][w] - D$]
G5[w_] := Gamma[2*\[Beta][w] + D$ - 2]
G6[w_] := Gamma[2 + \[Alpha][w] - \[Beta][w] - D$]
G6\[Sigma]\[Upsilon]\[Zeta][w_] :=
 Gamma[2 + \[Alpha]\[Sigma]\[Upsilon]\[Zeta][w] - \[Beta][w] - D$]
G7[w_] := Gamma[1 + \[Alpha][w] - \[Beta][w]]
G7\[Sigma]\[Upsilon]\[Zeta][w_] :=
 Gamma[1 + \[Alpha]\[Sigma]\[Upsilon]\[Zeta][w] - \[Beta][w]]

B[w_] := -1/Pi*((2/(w*rh*(1 + a$^2)^(1/(n + 1))))^(2*l + n + 1))*
  Sqrt[Ejlm[w] + a^2*w^2 + (n + 1)^2/4]*(G1[w]^2*G2[w]*G3[w]*G4[w])/(
  G5[w]*G6[w]*G7[w])
B\[Sigma]\[Upsilon]\[Zeta][
  w_] := -1/Pi*((2/(w*rh*(1 + a$^2)^(1/(n + 1))))^(2*l + n + 1))*
  Sqrt[Ejlm[w] + a^2*w^2 + (n + 1)^2/4]*(
  G1[w]^2*G2\[Sigma]\[Upsilon]\[Zeta][w]*
   G3\[Sigma]\[Upsilon]\[Zeta][w]*G4[w])/(
  G5[w]*G6\[Sigma]\[Upsilon]\[Zeta][w]*G7\[Sigma]\[Upsilon]\[Zeta][w])

A[w_] := (2*I*(B\[Sigma]\[Upsilon]\[Zeta][w] - B[w]))/(
 B\[Sigma]\[Upsilon]\[Zeta][w]*B[w] +
  I*(B\[Sigma]\[Upsilon]\[Zeta][w] - B[w]) + 1)

f2 = Plot[A[w], {w, 1.5, 2.9}, PlotRange -> {{1., 6.}, {-0.002, 1.}},
  AxesLabel -> {"w*rh", "|A|^2"}]
```

C.1.2 Energy emission

Code for calculating the differential energy emission rate for the emission of tensor-type gravitons in the case of a 7-dimensional ($n = 3$) rotating black hole with angular momentum parameter $a = 0.5$.

```
hr = 1;
n = 3;
astar = 0.5;                                        \

a = hr astar;
hawk = ((n + 1) + (n - 1) astar^2)/(4 \[Pi] (1 + astar^2) hr);
omega = astar/(hr (1 + astar^2));
far = 1000;
near = hr + 0.0001;
af[x_, w_] := 1
bf[x_, w_,
  m_] := -I (w - (m a)/(hr^2 +
       a^2)) (1 + (a/
       x)^2)/((1 + (a/x)^2 - (1 + (a/hr)^2) (hr/x)^(n + 1)))

iop = 0;
(w = 0.00001; int = 1; Label[w - loop];

 j = 2; Label[j - loop];
 l = 2; Label[l - loop];
 m = l - j; Label[m - loop];

 Ejlm = j (j + n +
      1) - (a w)^2 ((-1 + 2 l (l - 1) + 2 j (j + 1) - 2 m^2 +
        2 n (j + l) +
        n^2)/((2 j + n - 1) (2 j + n +
          3))) + (a w)^4 (((l - j + Abs[m]) (l + j - Abs[m] + n -
          1))/(16 (2 j + n - 3) (2 j + n - 1)^2) ((2 + l - j +
          Abs[m]) (l + j - Abs[m] + n - 3) -
        4 (2 j + n -
          3) ((-1 + 2 l (l - 1) + 2 j (j + 1) - 2 m^2 +
            2 n (j + l) +
            n^2)/((2 j + n - 1) (2 j + n + 3)))) - (((l - j +
          Abs[m] - 2) (l + j + n - Abs[m] + 1))/(16 (2 j + 5 +
          n) (2 j + n + 3)^2)) ((l - j + Abs[m] - 4) (j + l + n -
          Abs[m] + 3) +
        4 (2 j + n +
          5) ((-1 + 2 l (l - 1) + 2 j (j + 1) - 2 m^2 +
            2 n (j + l) + n^2)/((2 j + n - 1) (2 j + n + 3)))));
```

```
radialfn[r] =
 NDSolve[{r^(2 - n) (1 + (a/r)^2 - (1 + (a/hr)^2) (hr/r)^(n + 1))
       D[r^(2 + n) (1 + (a/r)^2 - (1 + (a/hr)^2) (hr/r)^(n + 1))
         R'[r], r] + (((r^2 + a^2) w -
            a m)^2 - (l (l + n - 1) a^2/r^2 + Ejlm -
            2 a m w + (a w)^2 )
          r^2 (1 + (a/r)^2 - (1 + (a/hr)^2) (hr/r)^(n + 1))) R[r] ==
    0, R[near] == af[near, w], R'[near] == bf[near, w, m]},
  R[r], {r, far - 1, far + 5}, AccuracyGoal -> Infinity,
  MaxSteps -> Infinity];
Rfn[r] = R[r] /. radialfn[r];
efn[r] = r^((n + 2)/2) Rfn[r];
ffn[r] = D[r^((n + 2)/2) Rfn[r], r];
pfn[w] = (1/2) Exp[-I w r] (efn[r] - I ffn[r]/w) /. r -> far;
qfn[w] = (1/2) Exp[I w r] (efn[r] + I ffn[r]/w) /. r -> far;
grayfn = (1 - Abs[( pfn[w])^2/( qfn[w])^2]);

f1 = If[j - l - Abs[m] >= 0, 1, 0];
f2 = If[Mod[j - l - Abs[m], 2] == 0, 1, 0];
ff = f1 f2;

Nl = (n + 1) (n + l) (2 l + n - 1) Factorial[
    l + n - 3]/(2 l (l + 1)
     Factorial[l - 2] (n - 1) Factorial[n - 3]);
iop =  iop +
  ff Nl w hr grayfn/(2 \[Pi] (Exp[(w - m omega)/hawk] - 1));

If[m < j - l, {m = m + 1, Goto[m - loop]}];
If[l < j, {l = l + 1, m = l - j, Goto[l - loop]}];
If[j < 8, {j = j + 1, l = 2, m = l - j, Goto[j - loop]}];

Do[{w, iop[[1]]} >>> ESpecj8a0n3.dat];
Print[w, " ", grayfn[[1]], " ", iop[[1]]];

If[w < 8, {w = w + 0.1, iop = 0, int = int + 1, Goto[w - loop]}];)
```

C.1.3 Angular momentum emission

Code for calculating the differential angular momentum emission rate for the emission of tensor-type gravitons in the case of a 7-dimensional ($n = 3$) rotating black hole with angular momentum parameter $a = 0.5$.

```
hr = 1;
n = 3;
astar = 0.5;                                    \

a = hr astar;
hawk = ((n + 1) + (n - 1) astar^2)/(4 \[Pi] (1 + astar^2) hr);
omega = astar/(hr (1 + astar^2));
far = 1000;
near = hr + 0.0001;
af[x_, w_] := 1
bf[x_, w_,
  m_] := -I (w - (m a)/(hr^2 +
       a^2)) (1 + (a/
       x)^2)/((1 + (a/x)^2 - (1 + (a/hr)^2) (hr/x)^(n + 1)))

iop = 0;
(w = 0.00001; int = 1; Label[w - loop];

 j = 2; Label[j - loop];
 l = 2; Label[l - loop];
 m >= -2; Label[m - loop];

 Ejlm = j (j + n +
      1) - (a w)^2 ((-1 + 2 l (l - 1) + 2 j (j + 1) - 2 m^2 +
        2 n (j + 1) +
        n^2)/((2 j + n - 1) (2 j + n +
          3))) + (a w)^4 (((l - j + Abs[m]) (l + j - Abs[m] + n -
          1))/(16 (2 j + n - 3) (2 j + n - 1)^2) ((2 + l - j +
          Abs[m]) (l + j - Abs[m] + n - 3) -
        4 (2 j + n -
          3) ((-1 + 2 l (l - 1) + 2 j (j + 1) - 2 m^2 +
            2 n (j + 1) +
            n^2)/((2 j + n - 1) (2 j + n + 3)))) - (((l - j +
          Abs[m] - 2) (l + j + n - Abs[m] + 1))/(16 (2 j + 5 +
          n) (2 j + n + 3)^2)) ((l - j + Abs[m] - 4) (j + l + n -
          Abs[m] + 3) +
        4 (2 j + n +
          5) ((-1 + 2 l (l - 1) + 2 j (j + 1) - 2 m^2 +
            2 n (j + 1) + n^2)/((2 j + n - 1) (2 j + n + 3)))))));
```

```
radialfn[r] =
 NDSolve[{r^(2 - n) (1 + (a/r)^2 - (1 + (a/hr)^2) (hr/r)^(n + 1))
      D[r^(2 + n) (1 + (a/r)^2 - (1 + (a/hr)^2) (hr/r)^(n + 1))
        R'[r], r] + (((r^2 + a^2) w -
           a m)^2 - (l (l + n - 1) a^2/r^2 + Ejlm -
           2 a m w + (a w)^2 )
         r^2 (1 + (a/r)^2 - (1 + (a/hr)^2) (hr/r)^(n + 1))) R[r] ==
    0, R[near] == af[near, w], R'[near] == bf[near, w, m]},
  R[r], {r, far - 1, far + 5}, AccuracyGoal -> Infinity,
  MaxSteps -> Infinity];
Rfn[r] = R[r] /. radialfn[r];
efn[r] = r^((n + 2)/2) Rfn[r];
ffn[r] = D[r^((n + 2)/2) Rfn[r], r];
pfn[w] = (1/2) Exp[-I w r] (efn[r] - I ffn[r]/w) /. r -> far;
qfn[w] = (1/2) Exp[I w r] (efn[r] + I ffn[r]/w) /. r -> far;
grayfn = (1 - Abs[( pfn[w])^2/( qfn[w])^2]);

f1 = If[j - l - Abs[m] >= 0, 1, 0];
f2 = If[Mod[j - l - Abs[m], 2] == 0, 1, 0];
ff = f1 f2;

Nl = (n + 1) (n + 1) (2 l + n - 1) Factorial[
    l + n - 3]/(2 l (l + 1)
     Factorial[l - 2] (n - 1) Factorial[n - 3]);
iop =  iop +
  ff Nl m hr grayfn/(2 \[Pi] (Exp[(w - m omega)/hawk] - 1));

If[m < j - l, {m = m + 1, Goto[m - loop]}];
If[l < j, {l = l + 1, m = l - j, Goto[l - loop]}];
If[j < 8, {j = j + 1, l = 2, m = l - j, Goto[j - loop]}];

Do[{w, iop[[1]]} >>> JSpecj8a0p5n3.dat];
Print[w, " ", grayfn[[1]], " ", iop[[1]]];

If[w < 12, {w = w + 0.1, iop = 0, int = int + 1, Goto[w - loop]}];)
```

C.2 Massive scalar emission

C.2.1 Absorption probability for the emission in the bulk

Code for calculating the graybody factor for the scalar mode $j, l, m = 1, 0, 1$ with mass parameter $M = 0.4$ propagating into the bulk in the case of a 6-dimensional ($n = 2$) rotating black hole with angular momentum parameter $a = 0.5$, both numerically (f_1) and analytically (f_2).

```
n = 2;
rh = 1;
j = 1;
l = 0;
m = 1;
a = 0.5;
M = 0.4;
far = 1000;
near = rh + 0.00001;
a$ = a/rh;


nh1[x_, w_] := 1
nh2[x_, w_, m_] := -\[ImaginaryI]*(w - (m*a)/(rh^2 + a^2))*(
  1 + a^2/x^2)/(1 + a^2/x^2 - (1 + a^2/rh^2)*(rh/x)^(n + 1))


A$ = (n + 1) + (n - 1)*a$^2;
D$ = 1 - (4*a$^2)/A$^2;
K$[w_] := (1 + a$^2)*w*rh - a$*m;
EjlmTilde[w_] :=
 j*(j + n + 1) - ((w^2 - M^2)*
    a^2)*((-1 + 2*l*(l - 1) + 2*j*(j + 1) - 2*m^2 + 2*n*(l + j) +
      n^2)/((2*j + n - 1)*(2*j + n + 3))) + ((w^2 - M^2)^2*
    a^4)*(((l - j + Abs[m])*(l + j - Abs[m] + n - 1))/(
     16*(2*j + n -
        3) (2*j + n -
       1)^2)*((2 + l - j + Abs[m])*(j + l - Abs[m] + n - 3) -
      4*(2*j + n -
        3)*(-1 + 2*l*(l - 1) + 2*j*(j + 1) - 2*m^2 + 2*n*(l + j) +
         n^2)/((2*j + n - 1)*(2*j + n + 3))) - ((l - j + Abs[m] -
      2)*(l + j - Abs[m] + n + 1))/(16*(2*j + n +
      5)*(2*j + n + 3)^2)*((l - j + Abs[m] - 4)*(l + j - Abs[m] +
       n + 3) +
      4*(2*j + n +
        5)*(-1 + 2*l*(l - 1) + 2*j*(j + 1) - 2*m^2 + 2*n*(l + j) +
         n^2)/((2*j + n - 1)*(2*j + n + 3))))
```

```
LjlmTilde[w_] := EjlmTilde[w] + a^2*w^2 - 2*a*m*w

(w = 0.02; Label[w - loop];
 s = NDSolve[{r^4*(1 + (a/r)^2 - (1 + (a/rh)^2)*(rh/r)^(n + 1))*
        D[r^n*r^2*(1 + (a/r)^2 - (1 + (a/rh)^2)*(rh/r)^(n + 1))*R'[r],
          r] + r^n*(r^2*((r^2 + a^2)*w - a* m)^2 - (l*(l + n - 1)*a^2 +
             LjlmTilde[w]*r^2 + M^2*r^4)*
            r^2*(1 + (a/r)^2 - (1 + (a/rh)^2)*(rh/r)^(n + 1)))*R[r] ==
      0,
     R[near] == nh1[near, w],
     R'[near] == nh2[near, w, m]},
    R[r], {r, far - 1, far + 5}, MaxSteps -> Infinity,
    AccuracyGoal -> Infinity];
 Rff[r] = R[r] /. s[[1]];
 R1[r] = r^((n + 2)/2)*Rff[r];
 R2[r] = D[r^((n + 2)/2)*Rff[r], r];
 Aout = 1/2*
    Exp[-\[ImaginaryI]*Sqrt[w^2 - M^2]*
      r]*(R1[r] - \[ImaginaryI]*R2[r]/Sqrt[w^2 - M^2]) /. r -> far;
 Ain = 1/2*
    Exp[\[ImaginaryI]*Sqrt[w^2 - M^2]*
      r]*(R1[r] + \[ImaginaryI]*R2[r]/Sqrt[w^2 - M^2]) /. r -> far;
 Absorption = 1 - Abs[Aout^2/Ain^2];
 Do[{w, Absorption} >>> Absn2l0j1m1a05M04.dat];
 Print[w, Absorption];
 If[w < 6.0, {w = w + 0.02, Goto[w - loop]}];)

data=
  Import["E:\\C disk\\PhD\\papers\\mathematica \
data\\bulk\\massive\\scalars\\absorption \
probability\\data\\Absn2j1l0m1a05M04.dat", "Table"];

f1 =
 ListPlot[data, Frame -> True, PlotJoined -> True,
  PlotRange -> {{0.00000001, 1.0}, {-0.000005, 0.00002}},
  PlotStyle -> {Dashing[{0.02, 0.02}], Thickness[0.005], Hue[1] },
  Ticks -> Automatic, ImageSize -> 72*5]

%%%%%%%%%%%%%%%%%%%%%%%%%%%%%%%%%%%%%%%%%%%%%%%%%%%%%%%%%%%%%%%%%%%%%%%%%%%

\[Alpha][w_]  := -K$[w]/A$*I
\[Alpha]\[Sigma]\[Upsilon]\[Zeta][w_] := K$[w]/A$*I
\[Beta][w_] :=
 1/2*((2 - D$) -
```

```
      Sqrt[(D$ - 2)^2 - (4*K$[w]^2)/A$^2 +
        1/A$^2 4*(l (l + n + 1)*a$^2 + M^2*rh^2 + LjlmTilde[w])*(1 +
          a$^2)])

G1[w_] := Gamma[Sqrt[EjlmTilde[w] + (w^2 - M^2)*a^2 + (n + 1)^2/4]]
G2[w_] := Gamma[\[Alpha][w] + \[Beta][w] + D$ - 1]
G2\[Sigma]\[Upsilon]\[Zeta][w_] :=
 Gamma[\[Alpha]\[Sigma]\[Upsilon]\[Zeta][w] + \[Beta][w] + D$ - 1]
G3[w_] := Gamma[\[Alpha][w] + \[Beta][w]]
G3\[Sigma]\[Upsilon]\[Zeta][w_] :=
 Gamma[\[Alpha]\[Sigma]\[Upsilon]\[Zeta][w] + \[Beta][w]]
G4[w_] := Gamma[2 - 2*\[Beta][w] - D$]
G5[w_] := Gamma[2 + \[Alpha][w] - \[Beta][w] - D$]
G5\[Sigma]\[Upsilon]\[Zeta][w_] :=
 Gamma[2 + \[Alpha]\[Sigma]\[Upsilon]\[Zeta][w] - \[Beta][w] - D$]
G6[w_] := Gamma[1 + \[Alpha][w] - \[Beta][w]]
G6\[Sigma]\[Upsilon]\[Zeta][w_] :=
 Gamma[1 + \[Alpha]\[Sigma]\[Upsilon]\[Zeta][w] - \[Beta][w]]
G7[w_] := Gamma[2*\[Beta][w] + D$ - 2]

B[w_] := -1/
    Pi*(2/(Sqrt[(w^2 - M^2)]*rh*(1 + a$^2)^(1/(n + 1))))^(2*l + n + 1)*
  Sqrt[EjlmTilde[w] + (w^2 - M^2)*a^2 + (n + 1)^2/4]*(
  G1[w]^2*G2[w]*G3[w]*G4[w])/(G5[w]*G6[w]*G7[w])
B\[Sigma]\[Upsilon]\[Zeta][
  w_] := -1/
    Pi*(2/(Sqrt[(w^2 - M^2)]*rh*(1 + a$^2)^(1/(n + 1))))^(2*l + n + 1)*
  Sqrt[EjlmTilde[w] + (w^2 - M^2)*a^2 + (n + 1)^2/4]*(
  G1[w]^2*G2\[Sigma]\[Upsilon]\[Zeta][w]*
   G3\[Sigma]\[Upsilon]\[Zeta][w]*G4[w])/(
  G5\[Sigma]\[Upsilon]\[Zeta][w]*G6\[Sigma]\[Upsilon]\[Zeta][w]*G7[w])

Absorption[w_] := (2*I*(B\[Sigma]\[Upsilon]\[Zeta][w] - B[w]))/(
 B[w]*B\[Sigma]\[Upsilon]\[Zeta][w] +
  I*(B\[Sigma]\[Upsilon]\[Zeta][w] - B[w]) + 1)

f2 = Plot[Absorption[w], {w, 0, 0.8},
  PlotRange -> {{0, 1.}, {-0.000005, 0.00002}},
  AxesLabel -> {"w*rh", "|A|^2"}]
```

C.2.2 Absorption probability for the emission on the brane

Code for calculating the graybody factor for the scalar mode $l, m = 1, 1$ with mass parameter $M = 0.4$ emitted on the brane by a 6-dimensional ($n = 2$) rotating black hole with angular momentum parameter $a = 0.5$, both numerically (f_1) and analytically (f_2).

```
n = 2;
l = 1;
m = 1;
a = 0.5;
rh = 1;
M = 0.4;
far = 1000;
near = rh + 0.00001;
a$ = a/rh;


nh1[x_, w_] := 1
nh2[x_, w_, m_] := -\[ImaginaryI]*(w - (m*a)/(rh^2 + a^2))*(
  1 + a^2/x^2)/(1 + a^2/x^2 - (1 + a^2/rh^2)*(rh/x)^(n + 1))
ElmTilde[w_] :=
 l*(l + 1) + (a*Sqrt[w^2 - M^2])^2*(
   2*m^2 - 2*l (l + 1) +
    1)/((2*l - 1)*(2*l + 3)) + (a*Sqrt[w^2 - M^2])^4*((
    2*(-3 + 17*l*(l + 1) +
       l^2*(l + 1)^2*(2*l - 3)*(2*l + 5)))/((2*l - 3)*(2*l +
      5) (2*l - 1)^3*(2*l + 3)^3) + (
    4*m^2)/((2*l - 1)^2*(2*l + 3)^2)*(1/((2*l - 1)*(2*l + 3)) - (
      3*l*(l + 1))/((2*l - 3)*(2*l + 5))) + (
    2*m^4*(48 + 5*(2*l - 1)*(2*l + 3)))/((2*l - 3)*(2*l +
      5) (2*l - 1)^3*(2*l + 3)^3))

LlmTilde[w_] := ElmTilde[w] + a^2*w^2 - 2*a*m*w
(w = 0.00000000001; Label[w - loop];
 s = NDSolve[{r^2*(1 + (a/r)^2 - (1 + (a/rh)^2)*(rh/r)^(n + 1))*
       D[r^2*(1 + (a/r)^2 - (1 + (a/rh)^2)*(rh/r)^(n + 1)) R'[r],
       r] + (((r^2 + a^2)*w - a* m)^2 - (LlmTilde[w] + M^2*r^2)*
         r^2*(1 + (a/r)^2 - (1 + (a/rh)^2)*(rh/r)^(n + 1))) R[r] ==
     0,
    R[near] == nh1[near, w],
    R'[near] == nh2[near, w, m]},
   R[r], {r, far - 1, far + 5}, MaxSteps -> Infinity,
   AccuracyGoal -> Infinity];
 Rff[r] = R[r] /. s[[1]];
```

```
R1[r] = r*Rff[r];
R2[r] = D[r*Rff[r], r];
Aout = 1/2*
   Exp[-\[ImaginaryI]*Sqrt[w^2 - M^2]*
    r]*(R1[r] - \[ImaginaryI]*R2[r]/Sqrt[w^2 - M^2]) /. r -> far;
Ain = 1/2*
   Exp[\[ImaginaryI]*Sqrt[w^2 - M^2]*
    r]*(R1[r] + \[ImaginaryI]*R2[r]/Sqrt[w^2 - M^2]) /. r -> far;
Absorption = 1 - Abs[Aout^2/Ain^2];
Do[{w, Absorption} >>> Absn2l1m1a05M04.dat];
Print[w, " ", " ", " ", Absorption];
If[w < 2.0, {w = w + 0.01, Goto[w - loop]}];)

data=
 Import["E:\\C disk\\PhD\\papers\\mathematica \
data\\brane\\massive\\scalars\\absorption \
probability\\data\\Absn2l1m1a05M04.dat", "Table"];

f1 =
 ListPlot[data, Frame -> True, PlotJoined -> True,
  PlotRange -> {{0.00000001, 1.0}, {-0.000005, 0.00002}},
  PlotStyle -> {Dashing[{0.02, 0.02}], Thickness[0.005], Hue[1] },
  Ticks -> Automatic, ImageSize -> 72*5]

%%%%%%%%%%%%%%%%%%%%%%%%%%%%%%%%%%%%%%%%%%%%%%%%%%%%%%%%%%%%%%%%%%%%%%%

A$ = (n + 1) + (n - 1)*a$^2;
D$ = 1 + (n*(1 + a$^2))/A$ - (4*a$^2)/A$^2;

K$[w_] := (1 + a$^2)*w*rh - a$*m;
ElmTilde[w_] :=
 l*(l + 1) + (a*Sqrt[w^2 - M^2])^2*(
   2*m^2 - 2*l (l + 1) +
   1)/((2*l - 1)*(2*l + 3)) + (a*Sqrt[w^2 - M^2])^4*((
    2*(-3 + 17*l*(l + 1) +
      l^2*(l + 1)^2*(2*l - 3)*(2*l + 5)))/((2*l - 3)*(2*l +
      5) (2*l - 1)^3*(2*l + 3)^3) + (
    4*m^2)/((2*l - 1)^2*(2*l + 3)^2)*(1/((2*l - 1)*(2*l + 3)) - (
      3*l*(l + 1))/((2*l - 3)*(2*l + 5))) + (
    2*m^4*(48 + 5*(2*l - 1)*(2*l) + 3))/((2*l - 3)*(2*l +
      5) (2*l - 1)^3*(2*l + 3)^3))

LlmTilde[w_] := ElmTilde[w] + a^2*w^2 - 2*a*m*w
```

```
\[Alpha][w_] := -K$[w]/A$*I
\[Alpha]\[Sigma]\[Upsilon]\[Zeta][w_] := K$[w]/A$*I
\[Beta][w_] :=
 1/2*((2 - D$) -
    Sqrt[(D$ - 2)^2 - (4*K$[w]^2)/A$^2 + (
      4*(M^2*rh^2 + LlmTilde[w])*(1 + a$^2))/A$^2])

G1[w_] := Gamma[Sqrt[ElmTilde[w] + a^2*(w^2 - M^2) + 1/4]]
G2[w_] := Gamma[\[Alpha][w] + \[Beta][w] + D$ - 1]
G2\[Sigma]\[Upsilon]\[Zeta][w_] :=
 Gamma[\[Alpha]\[Sigma]\[Upsilon]\[Zeta][w] + \[Beta][w] + D$ - 1]
G3[w_] := Gamma[\[Alpha][w] + \[Beta][w]]
G3\[Sigma]\[Upsilon]\[Zeta][w_] :=
 Gamma[\[Alpha]\[Sigma]\[Upsilon]\[Zeta][w] + \[Beta][w]]
G4[w_] := Gamma[2 - 2*\[Beta][w] - D$]
G5[w_] := Gamma[2 + \[Alpha][w] - \[Beta][w] - D$]
G5\[Sigma]\[Upsilon]\[Zeta][w_] :=
 Gamma[2 + \[Alpha]\[Sigma]\[Upsilon]\[Zeta][w] - \[Beta][w] - D$]
G6[w_] := Gamma[1 + \[Alpha][w] - \[Beta][w]]
G6\[Sigma]\[Upsilon]\[Zeta][w_] :=
 Gamma[1 + \[Alpha]\[Sigma]\[Upsilon]\[Zeta][w] - \[Beta][w]]
G7[w_] := Gamma[2*\[Beta][w] + D$ - 2]

B[w_] := -1/
   Pi*(2/(Sqrt[w^2 - M^2]*rh*(1 + a$^2)^(1/(n + 1))))^(2*l +
      1)*(ElmTilde[w] + a^2*(w^2 - M^2) + 1/4)*(
  G1[w]^2*G2[w]*G3[w]*G4[w])/(G5[w]*G6[w]*G7[w])
B\[Sigma]\[Upsilon]\[Zeta][
  w_] := -1/
   Pi*(2/(Sqrt[w^2 - M^2]*rh*(1 + a$^2)^(1/(n + 1))))^(2*l +
      1)*(ElmTilde[w] + a^2*(w^2 - M^2) + 1/4)*(
  G1[w]^2*G2\[Sigma]\[Upsilon]\[Zeta][w]*
   G3\[Sigma]\[Upsilon]\[Zeta][w]*G4[w])/(
  G5\[Sigma]\[Upsilon]\[Zeta][w]*G6\[Sigma]\[Upsilon]\[Zeta][w]*G7[w])

f2 =
Absorption[w_] := (2*I*(B\[Sigma]\[Upsilon]\[Zeta][w] - B[w]))/(
 B[w]*B\[Sigma]\[Upsilon]\[Zeta][w] +
  I*(B\[Sigma]\[Upsilon]\[Zeta][w] - B[w]) + 1)
Plot[Absorption[w], {w, 0, 1.35}, PlotRange -> {{0, 3}, {-0.002, 1.}},
  AxesLabel -> {"w*rh", "|A|^2"}]1
```

C.3 Angular profile of the Hawking radiation spectrum

We present the codes for the case of fermion emission since fermions exhibit the most interesting angular profile. The codes concerning boson and scalar emission are very similar.

C.3.1 Angular profile of specific fermionic modes

Code for calculating the angular profile of the emission of the fermionic (spin $\frac{1}{2}$) mode with $l = \frac{3}{2}$ and $m = \frac{1}{2}$ with energy parameter $w = 0.3$ by a rotating black hole with angular momentum parameter $a = 1$.

```
Clear[s, l, m, astar, w, max, HL1, HL, k1, k2, A0, B01, B02, B03, A1, \
B11, B12, B13, G12, C0, C1, C2, D0, D1, D2, D3, E1, E2, E3, E4, E5, \
E6,

s = 1/2;
l = 3/2;
m = 1/2;
astar = 1;
w = 0.3;
\[Alpha]\[Omega] = astar*w;

max = Abs[m];
HL1 = ((l + 1)^2 - max^2) ((l + 1)^2 - 1/4)/(2 (l + 1)^3);
HL = (l^2 - max^2) (l^2 - 1/4)/(2 l^3);
k1 = 1/2* Abs[m - s];
k2 = 1/2* Abs[m + s];

A0 = -2 (Abs[m - s] + 1);
B01 = 1/4*(Abs[m - s] + Abs[m + s])*(Abs[m - s] + Abs[m + s] + 2) -
   l (l + 1);
B02 = -2 (Abs[m - s] + s + 1) + (2 m s^2)/(l (l + 1));
B03 = -HL1 + HL;
A1 = -4 (Abs[m - s] + 2);
B11 = Abs[m - s] + Abs[m + s] + 2 +
   1/4*(Abs[m - s] + Abs[m + s])*(Abs[m - s] + Abs[m + s] + 2) -
   l (l + 1);
B12 = -4 - 2 (Abs[m - s] + s + 1) + (2 m s^2)/(l (l + 1));
B13 = -HL1 + HL;
\Gamma12 = Abs[m - s] + Abs[m + s] + 2 s + 2;

C0 = -B01/A0;
C1 = -B02/A0;
```

```
C2 = -B03/A0;
D0 = (B01*B11)/(A1*A0);
D1 = (B02*B11 + B01*B12)/(A1*A0) - G12/A1;
D2 = (B03*B11 + B02*B12 + B01*B13)/(A1*A0);
D3 = (B03*B13 + B02*B13)/(A1*A0);
E1 = 1 + C0 + D0;
E2 = C1 + D1;
E3 = C2 + D2;
E4 = C0 + 2 D0;
E5 = C1 + 2 D1;
E6 = C2 + D2;

Solve[D[(Exp[(\[Alpha]\[Omega]) x] (1 + x)^k1 (1 - x)^
      k2  (E1 + E2*(\[Alpha]\[Omega]) + E3*(\[Alpha]\[Omega])^2 +
       D3*(\[Alpha]\[Omega])^3 + (E4 + E5*(\[Alpha]\[Omega]) +
          E6*(\[Alpha]\[Omega])^2)*x + (D0 + D1*(\[Alpha]\[Omega]))*
        x^2))^2, x] == 0, x]

 Plot[(Exp[(\[Alpha]\[Omega]) x] (1 + x)^k1 (1 - x)^
      k2  (E1 + E2*(\[Alpha]\[Omega]) + E3*(\[Alpha]\[Omega])^2 +
       D3*(\[Alpha]\[Omega])^3 + (E4 + E5*(\[Alpha]\[Omega]) +
          E6*(\[Alpha]\[Omega])^2)*x + (D0 + D1*(\[Alpha]\[Omega]))*
        x^2))^2, {x, -1, 1}, PlotStyle -> Hue[1],
  PlotRange -> {{-1, 1}, {0, 123}}]
```

C.3.2 Angular profile of the energy flux carried away by fermions

Code for calculating the angular profile of the total energy ascribed to spin $\frac{1}{2}$ degrees of freedom emitted by a rotating black hole with angular momentum parameter $a = 1$.

```
Clear[s, l, m, astar, w, max, HL1, HL, k1, k2, A0, B01, B02, B03, A1, \
B11, B12, B13, G12, C0, C1, C2, D0, D1, D2, D3, E1, E2, E3, E4, E5, \
E6,

s = 1/2;
hr = 1;
n = 2;
astar = 0;                                          \
\

\[Alpha] = hr astar;
hawk = ((n + 1) + (n - 1) astar^2)/(4 \[Pi] (1 + astar^2) hr);
omega = astar/(hr (1 + astar^2));


iop = 0;
(x = 0; int = 1; Label[x - loop];
 \[Omega] = 0.0000001; Label[\[Omega] - loop];
 l = 1/2; Label[l - loop];
 m = -l; Label[m - loop];

 max = Abs[m];

 HL1 = ((l + 1)^2 - max^2) ((l + 1)^2 - 1/4)/(2 (l + 1)^3);

 HL = (l^2 - max^2) (l^2 - 1/4)/(2 l^3);

 k1 = 1/2* Abs[m - s];
 k2 = 1/2* Abs[m + s];
 A0 = -2 (Abs[m - s] + 1);
 B01 = 1/4*(Abs[m - s] + Abs[m + s])*(Abs[m - s] + Abs[m + s] + 2) -
   l (l + 1);
 B02 = -2 (Abs[m - s] + s + 1) + (2 m s^2)/(l (l + 1));
 B03 = -HL1 + HL;
 A1 = -4 (Abs[m - s] + 2);
 B11 = Abs[m - s] + Abs[m + s] + 2 +
   1/4*(Abs[m - s] + Abs[m + s])*(Abs[m - s] + Abs[m + s] + 2) -
   l (l + 1);
 B12 = -4 - 2 (Abs[m - s] + s + 1) + (2 m s^2)/(l (l + 1));
 B13 = -HL1 + HL;
 \Gamma12 = Abs[m - s] + Abs[m + s] + 2 s + 2;
```

```
C0 = -B01/A0;
C1 = -B02/A0;
C2 = -B03/A0;
D0 = (B01*B11)/(A1*A0);
D1 = (B02*B11 + B01*B12)/(A1*A0) - G12/A1;
D2 = (B03*B11 + B02*B12 + B01*B13)/(A1*A0);
D3 = (B03*B13 + B02*B13)/(A1*A0);
E1 = 1 + C0 + D0;
E2 = C1 + D1;
E3 = C2 + D2;
E4 = C0 + 2 D0;
E5 = C1 + 2 D1;
E6 = C2 + D2;


harm = (Exp[(\[Alpha]*\[Omega]) x] (1 + x)^k1 (1 - x)^
      k2 (E1 + E2*(\[Alpha]*\[Omega]) + E3*(\[Alpha]*\[Omega])^2 +
       D3*(\[Alpha]*\[Omega])^3 + (E4 + E5*(\[Alpha]*\[Omega]) +
          E6*(\[Alpha]*\[Omega])^2)*x + (D0 + D1*(\[Alpha]*\[Omega]))*
        x^2))^2;


iop =  iop +
  harm/(4 \[Pi] (Exp[(\[Omega] - m * omega)/hawk] + 1));


reducediop = iop/(1);


If[m < l, {m = m + 1, Goto[m - loop]}];
If[l < 15, {l = l + 1, Goto[l - loop]}];
If[\[Omega] < 0.5, {\[Omega] = \[Omega] + 0.01,
  Goto[\[Omega] - loop]}];


(* PutAppend[{w,  grayfn},"outgray.dat"];
Datagray=Table[{w, grayfn}, {w,0.000001, 0.21, 0.005}];
Export["outgray1.dat",Datagray, "Table"];*)
Print[x, "    ", l, "    ", m,
 "                                             ", iop,
 "          ", reducediop];
If[x < 1, {x = x + 0.02, iop = 0, int = int + 1, Goto[x - loop]}];)
```

Περίληψη

Η υπόθεση περί της ύπαρξης επιπλέον χωρικών διαστάσεων μεγάλου (συγκριτικά με το μήκος Planck) μεγέθους, που διατυπώθηκε πριν από περίπου 15 χρόνια, έχει πυροδοτήσει έκτοτε μια πληθώρα μελετών σχετικά με τις επιπώσεις της προτεινόμενης γεωμετρίας στο Σύμπαν που ζούμε καθώς και τον τρόπο, που θα μπορούσαμε να αποδείξουμε την ύπαρξή τους και να κατανοήσουμε τη φύση τους. Η γενική ιδέα είναι ότι το Σύμπαν μας είναι μια 4-διάστατη υπερεπιφάνεια (που ονομάζεται βράνη), η οποία ζει εμβαπτισμένη σε έναν $(4 + n)$-διάστατο υπερχώρο, με τα πλέον γνωστά μοντέλα βρανών να είναι τα επονομαζόμενα ADD [28, 29, 30] και Randall-Sundrum [33, 34]. Όλα τα συνηθισμένα σωματίδια του Καθιερωμένου Μοντέλου είναι εγκλωβισμένα επάνω στη βράνη, ενώ μόνο η βαρύτητα μπορεί να διαδίδεται σε ολόκληρο τον πολυδιάστατο χωροχρόνο. Αφού εμείς μπορούμε να διεξάγουμε πειράματα μόνο πάνω στη βράνη-Σύμπαν, όπου ζούμε, πρέπει να αναζητήσουμε κάποιο φαινόμενο, που αφενός μεν εκδηλώνεται στη βράνη μας αφετέρου δε επηρεάζεται από τη συνολική τοπολογία του χωροχρόνου. Αυτός είναι ο λόγος που η μελέτη των μελανών οπών παρουσιάζει τόσο μεγάλο ενδιαφέρον στα πλαίσια αυτών των θεωριών. Ως αμιγώς βαρυτικά αντικείμενα, οι μελανές οπές 'νιώθουν' την πλήρη $(4 + n)$-διάστατη γεωμετρία. Από την άλλη, η ακτινοβολία Hawkingπου εκπέμπουν σε μεγάλο βαθμό, εκπέμπεται επάνω στη βράνη, όπου και μπορεί να μελετηθεί. Επειδή οι λεπτομέρειες του φάσματος της εν λόγω ακτινοβολίας εξαρτώνται από παραμέτρους όπως το πλήθος των επιπλέον διαστάσεων, είναι προφανές ότι η μελέτη του φάσματος μπορεί να μας δώσει χειροπιαστές αποδείξεις σχετικά με την ύπαρξη επιπλέον χωρικών διαστάσεων στη φύση.

Το πιο ενδιαφέρον φαινόμενο, που ανακύπτει στα πλαίσια των προαναφερθέντων μοντέλων, είναι ότι η θεμελιώδης ενέργεια της βαρύτητας μπορεί να έχει εν γένει σημαντικά μικρότερη τιμή από τη συνηθισμένη κλίμακα Planck (10^{19}GeV). Μάλιστα η τιμή της θα μπορούσε να είναι της τάξης των λίγων Τε˘, δηλαδή ενέργειας που είναι πειραματικά προσεγγίσιμη από το Μεγάλο Αδρονικό Επιταχυντή (ΛΗ˘). Αυτό σημαίνει ότι συγκρούσεις σωματιδίων με αρκετή ενέργεια θα μπορούσαν να οδηγήσουν στη δημιουργία μελανών οπών σε απόλυτα ελεγχόμενες εργαστηριακές συνθήκες. Αυτές οι μελανές οπές στη συνέχεια θα εξαϋλώνονταν σε πολύ σύντομο χρόνο (της τάξης των 10^{-26}sec) μέσω της εκπομπής ακτινοβολίας Hawking, την οποία θα καταγράφουν οι ανιχνευτές μας με μεγάλη ακρίβεια. Είναι λοιπόν σαφές ότι για να αξιολογηθούν αυτές οι καταγραφές θα πρέπει να διαθέτουμε μια σαφή γνώση του πώς διαμορφώνεται το φάσμα ακτινοβολίας των πολυδιάστατων μελανών οπών συναρτήσει των επιπλέον διαστάσεων. Οι μελανές οπές δε, που θα δημιουργηθούν με αυτό τον τρόπο αναμένεται να διαθέτουν στροφορμή μιας και τα συγκρουόμενα σωματίδια θα έχουν μη-μηδενική παράμετρο σύγκρουσης. Η μετρική, που περιγράφει πολυδιάστατες

μελανές οπές με έναν άξονα περιστροφής (αυτόν επάνω στη βράνη δηλαδή) είναι μια απλοποιημένη εκδοχή της μετρικής Myers-Perry [49]

$$ds^2 = -dt^2 + \frac{\mu}{r^{D-5}\Sigma}(dt - \alpha\sin^2\theta d\phi)^2 + \frac{\Sigma}{\Delta}dr^2$$

$$+ \ \Sigma d\theta^2 + (r^2 + \alpha^2)\sin^2\theta d\phi^2 + r^2\cos^2\theta d\Omega_{D-4}^2,$$

όπου μ είναι η παράμετρος μάζας

$$\mu = \frac{16\pi\, G\, M}{(d-2)\, A_{d-2}},$$

$\alpha = (D-2)J/2M$ και για τα Σ και Δ έχουμε

$$\Sigma = r^2 + \alpha^2\cos^2\theta \ \text{ and } \ \Delta = r^2 + \alpha^2 - \frac{\mu}{r^{D-5}}, \qquad (˙.1)$$

αντίστοιχα.

Ξεκινώντας, λοιπόν, από την προαναφερθείσα μετρική μελετήσαμε (κεφάλαιο 2) την εκπομπή τανυστικών βαρυτονίων από μια τέτοια μελανή οπή. Η μελέτη έγινε χρησιμοποιώντας τόσο αναλυτικές όσο και αριθμητικές μεθόδους. Δείξαμε ότι η ενέργεια που εκπέμπεται με τη μορφή τανυστικών βαρυτικών διαταραχών αυξάνει όσο αυξάνει ο αριθμός των επιπλέον διαστάσεων, όπως επίσης και όσο ταχύτερα περιστρέφεται η μελανή οπή. Αν και η ενέργεια που μεταφέρεται μέσω των βαθμωτών πεδίων είναι μεγαλύτερη από αυτή που μεταφέρουν τα βαρυτόνια, όσο αυξάνει ο αριθμός των επιπλέον διαστάσεων η συνεισφορά των βαρυτονίων σε αυτή τη διαδικασία γίνεται ολοένα και πιο έντονη και σε κάθε περίπτωση θα πρέπει να τη συνυπολογίσουμε για να καθορίσουμε με ακρίβεια το τι ακριβώς αναμένουμε να δούμε [1] στους ανιχνευτές μας.

Στη συνέχεια, προχωρήσαμε στη μελέτη της εκπομπής έμμαζων βαθμωτών πεδίων από πολυδιάστατες μελανές οπές με έναν άξονα περιστροφής. Μελετήσαμε ξεχωριστά την εκπομπή αυτών επάνω στη βράνη και στον υπερχώρο και συγκρίναμε τη σημασία των δύο αυτών ' καναλιών εκπομπής ' βασιζόμενοι τόσο σε αναλυτικές τεχνικές όσο και σε αριθμητικούς υπολογισμούς. δείξαμε ότι σε κάθε περίπτωση η αύξηση του αριθμού των επιπλέον διαστάσεων ή/και της στροφορμής της μελανής οπής οδηγεί σε αύξηση της εκπομπής ενέργειας με τη μορφή βαθμωτών πεδίων. Αναμενόμενα, όσο βαρύτερα είναι τα μελετούμενα βαθμωτά σωματίδια τόσο πιο μικρότερη είναι η συνεισφορά τους στη συνολικά εκπεμπόμενη ενέργεια. Όσον αφορά τη σύγκριση της εκπομπής επάνω στη βράνη ως προς την αντίστοιχη στον υπερχώρο, είδαμε ότι η πρώτη είναι σε κάθε περίπτωση εντονότερη, με το φαινόμενο να αμβλύνεται όσο αυξάνει η μάζα των θεωρούμενων βαθμωτών σωματιδίων.

Ολοκληρώνοντας την ενασχόλησή μας με το φάσμα της ακτινοβολίας Hawking προσανατολιστήκαμε στη μελέτη της γωνιακής κατανομής της εκπεμπόμενης ενέργειας. Κίνητρό μας ήταν να βρούμε έναν τρόπο να διαχωρίσουμε την επίδραση της στροφορμής από την

---

[1] ή να μη δούμε, μιας και τα βαρυτόνια εκπέμπονται στον υπερχώρο και άρα δεν γίνονται αντιληπτά από παρατηρητές στη βράνη, οι οποίοι θα αποδώσουν σε αυτά το τμήμα της ενέργειας που λείπει κατά τη διαδικασία δημιουργίας/εξαΰλωσης της μελανής οπής.

επίδραση της παραμέτρου n (πλήθος επιπλέον διαστάσεων) στο ενεργειακό φάσμα[2] Τόσο αριθμητικά όσο και μέσω μιας προσεγγιστικής αναλυτικής μεθόδου, που αναπτύξαμε, δείξαμε (και επιβεβαιώσαμε παλαιότερες υπολογιστικές μελέτες) ότι σε χαμηλές ενέργειες τα μποζόνια εκπέμπονται κατά τη διεύθυνση του άξονα περιστροφής της μελανής οπής (οπότε η μελέτη τους θα μας καταδείξει τον προσανατολισμό του άξονα) ενώ το μέγιστο του ρυθμού εκπομπής ενέργειας μέσω των φερμιονίων εντοπίζεται σε συγκεκριμένη γωνία ως προς τον άξονα, η οποία καθορίζεται από τη στροφορμή της μελανής οπής (την οποία και προσδιορίζουμε μέσω του πειραματικού προσδιορισμού της εν λόγω γωνίας). Τέλος, σε υψηλότερες ενέργειες όλα τα σωματίδια τείνουν να εκπεμφθούν στο ισημερινό (ως προς τον άξονα περιστροφής) επίπεδο, επομένως οι χρήσιμες πληροφορίες, που αναφέρθηκαν προηγουμένως, χάνονται.

Επόμενο ερώτημα που μας απασχόλησε (στο κεφάλαιο 3) είναι η δυνατότητα κατασκευής μιας λύσης μελανής οπής στα πλαίσια του μοντέλου Randall-Sundrum τύπου II με μια βράνη και εάν μια τέτοια λύση μπορεί να υποστηριχθεί από ένα ρεαλιστικό μοντέλο θεωρίας πεδίου. Πιο συγκεκριμένα, ξεκινήσαμε από μια μετρική τύπου άιδψα στα πλαίσια του 5-διάστατου μοντέλου Randall-Sundrum , στην οποία η μάζα αφήνεται να έχει εξάρτηση τόσο από το χρόνο (παράμετρος u) όσο και από την επιπλέον διάσταση (παράμετρος y):

$$ds^2 = e^{2A(y)}\left[-\left(1 - \frac{2m(v,y)}{r}\right)dv^2 + 2\epsilon dvdr + r^2\left(d\theta^2 + \sin^2\theta d\varphi^2\right)\right] + dy^2 . \quad (˘.2)$$

Έπειτα προσδιορίσαμε τις αναλλοίωτες βαρυτικές ποσότητες και τα στοιχεία του τανυστή Einstein, που απορρέουν από αυτή. Προσπαθήσαμε να κατασκευάσουμε ένα μοντέλο, όπου από τη μια η κατανομή ενέργειας θα ικανοποιεί τις εξισώσεις Einsteinκαι από την άλλη θα υποστηρίζει μια συμπεριφορά της μάζας με τρόπο που να αποφεύγονται ανεπιθύμητοι απειρισμοί στις τιμές των βαθμωτών βαρυτικών ποσοτήτων. Αρχικά θεωρήσαμε την περίπτωση ελάχιστα συνδεδεμένων (minimally-coupled) με τη βαρύτητα βαθμωτών πεδίων στον υπερχώρο. Υποθέσαμε διαδοχικά την ύπαρξη ενός βαθμωτού πεδίου με μη-κανονικούς κινητικούς όρους, δύο αλληλεπιδρώντων βαθμωτών πεδίων με κανονικούς και μη-κανονικούς κινητικούς όρους καθώς δύο αλληλεπιδρώντων βαθμωτών πεδίων με κανονικούς και μη κινητικούς όρους και επιπλέον όρους ανάμειξης. Καμία όμως από αυτές τις υποθέσεις δεν κατόρθωσε να ικανοποιήσει τα κριτήριά μας. Στη συνέχεια, διερευνήσαμε την υπόθεση ύπαρξης ενός σύμμορφα συνδεδεμένου (conformally-coupled) με τη βαρύτητα βαθμωτού πεδίου στον υπερχώρο. Στην περίπτωση αυτή αν και δεν καταφέραμε να δομήσουμε ένα επιτυχές μοντέλο, κατορθώσαμε ωστόσο να δείξουμε ότι η εν λόγω υπόθεση δεν μπορεί σε καμία περίπτωση να μας δώσει τα επιθυμητά αποτελέσματα ανεξάρτητα από τον ακριβή τρόπο διασύνδεσης του βαθμωτού πεδίου με τη βαρύτητα, λόγω της μορφής των εξισώσεων Einstein.

Σειρά είχε το λεγόμενο παράδοξο της πληροφορίας, που εμφανίζεται στα συστήματα που περιλαμβάνουν μελανές οπές. Το ζήτημα έγκειται στο ότι οι μελανές οπές για έναν εξωτερικό παρατηρητή μπορούν να περιγραφούν μέσω μόνο τριών παραμέτρων (ήτοι μάζα,

---

[2]Τόσο στις δύο μελέτες μας που προαναφέρθηκαν όσο και σε όλες τις σχετικές μελέτες άλλων η τιμή της στροφορμής της μελανής οπής και το πλήθος των επιπλέον διαστάσεων επηρεάζουν την εκπομπή ενέργειας με πολύ παρόμοιο τρόπο, οπότε και δεν μπορεί να γίνει διαχωρισμός της επίδρασής τους μόνο με βάση τη συνολική εκπομπή ενέργειας.

στροφορμή και ηλεκτρικό φορτίο) ανεξάρτητα από το ποια ακριβώς ήταν η φύση της ύλης από την οποία διαμορφώθηκε. Αλλά και η ακτινοβολία Hawkingαυτής εξαρτάται μόνο από τα γεωμετρικά της χαρακτηριστικά, οπότε και η διαδικασία εκπομπής σωματιδίων εμφανίζεται επίσης 'αναίσθητη' ως προς το τι έχει απορροφήσει η μελανή οπή πέρα από το επίπεδο των τριών παραμέτρων, που προαναφέρθηκαν. Επιπλέον δε, η εν λόγω ακτινοβολία έχει αποδειχθεί να είναι θερμικού τύπου, δηλαδή ότι δεν υπάρχουν διασυνδέσεις μεταξύ των σωματιδίων που τη συναπαρτίζουν, συνεπώς δεν μπορεί να μεταφέρει καμία (ή σχεδόν καμία) πληροφορία σχετικά με το σύστημα από το οποίο προήλθε. Έτσι γεννιούνται εύλογα ερωτήματα σχετικά με το την τύχη των πληροφοριών, που εισέρχονται στη μελανή οπή κατά τη διάρκεια της ζωής της. Το αν αυτές καταστρέφονται ή διατηρούνται ή αποθηκεύονται σε απρόσιτες δομές κ.ο.κ. είναι ακόμα ανοιχτό σαν ερώτημα. Στο κεφάλαιο 4 παρουσιάζουμε δύο ιδέες, που θα μπορούσαν να επιλύσουν το παράδοξο αυτό. Από τη μία προτείνουμε την υπόθεση της διάκρισης των πληροφοριών σε δύο κατηγορίες. Πο πληροφορίες τύπου 1 είναι οι πλέον θεμελιώδεις, προστατεύονται σε κάθε περίπτωση από νόμους διατήρησης και ως προς αυτές δε υπάρχει απώλεια πληροφορίας. Σε αυτές συγκαταλέγονται η μάζα/ενέργεια, η στροφορμή, το ηλεκτρικό φορτίο και ενδεχομένως κάποιος συνδυασμός βαρυονικού και λεπτονικού αριθμού. Επειδή και τα εκπεμπόμενα από τη μελανή οπή σωματίδια περιέχουν τέτοιου είδους πληροφορίες, δεχόμαστε ότι το σύνολο των πληροφοριών τύπου 1 που περιέχουν τα εκπεμπόμενα σωματίδια ισούται με το σύνολο των τύπου 1 πληροφοριών, που διαθέτει η μελανή οπή, οπότε και εξασφαλίζεται η διατήρηση της πληροφορίας σε αυτό το επίπεδο. Όλες οι υπόλοιπες πληροφορίες (π.χ. το πως συνδυάζονται τα θεμελιώδη κβαντικά συστήματα για να σχηματίσουν υπερδομές όπως άτομα και μόρια, οι ιδιότητες των δομών αυτών κ.ο.κ.) χαρακτηρίζονται ως πληροφορίες τυπου 2 και μπορούν να καταστρέφονται. Οι μελενές οπές, ως τα πλέον ακραία αντικείμενα στο Σύμπαν θεωρούμε ότι καταστρέφουν το σύνολο των πληροφοριών τύπου 2, που εισέρχονται σε αυτές και ως εκ τούτου έχουν υψηλή εντροπία. Παράλληλα, προτείνουμε την ιδέα ότι για να μπορέσει να κατανοήσει κανείς πλήρως τη διαδικασία εξαΰλωση των μελανών οπών και το πώς μπορεί πληροφορίες από το εσωτερικό τους να διαφεύγουν προς το παρατηρήσιμο Σύμπαν, παρά την ύπαρξη του ορίζοντα γεγονότων, πρέπει να αναγνωρίσει την εκδήλωση του φαινομένου Einstein-Podolsky-Rosen[255] σαν βάση της διασύνδεσης μεταξύ των σωματιδίων της ακτινοβολίας Hawkingκαι του εσωτερικού της μελανής οπής. Η μη-τοπική φύση του φαινομένου, λοιπόν, σημαίνει ότι η επικοινωνία σωματιδίων-εσωτερικού καθίσταται εφικτή παρά τον (κλασικό) περιορισμό που θέτει η ύπαρξη του ορίζοντα γεγονότων. Υπό αυτό το πρίσμα, η διαδικασία δημιουργίας/εξαΰλωσης της μελανής οπής μπορεί να προσεγγιστεί σαν μια διαδικασία σκέδασης από τη μελανή οπή σωματιδίων, που την προσεγγίζουν προερχόμενα από μια ασυμπτωτικά επίπεδη περιοχή και τα οποία μετά την αλλελεπίδρασή τους με τη μελανή οπή καταλήγουν σε μια άλλη ασυμπτωτικά επίπεδη περιοχή, όπου και παρατηρούνται. Μάλιστα, στην περίπτωση της εργαστηριακής δημιουργίας μελανών οπών θα μπορούσαν να προσδιοριστούν πειραματικά τα στοιχεία του αντίστοιχου πίνακα σκέδασης και να αποκτήσουμε μια εικόνα περί της (άγνωστης μέχρι σήμερα) μικροφυσικής του εσωτερικού της μελανής οπής.

Το πλαίσιο, οι μέθοδοι, τα αποτελέσματα όλων αυτών των μελετών έχουν ήδη δημοσιευθεί στις κάτωθι εργασίες, οι οποίες και αποτέλεσαν τη βάση για τη συγγραφή της παρούσας

διατριβής:

- *"Graviton Emission in the Bulk by a Simply Rotating Black Hole"*, P. Kanti, H. Kodama, R.A. Konoplya, N. Pappas and A. Zhidenko, *Phys. Rev.* D **80**, 084016 (2009).

- *"Emission of Massive Scalar Fields by a Higher-Dimensional Rotating Black-Hole"*, P. Kanti and N. Pappas, *Phys. Rev.* D **82**, 024039 (2010).

- *"Bulk decay of (4 + n)-dimensional simply rotating black holes: Tensor-type gravitons"*, N. Pappas, *J. Phys. Conf. Ser.* **283** 012028 (2011).

- *"A New approach to information loss (no) problem for Black Holes"*, N. Pappas, *Int. J. Theor. Math. Phys.* **2N2**, 5-9 (2012).

- *"On the preservation of unitarity during black hole evolution and information extraction from its interior"*, N. Pappas, *Mod. Phys. Lett.* A**27**, 12501 (2012).

- *"Angular profile of Particle Emission from a Higher-dimensional Black Hole: Analytic Results"*, P. Kanti and N. Pappas, *JHEP* **1212**, 019 (2012).

- *"On the Localization of 4-Dimensional Brane-World Black-Holes"*, P. Kanti, N. Pappas and K. Zuleta Estrugo (submitted for publication to Class. Quant. Grav.).

Η παρακαταθήκη της διατριβής είναι ένα σύνολο γνώσεων, εμπειριών, ιδεών, προβληματισμών, εμπνεύσεων και, το κυριότερο, ανοιχτών ερωτημάτων προς διερεύνηση ως στόχος μελέτης για το επόμενο διάστημα, που αφορούν από τις λεπτομέρειες του φάσματος ακτινοβολίας των μελενών οπών μέχρι τη βαθύτερη φύση του χρόνου και την ενοποιημένη εικόνα, που επιθυμούμε να κατακτήσουμε για τη Φύση.

Bibliography

[1] H. Minkowski, *"Raum und Zeit"*, *Jahresberichte der Deutschen Mathematiker-Vereinigung*, 75-88 (1908/9).

[2] `www.link2universe.net/2010-11-04/un esperimento che usera un olometro mettera alla prova la teoria delluniverso come ologramma/`

[3] J. Forster and J. D. Nightingale, *"A short course in General Relativity"* (Springer Science, N.Y., 2006)

[4] R. d'Inverno, *"Introducing Einstein's relativity"* (Clarendon Press, Oxford, 1992)

[5] S. Hawking(ed.) and W. Israel(ed.), *"General Relativity: An Einstein centenary survey"* (Campbridge University Press, Campbridge, 1980)

[6] B. Schutz, *"A First Course in General Relativity"* (Campbridge University Press, Campbridge, 2009)

[7] M. V. Berry, *"Principles of Cosmology and Gravitation"* (IOP Publishing, 1989)

[8] W. Weinberg, *"Gravitation and Cosmology: Principles and Applications of the General Theory of Relativity"* (John Wiley & Sons, 1972)

[9] S. Carroll, *"Spacetime and Geometry: An Introduction to General Relativity "* (Addison-Wesley, 2003)

[10] J. B. Hartle *"Gravity: An Introduction to Einstein's General Relativity "* (Addison-Wesley, 2003)

[11] R. M. Wald, *"General Relativity "* (University Of Chicago Press, 1984)

[12] C. W. Misner, K. S. Thorne and J. A. Wheeler *"Gravitation"* (W. H. Freeman, 1973)

[13] R. Geroch *"General Relativity from A to B"* (University Of Chicago Press, 1981)

[14] V. Frolov and I. Novikov, *"Black Hole Physics"* (Springer, 1998)

[15] S. L. Shapiro and S. A. Teukolsky, *"Black Holes, White Dwarfs and Neutron Stars: The Physics of Compact Objects"* (Wiley-VCH, 1983)

[16] R. M. Wald, *'Black Holes and Relativistic Stars'"* (University Of Chicago Press, 1998)

[17] N. D. Pappas, "*A new approach to information loss (no) problem*", *Int. J. Theor. Math. Phys.* **2**, no 2 (2012).

[18] N. D. Pappas, "*On the preservation of unitarity during black hole evolution and information extraction from its interior*", *Mod. Phys. Lett.* A **27**, 12501 (2012).

[19] P. Kanti, H. Kodama, R. A. Konoplya, N. Pappas and A. Zhidenko, "*Graviton Emission in the Bulk by a Simply Rotating Black Hole*", Phys. Rev. D **80**, 084016 (2009).

[20] P. Kanti and N. Pappas, "*Emission of Massive Scalar Fields by a Higher-Dimensional Rotating Black-Hole*", *Phys. Rev.* D **82**, 024039 (2010).

[21] P. Kanti and N. Pappas, "*Angular profile of Particle Emission from a Higher-dimensional Black Hole: Analytic Results*", *JHEP* **1212**, 019 (2012).

[22] P. Kanti, N. Pappas and K. Zuleta Estrugo, "*On the Localization of 4-Dimensional Brane-World Black-Holes*", (submitted for publication to Phys. Rev. D).

[23] R. Sachs and H. Wu, "*General Realativity for Mathematicians*" (Springer-Verlag, 1977)

[24] T. Kaluza, "*On the Problem of Unity in Physics*", *Sitzungs-ber.Preuss.Akad.Wiss.Berlin*, 966-972 (1921).

[25] O. Klein, "*Quantum Theory and Five-Dimensional Theory of Relativity*", *Z.Phys.* **37**, 895-906 (1926).

[26] J.D. Bekenstein, "*Black Holes and the Second Law*", *Lett. Nuovo Cim.* **4**, 737 (1972).

[27] `www.bellarmine.edu/faculty/amahmood/tier3/research.html`

[28] N. Arkani-Hamed, S. Dimopoulos and G. R. Dvali, "*The hierarchy problem and new dimensions at a millimeter*", *Phys. Lett.* B **429**, 263 (1998).

[29] N. Arkani-Hamed, S. Dimopoulos and G. R. Dvali, "*Phenomenology, astrophysics and cosmology of theories with sub-millimeter dimensions and TeV scale quantum gravity*", *Phys. Rev.* D **59**, 086004 (1999).

[30] I. Antoniadis, N. Arkani-Hamed, S. Dimopoulos and G. R. Dvali, "*New dimensions at a millimeter to a Fermi and superstrings at a TeV*", *Phys. Lett.* B **436**, 257 (1998).

[31] I. Antoniadis, "*A possible new dimension at a few TeV*", *Phys. Lett.* B **246**, 377-384 (1990).

[32] J.C. Long, H.W. Chan, A.B. Churnside, E.A. Gulbis, M.C.M. Varney, and J.C. Price, *"Upper limits to submillimetre-range forces from extra space-time dimensions"*, *Nature* **421**, 922-925 (2003).

[33] L. Randal and R. Sundrum, *"Large mass hierarchy from a small extra dimension"*, *Phys. Rev. Lett.* **83**, 3370 (1999).

[34] L. Randall and R. Sundrum, *"An alternative to compactification"*, *Phys. Rev. Lett.* **83**, 4690 (1999).

[35] `www.learner.org/courses/physics/unit/text.html?unit=4&secNum=6`

[36] `www.thelivingmoon.com/41pegasus/01archives/Parallel_Dimensions.htm`

[37] M. Remazeilles, *"Dissipation and nonlocality in a general expanding braneworld universe"*, *Phys. Rev.* D **79**, 043523 (2009).

[38] M.J. Duff and J.T. Liu, *""Complementarity of the Maldacena and Randall-Sundrum Pictures"*, *Phys. Rev. Lett.* **85**, 2052-2055 (2000).

[39] `www.pitt.edu/~jdnorton/teaching/HPS_0410/chapters/black_holes/`

[40] R. Arnowitt, S. Deser and C.W. Misner, *"Dynamical Structure and Definition of Energy in General Relativity"*, *Physical Review* **116** 1322-1330 (1959).

[41] K. Schwarzschild, *"On the gravitational field of a mass point according to Einstein's theory "*, *Sitzungsber.Preuss.Akad.Wiss.Berlin*, 189-196 (1916).

[42] R.P. Kerr, *"Gravitational field of a spinning mass as an example of algebraically special metrics "*, *Phys.Rev.Lett.* **11**, 237-238 (1963).

[43] `www.daviddarling.info/encyclopedia/K/Kerr_black_hole.html`

[44] H. Thirring, *"Über die Wirkung rotierender ferner Massen in der Einsteinschen Gravitationstheorie"*, *Physikalische Zeitschrift* **19**, 33 (1918).

[45] J. Lense and H. Thirring, *"Über den Einfluss der Eigenrotation der Zentralkfrper auf die Bewegung der Planeten und Monde nach der Einsteinschen Gravitationstheorie"*, *Physikalische Zeitschrift* **19**, 156-163 (1918).

[46] C. W. F. Everitt et al., *"Gravity Probe B: Final Results of a Space Experiment to Test General Relativity"*, *Phys. Rev. Lett.* **106**, 221101 (2011).

[47] `large.stanford.edu/courses/2011/ph240/nagasawa2/`

[48] R. Penrose and R.M. Floyd, *"Extraction of rotational energy from a black hole "*, *Nature* **229**, 177-179 (1971).

[49] R. C. Myers and M. J. Perry, *"Black Holes In Higher Dimensional Space-Times"*, *Annals Phys.* **172**, 304 (1986).

[50] S. W. Hawking, *"Particle Creation By Black Holes"*, *Commun. Math. Phys.* **43**, 199 (1975).

[51] J. B. Hartle and S. W. Hawking, *"Path-integral derivation of black hole radiance"*, *Phys. Rev.* D **13**, 2188 (1976).

[52] minerva.union.edu/diiorios/physics123/hawkingradiation.html

[53] blog.emergingscholars.org/2012/11/science in review october 2012/

[54] J.M. Bardeen, B. Carter and S.W. Hawking, *"The four laws of black hole mechanics"*, *Commun. Math. Phys.* **31**, 161 (1973).

[55] J.D. Bekenstein, *"Black Holes and Entropy"*, *Phys. Rev.* D **7**, 2333 (1973).

[56] J.D. Bekenstein, *"Generalized second law of thermodynamics in black-hole physics"*, *Phys. Rev.* D **9**, 3292 (1974).

[57] S. W. Hawking, *"Information loss in black holes"*, *Phys. Rev.* **D 72**, 084013 (2005).

[58] J. D. Bekenstein and V. F. Mukhanov, *"Spectroscopy of the quantum black hole"*, *Phys. Lett.* **B 360**, 7 (1995).

[59] C. R. Stephens, G. 't. Hooft and B. F. Whiting, *"Black hole evaporation without information loss"*, *Class. Quant. Grav.* **11**, 621 (1994).

[60] S. Hod, *"Discrete black hole radiation and the information loss paradox"*, *Phys. Lett.* **A 299**, 144 (2002).

[61] V. F. Mukhanov, *"Are black holes quantized?"*, *Pis'ma. Zh. Eksp. Teor. Fiz.* **44**, 50 (1986).

[62] T. Vachaspati, D. Stojkovic, L. M. Krauss, *"Observation of incipient black holes and the information loss paradox"*, *Phys. Rev.* **D 76**, 024005 (2007).

[63] Y. Aharonov, A. Casher and S. Nussinov, *"The unitarity puzzle and planck mass stable remnants"*, *Phys. Lett.* **B 191**, 51 (1987).

[64] S. D. Mathur, *"The information paradox: A pedagogical introduction"*, *Class. Quant. Grav.* **26**, 224001 (2009).

[65] T. Vachaspati, D. Stojkovic, *"Quantum radiation from quantum gravitational collapse"*, *Phys. Lett.* **B 663**, 107-110 (2008).

[66] J. D. Bekenstein, *"Entropy bounds and black hole remnants"*, *Phys. Rev.* **D 49**, 1912 (1994).

[67] L. Susskind, *"Trouble for remnants"*, arXiv:hep-th/9501106.

[68] D. N. Page, *"Information in black hole radiation"*, *Phys. Rev. Lett.* **71**, 3743 (1993).

[69] V. Frolov, S. B. Giddings, A. Strominger, P. C. Argyres et al., *"Quantum aspects of gravity"*, arXiv:astro-ph/9412046.

[70] A. Ashtekar, V. Taveras and M. Varadarajan, *"Information is not lost in the evaporation of 2-dimensional black holes"*, *Phys. Rev. Lett.* **100**, 211302 (2008).

[71] A. Peet, L. Susskind and L. Thorlacius, *"Information loss and anomalous scattering"*, *Phys. Rev.* **D 46**, 3435 (1992).

[72] T. Banks, M. O'Loughlin and A. Strominger, *"Black hole remnants and the information puzzle"*, *Phys. Rev.* **D 47**, 4476 (1993).

[73] T. Banks, *"Lectures on black holes and information loss"*, *Nucl. Phys. Proc. Suppl.* **41**, 21 (1995).

[74] S. B. Giddings, *"Black holes and massive remnants"*, *Phys. Rev.* **D 46**, 1347 (1992).

[75] T. Banks, A. Dabholkar, M. R. Douglas and M. O'Loughlin, *"Are horned particles the endpoint of Hawking evaporation?"*, *Phys. Rev.* **D 45**, 3607 (1992).

[76] C. A. S. Silva, *"Fuzzy spaces topology change as a possible solution to the black hole information loss paradox"*, *Phys. Lett.* **B 677**, 318-321 (2009).

[77] J. Preskil, *"Do black holes destroy information?"*, arXiv:hep-th/9209058.

[78] S. B. Giddings, *"Toy models for black hole evaporation"*, arXiv:hep-th/9209113.

[79] S. W. Hawking, *"Breakdown of predictability in gravitational collapse"*, *Phys. Rev.* **D 14**, 2460 (1976).

[80] S. W. Hawking, *"The unpredictability of quantum gravity"*, *Commun. Math. Phys.* **87**, 395 (1982).

[81] T. Banks, L. Susskind and M. E. Peskin, *"Difficulties for the evolution of pure states into mixed states"*, *Nucl. Phys.* **B 244**, 125 (1984).

[82] J. Ellis, J. S. Hagelin, D. V. Nanopoulos and M. Srednicki, *"Search for violations of quantum mechanics"*, *Nucl. Phys.* **B 241**, 381 (1984).

[83] R. Emparan and H.S. Reall, *"Black Rings "*, *Class.Quant.Grav.* **23**, R169 (2006).

[84] P. Kanti, *"Black holes in theories with large extra dimensions: a review"*, *Int. J. Mod. Phys.* A **19**, 4899 (2004).

[85] S. B. Giddings and S. Thomas, *"High energy colliders as black hole factories: The end of short distance physics"*, *Phys. Rev.* D **65**, 056010 (2002).

[86] T. Banks and W. Fischler, *"A model for high-energy scattering in quantum gravity"*, arXiv:hep-th/9906038.

[87] D. M. Eardley and S. B. Giddings, *"Classical Black Hole Production in High-Energy Collisions"*, Phys. Rev. **D 66**, 044011 (2002).

[88] H. Yoshino and Y. Nambu, *"High-energy head-on collisions of particles and hoop conjecture"*, Phys. Rev. **D66**, 065004 (2002).

[89] H. Yoshino and Y. Nambu, *"Black hole formation in the grazing collision of high-energy particles"*, ibid. **D 67**, 024009 (2003).

[90] E. Kohlprath and G. Veneziano, *"Black holes from high-energy beam-beam collisions"*, JHEP **0206**, 057 (2002).

[91] V. Cardoso, O. J. C. Dias and J. P. S. Lemos, *"Gravitational radiation in D-dimensional spacetimes"*, Phys. Rev. D **67**, 064026 (2003).

[92] E. Berti, M. Cavaglia and L. Gualtieri, *"Gravitational energy loss in high energy particle collisions: Ultrarelativistic plunge into a multidimensional black hole"*, Phys. Rev. **D 69**, 124011 (2004).

[93] S. B. Giddings and V. S. Rychkov, *"Black holes from colliding wavepackets"*, Phys. Rev. D **70**, 104026 (2004).

[94] H. Yoshino and V. S. Rychkov, *"Improved analysis of black hole formation in high-energy particle collisions"*, Phys. Rev. D **71**, 104028 (2005).

[95] D. C. Dai, G. D. Starkman and D. Stojkovic, *"Production of black holes and their angular momentum distribution in models with split fermions"*, Phys. Rev. **73**, 104037 (2006).

[96] H. Yoshino and R. B. Mann, *"Black hole formation in the head-on collision of ultrarelativistic charges"*, Phys. Rev. **74**, 044003 (2006).

[97] H. Yoshino, T. Shiromizu and M. Shibata, *"Close-slow analysis for head-on collision of two black holes in higher dimensions: Bowen-York initial data"*, Phys. Rev. D **74**, 124022 (2006).

[98] P. Kanti, *"Black Holes at the LHC"*, Lect. Notes Phys. **769**, 387 (2009).

[99] P. Kanti, *"Brane-World Black Holes"*, J. Phys. Conf. Ser. **189**, 012020 (2009).

[100] M. Cavaglia, *"Black hole and brane production in TeV gravity: a review"*, Int. J. Mod. Phys. A **18**, 1843 (2003).

[101] G. L. Landsberg, *"Black holes at future colliders and in cosmic rays"*, Eur. Phys. J. C **33**, S927 (2004).

[102] K. Cheung, *"Collider phenomenology for a few models of extra dimensions"*, arXiv:hep-ph/0409028.

[103] S. Hossenfelder, *"What black holes can teach us"*, in *Focus on Black Hole Research* (Nova Science Publishers, 2005), pp155-192. arXiv:hep-ph/0412265.

[104] C. M. Harris, *"Physics beyond the standard model: exotic leptons and black holes at future colliders"*, arXiv:hep-ph/0502005.

[105] A. S. Majumdar and N. Mukherjee, *"Braneworld black holes in cosmology and astrophysics"*, *Int. J. Mod. Phys.* D **14**, 1095 (2005).

[106] E. Winstanley, *"Hawking radiation from rotating brane black holes"*, arXiv:hep-th/0708.2656.

[107] R. Emparan and H. S. Reall, *"Black Holes in Higher Dimensions"*, *Living Rev. Rel.* **11**, 6 (2008).

[108] E. Berti, V. Cardoso and A. O. Starinets, *"Quasinormal modes of black holes and black branes"*, *Class. Quant. Grav.* **26**, 163001 (2009).

[109] R. A. Konoplya, *"Gravitational quasinormal radiation of higher-dimensional black holes"*, Phys. Rev. D **68**, 124017 (2003).

[110] P. Kanti and R. A. Konoplya, *"Quasi-normal modes of brane-localised standard model fields"*, Phys. Rev. D **73**, 044002 (2006).

[111] H. Ishihara, M. Kimura, R. A. Konoplya, K. Murata, J. Soda and A. Zhidenko, *"Evolution of perturbations of squashed Kaluza-Klein black holes: escape from instability"*, Phys. Rev. D **77**, 084019 (2008).

[112] E. Berti, K. D. Kokkotas and E. Papantonopoulos, *"Gravitational stability of five-dimensional rotating black holes projected on the brane"*, Phys. Rev. D **68**, 064020 (2003).

[113] P. Kanti and J. March-Russell, *"Calculable corrections to brane black hole decay. I: The scalar case"*, *Phys. Rev.* D **66**, 024023 (2002).

[114] P. Kanti and J. March-Russell, *"Calculable corrections to brane black hole decay. II: graybody factors for spin 1/2 and 1"*, *Phys. Rev.* D **67**, 104019 (2003).

[115] C. M. Harris and P. Kanti, *"Hawking radiation from a (4+n)-dimensional black hole: Exact results for the Schwarzschild phase"*, *JHEP* **0310**, 014 (2003).

[116] A. Barrau, J. Grain and S. O. Alexeyev, *"Gauss-Bonnet black holes at the LHC: Beyond the dimensionality of space"*, *Phys. Lett.* B **584**, 114 (2004).

[117] J. Grain, A. Barrau and P. Kanti, *"Exact results for evaporating black holes in curvature-squared Lovelock gravity: Gauss-Bonnet graybody factors"*, *Phys. Rev.* D **72**, 104016 (2005).

[118] T. G. Rizzo, *"TeV-scale black hole lifetimes in extra-dimensional Lovelock gravity"*, *Class. Quant. Grav.* **23**, 4263 (2006).

[119] E. l. Jung, S. H. Kim and D. K. Park, *"Absorption cross section for S-wave massive scalar"*, *Phys. Lett.* B **586**, 390 (2004).

[120] E. l. Jung, S. H. Kim and D. K. Park, *"Low-energy absorption cross section for massive scalar and Dirac fermion by (4+n)-dimensional Schwarzschild black hole"*, *JHEP* **0409**, 005 (2004).

[121] E. l. Jung, S. H. Kim and D. K. Park, *"Proof of universality for the absorption of massive scalar by the higher-dimensional Reissner-Nordstroem black holes"*, *Phys. Lett.* B **602**, 105 (2004).

[122] E. l. Jung, S. H. Kim and D. K. Park, *"Ratio of absorption cross section for Dirac fermion to that for scalar in the higher-dimensional black hole background"*, *Phys. Lett.* B **614**, 78 (2005).

[123] E. Jung and D. K. Park, *"Absorption and emission spectra of an higher-dimensional Reissner-Nordstroem black hole"*, *Nucl. Phys.* B **717**, 272 (2005).

[124] E. Jung and D. K. Park, *"Bulk versus brane in the absorption and emission: 5D rotating black hole case"*, *Nucl. Phys.* B **731**, 171 (2005).

[125] P. Kanti, J. Grain and A. Barrau, *"Bulk and brane decay of a (4+n)-dimensional Schwarzschild-De-Sitter black hole: Scalar radiation"*, *Phys. Rev.* D **71**, 104002 (2005).

[126] A. S. Cornell, W. Naylor and M. Sasaki, *"Graviton emission from a higher-dimensional black hole"*, *JHEP* **0602**, 012 (2006).

[127] D. K. Park, *"Hawking radiation of the brane-localized graviton from a (4+n)-dimensional black hole"*, *Class. Quant. Grav.* **23**, 4101 (2006).

[128] V. Cardoso, M. Cavaglia and L. Gualtieri, *"Black hole particle emission in higher-dimensional spacetimes"*, *Phys. Rev. Lett.* **96**, 071301 (2006) [Erratum-ibid. **96**, 219902 (2006)].

[129] V. Cardoso, M. Cavaglia and L. Gualtieri, *"Hawking emission of gravitons in higher dimensions: Non-rotating black holes"*, *JHEP* **0602**, 021 (2006).

[130] S. Creek, O. Efthimiou, P. Kanti and K. Tamvakis, *"Graviton emission in the bulk from a higher-dimensional Schwarzschild black hole"*, *Phys. Lett.* B **635**, 39 (2006).

[131] O. Efthimiou, *"Graviton emission from a Schwarzschild black hole in the presence of extra dimensions"*, *J. Phys. Conf. Ser.* **68**, 012024 (2007).

[132] D. C. Dai, N. Kaloper, G. D. Starkman and D. Stojkovic, *"Evaporation of a black hole off of a tense brane"*, *Phys. Rev.* D **75**, 024043 (2007).

[133] V. P. Frolov and D. Stojkovic, *"Quantum radiation from a 5-dimensional rotating black hole"*, *Phys. Rev.* D **67**, 084004 (2003).

[134] D. Ida, K. y. Oda and S. C. Park, *"Rotating black holes at future colliders: graybody factors for brane fields"*, *Phys. Rev.* D **67**, 064025 (2003) [Erratum-ibid. D **69**, 049901 (2004)].

[135] H. Nomura, S. Yoshida, M. Tanabe and K. i. Maeda, *"The fate of a five-dimensional rotating black hole via Hawking radiation"*, *Prog. Theor. Phys.* **114**, 707 (2005).

[136] C. M. Harris and P. Kanti, *"Hawking radiation from a (4+n)-dimensional rotating black hole"*, *Phys. Lett.* B **633**, 106 (2006).

[137] D. Ida, K. y. Oda and S. C. Park, *"Rotating black holes at future colliders. II: Anisotropic scalar field emission"*, *Phys. Rev.* D **71**, 124039 (2005).

[138] D. Ida, K. y. Oda and S. C. Park, *"Rotating black holes at future colliders. III: Determination of black hole evolution"*, *Phys. Rev.* D **73**, 124022 (2006).

[139] E. Jung, S. Kim and D. K. Park, *"Condition for superradiance in higher-dimensional rotating black holes"*, *Phys. Lett.* B **615**, 273 (2005).

[140] E. Jung, S. Kim and D. K. Park, *"Condition for the superradiance modes in higher-dimensional rotating black holes with multiple angular momentum parameters"*, *Phys. Lett.* B **619**, 347 (2005).

[141] G. Duffy, C. Harris, P. Kanti and E. Winstanley, *"Brane decay of a (4+n)-dimensional rotating black hole: Spin-0 particles"*, *JHEP* **0509**, 049 (2005).

[142] M. Casals, P. Kanti and E. Winstanley, *"Brane decay of a (4+n)-dimensional rotating black hole. II: Spin-1 particles"*, *JHEP* **0602**, 051 (2006).

[143] M. Casals, S. R. Dolan, P. Kanti and E. Winstanley, *"Brane decay of a (4+n)-dimensional rotating black hole. III: Spin-1/2 particles"*, *JHEP* **0703**, 019 (2007).

[144] S. Creek, O. Efthimiou, P. Kanti and K. Tamvakis, *"graybody Factors for Brane Scalar Fields in a Rotating Black-Hole Background"*, *Phys. Rev.* D **75**, 084043 (2007).

[145] S. Creek, O. Efthimiou, P. Kanti and K. Tamvakis, *"graybody factors in a rotating black-hole background-II : fermions and gauge bosons"*, *Phys. Rev.* D **76**, 104013 (2007).

[146] S. Chen, B. Wang, R. K. Su and W. Y. Hwang, *"graybody factors for rotating black holes on codimension-2 branes"*, *JHEP* **0803**, 019 (2008).

[147] J. A. Frost, J. R. Gaunt, M. O. P. Sampaio, M. Casals, S. R. Dolan, M. A. Parker and B. R. Webber, *"Phenomenology of production and decay of spinning extra-dimensional black holes at hadron colliders"*, JHEP **0910**, 014 (2009).

[148] D-C. Dai, G. Starkman, D. Stojkovic, C. Issever, E. Rizvi, and J. Tseng, *"Black-Max: A black-hole event generator with rotation, recoil, split branes and brane tension"*, *Phys. Rev.* D **77**, 076007 (2008).

[149] R. Emparan, G. T. Horowitz and R. C. Myers, *"Black holes radiate mainly on the brane"*, *Phys. Rev. Lett.* **85**, 499 (2000).

[150] E. Jung and D. K. Park, *"Validity of Emparan-Horowitz-Myers argument in Hawking radiation into massless spin-2 fields"*, *Mod. Phys. Lett.* A **22**, 1635 (2007).

[151] M. Casals, S. R. Dolan, P. Kanti and E. Winstanley, *"Bulk Emission of Scalars by a Rotating Black Hole"*, JHEP **0806**, 071 (2008).

[152] S. Creek, O. Efthimiou, P. Kanti and K. Tamvakis, *"Scalar emission in the bulk in a rotating black hole background"*, *Phys. Lett.* B **656**, 102 (2007).

[153] T. Kobayashi, M. Nozawa, Y. Takamizu, *"Bulk scalar emission from a rotating black hole pierced by a tense brane"*, *Phys. Rev.* D **77**, 044022 (2008).

[154] M. Casals, S. R. Dolan, P. Kanti and E. Winstanley, *"Bulk Emission of Scalars by a Rotating Black Hole"*, *JHEP* **0806**, 071 (2008).

[155] H. K. Kunduri, J. Lucietti and H. S. Reall, *"Gravitational perturbations of higher dimensional rotating black holes: Tensor Perturbations"*, *Phys. Rev.* **D74**, 084021 (2006).

[156] H. Kodama, *"Superradiance and instability of black holes"*, *Prog. Theor. Phys. Supple.* **172**, 11 (2008).

[157] H. Kodama, R. A. Konoplya and A. Zhidenko, *"Gravitational stability of simply rotating Myers-Perry black holes: tensorial perturbations"*, *Phys. Rev.* D **81**, 044007 (2010).

[158] K. Murata and J. Soda, *"A Note on Separability of Field Equations in Myers-Perry Spacetimes"*, *Class. Quant. Grav.* **25**, 035006 (2008).

[159] H. Kodama, A. Ishibashi and O. Seto, *"Brane world cosmology: Gauge invariant formalism for perturbation"*, *Phys. Rev.* D **62**, 064022 (2000).

[160] H. Kodama, *"Perturbations and stability of higher-dimensional black holes"*, *Lect. Notes Phys.* **769**, 427 (2009).

[161] H. Kodama and A. Ishibashi, *"Stability of higher dimensional Schwarzschild black holes"*, *Prog. Theor. Phys.* **110**, 701 (2003).

[162] H. Kodama, R. A. Konoplya and A. Zhidenko, *"Gravitational instability of simply rotating Myers-Perry-AdS black holes"*, Phys. Rev. D **79**, 044003 (2009).

[163] R. A. Konoplya and A. Zhidenko, *"Stability of higher dimensional Reissner-Nordstrom-anti-de Sitter black holes"*, Phys. Rev. D **78**, 104017 (2008).

[164] D. Ida, Y. Uchida and Y. Morisawa, *"The scalar perturbation of the higher-dimensional rotating black holes"*, Phys. Rev. D **67** (2003) 084019.

[165] M. Abramowitz and I. Stegun, *Handbook of Mathematical Functions* (Academic, New York, 1996).

[166] E. Berti, V. Cardoso and M. Casals, *"Eigenvalues and eigenfunctions of spin-weighted spheroidal harmonics in four and higher dimensions"*, Phys. Rev. D **73**, 024013 (2006) [Erratum-ibid. D **73**, 109902(2006)].

[167] V. Cardoso, G. Siopsis and S. Yoshida, *"Scalar perturbations of higher dimensional rotating and ultra-spinning black holes"*, Phys. Rev. D **71**, 024019 (2005).

[168] H. Suzuki, E. Takasugi and H. Umetsu, *"Perturbations of Kerr-de Sitter black holes and Heun's equations"*, Prog. Theor. Phys. **100**, 491 (1998).

[169] R. A. Konoplya and A. Zhidenko, *"Decay of a charged scalar and Dirac fields in the Kerr-Newman-de Sitter background"*, Phys. Rev. D **76**, 084018 (2007).

[170] E.W. Leaver, *"An analytic representation for the quasi normal modes of Kerr black holes"* Proc. R. Soc. A **402**, 285 (1985).

[171] M.A. Rubin and C.R. Ordónez, *"Symmetric tensor eigen spectrum of the laplacian on N spheres"*, *J. Math. Phys.* **25**, 2888 (1984).

[172] J. Doukas, H. T. Cho, A. S. Cornell and W. Naylor, *"Graviton emission from simply rotating Kerr-de Sitter black holes: Transverse traceless tensor graviton modes"*, *Phys. Rev.* D **80**, 045021 (2009).

[173] S. B. Giddings and S. Thomas, *"High Energy Colliders as Black Hole Factories: The End of Short Distance Physics"*, Phys. Rev. D **65**, 056010 (2002).

[174] S. Dimopoulos and G. Landsberg, *"Black holes at the LHC"*, Phys. Rev. D **87**, 161602 (2001).

[175] P. C. Argyres, S. Dimopoulos and J. March-Russell, *"Black holes and sub-millimeter dimensions"*, Phys. Lett. B **441**, 96 (1998).

[176] U. Sperhake, V. Cardoso, F. Pretorius, E. Berti, T. Hinderer and N. Yunes, *"Cross section, final spin and zoom-whirl behavior in high-energy black hole collisions"*, Phys. Rev. Lett. **103**, 131102 (2009).

[177] A. Casanova and E. Spallucci, *"TeV mini black hole decay at future colliders"*, *Class. Quant. Grav.* **23**, R45 (2006).

[178] M. Casals, S. R. Dolan, P. Kanti and E. Winstanley, *"Angular profile of emission of non-zero spin fields from a higher-dimensional black hole"*, Phys. Lett. B **680**, 365 (2009).

[179] D. N. Page, *"Particle Emission Rates From A Black Hole. 3. Charged Leptons From A Nonrotating Hole"*, Phys. Rev. D **16**, 2402 (1977).

[180] M. O. P. Sampaio, *"Charge and mass effects on the evaporation of higher-dimensional rotating black holes"*, JHEP **0910**, 008 (2009).

[181] M. O. P. Sampaio, *"Distributions of charged massive scalars and fermions from evaporating higher-dimensional black holes"*, JHEP **1002**, 042 (2010).

[182] V. P. Frolov and D. Stojkovic, *"Particle and light motion in a space-time of a five-dimensional rotating black hole"*, Phys. Rev. D **68**, 064011 (2003).

[183] C. Muller, *Lecture Notes in Mathematics: Spherical Harmonics* (Springer-Verlag, Berlin-Heidelberg, 1966).

[184] S. S. Gubser, I. R. Klebanov and A. A. Tseytlin, *"String theory and classical absorption by three-branes"*, *Nucl. Phys.* **B499**, 217 (1997).

[185] S. D. Mathur, *"Absorption of angular momentum by black holes and D-branes"*, *Nucl. Phys. B* **514**, 204 (1998).

[186] S. S. Gubser, *"Can the effective string see higher partial waves?"*, *Phys. Rev. D* **56**, 4984 (1997).

[187] Y.B. Zel'dovich, *"Generation of waves by a rotating body"*, *JETP Lett.* **14**, 180 (1971).

[188] A. A. Starobinskii and S. M. Churilov, *"Amplification of electromagnetic and gravitational waves scattered by a rotational black hole"*, Sov. Phys.-JETP **38**, 1 (1974).

[189] E. D. Fackerell and R. G. Crossman, *"Spin-weighted angular spheroidal functions"*, J. Math. Phys. **18**, 1849 (1977).

[190] E. Seidel, *"A Comment On The Eigenvalues Of Spin Weighted Spheroidal Functions"*, Class. Quant. Grav. **6**, 1057 (1989).

[191] P. Kanti, *"Footprints of Higher-Dimensional Decaying Black Holes"*, *Rom. J. Phys.* **57**, 96 (2012).

[192] S. C. Park, *"Black holes and the LHC: A Review"*, *Prog. Part. Nucl. Phys.* **67**, 617 (2012).

[193] V. P. Frolov and D. Stojkovic, *"Black hole radiation in the brane world and recoil effect"*, *Phys. Rev. D* **66**, 084002 (2002).

[194] P. Nicolini and E. Winstanley, *"Hawking emission from quantum gravity black holes"*, JHEP **1111**, 075 (2011).

[195] A. Flachi, M. Sasaki and T. Tanaka, *"Spin polarization effects in micro black hole evaporation"*, *JHEP* **0905**, 031 (2009).

[196] M. O. P. Sampaio, *"Angular correlations in TeV-gravity black hole events"*, *JHEP* **1203**, 066 (2012).

[197] D. C. Dai and D. Stojkovic, *"Analytic explanation of the strong spin-dependent amplification in Hawking radiation from rotating black holes"*, *JHEP* **1008**, 016 (2010).

[198] S. A. Teukolsky, *"Rotating black holes - separable wave equations for gravitational and electromagnetic perturbations"*, *Phys. Rev. Lett.* **29**, 1114 (1972).

[199] S. A. Teukolsky, *"Perturbations of a rotating black hole. 1. Fundamental equations for gravitational electromagnetic and neutrino field perturbations"*, *Astrophys. J.* **185**, 635 (1973).

[200] W. H. Press and S. A. Teukolsky, *"Perturbations of a rotating black hole. II. Dynamical stability of the Kerr Metric"*, *Astrophys. J.* **185**, 649 (1973).

[201] F.R. Tangherlini, *"Schwarzschild field in n dimensions and the dimensionality of space problem"*, *Nuovo Cim.* **27**, 636 (1963).

[202] R. Maartens, *"Brane world gravity"*, *Living Rev. Rel.* **7**, 7 (2004).

[203] R. Gregory, *"Braneworld black holes"*, *Lect. Notes Phys.* **769**, 259 (2009).

[204] R. Maartens and K. Koyama, *"Brane-World Gravity"*, *Living Rev. Rel.* **13**, 5 (2010).

[205] A. Chamblin, S.W. Hawking and H.S. Reall, *"Brane-world black holes"*, *Phys. Rev. D* **61**, 065007 (2000).

[206] R. Gregory and L. Laflamme, *"Black strings and p-branes are unstable"*, *Phys. Rev. Lett.* **70**, 2837 (1993).

[207] R. Gregory, *"Black string instabilities in anti-de Sitter space"*, *Class. Quant. Grav.* **17**, L125 (2000).

[208] N. Dadhich, R. Maartens, P. Papadopoulos and V. Rezania, *"Black holes on the brane"*, *Phys. Lett. B* **487**, 1 (2000).

[209] G. Kofinas, E. Papantonopoulos and V. Zamarias, *"Black hole solutions in braneworlds with induced gravity"*, *Phys. Rev. D* **66**, 104028 (2000).

[210] P. Kanti and K. Tamvakis, *"Quest for localized 4-D black holes in brane worlds"*, *Phys. Rev. D* **65**, 084010 (2002).